DOCTOR OF PHILOSOPHY

Giving molecular cavity wall extensions (and other topology changes) to pseudo [M7] (M = Co, Ni and Zn) metallocalix[n]arenes (n = 4, 6)

Slater-Parry, Mari

Award date:
2024

Awarding institution:
Bangor University

Giving molecular cavity wall extensions (and other topology changes) to *pseudo* [M_7] (M = Co, Ni and Zn) metallocalix[n]arenes (n = 4, 6)

PRIFYSGOL
BANGOR
UNIVERSITY

A THESIS SUBMITTED BY

MARI ELENA SLATER-PARRY

IN ACCORDANCE WITH THE REQUIRMENTS FOR THE DOCTOR OF PHILOSOPHY

SCHOOL OF CHEMISTRY

BANGOR UNIVERSITY

September 2023

Declaration

I hereby declare that this thesis is the results of my own investigations, except where otherwise stated. All other sources are acknowledged by bibliographic references. This work has not previously been accepted in substance for any degree and is not being concurrently submitted in candidature for any degree unless, as agreed by the University, for approved dual awards.

Yr wyf drwy hyn yn datgan mai canlyniad fy ymchwil fy hun yw'r thesis hwn, ac eithrio lle nodir yn wahanol. Caiff ffynonellau eraill eu cydnabod gan droednodiadau yn rhoi cyfeiriadau eglur. Nid yw sylwedd y gwaith hwn wedi cael ei dderbyn o'r blaen ar gyfer unrhyw radd, ac nid yw'n cael ei gyflwyno ar yr un pryd mewn ymgeisiaeth am unrhyw radd oni bai ei fod, fel y cytunwyd gan y Brifysgol, am gymwysterau deuol cymeradwy.

Contents

Abstract

This thesis details the synthesis and structural characterisation of twenty-nine (**1**-**29**) new 1st row transition metal complexes constructed using a series of structurally related organic ligands based on a common phenol building block. A chapter content breakdown is given below.

Chapter 2 describe the synthesis of a sixteen (**1**-**16**) member family of solid-state host-guest complexes. Here we have successfully encapsulated a series of organic guest moieties (2-furaldehyde, 3-furaldehyde, benzaldehyde, thiophenecarboxaldehyde, 2-acetylfuran and acetophenone) into the molecular cavities within $[M(II)_7(OR)_6(L_1)_6](NO_3)_2$ (M = Co, Ni and Zn; R = H or CH_3 and L_1H = 2-Methoxy-6-[(E)-(methylimino)methyl]phenol) *pseudo* metallocalix[6]arene host complexes. Guest encapsulation has been confirmed using a variety of techniques including FT-IR, single crystal X-ray diffraction and solid-state NMR (in the case of $[(2\text{-fur})\subset Zn(II)_7(OMe)_6(L_1)_6](NO_3)_2{\cdot}3H_2O$ (**1**) and $[(benz)\subset Zn(II)_7(OMe)_6(L_1)_6](NO_3)_2{\cdot}5H_2O$ (**7**).

In Chapter 3 we describe the synthesis and characterisation of the ligands 2-Methoxy-6-{(E)-[(2-methoxyphenyl)imino]methyl}phenol (L_3H), Methyl 4-[(E)-(2-hydroxy-3-methoxybenzylidene)amino]benzoate (L_4H), 2-[(E)-(Benzylimino)methyl]-6-methoxyphenol (L_5H)**,** 2-[(Benzylamino)methyl]-6-methoxyphenol (L_6H) and 2-[(benzylamino)methyl]-4-bromo-6-methoxyphenol (L_7H). These ligands are structurally related to the ligand 2-Methoxy-6-[(E)-(methylimino)methyl]phenol (L_1H) used in the construction of the $[M_7]$ (M = Co(II), Ni(II) and Zn(II)) host complexes described in Chapter 2. Here we have investigated how the deliberate structural modifications of ligands L_1H and L_2H (in the form of $L_{3\text{-}7}H$) give rise to a variety of new complexes with varying nuclearities and topologies. For instance, we present the rare ferromagnetically coupled dinuclear complex $[Ni(II)_2(L_3)_3(H_2O)](NO_3){\cdot}2H_2O{\cdot}3MeOH$ (**17**) as characterised using a combination of SQUID and High-Field, High-Frequency EPR studies. We also discuss the structural and magnetic characterisation of the tetranuclear analogues $[(NO_3)\subset Co(II)_4(\mu_3\text{-}OH)_2(L_6)_4(H_2O)_2](NO_3){\cdot}H_2O$ (**21**), $[(NO_3)\subset Ni(II)_4(\mu_3\text{-}OH)_2(L_6)_4(H_2O)_2](NO_3){\cdot}H_2O$ (**22**) and $[Ni(II)_4(\mu_3\text{-}OH)_2(L_7)_4](NO_3)_2{\cdot}MeCN$ (**23**), whose *'butterfly'* core topologies

are discussed in relation to their heptanuclear *pseudo* metallocalix[6]arene ancestors $[Ni(II)_7(\mu_3\text{-}OH)_6(L_1)_2](NO_3)_2$ and $[Co(II)_7(\mu_3\text{-}OH)_6(L_1)_6](NO_3)_2$ (previously reported by the Jones group).

Magnetic susceptibility and magnetisation studies on complex $[(NO_3)\subset Co(II)_4(\mu_3\text{-}OH)_2(L_6)_4(H_2O)_2](NO_3)\cdot H_2O$ (**21**) and $[Ni(II)_4(\mu_3\text{-}OH)_2(L_7)_4](NO_3)_2\cdot MeCN$ (**23**) indicate competing anti- and ferromagnetic exchange between the Co(II) centres in **21** and dominant antiferromagnetic exchange between the Ni(II) ions in **23**.

In Chapter 4 we have taken the original ligand 2-Methoxy-6-[(E)-(methylimino)methyl]phenol (L_1H) and modified it at the upper rim location by attaching phenyl and tolyl functional groups to give the ligands 2-Methoxy-4-phenyl-6-[(E)-(methylimino)methyl]phenol (L_8H) and 2-Methoxy-4-tolyl-6-[(E)-(methylimino)methyl]phenol (L_9H), respectively. Interestingly and despite significant structural changes both L_8H and L_9H still produce the *pseudo* metallocalix[6]arenes complexes in the form of $[Ni(II)_7(OMe)_6(L_8)_6](NO_3)_2\cdot 2H_2O$ (**25**), $[Zn(II)_7(OH)_2(OMe)_4(L_8)_6](NO_3)_2\cdot 4MeOH\cdot 10H_2O$ (**26**) and $[Zn(II)_7(OMe)_6(L_9)_6](NO_3)_2\cdot 10MeOH\cdot 13H_2O$ (**27**). As intended, this upper rim functionalisation provides the family with extensions to their molecular cavity walls when compared to their previously reported siblings.

We also demonstrate how upper *and* lower rim functionalisation of the 2-Methoxy-6-[(E)-(methylimino)methyl]phenol (L_1H) gives rise to a new duo of ligands employed in the production of the complexes: $[Ni(II)_2(L_{10})_2(H_2O)(NO_3)_2].2MeCN$ (**28**) and $[Zn(L_{11})_2]$ (**29**) (where $L_{10}H$ is 2-Methoxy-4-phenyl-6-{(E)-[(2-methoxyphenyl)imino]methyl}phenol and $L_{11}H$ is 2-[(E)-(Benzylimino)methyl]-4-phenyl-6-methoxyphenol.

Acknowledgements

I would like to give a very special thank you to my Nain and Taid that are sadly no longer here to share in this moment. Without their encouragement and belief in my ability from a young age I'm not sure if I'd be the person I am today, let alone achieving a PhD. I'll be forever thankful for their kindness.

Secondly my parents for guiding me in this direction in the first place, life would have been very different as a beauty therapist and definitely not as interesting. Thank you for putting up with me for so many years as a student and helping in any way you could.

A big thank you to my partner James for listening to every rant and moan I had about this PhD and giving me nothing but encouragement to finish it. Through all the late nights and tears I've very glad that I had you to lend me a hand, even if it was sometimes just to make me a cup of tea. A special thank you to my son Macsen for being the reason I want to excel at my career and complete this thesis.

A thank you to all the 3rd and 4th year students I had along the way for the great laughs in team meetings and the lab as well as any contributions they made to the group work. To all the staff at Bangor University's Chemistry department, it really was like a family and it's a shame that future generations won't get to experience the same atmosphere. A special mention to Dr. Lorrie Murphy for her help and encouragement to finish this thesis long after she needed to.

And the biggest thank you of all goes to Dr. Leigh Jones. Firstly, for taking me on as a PhD student, and taking that chance in the first place. To all the help and encouragement, he had for me from the very beginning back in 2014 to present day 2024 (Yes it's really been that long!). You truly are an excellent supervisor and although I'm sure there were moments where you thought this day might not come, I'm forever grateful that you stuck with me to the end.

Acknowledgements – Data/Results

I would like to thank the following institutions for their help in attaining data that is included in this thesis.

Single crystallography	National Crystallography service at the University of Southampton. Crystallographers were Simon J. Coles, Peter N. Horton, Mateusz Pitak and Wim Klooster.
Elemental analysis	OEA laboratories
SQUID measurements	Helen O'Conner and Prof. Euan Brechin at University of Edinburgh.
Solid state NMR	Dr David Apperley at the University of Durham.
Powder XRD	Most were measured at Bangor University with assistance from Nick Welsby and Glynne Evans. Some were measured at Wolverhampton University by David Townrow and Dr Leigh Jones.
EPR	Anne-Laure Barra at CNRS.

Abbreviations

2-Acetyl	2-Acetylfuran
Acetop	Acetophenone
aq.	Aqueous
Benzal	Benzaldehyde
BVS	Bonding valence model
Cat.	Catalyst
Conc.	Concentrated
DCM	Dichloromethane
DMSO	Dimethylsulfoxide
DMSO-d_6	Deuterated dimethyl sulfoxide
Equiv.	Equivalent
FT-IR	Fourier-transform infrared spectroscopy
Fur	Furaldehyde (2 or 3)
$L_{10}H$	3,4'-dimethoxy-5-[(methylimino)methyl]-(1,1'-biphenyl)-4-ol
$L_{11}H$	4'-mercapto-3-methoxy-5-((methylimino)methyl)-[1,1'-biphenyl]-4-ol
$L_{12}H$	3-methoxy-5-(((2-methoxyphenyl)imino)methyl)-[1,1'-biphenyl]-4-ol
$L_{13}H$	3-((benzylimino)methyl)-5-methoxy-[1,1'-biphenyl]-4-ol
$L_{14}H$	3-methoxy-5-((phenylimino)methyl)-[1,1'-biphenyl]-4-ol
L_1H	2-methoxy-6-[(methylimino)methyl]phenol
L_2H	2-methoxy-6-[(phenylimino)methyl]phenol
L_3H	2-methoxy-6-{[(2-methoxybenzyl)imino]methyl}phenol
L_4H	4-[(2-hydroxy-3-methoxybenzylidene)amino]benzoate
L_5H	2-[(benzylimino)methyl]-6-methoxyphenol

L_6H	2-[(benzylamino)methyl]-6-methoxyphenol
L_7H	2-[(benzylamino)methyl]-4-bromo-6-methoxyphenol
L_8H	3-methoxy-5-[(methylimino)methyl]-(1,1'-biphenyl])-4-ol
L_9H	3-methoxy-4'-methyl-5-[(methylimino)methyl]-(1,1'-biphenyl)-4-ol
Me	Methyl group
MS	Mass spectroscopy
NMR	Nuclear magnetic resonance
PC1	2-((benzylimino)methyl)-4-bromo-6-methoxyphenol
PC2	4-hydroxy-5-methoxy-[1,1'-biphenyl]-3-carbaldehyde
PC3	4-hydroxy-5-methoxy-4'-methyl-[1,1'-biphenyl]-3-carbaldehyde
PC4	4-hydroxy-4',5-dimethoxy-[1,1'-biphenyl]-3-carbaldehyde
PC5	4-hydroxy-4'-mercapto-5-methoxy-[1,1'-biphenyl]-3-carbaldehyde
rt	Room temperature
S.E	Symmetry equivalent
SMM	Single molecular magnet
Thio	Thiophenecarboxaldehyde
TLC	Thin layer chromatography
XRD	X-ray crystallography

List of organic ligands used in this work

2-Methoxy-6-[(E)-(methylimino)methyl]phenol (L_1H)

2-methoxy-6-[(E)-(phenylimino)methyl]phenol (L_2H)

2-Methoxy-6-{(E)-[(2-methoxyphenyl)imino]methyl}phenol (L_3H)

Methyl 4-[(E)-(2-hydroxy-3-methoxybenzylidene)amino]benzoate (L_4H)

2-[(E)-(Benzylimino)methyl]-6-methoxyphenol (L_5H)

2-[(Benzylamino)methyl]-6-methoxyphenol (L_6H)

2-[(benzylamino)methyl]-4-bromo-6-methoxyphenol (L_7H)

2-Methoxy-4-phenyl-6-[(E)-(methylimino)methyl]phenol (L_8H)

2-Methoxy-4-tolyl-6-[(E)-(methylimino)methyl]phenol (L_9H)

2-Methoxy-4-phenyl-6-{(E)-[(2-methoxyphenyl)imino]methyl}phenol ($L_{10}H$)

2-[(E)-(Benzylimino)methyl]-4-phenyl-6-methoxyphenol ($L_{11}H$)

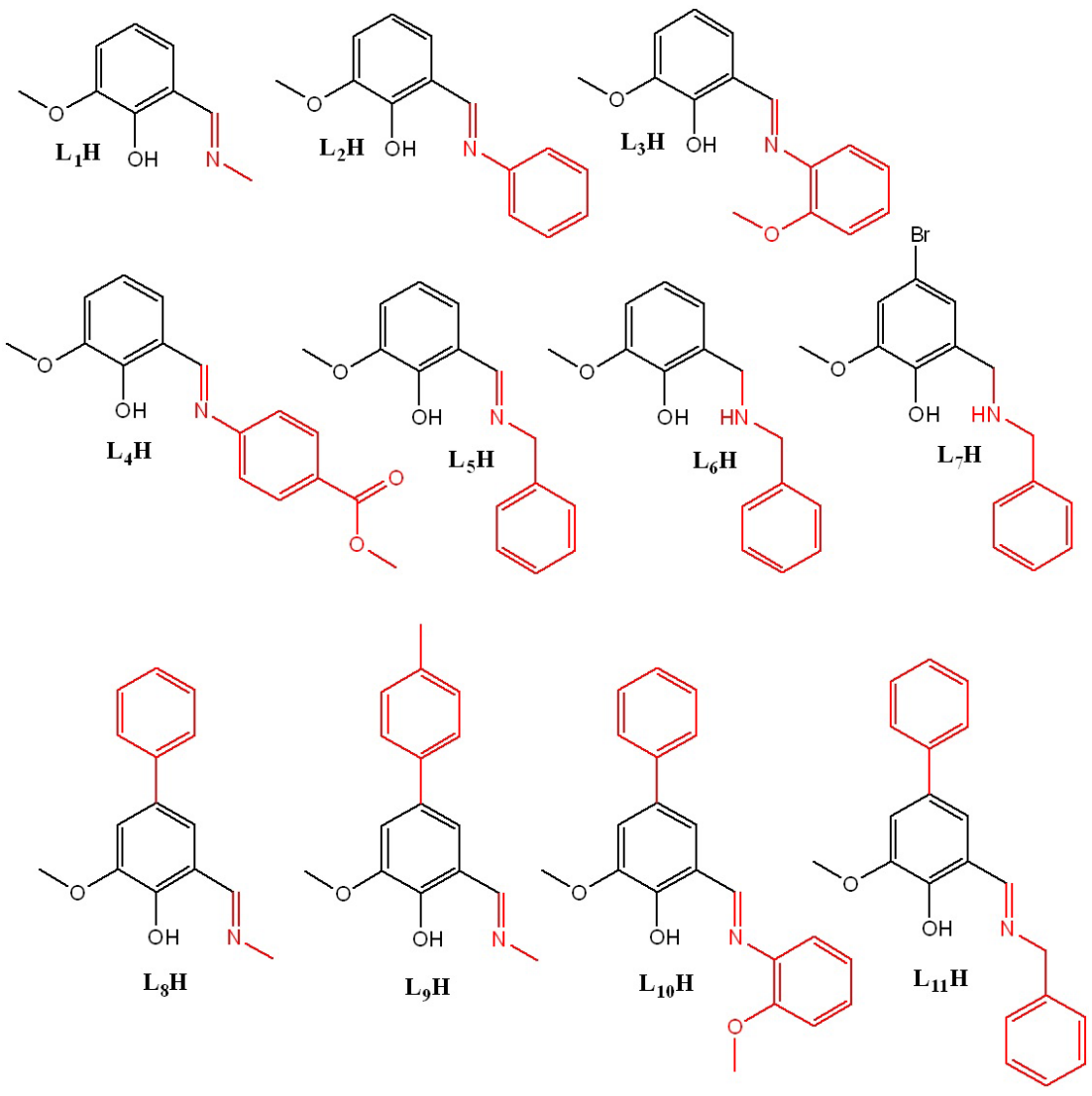

List of Complexes

Chapter 2

[(2-fur)⊂$Zn(II)_7(OMe)_6(L_1)_6$]$(NO_3)_2 \cdot 3H_2O$ (**1**)

[(2-fur)⊂$Ni(II)_7(OH)_6(L_1)_6$]$(NO_3)_2$ (**2**)

[(2-fur)⊂$Co(II)_7(OH)_6(L_1)_6$]$(NO_3)_2 \cdot 3H_2O$ (**3**)

[(3-fur)⊂$Zn(II)_7(OH)_6(L_1)_6$]$(NO_3)_2$ (**4**)

[(3-fur)⊂$Ni(II)_7(OH)_6(L_1)_6$]$(NO_3)_2 \cdot 3H_2O$ (**5**)

[(3-fur)⊂$Co(II)_7(OH)_6(L_1)_6$]$(NO_3)_2 \cdot 4.5H_2O$ (**6**)

[(benz)⊂$Zn(II)_7(OMe)_6(L_1)_6$]$(NO_3)_2 \cdot 5H_2O$ (**7**)

[(benz)⊂$Ni(II)_7(OH)_6(L_1)_6$]$(NO_3)_2$ (**8**)

[(2-Thio)⊂$Zn(II)_7(OH)_6(L_1)_6$]$(NO_3)_2$ (**9**)

[(2-Thio)⊂$Ni(II)_7(OH)_6(L_1)_6$]$(NO_3)_2$ (**10**)

[(2-acetyl)⊂$Zn(II)_7(OH)_6(L_1)_6(NO_3)_2$] (**11**)

[(2-acetyl)$Ni(II)_7(OMe)_6(L_1)_6$]$(NO_3)_2 \cdot 3H_2O$ (**12**)

[(2-acetyl)⊂$Co(II)_7(OMe)_6(L_1)_6$]$(NO_3)_2 \cdot 7H_2O$ (**13**)

[(acetoph)⊂$Zn(II)_7(OH)_6(L_1)_6$]$(NO_3)_2$ (**14**)

[(acetoph)⊂$Ni(II)_7(OMe)_6(L_1)_6$]$(NO_3)_2$ (**15**)

[(acetoph)⊂$Co(II)_7(OMe)_6(L_1)_6$]$(NO_3)_2 \cdot 7H_2O$ (**16**)

Chapter 3

[$Ni(II)_2(L_3)_3(H_2O)$]$(NO_3) \cdot 2H_2O \cdot 3MeOH$ (**17**)

[Na(I)$Ni(II)_2(\mu_3\text{-}OH)(L_4)_3(H_2O)_2$]$(NO_3)$ (**18**)

[$Ni(II)(L_5)_2$] (**19**)

[$Co(III)(L_5)_3$]$\cdot H_2O \cdot MeOH$ (**20a**)

[$Co(II)_7(OMe)_6(L_5)_6$]$(NO_3)_2 \cdot 0.5H_2O \cdot 4MeOH$ (**20b**)

[(NO_3)⊂$Co(II)_4(\mu_3\text{-}OH)_2(L_6)_4(H_2O)_2$]$(NO_3) \cdot H_2O$ (**21**)

[(NO_3)⊂$Ni(II)_4(\mu_3\text{-}OH)_2(L_6)_4(H_2O)_2$]$(NO_3) \cdot H_2O$ (**22**)

[$Ni(II)_4(\mu_3\text{-}OH)_2(L_7)_4(NO_3)_2$]$\cdot MeCN$ (**23**)

Chapter 4

$[Co(II)_7(OMe)_6(L_8)_6](NO_3)_2 \cdot H_2O \cdot 3MeOH$ (**24**) (originally synthesised by Sean Meally at NUI Galway)

$[Ni(II)_7(OMe)_6(L_8)_6](NO_3)_2 \cdot 2H_2O$ (**25**)

$[Zn(II)_7(OH)_2(OMe)_4(L_8)_6](NO_3)_2 \cdot 4MeOH \cdot 10H_2O$ (**26**)

$[Zn(II)_7(OMe)_6(L_9)_6](NO_3)_2 \cdot 10MeOH \cdot 13H_2O$ (**27**)

$[Ni(II)_2(L_{10})_2(H_2O)(NO_3)_2] \cdot 2MeCN$ (**28**)

$[Zn(L_{11})_2]$ (**29**)

Chapter 1:

Introduction

1. Introduction

1.1 Overview

The work described in this thesis entails the synthesis and full characterisation of a number of new complexes centred on a family of *pseudo* [M(II)$_7$] (M = Co, Ni and Zn) metallocalix[n]arenes and their analogues. As will become clear as the thesis proceeds, these complexes have been shown to display interesting physical properties such as targeted guest encapsulation and magnetic behaviour (when M(II) = Co or Ni). As a result, this thesis naturally lies within the fields of coordination, supramolecular and magneto-chemistry and we will therefore introduce these concepts below.

1.2 Coordination Chemistry

Modern coordination chemistry is largely based on the work of Alfred Werner who theorised the idea of variable valence in 1893, as part of his doctorate studying nitrogen compounds.[1] Werner had previously theories that nitrogen with three valence bonds would form a tetrahedron shape with the three ligands being extended to the three corners of the base triangle and the nitrogen itself occupying the fourth corner. This theory explained why certain nitrogen compounds showed optical isomerism. Werner later (1898) theorised that in terms of inorganic molecular compounds that they would contain a single central atom that acted like a nuclei where by all the other atoms, radicals or other molecules would spread out from. He theorised that these would space out into simple geometric patterns that allowed maximum amount of space around them. This was very different to the thinking at the time where compounds such as [Co(III)(NH$_3$)$_6$]Cl$_3$ would be depicted as a long chain molecule and not as the octahedron we recognise today (Fig. 1.1).[2]

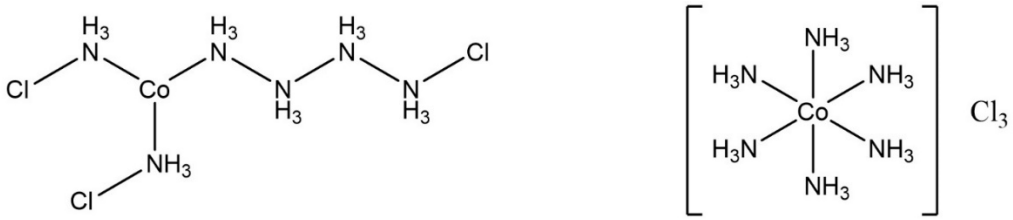

Christian Blomstrand & Sophus Jorgensen proposed structure

Alfred Werner proposed structure

Figure 1.1 (Left) proposed structure of $[Co(III)(NH_3)_6]Cl_3$, depicted as a long chain molecule. (Right) Alfred Werner`s proposed structure where the Co(III) is the central atom ligated to NH_3 ligands.

While trying to work out the geometry of the cobalt compound $[Co(III)(NH_3)_6]Cl_3$, Werner had two theories that he set out to prove or disprove. The first was that the six amine groups could orientate themselves three above and three below the cobalt plane, the second was to have four of the amines in a square orientation on the cobalt plane with one amine above and one below the plane. The difference between the two would be the number of isomers formed when you exchange two amine groups for two chlorine groups. The first could give three isomers and the second only two isomers. Through numerous investigations he was able to prove that only two isomers could be formed in this example, thus forming his thinking that the compound in fact orientated octahedrally.[3] Over the next 20 years (1898-1919) Werner and his collaborators prepared and studied hundreds of compounds and this work would go on to be the building blocks of coordination chemistry that then grew to be interdisciplinary field of supramolecular chemistry. For his work on the topic, he was awarded the 1913 Nobel prize for Chemistry.

1.3 Supramolecular Chemistry: A potted history

Supramolecular chemistry is defined as *chemistry beyond the molecule* and focuses on how two or more molecules associate through reversible intermolecular forces to form larger non-covalent assemblies whose physical properties (e.g. *chirality*, *magnetism, photoluminescence*) have been introduced and often enhanced through careful building block selection.[4] The field of supramolecular chemistry lies at the interface of biology,

chemistry and physics covers a wide variety of multidisciplinary subject areas such as host-guest chemistry (e.g. molecular recognition and sensing),[5] molecular self-assembly[6] and Dynamic Covalent Chemistry (DCvC).[7]

Although the roots of supramolecular chemistry were planted in the late 1800s (e.g. Fisher`s lock and key principal), the term supramolecular chemistry was first coined in the mid-to-late 1960's when many new developments concerning macrocycles and their metal coordination were being investigated.[8] The first example of the concepts behind supramolecular chemistry can be traced back to 1810 when Sir Humphry Davy more famously known for his work on electrolysis discovered chlorine hydrate.[9] This system was one of the first recorded instances of a compound that existed due to ion-ion binding rather than conventional covalent bonding. In 1894 Emil Fischer developed the concept of *'lock and key'* more widely known in biological systems but provided great ambition for modern day host-guest chemists to produce systems that can replicate this selectivity observed in nature.[10] Following this, in 1906 Paul Ehrlich introduced the concept of receptors, again more commonly known in biology but provided the foundation for research areas such as molecular switches and catalysts.[11] With more than a little help from Rosalind Franklin, 1953 saw Watson, Crick and Wilkins solve the structure of DNA, whose double helix shape was found to be driven by H-bonding (Fig. 1.2)[12]

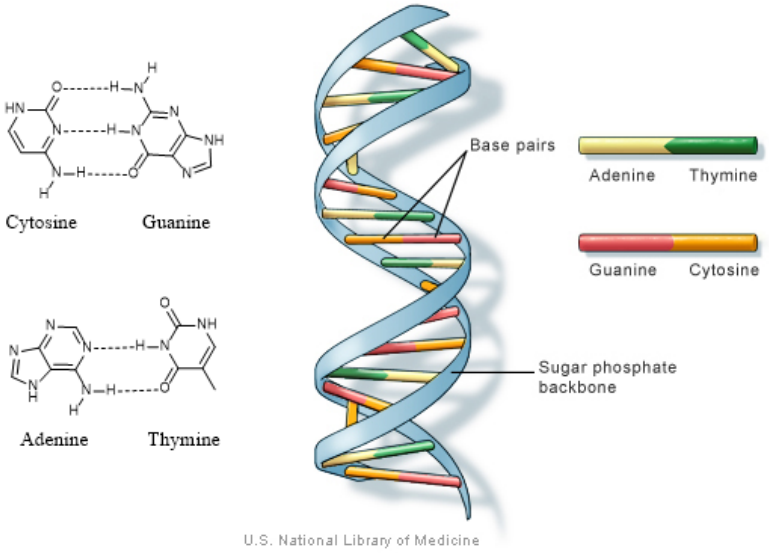

Figure 1.2 (Left) Diagram of the hydrogen bonds formed between GC and AT base pairs. Created in chemdraw. (Right) Visual diagram of the base pairs producing the double helix structure through stacking and sugar phosphate backbone.[13]

1.3.1 Crown ethers, carcerands and cryptands

The 1960's saw four fundamental systems developed, three of which were Schiff base condensation reactions of an aldehyde with an amine to give the corresponding imine.[14] These were produced by Curtis (1961),[15] Busch (1964),[16] Jäger (1964)[17] and Pedersen (1967).[18] Each of these systems were seen as developments upon natural macrocyclic systems (Fig. 1.3).

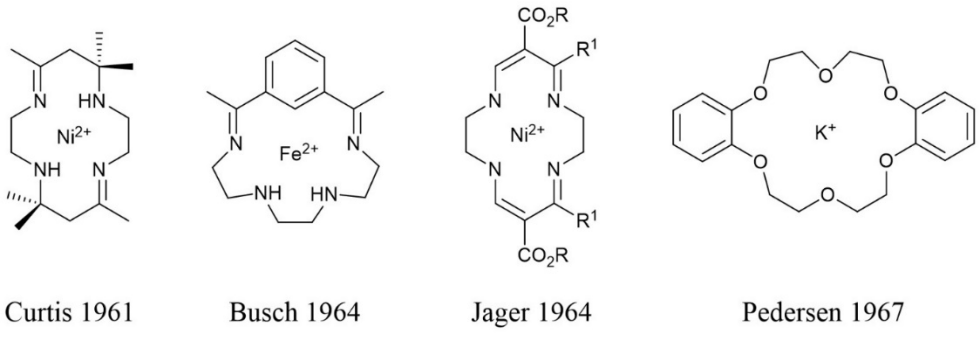

Figure 1.3 The four fundamental systems of supramolecular chemistry as outlined by Steed *et al* in the book 'Supramolecular Chemistry.'[19]

While working at DuPont in the 1960s, Charles Pedersen was investigating vanadium coordination chemistry when he serendipitously produced a small (but intriguing) amount of byproduct. This turned out to be a crown ether (18-crown-6). Indeed, he quickly noticed how this molecule was able to aid the dissolution of potassium permanganate while in benzene. He proposed that the K^+ ion fell into the hole (Fig. 1.4a).

Building upon Pedersen`s fascinating 2-D organic host structures, Cram began investigating -3-D structures towards producing cavities that would tightly bind certain guest units. He coined these materials carcerands and hemicarcerands (Fig. 1.4b). The difference between the two being the complete and irreversible guest encapsulation within carcerands, while guests may egress hemicarcerand cavities at higher temperatures.

In 1968, Lehn and co-workers produced a caged molecule with a cavity that can accommodate a guest compound. This organic cage was christened a cryptand, as it entombed its guest ion. Lehn was then able to use his extensive knowledge of organic chemistry to produce a variety of organic host units whose cavity sizes could be controlled and therefore guest ingression tailored accordingly (Fig. 1.4c).

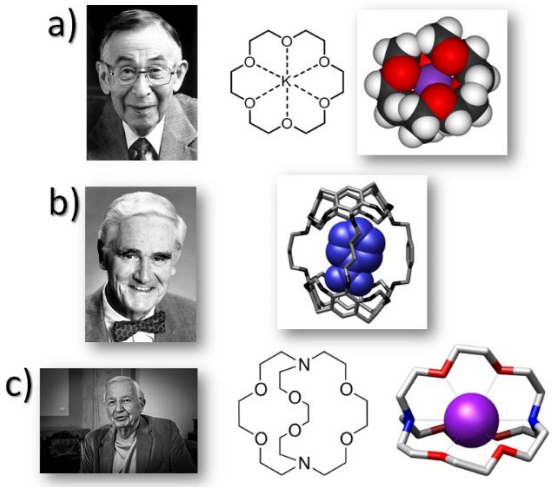

Figure 1.4 (a) Charles Pedersen alongside a K^+ bound macrocycle in both ChemDraw and crystal form. (b) Donald Cram alongside a crystal structure of a carcerand. (c) Jean-Marie Lehn alongside ChemDraw and crystal structure representations of a K^+ bound [2.2.2]-cryptand. [19]

In 1987, Jean-Marie Lehn, Donald J. Cram and Charles J. Pederson won the Nobel Prize *'for their development and use of molecules with structure specific interactions of high selectivity.'* giving rise to new applications, for example molecular sensor and storage systems.[20] Other Nobel prizes awarded in the field of supramolecular chemistry went to Harry Kroto, Richard Smalley and Robert Curl (1996) for their work of the chemistry of fullerenes[21] and more recently (2016) to Sir J. Fraser Stoddart, Jean-Pierre Sauvage and Ben L. Feringa for their pioneering work on molecular machines (Fig. 1.5).[23]

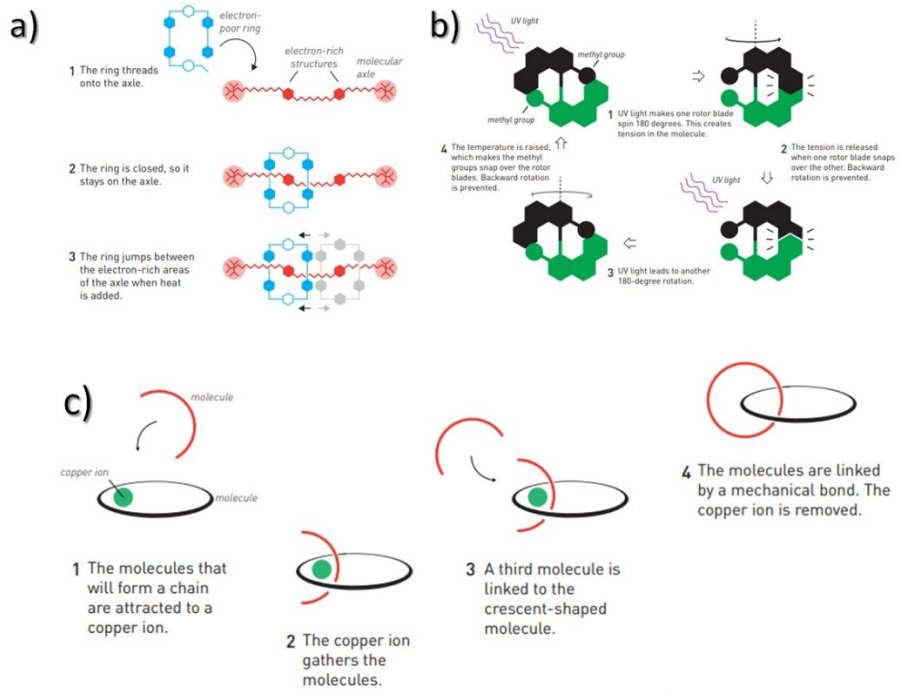

Figure 1.5 Schematics demonstrating the 2016 Chemistry Nobel prize winning work on molecular machines in the form of (a) Stoddart`s rotaxane molecular rings, (b) Feringa`s molecular motor and (c) Sauvage`s mechanically bonded cantenane molecule.[23]

Supramolecular chemistry is a fast-growing discipline due to its ability to attract wide ranging collaboration between chemists, biochemists, biologists, physicists and computational modellers to name a few.

1.3.2 Dynamic Covalent Chemistry (DCvC)

Dynamic Covalent Chemistry is a synthetic methodology that takes advantage of the reversible nature of specific covalent bonds (e.g. M-L bonds, C=N imine bonds; S-S disulfide bonds) in order to produce elaborate extended architectures of both inorganic

and organic origin. Such methods also produce much higher yields than traditional step by step bond formation synthesis. The thermodynamic component of DCvC also allows a degree of control when it comes to the formation of the new molecules and the reversibility of the method gives the option of 'undoing' (or error checking) the reaction should it not progress as expected.[24]

An excellent example of DCvC in action comes in the self-assembly of the spherical and extremely large $[Pd(II)_{24}(L)_{48}].(BF_4)_{48}$ architecture (Fig. 1.6).[25] This superstructure is commensurate in size to biological assemblies and represented an early example of emergent behaviour that could provide vital insights into the formation of complex biological structures.

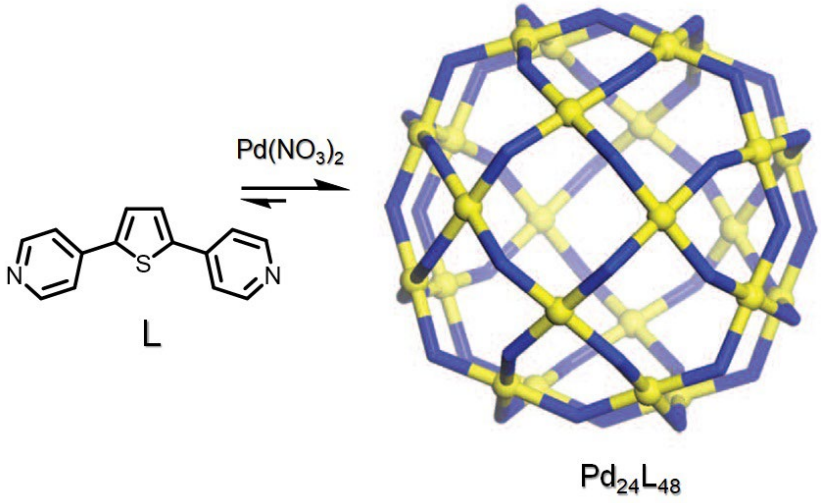

Figure 1.6 Schematic showing the successful self-assembly of the multicomponent sphere $Pd_{24}L_{48}$ produced upon reaction of palladium nitrate and a bent dipyridylthiophene which was specifically chosen to provide the correct angle and subsequent spherical topology when coordination to Pd(II)). [25]

In 2017, Hsu *et al* discusses the self-sorting properties of DCvC and interestingly highlights metal-organic systems produced by Lehn.[26] A mixture of two ligands produced (**26** and **27** as numbered by the author) were introduced to Cu(I) in solution and the self-sorting resulted in two distinct helicates in the form of $[\mathbf{26}_2Cu_2]^{2+}$ and $[\mathbf{27}_2Cu_3]^{3+}$ (Fig. 1.7). This work showed that in this case the self-sorting forms exclusively homomeric complexes.

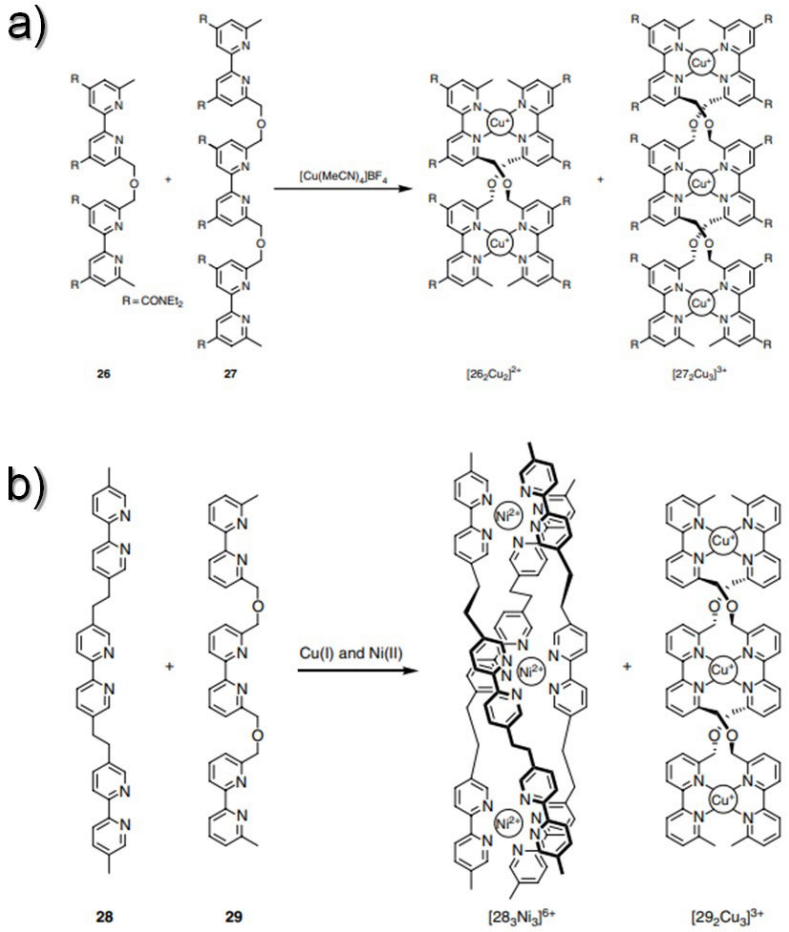

Figure 1.7 Abstract figures taken from Hsu and coworkers 2017 publication showing the self-assembly of ligands **26**, **27**, **28** and **29** when exposed to Cu(I) and Ni(II) solutions.[26]

Another example given is work emanating from the Nitschke group where they combined two dynamic reactions, an imine exchange and a ligand-metal coordination. Interestingly the reaction (between 8-aminoquinoline, 1,10-phenantholine-2,9-dicarbaldehyde, and copper(I)) took place in aqueous solution, even though imines are quickly hydrolysed in water. However, it was convincingly proposed that transition metal binding stabilised both the Cu(I) oxidation state and imine bonds to give the helicate complex [**30**$_2$Cu(I)$_3$]$\cdot$(BF$_4$)$_3$ as shown below in quantitative yield (Fig. 1.8).[27]

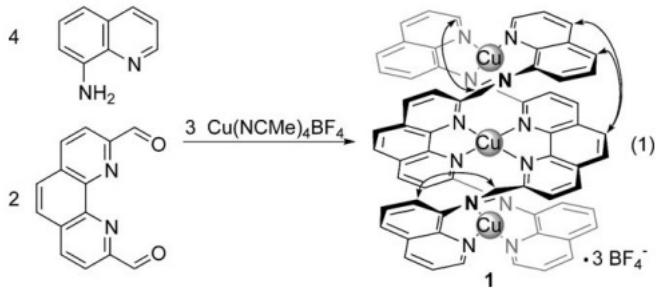

Figure 1.8 ChemDraw schematic illustrating the quantitative formation of a Cu(I) helicate $[30_2Cu(I)_3]\cdot(BF_4)_3$.[27]

1.3.3 Supramolecular chemistry in nature

Supramolecular systems exist in nature in vast numbers, and it could be said that supramolecular research is the pursuit in mimicking nature. For example, Valinomycin is found in cells around the body and is responsible for facilitating the movement of potassium ions through lipid membranes.[28] Valinomycin is a dodecadepsipeptide which is formed when twelve alternating amino acids and esters bond together to form a macrocyclic molecule (Fig. 1.9). These molecules are formed in such a way as to be as highly selective to potassium ions as opposed to sodium ions (that are found as electrolytes within the body and are transported using intramolecular forces).[29] Such systems provide inspiration for supramolecular chemistry, as these types of compounds requires not only organic but also inorganic chemistry. This type of chemistry allows for ligands to be predesigned to exhibit certain properties.[30] The properties of these biological systems are also of interest to various scientists as they can be used as sensors for cations, anions and photo-active molecules.[31]

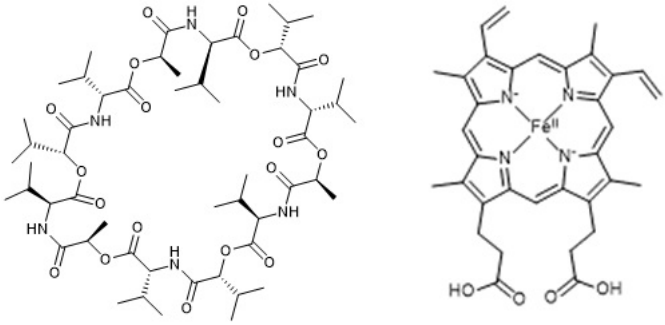

Figure 1.9 ChemDraw representations of the structures of valinomycin (right) and a Fe(II) coordinated heme molecule (right).

Another biological system that supramolecular chemists take inspiration from are heme molecules present in haemoglobin and myoglobin.[32] These molecules are porphyrin-based complexes that accommodate iron ion at their centre, thus allowing the heme molecule to bind to oxygen.[33] Porphyrins are an important class of chelating agents in biological systems and are a basis for a lot of current supramolecular research as they contain four or more nitrogen atoms that act as electron pair donors allowing easy binding to metals in the centre.

1.3.4 Host-Guest Chemistry

Although not the first concept people would think of when discussing supramolecular chemistry, host-guest chemistry is based upon three historical concepts better known in biology by the lock and key analogy:[19]

1. *'The recognition that molecules do not act if they do not bind' (Paul Ehrlich in 1906).*[34]

2. *'That binging must be selective, in which the guest has a geometric size or shape complementary to the receptor molecule'* (Emil Fischer in 1894)[35]

Fischer produced the lock and key image still used to this day to show how a host can be selective to one guest even when in the presence of several different guest molecules.

3. *'Selective binding must involve attraction or mutual affinity between host and guest molecules'* (Alfred Werner 1893).[36]

Therefore, host-guest chemistry in its simplest form refers to when a smaller molecule of the right size binds non-covalently to a cavity in a larger host molecule (Figure 1.10). These host molecules can be anything from enzymes[37] to synthetic cyclic molecules[38] if they possess a sizable central hole or cavity which contain convergent binding sites such as Lewis basic donor atoms or hydrogen bond donors etc. The guest molecules can be anything from a simple organic molecule or inorganic anion to a larger molecule such as a hormone or pheromone, they again would just need to contain a binding site such as a Lewis acidic metal cation or a hydrogen bond acceptor etc. Once bound together these host-guest systems produce a supramolecule which exist in both the liquid and the solid state, an example of such a system is polyoxovanadates (POVs).[39]

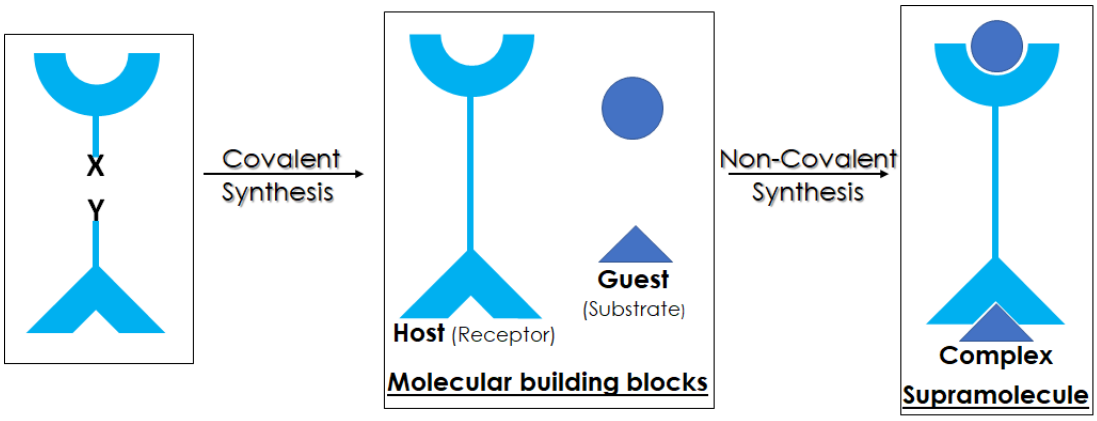

Figure 1.10 Simplified depiction of the formation of a supramolecule. Where X and Y can be any number of functional groups used to form covalent bonds. This figure has been adapted from Supramolecular chemistry textbook by Jonathan W. Steed & Jerry L. Atwood.

Of course, these host-guest systems are not just as easy as picking a host and guest molecule, a general rule of thumb was outlined by Rebek where he found that for optimum binding within a host-guest system the guest should fill 55% ± 9% of the cavity void.[40] Guest molecules too large would result in sterical hindrance stopping them from being contained within the cavity while smaller guest molecules would not be large enough to take advantage of the convergent binging sites. Although there are examples were multiple small guest molecules can be encapsulated in a host molecule in the solid state.[41]

1.3.4.1 Host-Guest Binding

Host-guest systems are held together by non-covalent bonds; this encompasses numerous types of bonding some of such bonding types will be described below with their relative bond energies and examples of supramolecular systems using such bonds.

Table 1.1 Examples of non-covalent interactions observed in nature and the scientific literature.

Non-covalent interaction and typical strength	Example
Ion-Ion interactions (100-350 kJ mol^{-1})	• The strongest type of noncovalent bond. • Best known example is the NaCl cubic lattice.
Ion-dipole interactions (50-200 kJ mol^{-1})	• Occurs when an ion bonds with a polar molecule. • Common examples are crown ethers.
Dipole-dipole interactions (5-50 kJ mol^{-1})	• *Type 1)* dipole interacts with on dipole on the adjacent molecule. *Type 2)* A pair of dipoles interact with a pair of dipoles on the adjacent molecule. • HCl···HCl; *etc*
Hydrogen bonding (4-120 kJ mol^{-1})	• Type of dipole-dipole interaction, hydrogen atom attached to an electron withdrawing group is attracted to a neighbouring dipole on a adjacent molecule. HF---HF *etc* • Responsible for the overall shape of a double helix observed in DNA. (Figure 1.3); Structure of water (e.g. porous nature of ice).
π-π Stacking (0-50 kJ mol^{-1})	• Weak electrostatic attractions occurring between aromatic rings. Two types, face to face and edge to face. • Face to face example observed in graphite layering. • Edge to face example observed in benzene packed into herringbone structures.
Van der Waals forces (< 5 kJ mol^{-1})	• Weak electrostatic attraction caused by polarisation of an electron cloud, due to its proximity to adjacent nucleus.

	• Example is the interaction between toluene as a guest molecule in p-tert-butylcalix[4]arene.
Hydrophobic effects	• Although not a force, it relates to the exclusion from a polar solvent. • Most common example is mineral oil in water causing the oil to form droplets. • Another example is the binding of organic guests to hosts such as cyclodextrins and cyclophane.
Close packing in the solid state	• Very few structures exhibit empty spaces in solid state. Complexes favour topologies that have maximum number of interactions, adopting structures that sometimes intertwin to achieve this state.

1.4 Calixarenes: Hosts for a myriad of guests

Calix[*n*]arenes (*n* = 1, 2, 3, 4, 5, 6, 8) are a group of compounds best described as cyclic arrays of phenolic moieties linked by methylene groups (e.g. p-*tert*-butylcalix-[4]arene in Figure. 1.11). This calix[4]arene can form four different conformations: *cone*, *partial cone*, *1,3-alternate* and *1,2-alternate*. [42] The cone conformer is the most common due to stabilisation by the hydrogen bonding between the phenolic OH groups.[43] When the lower rim is deprotonated it can bind alkali metal cations and is even capable of transporting them through model membrane systems.[44] An example of this is the tetraester complex of p-*tert*-butylcalix-[4]arene which has been shown using UV spectroscopy to be highly selective to sodium cations over any other group 1 cations.[45]

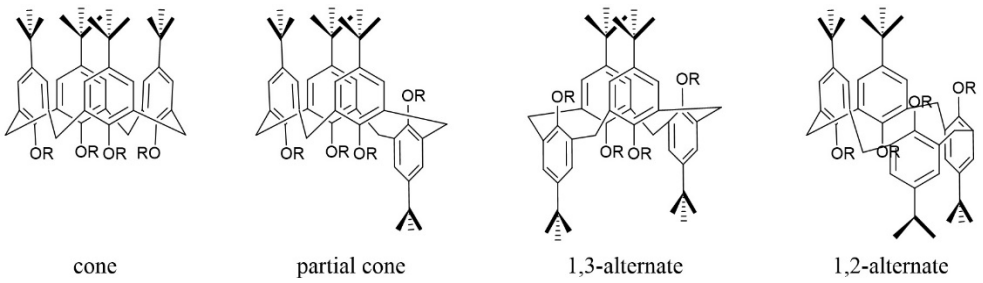

Figure 1.11 The four possible conformations observed by the calix[4]arene para-*tert*-butylcalix-[4]arene.

1.4.1. Metallocalix[n]arenes: Calix[n]arenes as ligands in metal complexation

The transition metalation of calix[n]arene moieties was first realised in 1985 by Power and co-workers when they showed that reaction of $Ti(NMe_2)_4$ and p-*tert*-butylcalix[4]areneH_4 produced the dimeric complex [{Ti(IV)(p-*tert*-butylcalix[4]arene)}$_2$]·6PhMe.[46] Furthermore, Co and Fe analogues were also produced and discussed in the same publication. These findings forged a new research avenue that continues to provide interesting materials employed in such areas as molecular magnetism, magnetic cooling and catalysis.[47] For instance, in the late 2000s, the collaboration between Brechin and Dalgarno began to produce a plethora of 3d and 3d-4f calix[n]arene complexes. For instance, 2008 saw the publication of the magnetic coolant complex $[Mn(III)_2Mn(II)_2(OH)_2(TBC4)_2(DMF)_6]$, constructed with p-*tert*-butylcalix[4]arene and exhibiting a $-\Delta S_m$ value of 19.0 J Kg^{-1} K^{-1} at 4 K.[48]

In a paper published in 2017, Dalgarno and co-workers discuss the production of a new family of bis-calix[4]arene supported 3d-4f metal clusters which included the complexes $[Cu(II)_4Tb(III)_5(bis\text{-}C[4])_2(\mu_3\text{-}OMe)(\mu\text{-}OMe)(\mu_3\text{-}OH)(\mu_4\text{-}NO_3)(\mu_5\text{-}NO_3)(MeOH)(DMF)_6(H_2O)_4]\cdot(OH)_2(DMF)_6(H_2O)$, $[Fe(III)_5Gd(III)(C[4])_2(\mu_4\text{-}O)_2(\mu_3\text{-}O)_2(\mu_3\text{-}NO_3)_2(DMF)_8(H_2O)_6](OH)$ and $[Mn(III)_4Gd(III)4(bis\text{-}C[4])_2(\mu_3\text{-}OH)_4(\mu\text{-}CO_3)_2(DMF)_8(H_2O)_4](MeOH)(DMF)$ (where p-tBu-calix[4]arene and calix[4]arene = TBC4 and C4, respectively) (Fig. 1.12).Variable temperature magnetic susceptibility studies on all three complexes indicated the presence of competing ferro- and antiferromagnetic exchange.[49] More recently (2020), Dalgarno *et al* described the formation of the first example of a heterometallic triangle containing Mn centres in the trivalent and bivalent states. This partial cubane structure represented one of only a few examples where Mn(III) was observed *within* a metallocalixarene structure. Due to the steric constraints of the structure the complex has an unoccupied pocket at the lower rim which is very unusual.

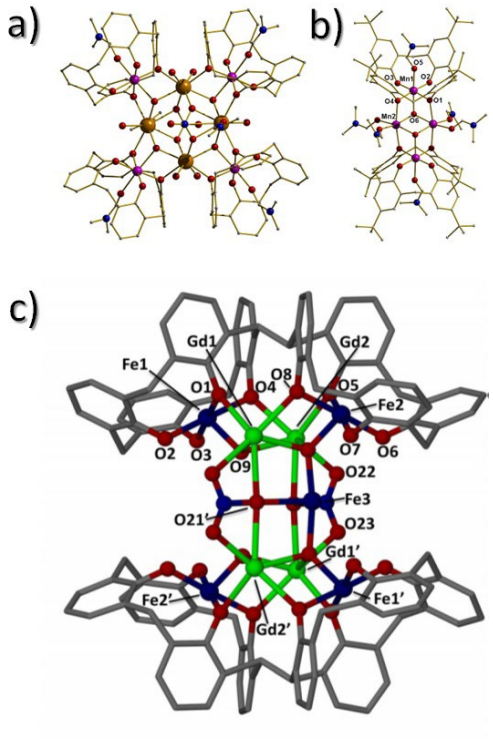

Figure 1.12 Crystal structures of the calix[4]arene bound complexes (a) $[Mn(III)_4Gd(III)_4(OH)_4(C4)_4(NO_3)_2(DMF)_6(H_2O)_6](OH)_2$, (b) $[Mn(III)_2Mn(II)_2(OH)_2(TBC4)_2(DMF)_6]$ and (c) $[Fe(III)_5Gd(III)(C[4])_2(\mu_4\text{-}O)_2(\mu_3\text{-}O)_2(\mu_3\text{-}NO_3)_2(DMF)_8(H_2O)_6](OH)$ (where p-tBu-calix[4]arene and calix[4]arene = TBC4 and C4, respectively).[48,50,51]

1.4.2 *Pseudo* metallocalix[n]arenes

In 2010, the Jones group published the complex $[Ni(II)_7(OH)_6(L_1)](NO_3)_2$ (L_1H = 2-Methoxy-6-[(E)-(methylimino)methyl]phenol) which was described as a *pseudo* metallocalix[6]arene.[52] The inorganic core comprises a planar body centred hexagon motif connected by bridging μ_3-OH^-. The outer Ni(II) ions are further connected by six $\eta^1{:}\eta^2{:}\eta^1{:}\mu$-bridging L_1^- units. These functionalised phenolic ligands effectively form a double-bowl topology within this complex and gives rise to its *pseudo* metallocalix[6]arene moniker (Fig. 1.13). Since the inception of this complex, the Jones group have reported on a number of Zn(II) and Co(II/III) analogues in the form of (for example): $[(MeOH)_2{\subset}Ni(II)_7(OH)_6(L_1)](NO_3)_2$, $[(MeOH)_2{\subset}Zn(II)_7(OH)_6(L_1)](NO_3)_2$ and $[(MeOH)_2{\subset}Co(II)_7(OH)_6(L_1)](NO_3)_2$ (Fig. 1.14 and Fig. 1.15). Indeed (and as discussed below) this family of complexes formed the basis for the work described here.

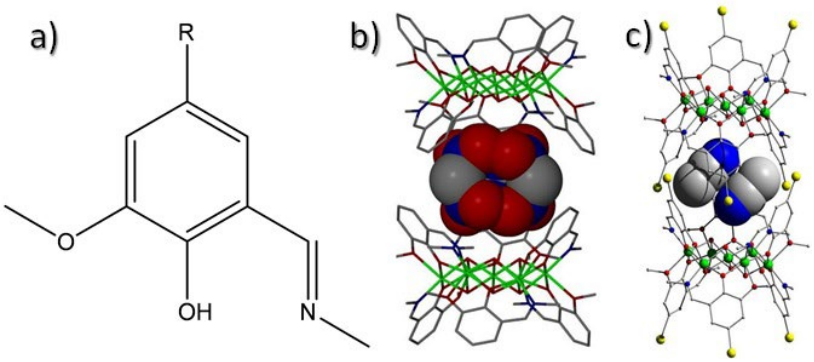

Figure 1.13 (a) ChemDraw representation of the ligands 2-Methoxy-6-[(E)-(methylimino)methyl]phenol (L_1H; when R = H) and 2-iminomethyl-4-bromo-6-methoxy-phenol (L_2H; R = Br) used in the construction of pseudo [M_7] (M = Co(II)/(III), Ni(II), Zn(II) metallocalix[6]arenes such as $[(MeNO_2)_3{\subset}Ni(II)_7(OH)_6(L_1)_6](NO_3)_2$ (b) and $[(MeCN)_2{\subset}Ni(II)_7(OH)_6(L_2)_6](NO_3)_2$ (c). The guest $MeNO_2$ and MeCN molecules are space-fill represented.[52]

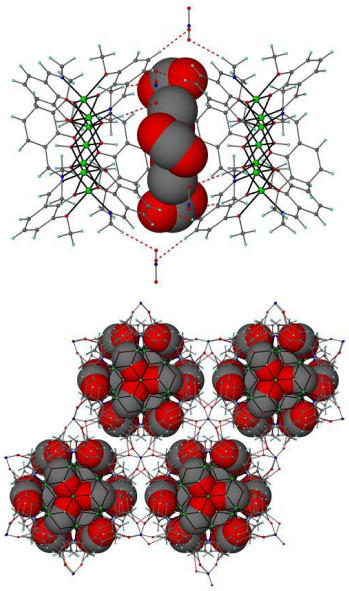

Figure 1.14 Crystal structure (top) and packing arrangement (bottom) for the *pseudo* [Ni(II)$_7$] metallocalix[6]arene $[(MeOH)_2{\subset}Ni(II)_7(OH)_6(L_1)_6](NO_3)_2$ (L_1H = 2-Methoxy-6-[(E)-(methylimino)methyl]phenol)[52]

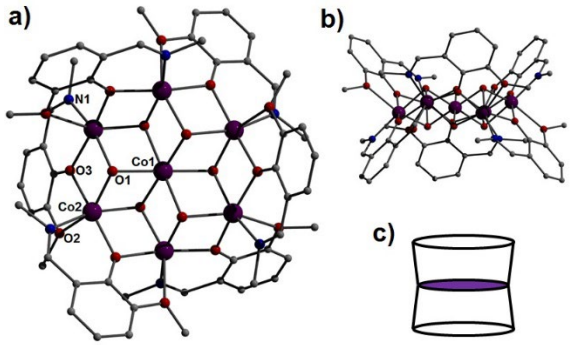

Figure 1.15 Crystal structure of the pseudo [Co(II)$_7$] metallocalix[6]arene [(MeOH)$_2$⊂Co(II)$_7$(OH)$_6$(L$_1$)$_6$](NO$_3$)$_2$ (L$_1$H = 2-Methoxy-6-[(E)-(methylimino)methyl]phenol) as viewed perpendicular (a) and parallel (b) to the {Co(III)Co(II)$_6$} core. (c) A schematic highlighting the double bowl topology formed by this complex (and its analogues).[52]

1.5 Molecular magnetism

Traditional magnets are found in many households across the world within a plethora of technologies of varying complexities ranging from the humble fridge magnets to the magnetic materials that store our information in personal computers. This ability to store information emanates from their long-range magnetic domain structure and their ability to exhibit magnetic hysteresis. In a similar vein, certain paramagnetic complexes have much more recently been shown to exhibit magnetic hysteresis on a molecular level below a certain blocking temperature (T_B) and have been coined Single-Molecule Magnets (SMMs)[53] In effect, there is a barrier to the reorientation of the magnetisation of these materials with barriers (U) commensurate to S^2D (S = total spin and D = zero-field splitting parameter), although Quantum Tunnelling of Magnetisation (QTM) often reduces this value when found experimentally (given as U_{eff}) (Figures 1.16 and 1.17). So what uses could we have for such phenomena? We live in a fast-growing modern society where data storage on technologies is always expected to be larger and faster than our current abilities. Future uses for SMMs could include ultra-high density data storage among other possible applications such as magnetic optical switches, quantum computation, MRI contrast agents and molecular spintronics.[54,55,56]

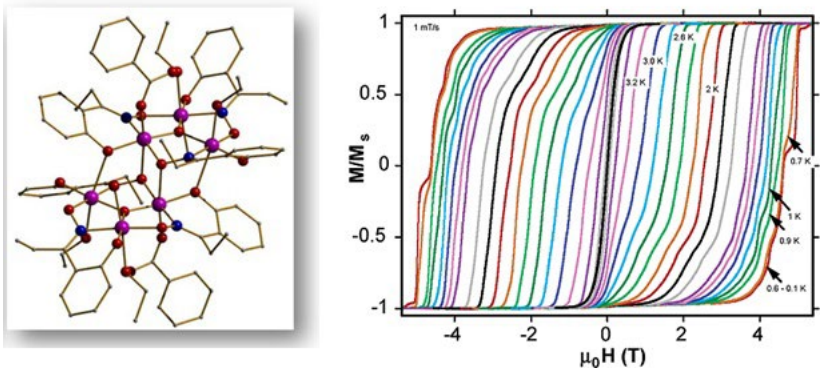

Figure 1.16 Magnetic hysteresis loops at various temperatures (ranging from 1.8 to 4.2 K) obtained from a single crystal of the SMM $[Mn(III)_6(O)_2(Et\text{-}sao)_6(L)_2(EtOH)_2]$ (Et-saoH$_2$ = Ethyl salicyaldoxime; L = 3,5-dimethylbenzoic acid) (left).[57]

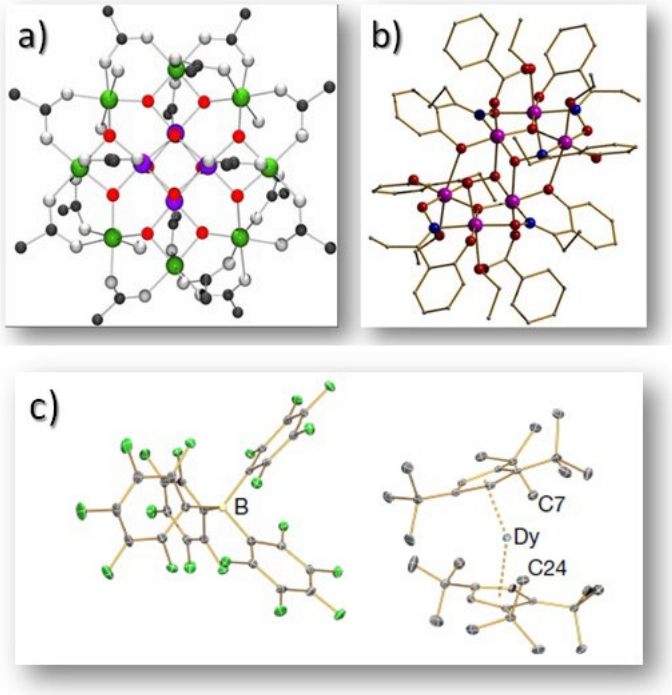

Figure 1.17 Crystal structures of the high performance SMMs (a) $[Mn_{12}O_{12}(OAc)_{16}(H_2O)_4]$ (U_{eff} = 42 cm^{-1}; T_B = 3 K)[58], (b) $[Mn(III)_6(O)_2(Et\text{-}sao)_6(L)_2(EtOH)_2]$ (Et-saoH$_2$ = Ethyl salicyaldoxime; L = 3,5-dimethylbenzoic acid) (U_{eff} = 86.4 cm^{-1}; T_B = 4.5 K)[57] and (c) $[Dy(Cp^{ttt})_2][B(C_6F_5)_4]$ (U_{eff} = 1,223 cm^{-1} and T_B = 60 K).[60]

1.5.1 Fundamentals of molecular magnetic behaviour

Before we discuss SMMs in more detail, we should outline the basics of magnetic behaviour. All magnetic materials have one thing in common in that they are made up of paramagnetic metal ions (e.g. Fe(II) and Fe(III) in magnetite ($Fe(III)_2Fe(III)O_4$) and therefore have unpaired electrons. Each unpaired electron has an inherent magnetic moment (μ) emanating from its spin and is quantified by its spin quantum number, S. From this the magnetic moment for any paramagnetic metal centre can be determined using the spin-only formula (Equation 1) given below:

$$\textit{Equation 1} \qquad \mu = \sqrt{[n(n+2)]} \qquad \textbf{\textit{or}} \qquad \mu = 2\sqrt{[S(S+1)]}$$

-where μ is magnetic moment, n is number of unpaired electrons and S is the spin quantum number of the metal ion.

1.5.2 Magnetic ordering classifications

There are five different classifications of magnetic behaviour with respect to how they respond to an external magnetic field as a function of temperature (Fig. 1.19). These are *diamagnetism*, *paramagnetism*, *ferromagnetism*, *antiferromagnetism* and *ferrimagnetism* and are described below.

Diamagnetism

Diamagnetic materials have no net magnetic moment due to the material having a full electron shell, therefore diamagnetism is a property of all materials. In the presence of a magnetic field diamagnetic materials give a negative susceptibility reading as they repel the magnetic field and is why they appear lighter in a magnetic field.

Paramagnetism

This property occurs when metal ions have unpaired electrons resulting in a magnetic moment. These magnetic moments can represent as spins, as each unpaired electron has a spin of ½. Paramagnetic materials are disordered without the application of a magnetic field, but when a magnetic field is applied the moments align with the field. Therefore, like diamagnetism, the net magnetisation of paramagnetic materials is zero without the field. In the presence of the magnetic field the material will display positive susceptibility and will appear heavier in weight. The efficiency of the field in aligning

the magnetic moments is temperature dependent and this is known as the Curie Law. At normal temperature and in a moderate magnetic field the paramagnetic susceptibility is small but still greater than its diamagnetic contribution. However, under a very high magnetic field or at very low temperature the material will possess a high susceptibility (Fig. 1.18a).

Ferromagnetism

Ferromagnetism is when the individual magnetic moments align in a parallel fashion, thus giving them a directional magnetic moment. This magnetic ordering occurs below the Curie temperature (T_c) and will become randomised when the temperature is raised above T_c and paramagnetic in nature (Fig. 1.18b).

Antiferromagnetism

Antiferromagnetic ordering is observed when individual magnetic moments align in opposite directions and effectively cancel each other out to give no net magnetisation. The temperature at which such ordering occurs is the Néel temperature (T_N) (Fig. 1.18c).

Ferrimagnetism

This type of magnetism occurs in materials comprising metal ions with differing magnetic moments. More specifically, when these unequal individual magnetic moments aligned in opposite (antiferromagnetic) directions a net directional magnetisation persists. A good example of such ordering is observed between the Fe(III) and Fe(II) ions in magnetite ($Fe(III)_2Fe(II)O_4$) and is the reason for its significant magnetic behaviour (Fig. 1.18d).[60]

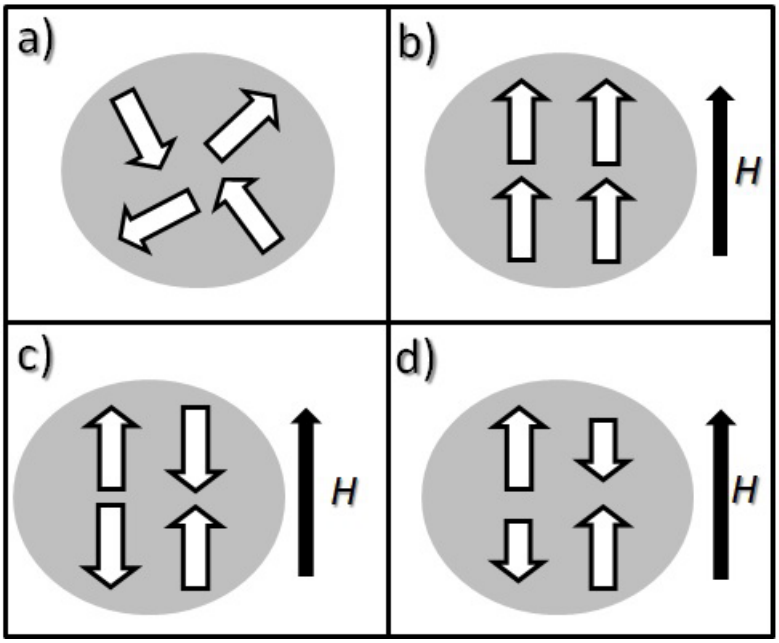

Figure 1.18 Schematic showing (a) paramagnetic, (b) ferromagnetic, (c) antiferromagnetic and (d) ferrimagnetic interactions (where H = external magnetic field). Each arrow represents a single magnetic moment emanating from a paramagnetic metal centre.

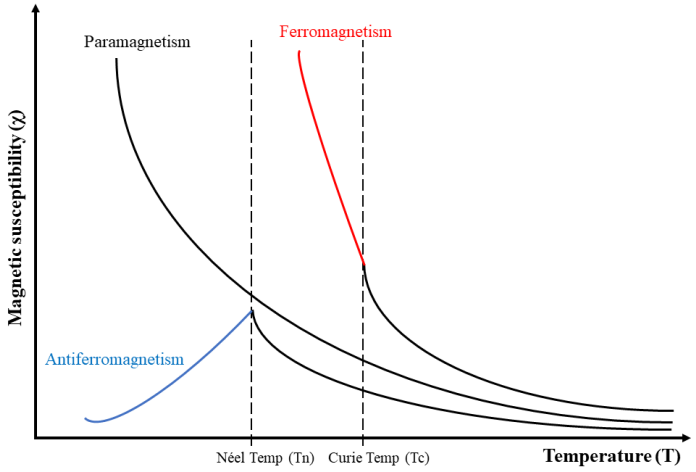

Figure 1.19 A schematic highlighting the temperature effects on magnetic susceptibility (χ) for different types of magnetic materials as a function of temperature. The antiferromagnetic (T_N) and ferromagnetic ordering (Tc) temperatures are also shown.

1.5.3 Linking magnetic behaviour to molecular structure

The spin only formula described in Equation 1 is regularly employed by magneto-chemists to assess sample purity and this is done by comparing experimental and theoretical room temperature magnetic susceptibility measurements. This endeavour takes advantage of the fundamental and vital link between molecular and electronic structure; together playing a vital role in the development of molecular and solid-state chemistry and physics. An excellent early example of this connection was highlighted by Bleaney and Bowers in 1952.[61] A previous report by Guha and co-workers described how the magnetic susceptibility of copper acetate decreased rapidly with lowering temperature and was heading to a value of zero at approx. 50 K (Fig. 1.20).[62] These findings piqued the interest of Bleaney and Bowers, who after conducting Electron Paramagnetic Resonance (EPR) studies on copper acetate, deduced that the material was not monomeric (as first assumed), but in fact dimeric in nature (later confirmed using single crystal X-ray diffraction) and its magnetic susceptibility behaviour was consistent with antiferromagnetic exchange between the juxtaposed Cu(II) centres.

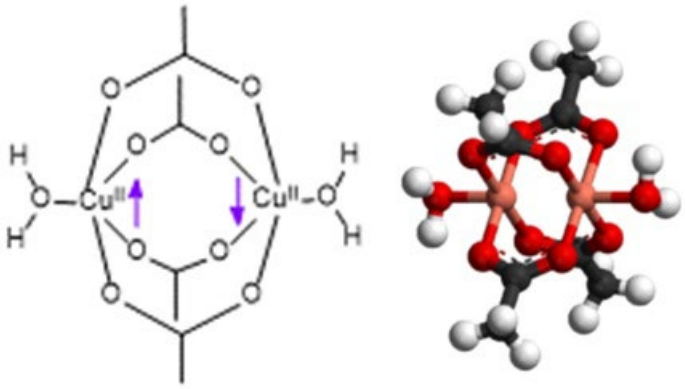

Figure 1.20 Schematic (left) and crystal structure (right) of the complex copper acetate ($[Cu(II)_2(OAc)_4(H_2O)_2]$). The arrows represent the antiferromagnetic exchange observed using electron paramagnetic resonance studies and magnetic susceptibility data.

1.6 Project aims and objectives.

The project described in this thesis focused on two related areas of research, both of which centred on extrapolating upon the coordination and host-guest chemistry of the previously reported family of heptanuclear *pseudo* $[M_7]$ (M = Co(II)/(III), Ni(II) and Zn(II)) metallocalix[6]arene complexes (as introduced in Section 1.4.2), first

discovered by the Jones group.[52] The two major aims of this project are described below:

1.6.1 Research area 1

This work focused on attempts to replace guest solvate molecules normally encapsulated within the molecular cavities of *pseudo* [M_7] metallocalix[6]arenes (e.g. $MeNO_2$ guest units in Figure 1.21 below) with larger more complex organic moieties towards producing new host-guest materials. These studies were aimed at testing the tolerances of this family of *pseudo* [$M(II)_7$] (M = Co, Ni and Zn) metallocalix[6]arenes in terms of their hosting abilities when confronted with various guests of varying shapes, sizes and topologies.

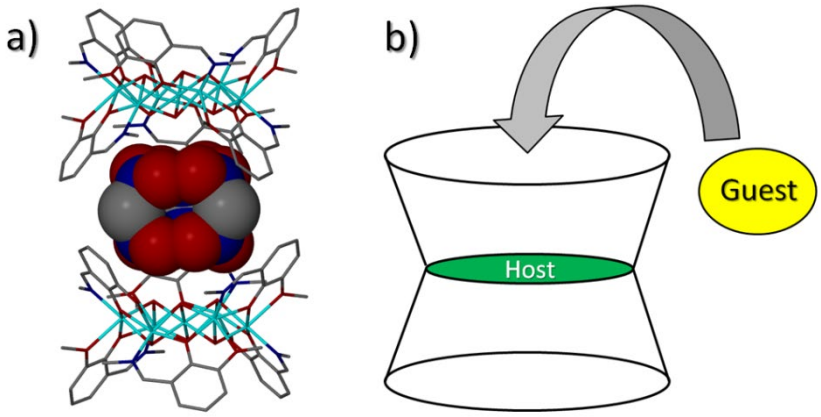

Figure 1.21 (Left) Space-fill represented $MeNO_2$ guests encapsulated within the molecular cavity formed by two *pseudo* $[(MeNO_2)_3 \subset Zn(II)_7(OH)_6(L_1)_6](NO_3)_2$ (L_1H = 2-Methoxy-6-[(E)-(methylimino)methyl]phenol) metallocalix[6]arenes in the solid state. (Right) Schematic cartoon highlighting the encapsulation of a target guest molecule within a *pseudo* [M_7] (M = Co(II), Ni(II) and Zn(II)) metallocalix[6]arene host unit.

1.6.2 Research area 2

The second area of research aimed to modify the ligand 2-iminomethyl-6-methoxy-phenol at two disparate sections (R^1 and R^2) which we have coined the *upper rim* and *lower rim* positions (Figure 1.21). As illustrated by Figure 1.22b, the altering the *upper rim* of the ligand would transform the topology of the double-bowl motif previously observed by the *pseudo* metallocalix[6]arenes and lead to new larger molecular cavities and therefore modified host behaviour. Likewise, we also aimed to evaluate

the effect of lower rim modification in order to ascertain whether we would still produce [M(II)$_7$] (M = Co, Ni and Zn) *pseudo* metallocalix[6]arenes or produce entirely different complexes upon metal complexation. The final aim of this section of the project would investigate the metal coordinating ability of novel ligands formed by modifying 2-iminomethyl-6-methoxy-phenol at *both* the R^1 and R^2 positions. All new materials emanating from this work would then be assessed both structurally (topology analysis and host-guest assessment) and physically (e.g., magnetic behaviour; photo-physical behaviour).

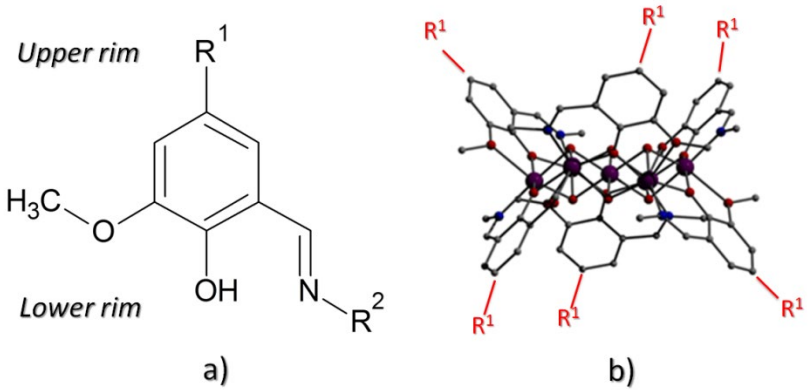

Figure 1.22 (a) Chemsketch of a phenolic ligand used in the construction of *pseudo* [M_7] (M = Co(II), Ni(II) and Zn(II)) metallocalix[6]arenes that will be modified at positions R^1 (*upper rim*) and / or R^2 (*lower rim*). Modifications at the R^1 position would be expected to extend the double bowl topology observed by such *pseudo* metallocalix[6]arenes (b). We also aim to functionalise at the R^2 position to investigate their subsequent metal complexation.

1.7 References

1. G. B. Kauffman, *Bull. Hist. Chem*. 20 (1997).

2. N. P. E. Barry and P. J. Sadler, *Pure Appl. Chem*. 2014, **86(12)**, 1897–1910.

3. J. M. Harrowfield , M. I. Ogden, B. W. Skelton, A. H. White, *C. R. Chimie.* 2005, **8**, 121–128.

4. O. Santoro, M. R. J. Elsegood, S. J. Teat, T. Yamato and C. Redshaw, *RSC Advances*., 2021, **11**, 11304.

5. W.-L. Leong and J. J. Vittal, *New J. Chem*., 2010, **34**, 2145–2152.

6. P. P. Cholewa and S. J. Dalgarno, *CrystEngComm*, 2014, **16**, 3655.

7. H. Ding, R. Chen, and C. Wang, Ch 4: *Organic Cages through Dynamic Covalent Reactions*. Dynamic Covalent Chemistry: Principles, Reactions and Application. (Wiley Publishers) 2017, 165-205.

8. L. Y. Martin, L. J. DeHayes, L. J. Zompa, and D. H. Busch, *J. Am. Chem. Soc*. 1974, **96(12)**, 4046–4048.

9. Proc. Natl. Acad. Sci. U.S.A.,L. Pauling and R. E. Marsh, PNAS, 1952, **38(2)**, 112-118.

10. W.-D. Jang, K. M. Kamruzzaman Selim, C.-H. Lee, I.-K. Kang, *Progress in Polymer Science.* 2009, **34(1)**, 1-23.

11. P. Yang, M. Elcheikh Mahmoud, Y. Xiang, Z. Lin, X. Ma, J. H. Christian, J. K. Bindra, J. S. Kinyon, Y. Zhao, C. Chen, T. Nisar, V. Wagner, N. S. Dalal and U. Kortz, *Inorg. Chem.* 2022, **61**, 18524–18535.

12. C. Fonseca Guerra, F. M. Bickelhaupt, J. G. Snijders and E. Jan Baerends, *J. Am. Chem. Soc.* 2000, **122(17)**, 4117–4128.

13. U.S. National Library of Medicine, discovery of the double helix. Website: https://profiles.nlm.nih.gov/spotlight/sc/feature/doublehelix

14. R. Gheorghe, G. A. Ionita, C. Maxim, A. Caneschi, L. Sorace, M. Andruh. *Polyhedron* 2019, **171**, 269–278.

15. M. M. Blight and N. F. Curtis, *J. Chem. Soc.,* 1962, 1204-1207.

16. D. H. Busch and S. C. Cummings. *Inorg. Chem.* 1971, **10(6)**, 1220–1224.

17. E.-G. Jager, J. Knaudt, M. Rudolph, and M. Rost. *Chem. Berichte.* 1996, **129(9)**, 981-1142.

18. G. Filomeni, G. Cerchiaro, A. M. Da Costa Ferreira, A. De Martino, J. Z. Pedersen, G. Rotilio, and M. R. Ciriolo. *J. Biol. Chem*., 2007, **282(16)**, 12010 –1202.

19. J. W. Steed and J. L. Atwood. *Supramolecular Chemistry* (Wiley Publishers). 3rd Edition.

20. R. M. Izatta. *Chem. Soc. Rev*., 2007, **36**, 143-147.

21. R. F. Curl and R. E. Smalley, *Scientific American.* 1991, **265(4)**, 54-63.

22. J. C. Barnesa and C. A. Mirkin. PNAS, 2017, 114(4), 620-625.

23.https://www.nobelprize.org/prizes/chemistry/2016/press-release/(25/09/2023 16:26)

24. Y. Jin, C. Yu, R. Denman, W. Zhang, *Chem. Soc. Rev.*, 2013, **42**, 6634-6654.

25. Q. Sun, J. Iwasa, D. Ogawa, Y. Ishido, S. Sato, T. Ozeki, Y. Sei, K. Yamaguchi, M. Fujita, *Science.* 2010, **328**, 1144-1147.

26. C. Hsu and O. Miljanić. Ch 6: *Self Sorting through Dynamic Covalent Chemistry*. Dynamic Covalent Chemistry: Principles, Reactions and Application. (Wiley Publishers) 2017, 253-286.

27. M. Hutin, R. Frantz and J. Nitschke, *Chem. Eur. J.* 2006, **12**, 4077–4082.

28. Ehud. Eyal and G. A. Rechnitz, *J. Anal. Chem*. 1971, **43(8)**, 1090-1093.

29. S. Varma, D. Sabo and S. B. Rempe. *J. Mol. Biol.*, 2008, **376(1)**, 13-22.

30. Q.-D. Hu, G.-P. Tang and P. K. Chu, *Acc. Chem. Res*. 2014, **47(7)**, 2017-2025.

31. S.-H. Zhang, R.-X. Zhao, G. Li, H.-Y. Zhang, C.-L. Zhang and G. Muller, *RSC Advances*. 2014, **4**, 54837-54846.

32. J. P. Collman and L. Fu, *Acc. Chem. Res.* 1999, **32(6)**, 455–463.

33. Q. Gibson. *J. Biol. Chem.* 1970, **245(13)**, 3285-3288.

34. K. Strebhardt and A. Ullrich. *Nat Rev Cancer*. 2008, **8**, 473-480.

35. J. Damborsky, J. Brezovsky. *Current Opinion in Chemical Biology*. 2009, **13(1)**, 26-34.

36. N. P. E. Barry and P. J. Sadler. *Pure and Applied Chemistry*. 2014, **86(12)**, 1897-1910.

37. M. Sayed and H. Pal. *Phys. Chem. Chem. Phys.*, 2021, **23**, 26085-26107.

38. C. Redshaw. *Coord. Chem. Rev*. 2003, **244**, 45-70.

39. M. Aureliano, N. I. Gumerova, G. Sciortino, E. Garribba, A. Rompel and D. C. Crans. *Coord. Chem. Rev*. 2021, **447**, 214143.

40. S. Mecozzi and J. Rebek, Jr. *Chem. Eur. J.* 1998, 4(6), 0947-6539.

41. F. Hof, S. Craig, C. Nuckolls and J. Rebek, Jr. *Angew. Chem. Int. Ed.* 2002, **41**, 1488-1508.

42. L. Wilson, M. Coletta, M. Singh, S. Teat, A. Brookfield, M. Shanmugam, E. J. L. M. McInnes, S. Piligkos, S. J. Dalgarno and E. K. Brechin, *Dalton Trans.*, 2023, **52**, 8956.

43. G. Crini, *Chem. Rev.* 2014, **114**, 10940−10975.

44. T. Jin, M. Kinjo, T. Koyama, Y. Kobayashi and H. Hirata, *Langmuir* 1996, **12(11)**, 2684–2689.

45. L. Baklouti, R. Abidi, J. Vicens, Z. Asfari, J. Harrowfield and R. Rokbani. *Journal of Inclusion Phenomena*. 2002, **42**, 197-201.

46. M. Olmstead, G Sigel, H Hope, X Xu and P. Power, *J. Am. Chem. Soc.* 1985, **107**, 8087-8091.

47. C. Redshaw, *Dalton Trans.*, 2016, **45**, 9018-9030.

48. G. Karotsis, M. Evangelisti, S. J. Dalgarno and E. K. Brechin, *Angew. Chem. Int. Ed.,* 2009, **48,** 9928-9931.

49. M. Coletta, R. McLellan, S. Sanz, K. Gagnon, S. Teat, E. K. Brechin and S. J. Dalgarno, *Chem. Eur. J.* 2017, **23**, 14073-14079.

50. G. Karotsis, S. Teat, W. Wernsdorfer, S. Piligkos, S. Dalgarno and E. K. Brechin. *Angew. Chem. Int. Ed*., 2009, **48**, 8285-8288.

51. M. Coletta, R. McLellan, S. Sanz, K. Gagnon, S. Teat, E. K. Brechin and S. J. Dalgarno. *Chem. Eur. J.* 2017, **23**, 14073-14079.

52. S. T. Meally, G. Karotsis, E. K. Brechin, G. S. Papaefstathiou, P. W. Dunne, P. McArdle and L. F. Jones. *CrystEngComm.,* 2010, **12**, 59.

53. A. Caneschi, D. Gatteschi and R. Sessoli, *J. Am. Chem. Soc.* 1991, **113**, 5873-5874.

54. A. Zabala-Lekuona and J. Seco, E. Colacio, *Coord. Chem. Rev*. 2021, **441**, 213984.

55. F. Guo, B. Day, Y. Chen, M. Tong, A. Mansikkamäki and R. Layfield. *Angew. Chem. Int. Ed.,* 2017, **56**, 11445-11449.

56. C. Gould, K. Randall McClain, J. Yu, T. Groshens, F. Furche, B. Harvey and J. Long, *J. Am. Chem. Soc.* 2019, **141(33)**, 12967-12973.

57. C. Milios, A. Vinslava, W. Wernsdorfer, S. Moggach, S. Parsons, S. Perlepes, G. Christou, and E. K. Brechin, *J. Am. Chem. Soc*., 2007, **129(10)**, 2754–2755.

58. R. Sessoli, H. Tsai, A. Schake, S. Wang, J. Vincent, K Foiling, D. Gatteschi, G. Christou and D. N. Hendrickson, *J. Am. Chem. Soc.* 1993, **115**, 1804-1816.

59. C. Goodwin, F. Ortu, D. Reta, N. Chilton and D. Mills, *Nature*, 2017, **548**, 442.

60. V. L. Mazzocchi and C. B. R. Parente. *J. Appl. Cryst.* 1998, **31**, 718-725

61. B. Bleaney and K. D. Bowers. *Proc Roy. Soc. A*. 1952, 451-465.

62. B. Guha. Proceedings of the Royal Society of London. Series A, Mathematical and Physical Sciences, 1951, **206(1086)**, 353–373.

Chapter 2:

Providing new guests to heptanuclear $[M(II)_7]$ (M = Co, Ni, Zn) pseudo metallocalix[6]arenes

2. Introduction

2.1 Overview

There is currently a wholly justifiable clamour for the premeditated introduction of pores, channels and/or cavities within both inorganic and organic materials due to their potential applications in fields such as catalysis (where cavities represent nano-reactors),[1] molecular storage[2] and separation.[3] Discrete assemblies with the propensity to possess such structural properties include self-assembled coordination cages (a.k.a. molecular flasks)[4] and porous organic cages (POCs),[5] while Covalent Organic Frameworks (COFs)[6] and the more established Metal-Organic Frameworks (MOFs)[7] represent exemplar porous extended network materials. With these thoughts in mind, previous work by the Jones group detailed the synthesis of a family of heptanuclear *pseudo* [M_7] (M = Co(II), Ni(II), Zn(II)) metallocalix[6]arenes of general formula $[M(II)_7(\mu_3\text{-}OH)_6(L_1)_6](NO_3)_2$ (L_1H = 2-Methoxy-6-[(E)-(methylimino)methyl]phenol**)**. In this work each sibling was shown to accommodate guest solvent molecules within their self-assembled H-bonded molecular cavities as shown in Scheme 2.1 (centre). Building upon these initial findings, we set out to test the tolerances of our *pseudo* metallocalix[6]arene hosts with respect to guest encapsulation. We began by screening various guest molecules. Failures included naphthalene and anthracene (selected for potentially interesting photophysics) before hitting upon smaller guest aromatics. To this end, we present in this work the successful solid-state encapsulation of six new organic guest moieties (such as 2- and 3-furaldehyde, benzaldehyde and acetophenone; Scheme 1) within our [M_7] (M = Co(II), Ni, Zn(II)) host architectures giving rise to a 16 strong family of heptametallic inclusion complexes (**1**-**16**; Table 2.1). As described in the experimental section, each inclusion complex is formed by introducing a slight excess of guest to a methanolic solution comprising the selected [$M(II)_7$] host (Host : Guest = 1 : 1.43). Despite the significant excess of MeOH, itself a guest in the previously published $[(MeOH)_2{\subset}Zn(II)_7(OH)_6(L_1)_6](NO_3)_2$ complex,[8] small organic guest encapsulation is preferred.

2.2 Results and Discussion

We present here the synthesis and full characterisation of a family of *pseudo* metallocalix[6]arene complexes of general formula: [(guest)⊂M(II)$_7$(μ_3-OR)$_6$(L_1)$_6$](NO_3)$_2$ (where guest = 2- and 3-furaldehyde, benzaldehyde, 2-thiophenecarboxaldehyde, 2-acetylfuran and acetophenone; M = Co, Ni, Zn and R = H or CH_3; L_1H = 2-Methoxy-6-[(E)-(methylimino)methyl]phenol) (see Table 2.1 for the full list). Although previous Jones group work was attempted using anthracene and naphthalene compounds with hopes to take advantage of their photochemical properties, attempts at encapsulation were unsuccessful likely due to the size of these guests being too large. In this work, aldehydes and ketones are investigated as guest molecules, due to their potential to produce radicals. Evidence of guest encapsulation has been provided using a combination of FT-IR, single-crystal and powder X-ray diffraction and solid-state NMR. Initial evidence of successful guest encapsulation was sought from FT-IR as each guest moiety (Scheme 2.1) possesses distinct νC=O stretching frequencies lying in the 1653-1676 cm^{-1} (Table 2.1 and Figures 2.1-2.4). Each host [M(II)$_7$] unit exhibits signature peaks associated with C=N imine (1625-1639 cm^{-1}) and C-H (alkyl: ~2900 cm^{-1}; aromatic: ~3000 cm^{-1}) stretches, respectively.[9] It should also be noted that the latter assignments will also comprise of contributions from the various organic guests housed within these host units. Likewise, in each spectra there are broad resonances centred around 3200-3600 cm^{-1} and are attributed to OH^- stretching frequencies associated with a combination of guest waters of crystallisation and (if present) μ_3-bridging OH^- ions.[10] Likewise, resonances observed in the 2690-2850 cm^{-1} are attributed to the presence of C-H (aldehyde) stretching vibrations belonging to guest aldehydes such as (among others) 2- and 3-furaldehyde (in complexes **1**-**6**) and benzaldehyde (in **7** and **8**).

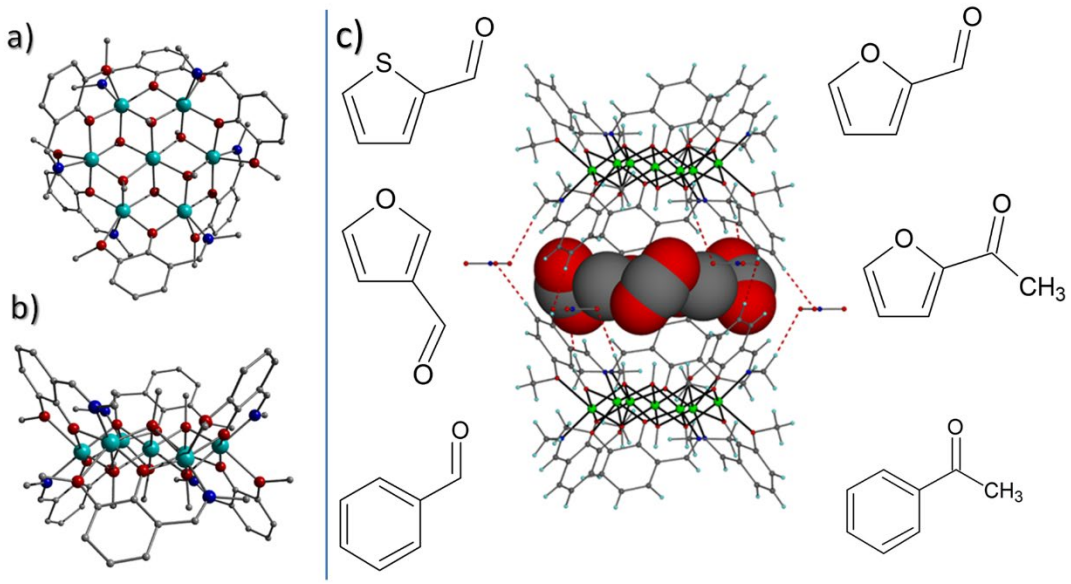

Scheme 2.1 Crystal structure of the host guest complex [(2-fur)⊂$Zn(II)_7(OMe)_6(L_1)_6$]$(NO_3)_2 \cdot 3H_2O$ (**1**) as viewed perpendicular (a) and parallel (b) to the planar body centred hexagonal core. The NO_3^- counter anions and the majority of H atoms have been omitted for clarity. Colour code: Light blue (Zn), Red (O), Blue (N), Grey (C). (c) The eight guest organic molecules used in this work: (2- and 3-furaldehyde (2-, 3-fur), benzaldehyde (bzal), 2-thiophenecarboxaldehyde (2-thio), 2-acetylfuran (2-acetylfuran) and acetophenone (acetoph). Inset: A typical host *pseudo* metallocalix[6]arene in the form of the complex [$(MeOH)_2$⊂$Ni(II)_7(OH)_6(L_1)_6$]$(NO_3)_2$ exhibiting a molecular cavity that accommodates (in this instance) MeOH guest moieties (space-fill represented).[8] Colour code: Green (Ni), Red (O), Blue (N), Grey (C), Light blue (H). Dashed lines represent H-bonding interactions.

Table 2.1 FT-IR νCO stretching frequencies obtained from the encapsulated and free-form aldehyde / ketone guest molecules compared to when encapsulated within [M_7] (M = Zn(II), Ni(II) and Co(II)) pseudo metallocalix[6]arene host materials.

Host-guest complex	**νC=O stretch (encapsulated / free form) (cm^{-1})**
[(2-fur)⊂$Zn(II)_7$] (**1**)	1667 / 1668
[(2-fur)⊂$Ni(II)_7$] (**2**)	1669 / 1668
[(2-fur)⊂$Co(II)_7$] (**3**)	1671 / 1668
[(3-fur)⊂$Zn(II)_7$] (**4**)	1676 / 1677
[(3-fur)⊂$Ni(II)_7$] (**5**)	1676/ 1677
[(3-fur)⊂$Co(II)_7$] (**6**)	1678 / 1677
[(bzal)⊂$Zn(II)_7$] (**7**)	1689 / 1697
[(bzal)⊂$Ni(II)_7$] (**8**)	1689 / 1697
[(2-thio)⊂$Zn(II)_7$] (**9**)	1653 / 1668
[(2-thio)⊂$Ni(II)_7$] (**10**)	1656 / 1668
[(2-acetylfuran)⊂[$Zn(II)_7$] (**11**)	1667 / 1671
[(2-acetylfuran)⊂[$Ni(II)_7$] (**12**)	1665 / 1671
[(2-acetylfuran)⊂[$Co(II)_7$] (**13**)	1670 / 1671
[(acetoph)⊂$Zn(II)_7$] (**14**)	1676 / 1680
[(acetoph)⊂[$Ni(II)_7$] (**15**)	1674 / 1680
[(acetoph)⊂$Co(II)_7$] (**16**)	1676 / 1680

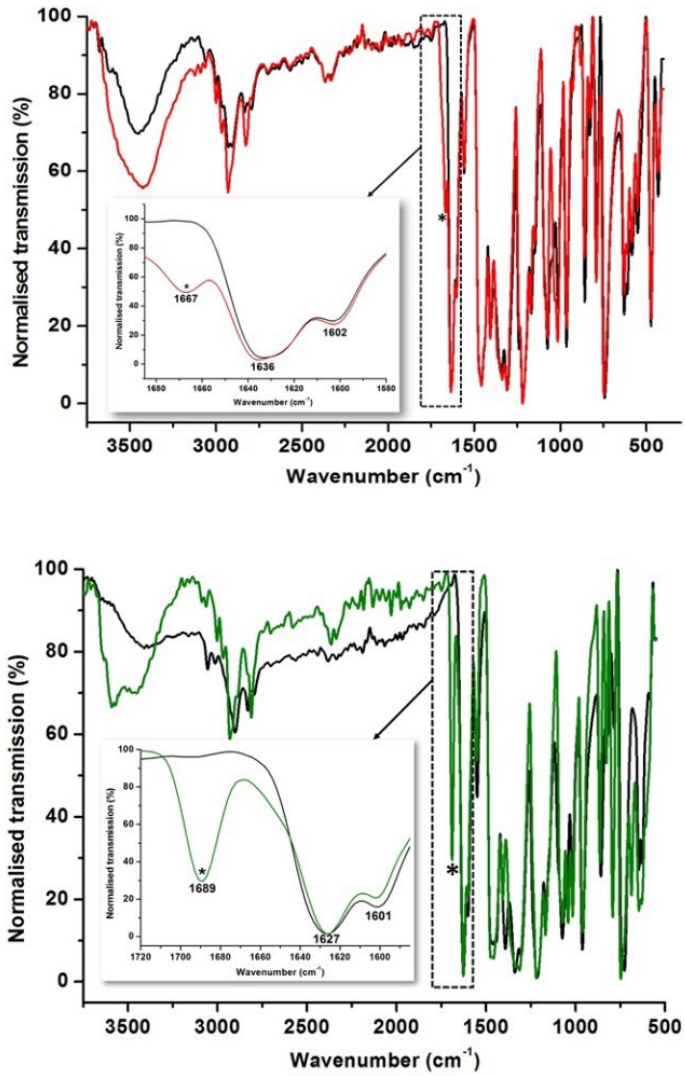

Figure 2.1 (Top) IR spectra overlay of $[(MeOH)_2 \subset Zn(II)_7(OH)_6(L_1)_6](NO_3)_2$ (black line) and the 2-furaldehyde accommodated complex $[(2\text{-fur}) \subset Zn(II)_7(OMe)_6(L_1)_6](NO_3)_2$ (**1**; red line). (Inset) Expansion of the 1720-1585 cm^{-1} region of the spectra highlighting the CO aldehyde stretch (*) of the 2-furaldehyde guests in **1**. (Bottom) IR spectra overlay of $[(MeOH)_2 \subset Ni(II)_7(OH)_6(L_1)_6](NO_3)_2$ (black line) and the benzaldehyde accommodated complex $[(bzal) \subset Ni(II)_7(OMe)_6(L_1)_6](NO_3)_2$ (**8**; green line). (Inset) Expansion of the 1720-1585 cm^{-1} region of the spectra highlighting the CO aldehyde stretch (*) of the benzaldehyde guests in **8**.

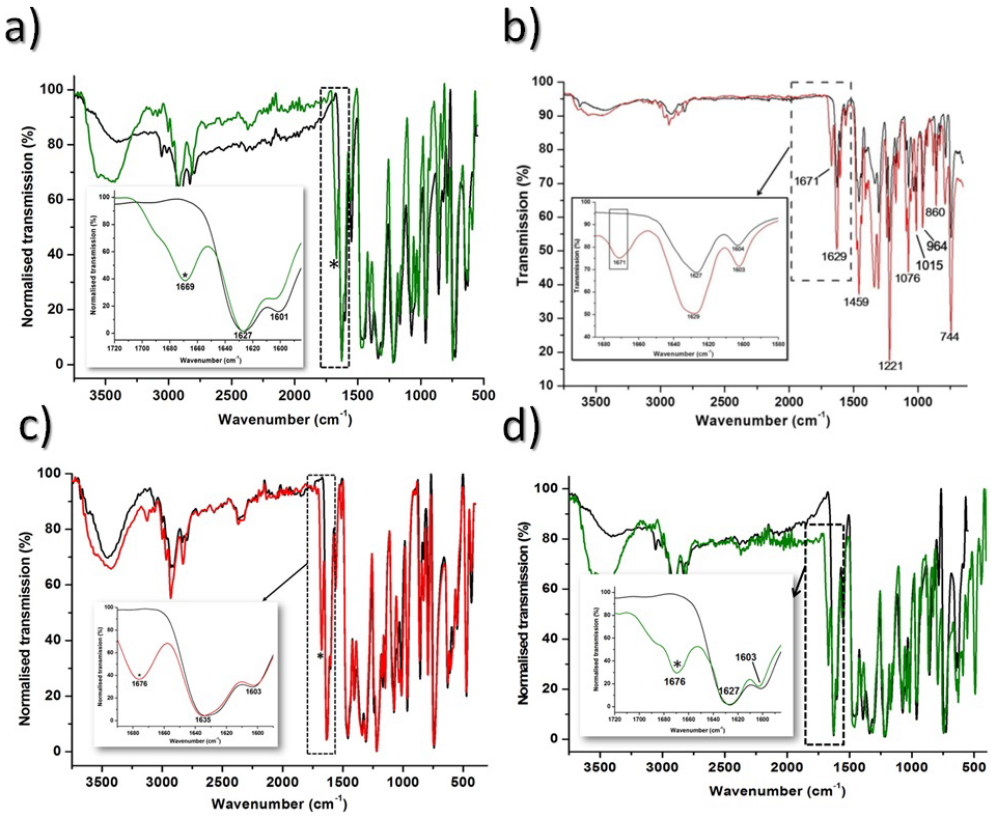

Figure 2.2 IR spectra overlay of $[(MeOH)_2 \subset Zn(II)_7(OH)_6(L_1)_6](NO_3)_2$ (black lines) and the guest accommodated complexes (a) $[(2\text{-fur}) \subset Ni(II)_7(OMe)_6(L)_6](NO_3)_2 \cdot 3H_2O$ (**2**; green line), (b) $[(2\text{-fur}) \subset Co(II)_7(OH)_6(L)_6](NO_3)_2 \cdot 3H_2O$ (**3**; red line), $[(3\text{-fur}) \subset Zn(II)_7(OMe)_6(L)_6](NO_3)_2$ (**4**; red line) and (d) $[(3\text{-fur}) \subset Ni(II)_7(OMe)_6(L)_6](NO_3)_2 \cdot 3H_2O$ (**5**; green line). The inset expansions highlight the 1720-1585 cm^{-1} region of the spectra highlighting the CO aldehyde guest stretches (*).

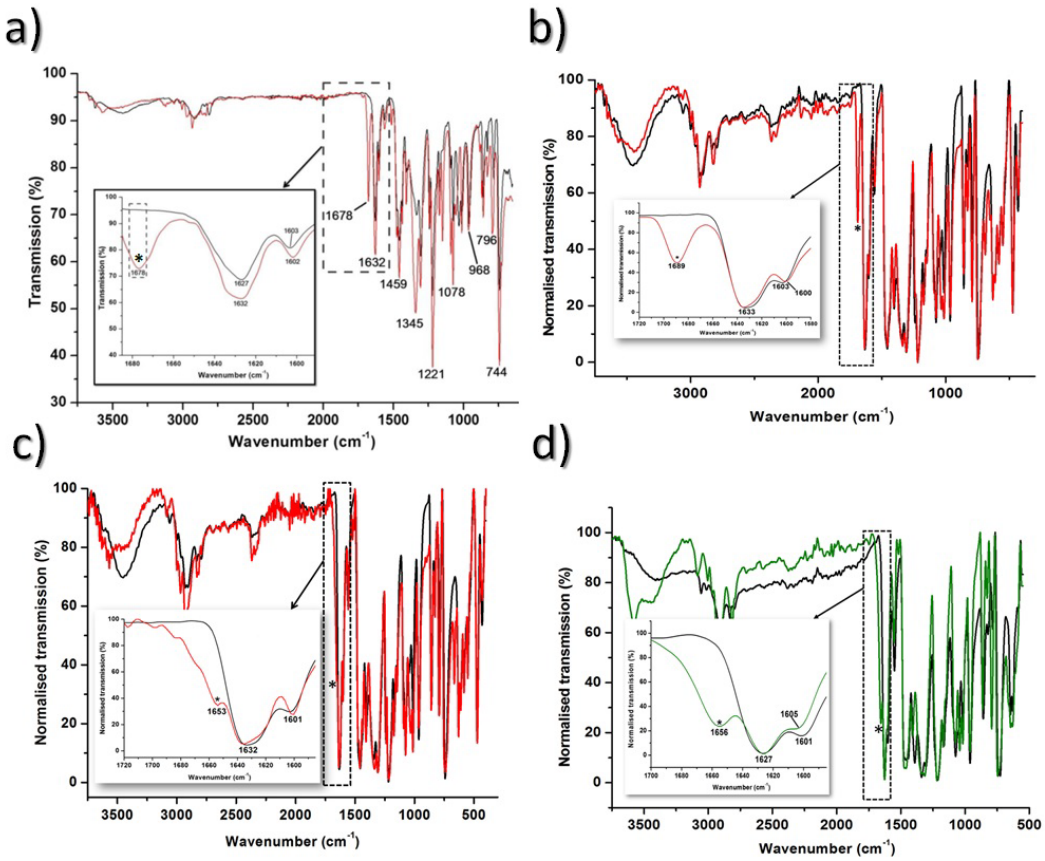

Figure 2.3 IR spectra overlay of $[(MeOH)_2 \subset Zn(II)_7(OH)_6(L_1)_6](NO_3)_2$ (black lines) and the guest accommodated complexes (a) $[(3\text{-fur}) \subset Co(II)_7(OH)_6(L)_6](NO_3)_2 \cdot 4.5H_2O$ (**6**; red line), (b) $[(bzal) \subset Zn(II)_7(OMe)_6(L)_6](NO_3)_2 \cdot 5H_2O$ (**7**; red line), (c) $[(2\text{-thio}) \subset Zn(II)_7(OH)_6(L)_6](NO_3)_2$ (**9**; red line) and (d) $[(2\text{-thio}) \subset Ni(II)_7(OH)_6(L)_6](NO_3)_2$ (**10**; green line). The inset expansions highlight the 1720-1585 cm^{-1} region of the spectra highlighting the CO aldehyde guest stretches (*).

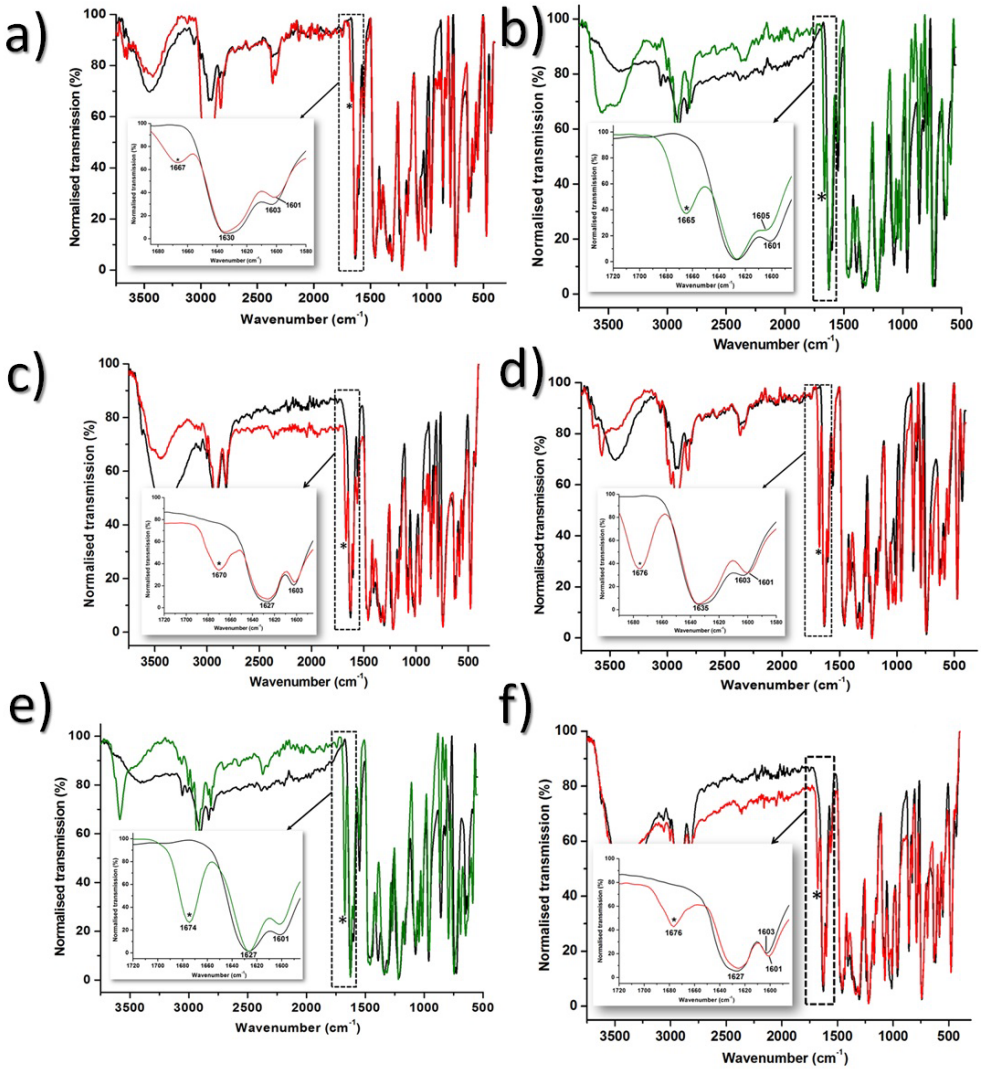

Figure 2.4 IR spectra overlay of $[(MeOH)_2 \subset Zn(II)_7(OH)_6(L_1)_6](NO_3)_2$ (black lines) and the guest accommodated complexes (a) $[(2\text{-acetylfuran}) \subset Zn(II)_7(OH)_6(L)_6](NO_3)_2$ (**11**; red line) (b) $[(2\text{-acetylfuran}) \subset Ni(II)_7(OMe)_6(L)_6](NO_3)_2 \cdot 3H_2O$ (**12**; green line) (c) $[(2\text{-acetylfuran}) \subset Co(II)_7(OMe)_6(L)_6](NO_3)_2 \cdot 7H_2O$ (**13**; red line) (d) $[(\text{acetoph}) \subset Zn(II)_7(OH)_6(L)_6](NO_3)_2$ (**14**; red line) (e) $[(\text{acetoph}) \subset Ni(II)_7(OMe)_6(L)_6](NO_3)_2$ (**15**; green line) and (f) $[(\text{acetoph}) \subset Co(II)_7(OMe)_6(L)_6](NO_3)_2 \cdot 7H_2O$ (**16**; red line). The inset expansions highlight the 1720-1585 cm^{-1} region of the spectra highlighting the CO aldehyde guest stretches (*).

2.2.1 Solid state NMR studies

In order to garner further evidence of guest incorporation, Cross-Polarisation Magic Angle Spinning (CP-MAS) solid-state ^{13}C NMR spectrum was obtained at room temperature from polycrystalline samples of $[(2\text{-fur}) \subset Zn(II)_7(OMe)_6(L_1)_6](NO_3)_2$ (**1**)

and [(bzal)⊂$Zn(II)_7(OMe)_6(L_1)_6$]$(NO_3)_2$ (**7**) (samples gave poorly resolved proton spectra). Powder X-ray diffraction measurement on complexes **1**) and **7** (as shown in Figure 2.13) provided reliability in terms of bulk purity. The spectra in Figures 2.5 and 2.6 show a range of intense resonances (45.69 – 173.70 ppm in **1** and 45.41-173.14 ppm in **7**), which are attributed to the [$Zn(II)_7$] host units. The low intensity signals below 40 and above 230 ppm are spinning sidebands associated with these host signals. The signals at 112.43, 122.07 and 177.06 ppm in **1** and 135.15 and 193.21 ppm in **7** are consistent with the presence of 2-furaldehyde and benzaldehyde guest moieties, respectively. Although there are host signals in this area the mismatch in intensity between the direct excitation (DE) and continuous phase (CP) spectra suggests guest aromatic carbons are indeed present in both cases. More specifically, in order to further differentiate host and guest signals, a second spectrum of both **1** and **7** was obtained using a short-recycle, direct excitation experiment (with background suppression). Here, differences in (carbon) relaxation behaviour should be more apparent and signals from the carbon atoms within the [$Zn(II)_7$] hosts in **1** and **7** should be under-represented relative to signals from a more mobile and rapidly relaxing 2-furaldehyde and benzaldehyde guest molecules, respectively. The overlay plots in Figure 2.5 illustrates this more clearly. To this end, three signals in **1** (112.43, 122.07 and 177.06 ppm) and two signals in **7** (135.15 and 193.21 ppm) are more intense in the DE spectrum than its CP counterpart; indicating 2-furaldehyde and benzaldehyde guest inclusion in **1** and **7**, respectively. However, these spectral lines remain broad and rules out fast isotropic tumbling of the mobile guest species, which is consistent with their encapsulated nature.

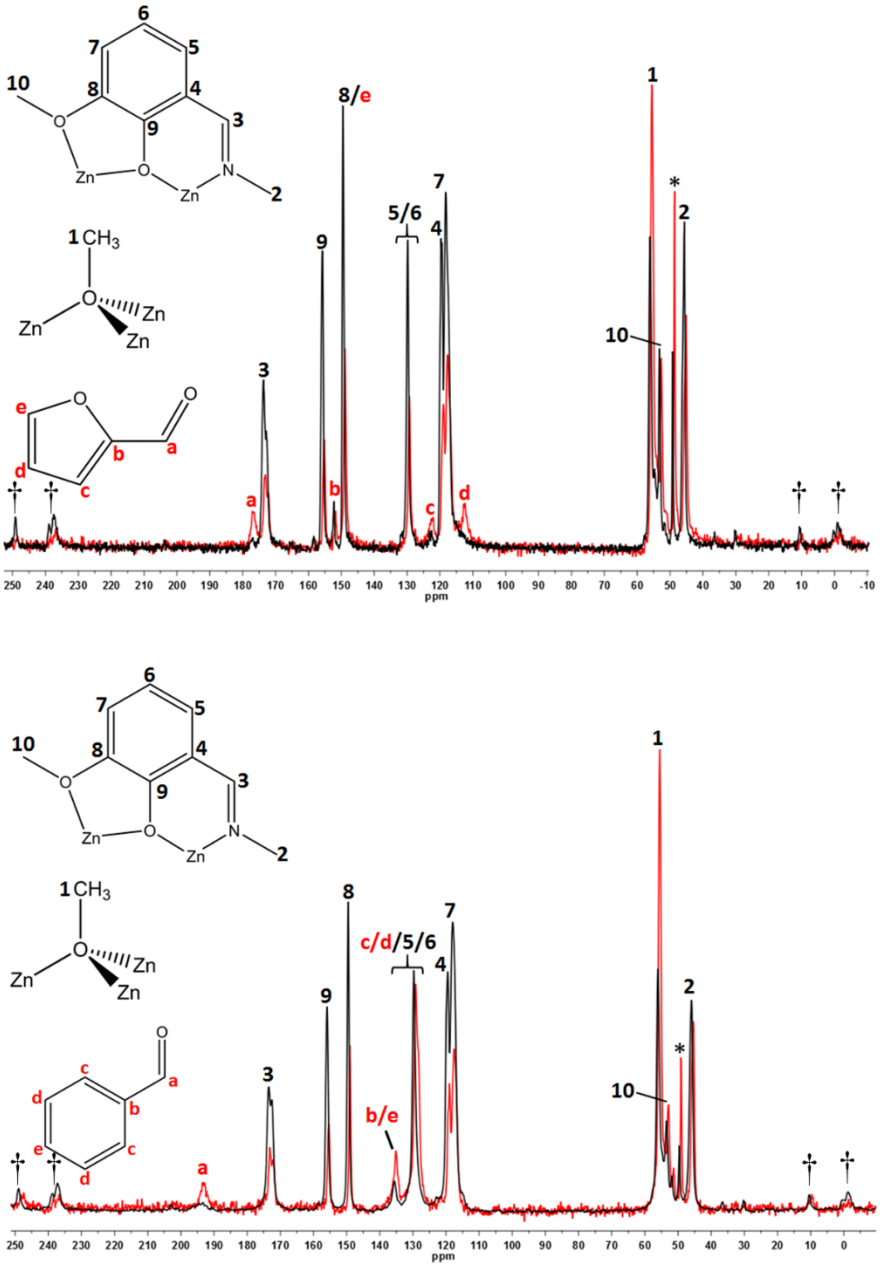

Figure 2.5 Direct overlays of the ^{13}C CP-MAS (black line) and ^{13}C CP/MAS short-recycle, direct excitation (red line) spectra from a polycrystalline sample of [(2-fur)⊂Zn(II)$_7$] (**1**; top) and [(Bzal)⊂Zn(II)$_7$] (**7**; bottom), highlighting the faster relaxation of the guest molecules when compared to the host [Zn$_7$] complex. Star (*) symbol represents trace methanol generated through exchange between bridging μ_3-OMe$^-$ bridges and encapsulated waters of crystallisation. Dagger (†) symbols represent spinning sidebands.

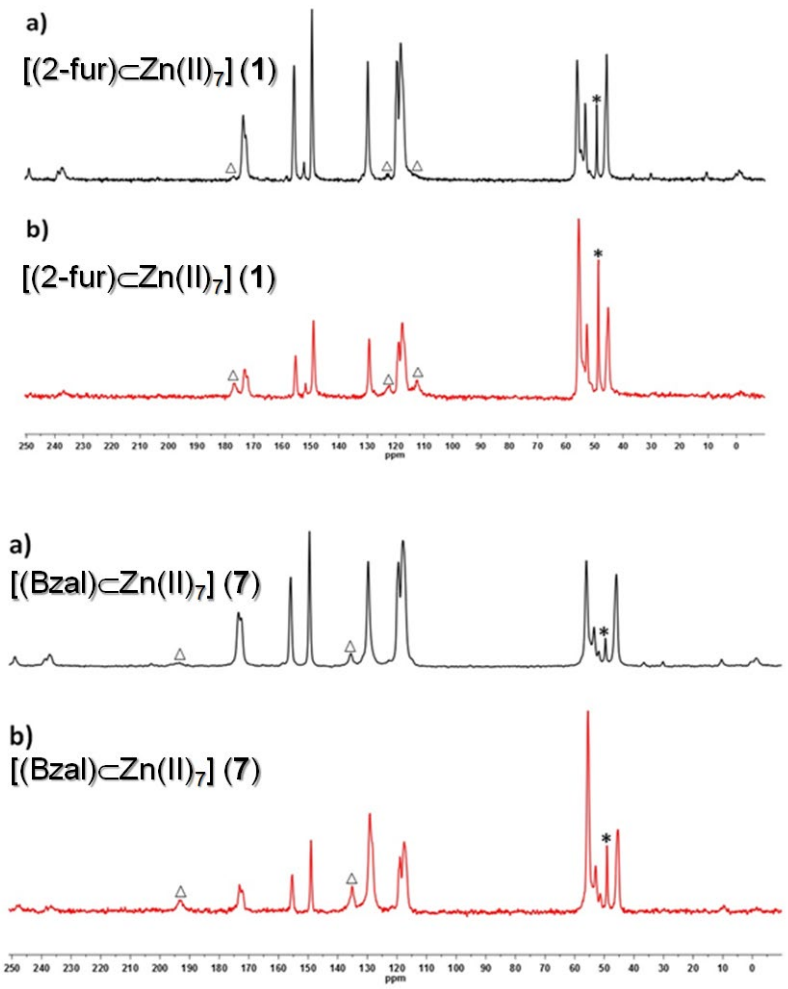

Figure 2.6 (Top) (a) Room temperature ^{13}C CP/MAS spectrum of [(2-fur)⊂Zn(II)$_7$] (**1**) recorded at a spinning speed of 12 KHz. Triangles (Δ) trace the ^{13}C signals of 2-furaldehyde guest. (b) ^{13}C CP/MAS short-recycle, direct excitation spectrum of [(2-fur)⊂Zn(II)$_7$] (**1**) recorded at a spinning speed of 12 KHz at room temperature. Star (*) symbol represents trace methanol. (Bottom) (a) Room temperature ^{13}C CP/MAS spectrum of [(Bzal)⊂Zn(II)$_7$] (**7**) recorded at a spinning speed of 12 KHz. Triangles (Δ) trace the ^{13}C signals of benzaldehyde guest. (b) ^{13}C CP/MAS short-recycle, direct excitation spectrum of [(Bzal)⊂Zn(II)$_7$] (**7**) recorded at a spinning speed of 12 KHz at room temperature. Star (*) symbol represents trace methanol.

2.2.2 X-ray diffraction studies

Single crystal X-ray diffraction data was obtained from crystalline samples of complexes **1**, **3**, **5**-**7**, **12**, **13** and **16** (for X-ray data see Tables 2.5-2.7). Close inspection of a number of crystalline samples highlights that guest encapsulation often causes a

slight colour change to the resultant inclusion complex. For instance, 2-furaldehyde encapsulation provides a yellow / orange colouration of the crystalline product of [(2-fur)⊂$Zn(II)_7(OMe)_6(L_1)_6$]$(NO_3)_2 \cdot 3H_2O$ (**1**) when compared to our previously reported *pseudo* metallocalix[6]arene [$(MeOH)_2$⊂$Zn(II)_7(OH)_6(L_1)_6$]$(NO_3)_2$ (Figure 2.4). As observed in our *pseudo* [M_7] metallocalix[6]arenes,[8,11] all sibling exhibit a disk-like heptanuclear body centred hexagonal inorganic core[12] connected by either μ_3-OH^- or μ_3-OMe^- anions and a double-bowl topology directed by the six singly deprotonated L_1^- ligands. Furthermore, the individual [$M(II)_7$] (M = Co, Ni and Zn) host units are arranged in 1D columns along the *c* unit cell directions and as a result produce the host cavities in all cases with [$M(II)_7$]···[$M(II)_7$] distances ranging from 11.35 Å (in **3**) to 11.62 Å (in **12**) and bowl dimensions (Figure 2.7) as given in Table 2.2 (for packing diagrams see Fig. 2.11). For all [$Co(II)_7$] analogues (complexes **3**, **6**, **13** and **16**), Bond Valence Sum (BVS) calculations were employed to confirm their Co(II) oxidation states (Table 2.3). Despite numerous attempts, modelling of the guest moieties within these complexes (**1**, **3**, **5**-**7**, **12**, **13** and **16**) remained futile. However, from looking at the Q-peak data on all collections, we could ascertain that all guests are indeed located within the molecular cavities (1 per cavity) and lie parallel and at the midpoint of the two juxtaposed [$M(II)_7$] planes. Moreover, each guest is disordered over three sites, lying around the three-fold axis located along the central M(II) ion and lying perpendicular to the [$M(II)_7$] plane (Fig. 2.10 and Fig. 2.12). It is worth noting that these guest positions are at (approx.) the correct distances to be able to interact with their host aromatic ligand groups presumably through C-H···π and / or π···π intermolecular interactions (Fig. 2.10). Furthermore, the positioning of these guest moieties (parallel to [M_7] planes) strongly suggests that no interactions are occurring with respect to the inner core of the host complexes and encapsulation is driven by entropic (displacement of interstitial MeOH and H_2O) and hydrophobic effects (guests sitting within hydrophobic cavity). However, we cannot rule out that guests may also partake in H-bonding interactions with interstitial waters of crystallisation.

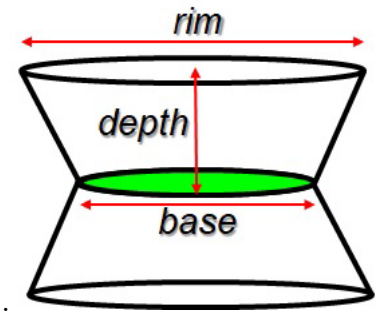

Figure 2.7 Diagram showing where the base, depth and rim dimensions as measured within the [M_7] pseudo metallocalix[6]arenes.

Table 2.2 Molecular cavity dimensions observed in the crystals of **1**, **3**, **5**-**7**, **12**, **13** and **16**.

Host-guest complex	**$[M_7]_{plane}$-$[M_7]_{plane}$ distance (Å)***	**Cavity dimensions (Å) (base × depth × rim)**
[(2-fur)⊂$Zn(II)_7$] (**1**)	11.53	6.25 × 4.88 × 13.20
[(2-fur)⊂$Co(II)_7$] (**3**)	11.35	6.27 × 4.72 × 13.47
[(3-fur)⊂$Ni(II)_7$] (**5**)	11.59	6.20 × 4.90 × 12.71
[(3-fur)⊂$Co(II)_7$] (**6**)	11.35	6.25 × 4.74 × 13.45
[(bzal)⊂$Zn(II)_7$] (**7**)	11.50	6.24 × 4.86 × 13.26
[(2-acetyl-furan)⊂$Ni(II)_7$] (**12**)	11.62	6.19 × 4.96 × 12.72
[(2-acetyl-furan)⊂[$Co(II)_7$] (**13**)	11.50	6.26 × 4.80 × 13.29
[(acetoph)⊂[$Co(II)_7$] (**16**)	11.47	6.26 × 4.72 × 13.48

***** Includes **all** voids in the crystal structure and not just molecular cavities. Each unit cell contains two solvent accessible voids and represents one void per [M_7] unit (Z = 2).

Table 2.3 Bond Valence Sum (BVS) analysis on complexes **3**, **6**, **13** and **16**.

[(2-fur)⊂Co(II)$_7$(OH)$_6$(L)$_6$](NO$_3$)$_2$·3H$_2$O (**3**)	
Atom label	***Metal oxidation state from BVS analysis***
Co1	2.01
Co2	2.09
[(3-fur)⊂Co(II)$_7$(OH)$_6$(L)$_6$](NO$_3$)$_2$·4.5H$_2$O (**6**)	
Atom label	***Metal oxidation state from BVS analysis***
Co1	*2.00*
Co2	*2.02*
[(2-acetylfuran)⊂[Co(II)$_7$(OMe)$_6$(L)$_6$](NO$_3$)$_2$·7H$_2$O (**13**)	
Atom label	***Metal oxidation state from BVS analysis***
Co1	*1.93*
Co2	*2.02*
[(acetoph)⊂[Co(II)$_7$(OMe)$_6$(L)$_6$](NO$_3$)$_2$·7H$_2$O (**16**)	
Atom label	***Metal oxidation state from BVS analysis***
Co1	*1.92*
Co2	*2.02*

To provide further corroborative evidence of successful guest encapsulation, The SQUEEZE program was employed to account for the residual electron densities within the solvent accessible molecular cavities in all host-guest complexes and used to obtain their final chemical formulae as given in Table 2.4.[13] In all nine complexes the SQUEEZE data was consistent with the presence of one guest small organic molecule per [M(II)$_7$] cage along with a number (ranging from 3 to 7) of interstitial waters of crystallisation (Table 2.4).

Table 2.4 Void and electron count values obtained from the SQUEEZE[13] analysis of single crystal data obtained for a variety of host-guest pseudo metallocalix[6]arene complexes.

Host-guest complex	Void volume per [M$_7$] cage (Å^3)*	Electron count per molecular cavity
[(2-fur)⊂Zn(II)$_7$(OMe)$_6$(L)$_6$](NO$_3$)$_2$·3H$_2$O (**1**)	403	85
[(2-fur)⊂Co(II)$_7$(OH)$_6$(L)$_6$](NO$_3$)$_2$·3H$_2$O (**3**)	477	83
[(3-fur)⊂Ni(II)$_7$(OH)$_6$(L)$_6$](NO$_3$)$_2$ ·3H$_2$O (**5**)	481	82
[(3-fur)⊂Co(II)$_7$(OH)$_6$(L)$_6$](NO$_3$)$_2$·4.5H$_2$O (**6**)	479	98
[(bzal)⊂Zn(II)$_7$(OMe)$_6$(L)$_6$](NO$_3$)$_2$·5H$_2$O (**7**)	402	114
[(2-acetylfuran)⊂[Ni(II)$_7$(OMe)$_6$(L)$_6$](NO$_3$)$_2$·3H$_2$O (**12**)	388	86
[(2-acetylfuran)⊂[Co(II)$_7$(OMe)$_6$(L)$_6$](NO$_3$)$_2$·7H$_2$O (**13**)	406	128
[(acetoph)⊂[Co(II)$_7$(OMe)$_6$(L)$_6$](NO$_3$)$_2$·7H$_2$O (**16**)	418	135

***** Includes **all** voids in the crystal structure and not just molecular cavities. Each unit cell contains two solvent accessible voids and represents one void per [M$_7$] unit (Z = 2).

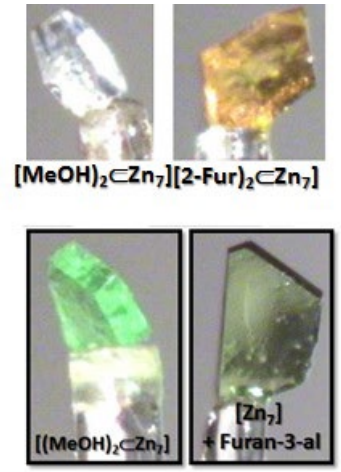

Figure 2.8 The single crystals of $[(MeOH)_2{\subset}Zn(II)_7(OH)_6(L_1)_6](NO_3)_2$ and $[(2\text{-fur}){\subset}Zn(II)_7(OH)_6(L_1)_6](NO_3)_2$ (**1**) used for their X-ray diffraction collections, highlighting the colour difference upon guest encapsulation. (Bottom) Another example of guest influence on crystal colour using the complexes $[(MeOH)_2{\subset}Ni(II)_7(OH)_6(L_1)_6](NO_3)_2$ and $[(3\text{-Fur}){\subset}Ni(II)_7(OH)_6(L_1)_6](NO_3)_2{\cdot}3H_2O$ (**5**).

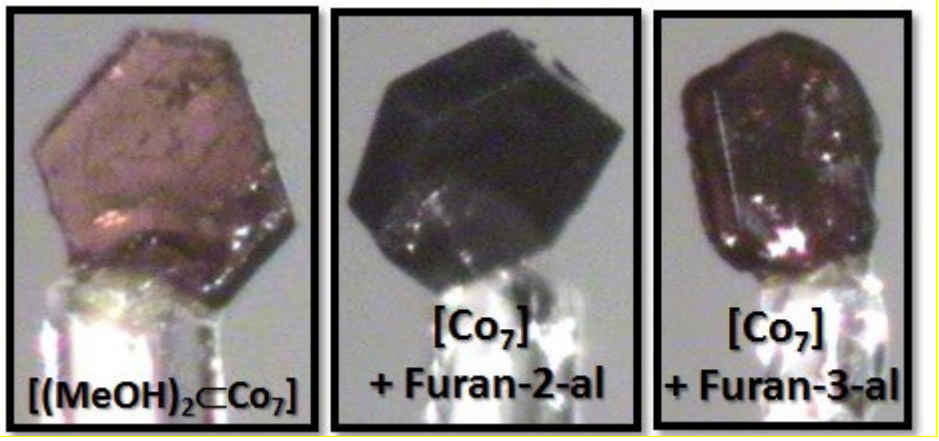

Figure 2.9 The single crystals of $[(MeOH)_2{\subset}Co(II)_7(II)_7(OH)_6(L_1)_6](NO_3)_2$, $[(2\text{-Fur}){\subset}Co(II)_7(OH)_6(L_1)_6](NO_3)_2{\cdot}3H_2O$ (**3**) and $[(3\text{-Fur}){\subset}Co(II)_7(OH)_6(L_1)_6](NO_3)_2{\cdot}4.5H_2O$ (**6**) used for their X-ray diffraction collections.

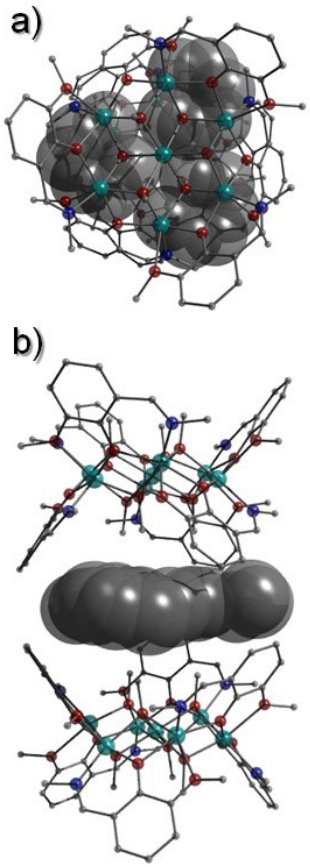

Figure 2.10 Two views of the crystal structure in $[(bzal)\subset Zn(II)_7(OMe)_6(L_1)_6](NO_3)_2{\cdot}5H_2O$ (**7**) highlighting a disordered benzaldehyde guest located parallel and at the midpoint of two juxtaposed $[Zn(II)_7]$ planes. The guest units in **7** are disordered over three sites and sit around the three-fold axis located at the central Zn(II) ion and lying perpendicular to the $[Zn(II)_7]$ plane (a). ***Note:*** Attempts at modelling the guest benzaldehyde units in **7** were fruitless and so these figures have been generated to aid guest location discussions only. Colour code: Aqua Blue (Zn), Grey (C and guest Q peaks), Dark Blue (N), Red (O). Hydrogen atoms have been omitted for clarity.

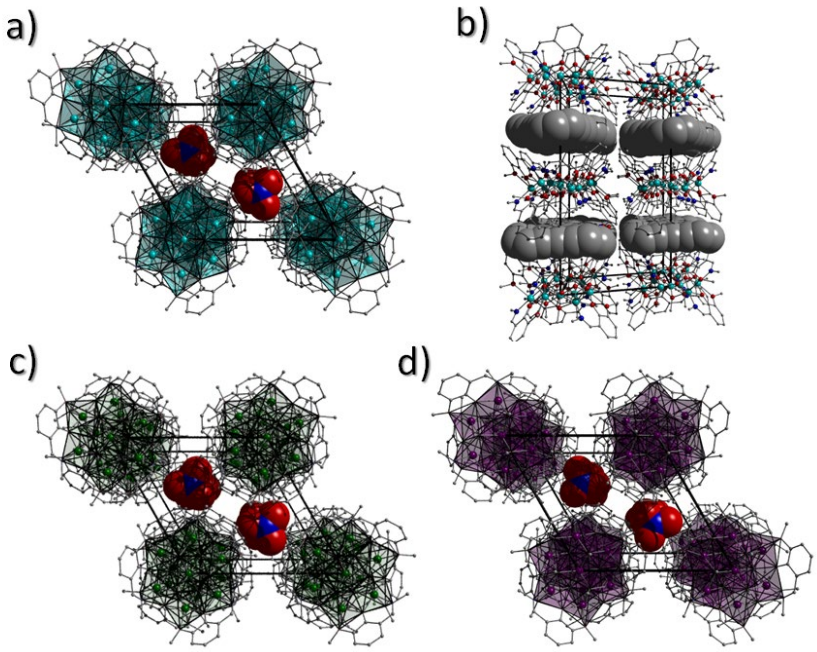

Figure 2.11 Packing arrangements observed in complexes (a) [(2-fur)⊂Zn(II)$_7$(OMe)$_6$(L$_1$)$_6$](NO$_3$)$_2$·3H$_2$O (**1**) [(bzal)⊂Zn(II)$_7$(OMe)$_6$(L$_1$)$_6$](NO$_3$)$_2$·5H$_2$O (**7**), (c) [(3-fur)⊂Ni(II)$_7$(OMe)$_6$(L$_1$)$_6$](NO$_3$)$_2$·3H$_2$O (**5**) and (d) [(2-acetylfuran)⊂Co(II)$_7$(OMe)$_6$(L$_1$)$_6$](NO$_3$)$_2$·7H$_2$O (**13**). All hydrogen atoms have been omitted for clarity. All NO_3^- counter anions are shown in space-fill mode. The grey space-fill molecules in Figure b represent the disordered benzaldehyde guests. Note that attempts at modelling the guest benzaldehyde units in **7** were fruitless and so this figure has been generated to aid guest location discussions only (as employed in Figure 2.10).

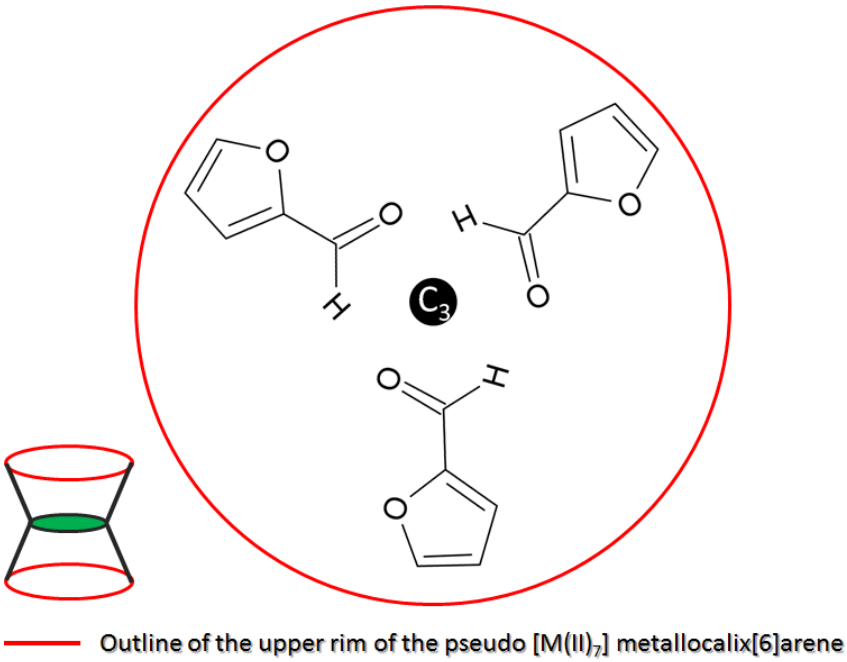

Figure 2.12 Schematic showing a guest 2-furaldehyde unit disordered over three sites related by a C_3 rotation axis lying central and perpendicular to the $\{M(II)_7\}$ plane. We propose this is the case for all inclusion complexes discussed in this chapter.

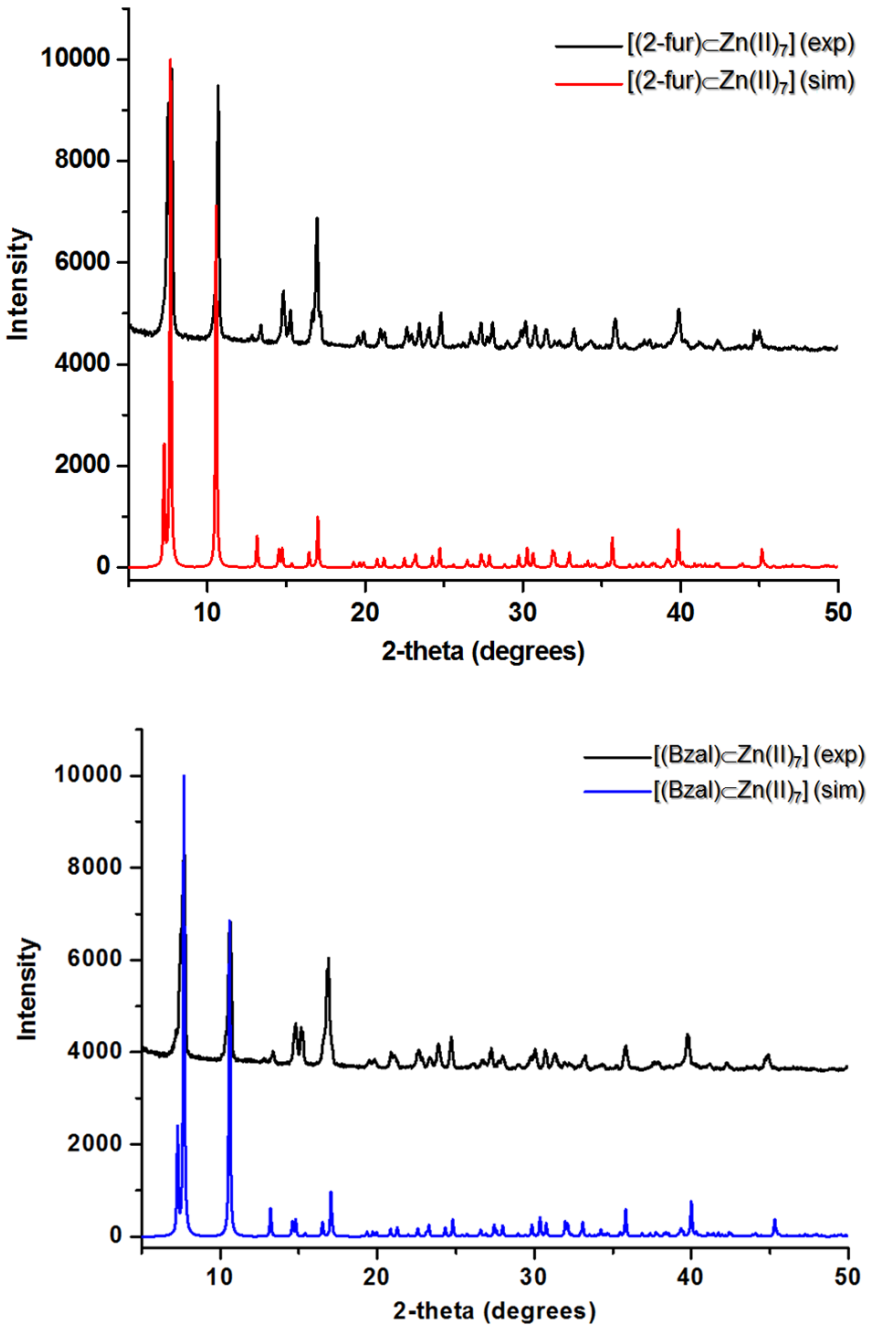

Figure 2.12 Stacked plots showing experimental and simulated powder X-ray diffraction spectra for $[(2\text{-fur})\subset Zn(II)_7(OMe)_6(L_1)_6](NO_3)_2{\cdot}3H_2O$ (**1**) (top) and $[(bzal)\subset Zn(II)_7(OMe)_6(L_1)_6](NO_3)_2{\cdot}5H_2O$ (**7**) (bottom). Simulations were performed using the Mercury program.[14]

Table 2.5 Crystallographic data[15] obtained from complexes **1, 3** and **5**.

	1·3H$_2$O	**3**·3H$_2$O	**5**·3H$_2$O
Formula[a]	$C_{65}H_{88}N_8O_{29}Zn_7$	$C_{59}H_{76}N_8O_{29}Co_7$	$C_{59}H_{76}N_8O_{29}Ni_7$
M_W	1903.08	1773.81	1772.13
Crystal System	Trigonal	Trigonal	Trigonal
Space group	P-3c1	P-3c1	P-3c1
a/Å	14.064(2)	14.100(2)	13.8183(5)
b/Å	14.064(2)	14.100(2)	13.8183(5)
c/Å	23.056(5)	22.702(5)	23.1848(14)
α/°	90	90	90
β/°	90	90	90
γ/°	120	120	120
V/Å^3	3949.3(14)	3908.7(11)	3833.9(4)
Z	2	2	2
T/K	150(2)	150(2)	150(2)
λ[b]/Å	0.71073	0.71073	0.71073
D_c/g cm^{-3}	1.474	1.380	1.405
μ(Mo-Ka)/ mm^{-1}	2.162	1.518	1.752
Meas./indep.(R_{int}) refl.	7622 / 2416 (0.0660)	2388 / 1897 (0.0409)	7199 / 2344 (0.0337)
wR2 (all data)[c]	0.1656	0.2461	0.2398
$R1$[d,e]	0.0582	0.0784	0.0793
Goodness of fit on F^2	1.055	1.149	1.125

[a] Includes guest molecules.[b] Mo-Kα radiation, graphite monochromator. [c] $wR2$= [$\Sigma w(|F_o^2| - |F_c^2|)^2$/ $\Sigma w|F_o^2|^2]^{1/2}$. [d]For observed data. [e] $R1$= $\Sigma||F_o| - |F_c||$/ $\Sigma|F_o|$.

Table 2.6 Crystallographic data obtained from complexes **6**, **7** and **12**.

	6·4.5H_2O	**7**·5H_2O	**12**·3H_2O
Formula[a]	$C_{59}H_{79}N_8O_{30.5}Co_7$	$C_{67}H_{82}N_8O_{30}Zn_7$	$C_{60}H_{78}N_8O_{24}Ni_7$
M_W	1800.83	1937.05	1870.31
Crystal System	Trigonal	Trigonal	Trigonal
Space group	P-3c1	P-3c1	P-3c1
a/Å	14.098(2)	14.010	13.811(2)
b/Å	14.098(2)	14.010	13.811(2)
c/Å	22.706(5)	23.002	23.235(2)
α/°	90	90	90
β/°	90	90	90
γ/°	120	120	120
V/Å^3	3909.5(11)	3909.9	3838.35(6)
Z	2	2	2
T/K	150(2)	173(2)	100(2)
λ[b]/Å	0.71073	0.6889	0.71073
D_c/g cm^{-3}	1.380	1.489	1.476
μ(Mo-Ka)/ mm^{-1}	1.518	2.184	1.754
Meas./indep.(R_{int}) refl.	2388 / 1561 (0.0760)	82320 / 6611 (0.0470)	66489 / 2358 (0.0330)
wR2 (all data)[c]	0.2955	0.1373	0.2240
$R1$[d,e]	0.0953	0.0416	0.0753
Goodness of fit on F^2	1.188	1.069	1.113

[a] Includes guest molecules.[b] Mo-Kα radiation, graphite monochromator. [c] $wR2= [\Sigma w(|F_o^2|- |F_c^2|)^2/ \Sigma w|F_o^2|^2]^{1/2}$. [d]For observed data. [e] $R1= \Sigma||F_o|- |F_c||/ \Sigma|F_o|$.

Table 2.7 Crystallographic data obtained from complexes **13** and **16**.

	13 $7H_2O$	**16**·$7H_2O$
Formula[a]	$C_{66}H_{98}N_8O_{33}Co_7$	$C_{62}H_{100}N_8O_{32}Co_7$
M_W	1944.05	1954.09
Crystal System	Trigonal	Trigonal
Space group	P-3c1	P-3c1
a/Å	14.053(2)	14.143(2)
b/Å	14.053(2)	14.143(2)
c/Å	23.008(2)	22.940(3)
α/°	90	90
β/°	90	90
γ/°	120	120
V/Å^3	3934.91(5)	3973.90(5)
Z	2	2
T/K	100(2)	100(2)
λ[b]/Å	1.54184	1.54184
D_c/g cm^{-3}	1.441	1.427
μ(Mo-Ka)/ mm^{-1}	11.890	11.733
Meas./indep.(R_{int}) refl.	2416/2385 (0.0355)	2439/2343 (0.0409)
wR2 (all data)[c]	0.1486	0.1658
$R1$[d,e]	0.0482	0.0594
Goodness of fit on F^2	1.122	1.110

[a] Includes guest molecules. [b] Mo-Kα radiation, graphite monochromator. [c] $wR2 = [\Sigma w(|F_o^2| - |F_c^2|)^2 / \Sigma w|F_o^2|^2]^{1/2}$. [d] For observed data. [e] $R1 = \Sigma||F_o| - |F_c|| / \Sigma|F_o|$.

2.2.3 Packing coefficient calculations

Using the OLEX2,[16] PLATON[13] and CrystalExplorer[17] programs, the molecular cavity volumes were obtained for inclusion complexes **1**, **3**, **5**-**7**, **12**, **13** and **16** with void volumes ranging from 381.2 Å^3 (in [(2-acetylfuran)⊂Ni(II)$_7$(OMe)$_6$(L$_1$)$_6$](NO$_3$)$_2$·3H$_2$O (**12**)) to 481.0 Å^3 (in [(3-fur)⊂Ni(II)$_7$(OH)$_6$(L$_1$)$_6$](NO$_3$)$_2$·3H$_2$O (**5**)). Furthermore, all guest volumes (including waters of crystallisation) were calculated using the 3V program.[18] The six guests (2- and 3-furaldehyde, benzaldehyde, 2-acetyl-furan and acetophenone) were first drawn out on the online quantum chemistry program Webmo and the optimized structures saved as PDB files, before being run through the online volume assessor program 3V, at high grid resolution (probe radius of 3). Using an average molecular cavity void volume, coupled with the guest van der Waals volume values previously calculated, packing coefficients were produced to give values ranging from 35.3% (in [(3-Fur)⊂Ni(II)$_7$(OH)$_6$(L$_1$)$_6$](NO$_3$)$_2$·3H$_2$O (**5**)) to 72.5% (in [(2-acetylfuran)⊂[Co(II)$_7$(OMe)$_6$(L$_1$)$_6$](NO$_3$)$_2$·7H$_2$O (**13**)), many of which are broadly in line with the Rebek rule (55%+0.09) (Table 2.8).[19] Deviations from this rule may be attributed to the rather splayed double bowl topologies within the host structures giving rise to significant openings to the exterior of their molecular cavities, thus not allowing precise internal molecular cavity calculations.[19] It should also be noted that packing coefficients of approximately 70% are reasonable when multiple guests are encapsulated (guest + xH$_2$O (x = 3-7) in our case).[20]

Table 2.8 Packing coefficient calculations for complexes **1**, **3**, **5-7**, **12**, **13** and **16** using software platforms OLEX2,[16] PLATON[13], Crystal Explorer,[17] and 3V.[18]

	Molecular cavity volume calculations per void*				Guest volume calculations		
Complex	**OLEX2 ($Å^3$)**	**PLATON (squeeze) ($Å^3$)**	**Crystal Explorer ($Å^3$)**	**Average cavity volume ($Å^3$)**	**Guest volume ($Å^3$)**	**Total volume of H_2O per cavity****	**Packing Coefficient (%)**
[(2-fur)⊂$Zn(II)_7$] (**1**)	391.0	403.0	433.6	409.2	100	63	39.9
[(2-Fur)⊂$Co(II)_7$] (**3**)	470.9	477.0	434.6	460.8	100	63	35.4
[(3-fur)⊂$Ni(II)_7$] (**5**)	476.0	481.0	428.2	461.7	100	63	35.3
[(3-Fur)⊂$Co(II)_7$] (**6**)	468.6	479.0	434.6	460.7	100	94.5	42.2
[(Bzal)⊂$Zn(II)_7$] (**7**)	390.3	402.0	341.8	378.0	123	105	60.3
[(2-AF)-$Ni(II)_7$] (**12**)	384.1	388.0	336.4	369.5	124	63	50.6
[(2-AF)⊂[$Co(II)_7$] (**13**)	381.2	406.0	350.3	379.2	124	147	71.5
[(Acetoph)⊂[$Co(II)_7$] (**16**)	392.1	418.0	363.0	391.0	135	147	72.1

* There are two solvent accessible voids per unit cell in all complexes.

** Calculated using SQUEEZE and a volume of 21 $Å^3$ per H_2O molecule (taken from 3V program).[17]

2.3 Concluding Remarks

This chapter demonstrates how a family of host *pseudo* [M(II)$_7$] (M = Co, Ni and Zn) metallocalix[6]arenes are able to encapsulate a range of small molecule organic guest substrates even when in competition with ubiquitous solvent molecules with a history of ingression within these polymetallic hosts. Guest encapsulation was proven using a combination of FT-IR, X-ray diffraction and solid state NMR studies. Packing coefficients were calculated for a number of family members and were found to be broadly in-line with the 55% Rebek rule. Future work from within the Jones group will entail the water solubilisation of [Zn(II)$_7$] host units towards potential NMR host-guest titration studies. This will be achieved through ligand modification in order to: *1)* achieve improved solubilisation, *2)* improve guest affinity and *3)* narrow the apertures within the rather splayed double-bowl topologies currently observed within our host metallocalix[6]arene complexes.

2.4 Experimental section

All chemicals and reagents were purchased from Sigma Aldrich (UK) or Fischer Scientific (UK), and used as supplied, without further purification. Infra-red spectra obtained from complexes **1**, **3**, **5** and **6** were recorded on a Perkin Elmer FT-IR Spectrum One spectrometer equipped with a Universal ATR Sampling accessory (NUI Galway). Spectra corresponding to complexes **2**, **4**, **7** and **8**-**16** were obtained from a Bruker Alpha FT-IR Platinum ATR spectrometer (School of Natural Sciences, Bangor University). Multi-element NMR were recorded in $CDCl_3$ or DMSO at room temperature (298K) on a Bruker Ultrashield^{TM} Plus 400, operating at 400 MHz for ^{1}H and 100 MHz for ^{13}C. All NMR were recorded using TopSpin^{TM} 3.2 software package and were analysed using MestReNova Version 11.0.2-1853. Solid state CP-MAS ^{13}C NMR spectra on **1** and **7** were obtained at room temperature on a Bruker Avance III HD spectrometer located at the Solid-State NMR facility at Durham University.

2.4.1 Collection and refinement details

*2.4.1.1 X-ray diffraction details on the collection of complexes **1**, **3**, **5**-**7**, **12**, **13** and **16**.*

Data obtained from structures of **1, 3**, **5** and **6** were collected on an Xcalibur S single crystal diffractometer (Oxford Diffraction) using an enhanced Mo source (located at NUI Galway, Ireland). Each data reduction was carried out on the CrysAlisPro software package. Complexes **12, 13** and **16** were collected on an Rigaku AFC12 goniometer equipped with an enhanced sensitivity (HG) Saturn724+ detector mounted at the window of an FR-E+ Super Bright molybdenum rotating anode generator with HF Varimax optics (100 m focus) (National Crystallographic Service, School of Chemistry, University of Southampton). The cell determination and data collection of each complex was carried out using the CrystalClear-SM Expert package (Rigaku, 2012). In an attempt to obtain better data and successfully model the encapsulated benzaldehyde guests in the complex $[(bzal)\subset Zn(II)_7(OMe)_6(L_1)_6](NO_3)_2 \cdot 5H_2O$ (**7**), a data set was collected at the Diamond Light source (I19 beamline; Didcot, Oxford, wavelength of 0.6889) using a three-circle diffractometer (custom built fixed Chi) and a Dectris Pilatus 2M detector.

Data reduction, cell refinement and absorption corrections on all complexes were carried out using CrysAlisPro software (Rigaku OD, 2015),[21] while all structures were solved and refined using SHELXT and SHELXL-2018.[22] All hydrogen atoms were placed in calculated positions and all non-hydrogen atoms were refined as anisotropic. The SQUEEZE program was employed to account for the residual electron densities within the solvent accessible molecular cavities in all host-guest complexes and used to obtain their final chemical formulae.[13]

2.4.2 Synthesis of 2-Methoxy-6-[(E)-(methylimino)methyl]phenol (L_1H)

Ortho-vanillin (5.0 g, 33.0 mmol) was dissolved in 50 cm^3 of methanol before 33% methylamine solution (4.1 cm^3, 33.0 mmol) was added. The resulting mixture was allowed to stir at room temperature for 4 hours, before a 100 cm^3 of brine solution was added. The product was then extracted using 3 x 40 cm^3 portions of $CHCl_3$. The combined extracts were dried over magnesium sulphate before being concentrated in

vacuum, the product was allowed to dry over a 24 hour period and yielded a yellow solid (yield = 98%). ^{1}H NMR (400 MHz, $CDCl_3$) δ 13.86 (s, 1H), 8.32 (d, 1H, *J* = 1.3 Hz), 6.91 (dd, 1H, *J* = 7.8, 1.4 Hz), 6.86 (dd, 1H, *J* = 7.8, 1.5 Hz), 6.79 (t, 1H, *J* = 7.8 Hz,), 3.90 (s, 3H), 3.49 (d, 3H, *J* = 1.3 Hz).^{13}C NMR (100 MHz, $CDCl_3$): δ 166.39, 152.32, 148.69, 122.81, 118.74, 117.79, 113.88, 56.21, 45.72. FT-IR (cm^{-1}): 2994 (w), 2944 (w), 2905 (w), 2838 (w), 2774 (w), 1631 (s), 1463 (s), 1438 (m), 1406 (m), 1393 (m), 1373 (m), 1335 (w), 1320 (w), 1251 (s), 1226 (s), 1188 (m), 1167 (m), 1077 (s), 1006 (m), 979 (m), 962 (s), 867 (m), 837 (m), 779 (s), 735 (s), 637 (w), 620 (m), 580 (w), 565 (w), 485 (w). ESI MS: m/z (% Rel. Ab.); 165.10 (75, $\{M\}^+$), 150.15 (100, $\{M\text{-}CH_3\}^+$), 136.22 (25, $\{M\text{-}N\text{-}CH_3\}^+$), 122.20 (15, $\{M\text{-}C_2H_7N\}^+$).

2.4.3 Preparation of complexes

All reactions were performed under aerobic conditions and all reagents and solvents were used as purchased. *Caution*: Although no problems were encountered in this work, care should be taken when manipulating the potentially explosive nitrate salts.

*2.4.3.1 Synthesis of [(2-fur)⊂Zn(II)$_7$(OMe)$_6$(L$_1$)$_6$](NO$_3$)$_2$·3H$_2$O (**1**)*

To a solution of L_1H (0.139 g, 0.84 mmol) in 30 cm^3 of methanol, NaOH (0.034 g, 0.84 mmol) and $Zn(NO_3)_2{\cdot}6H_2O$ (0.25 g, 0.84 mmol) were added. The solution was allowed to stir for 1 hour before 2-furaldehyde (0.70 cm^3, 8.4 mmol) was added and the solution stirred for a further 3 hours. The resultant solution was then allowed to settle for 30 minutes before filtration. X-ray quality crystals of **1** were obtained after 3 weeks in 17% yield. Elemental analysis (%) calculated (found) for **1**: ($C_{65}H_{88}N_8O_{29}Zn_7$): C 41.02 (41.09), H 4.66 (4.30), N 5.89 (5.85). FT-IR (cm^{-1}): 3431 (vb), 2998 (w), 2965 (w), 2929 (m), 2828 (w), 1857 (w), 1667 (m), 1639 (s), 1602 (m), 1561 (w), 1476 (s), 1461 (s), 1436 (m), 1409 (m), 1383 (s), 1340 (b/m), 1311 (s), 1241 (m), 1222 (s), 1172 (m), 1148 (w), 1093 (m), 1077 (m), 1036 (m), 1014 (m), 966 (m), 928 (w), 881 (w), 859 (w), 829 (w), 793 (m), 747 (m). Solid state ^{13}C NMR (ppm) (spinning speed = 12 KHz) (Prominent guest peaks in bold): **177.06**, 173.70, 155.75, 151.74, 149.49, 129.80, **122.07**, 119.62, 118.22, **112.43**, 56.11, 53.25, 45.69.

*2.4.3.2 Synthesis of [(2-fur)⊂Ni(II)$_7$(OH)$_6$(L$_1$)$_6$](NO$_3$)$_2$ (**2**)*

To a solution of L_1H (0.139 g, 0.84 mmol) in 30 cm^3 of methanol, NaOH (0.034 g, 0.84 mmol) and $Ni(NO_3)_2 \cdot 6H_2O$ (0.250 g, 0.84 mmol) were added. The solution was allowed to stir for 1 hour before 2-furaldehyde (0.71 cm^3, 8.4 mmol) was added and the reaction mixture stirred for a further 3 hours. The resultant solution was then filtered to give X-ray quality crystals of **2** in 20% yield over a 3 week period. Elemental analysis (%) calculated (found) for **2** ($C_{59}H_{70}N_8O_{26}Ni_7$): C 41.25 (41.56), H 4.22 (4.22), N 6.54 (6.24). FT-IR (cm^{-1}): 3411 (vb), 3122 (w), 3088 (w), 3002 (w), 2932 (m), 2815 (w), 2704 (w), 2579 (w), 2400 (w), 2036 (w), 1973 (w), 1933 (w), 1857 (w), 1669 (m), 1630 (s), 1603 (m), 1561 (m), 1552 (m), 1478 (s), 1407 (s), 1382 (s), 1354 (s), 1317 (s), 1224 (s), 1170 (m), 1149 (m), 1087 (m), 1073 (m), 1044 (m), 1018 (m), 963 (m), 928 (w), 864 (m), 829 (w), 793 (m), 748 (s), 643 (m), 627 (m), 591 (w), 555 (w), 492 (m), 438 (w), 402 (m).

*2.4.3.3 Synthesis of [(2-fur)⊂Co(II)$_7$(OH)$_6$(L$_1$)$_6$](NO$_3$)$_2$·3H$_2$O (**3**)*

A mixture of $Co(NO_3)_2.6H_2O$ (0.25 g, 0.86 mmol) and L_1H (0.14 g, 0.86 mmol) were stirred in EtOH (25 cm^3) until complete dissolution of solid material was achieved. NaOH (0.034 g, 0.06 mmol) was then added effecting a colour change from purple-red to dark red-brown. 2-furaldehyde (0.71 cm^3, 8.4 mmol) was then added and the red-brown opaque solution stirred for a further 4 hours following which it was filtered to afford a purple-brown mother liquor. Purple-brown blocks of **3** were harvested both from the mother liquor and Et_2O diffused samples of the mother liquor with a combined yield of 22% after 2 weeks. Elemental analysis (%) calculated (found) for **3** ($C_{59}H_{76}N_8O_{29}Co_7$): C 39.95 (41.18), H 4.32 (3.78), N 6.32 (6.27). FT-IR (cm^{-1}): 3464 (w), 2932 (w), 1671 (m), 1629 (m), 1602 (w), 1560 (w), 1474 (m), 1459 (m), 1436 (m), 1407 (w), 1339 (m), 1306 (m), 1240 (m), 1221 (s), 1171 (w), 1149 (w), 1090 (m), 1076 (m), 1054 (w), 1015 (m), 964 (m), 927 (w), 882 (w), 860 (m), 830 (w), 788 (m), 744 (s).

*2.4.3.4 Synthesis of [(3-fur)⊂Zn(II)$_7$(OH)$_6$(L$_1$)$_6$](NO$_3$)$_2$ (**4**)*

To a 30 cm^3 methanolic solution of L$_1$H (0.139 g, 0.84 mmol) were added NaOH (0.034 g, 0.84 mmol) and Zn(NO$_3$)$_2$·6H$_2$O (0.25 g, 0.84 mmol). The resultant solution was allowed to stir for 1 hour before 3-furaldehyde (0.73 cm^3, 8.4 mmol) was added and the mixture stirred for a further 3 hours. The solution was then allowed to settle for 30 minutes before filtration. X-ray quality crystals of **4** were obtained after 3 weeks in 18 % yield. Elemental analysis (%) calculated (found) for **4**.2H$_2$O ($C_{59}H_{74}N_8O_{28}Zn_7$): C 39.34 (39.33), H 4.14 (4.23), N 6.22 (6.37). FT-IR (cm^{-1}): 3429 (vb), 2929 (m), 2829 (w), 1859 (w), 1676 (m), 1639 (s), 1602 (m), 1560 (w), 1475 (s), 1461 (s), 1436 (m), 1409 (m),1383 (s),1356 (b/m), 1311 (s), 1241 (m), 1222 (s), 1172 (m), 1149 (m), 1093 (m), 1076 (m), 1035 (m), 1013 (m), 966 (m), 860 (w), 829 (w), 795 (m), 746 (m).

*2.4.3.5 Synthesis of [(3-fur)⊂Ni(II)$_7$(OH)$_6$(L$_1$)$_6$](NO$_3$)$_2$·3H$_2$O (**5**)*

To a 30 cm^3 methanolic solution of L$_1$H (0.139 g, 0.84 mmol) were added NaOH (0.034 g, 0.84 mmol) and Ni(NO$_3$)$_2$·6H$_2$O (0.250 g, 0.84 mmol). The solution was allowed to stir for 1 hour before 3-furaldehyde (0.74 cm^3, 8.4 mmol) was added and the reaction mixture stirred for a further 3 hours. The resultant solution was filtered and X-ray quality crystals of **5** were obtained in 10% yield over a 3 week period. Elemental analysis (%) calculated (found) for **5** ($C_{59}H_{76}N_8O_{29}Ni_7$): C 39.99 (40.25), H 4.32 (4.23), N 6.32 (6.24). FT-IR (cm^{-1}): 3438 (vb), 3002 (w), 2932 (w), 2814 (w), 1676 (m), 1626 (s), 1603 (m), 1561 (w), 1550 (w), 1511 (w), 1459 (s), 1436 (m), 1407 (m), 1336 (s), 1315 (s), 1239 (m), 1222 (s), 1210 (s), 1169 (m), 1149 (m), 1086 (m), 1072 (m), 1044 (m), 1017 (m), 957 (m), 866 (m), 828 (m), 792 (m), 742 (s), 727 (m), 641 (m), 627 (m), 599 (m), 555 (m), 492 (m).

*2.4.3.6 Synthesis of [(3-fur)⊂Co(II)$_7$(OH)$_6$(L$_1$)$_6$](NO$_3$)$_2$·4.5H$_2$O (**6**)*

A solution of Co(NO$_3$)$_2$.6H$_2$O (0.25 g, 0.86 mmol) and L$_1$H (0.142 g, 0.86 mmol) were stirred in EtOH (25 cm^3) and placed in a glass-lined CEM Discovery® microwave reactor, adopting a purple-red colour in the process. Solid NaOH (0.034 g, 0.86 mmol, 1.0 eq.) and 3-furaldehyde (3-fur) (0.74 cm^3, 8.6 mmol) were then added neat and the

system isolated from its surroundings by capping with a Teflon seal. The solution was heated under microwave conditions (110°C, 110 psi, 200 W, 20 mins) affording a dark, red-brown solution which was filtered to afford a similarly coloured mother liquor. Et_2O diffusion of the mother liquor afforded purple-brown blocks of **6** after one week which were harvested with a combined yield of 10%. Elemental analysis (%) calculated (found) for $C_{59}H_{70}N_8O_{26}Co_7$ (loss of waters): C 39.35 (40.53), H 4.42 (4.58), N 6.22 (6.63). FT-IR (cm^{-1}): 3575 (w), 2932 (w), 1678 (m), 1632 (s), 1601 (m), 1562 (w), 1512 (w), 1474 (w), 1459 (s), 1436 (m), 1407 (m), 1345 (s), 1306 (s), 1239 (m), 1221 (s), 1171 (m), 1149 (m), 1089 (m), 1078 (s), 1055 (w), 1011 (m), 968 (m), 869 (w), 858 (m), 796 (m), 744 (s).

*2.4.3.7 Synthesis of [(bzal)⊂Zn(II)$_7$(OMe)$_6$(L$_1$)$_6$](NO$_3$)$_2$·5H$_2$O (**7**)*

To a 30 cm^3 methanolic solution of L_1H (0.139 g, 0.84 mmol) were added NaOH (0.034 g, 0.84 mmol) and $Zn(NO_3)_2 \cdot 6H_2O$ (0.25 g, 0.84 mmol). The resultant solution was allowed to stir for 1 hour before benzaldehyde (0.85 cm^3, 8.4 mmol) was added and the mixture stirred for a further 3 hours. The solution was then allowed to settle for 30 minutes before filtration. X-ray quality crystals of **7** were obtained after 3 weeks in 15% yield. Elemental analysis (%) calculated (found) for **7** ($C_{67}H_{82}N_8O_{30}Zn_7$): C 41.54 (41.68), H 4.27 (4.43), N 5.78 (5.51). FT-IR (cm^{-1}): 3435 (vb), 2938 (b/w), 2825 (w), 1826 (w), 1689 (m), 1643 (s), 1599 (m), 1556 (w), 1472 (s), 1351 (b/s), 1315 (s), 1230 (m), 1221 (s), 1176 (w), 1080 (m), 1032 (m), 961 (m), 857 (m), 827 (w), 789 (m), 753 (s). Solid state ^{13}C NMR (ppm) (spinning speed = 12 KHz) (Prominent guest peaks in bold): **193.21**, 173.14, 155.36, 149.00, **135.15**, 129.16, 118.94, 117.59, 55.53, 52.90, 45.41.

*2.4.3.8 Synthesis of [(bzal)⊂Ni(II)$_7$(OH)$_6$(L$_1$)$_6$](NO$_3$)$_2$ (**8**)*

To a 30 cm^3 methanolic solution of L_1H (0.139 g, 0.86 mmol) were added NaOH (0.034 g, 0.86 mmol) and $Ni(NO_3)_2 \cdot 6H_2O$ (0.25 g, 0.86 mmol). The solution was allowed to stir for 1 hour before benzaldehyde (0.87 cm^3, 8.6 mmol) was added and the resultant mixture stirred for a further 3 hours. The solution was filtered and X-ray quality crystals of **8** were obtained after 3 weeks in 17% yield. Elemental analysis (%) calculated (found) for **8**.2H_2O ($C_{61}H_{76}N_8O_{27}Ni_7$): C 41.53 (41.21), H 4.34 (4.19), N

6.35 (6.63). FT-IR (cm^{-1}): 3568 (w), 3439 (vb), 3003 (w), 2932 (w), 2811 (w), 1689 (m), 1626 (s), 1602 (m), 1549 (w), 1458 (s), 1437 (w), 1407 (m), 1337 (s), 1315 (s), 1239 (w), 1222 (s), 1209 (s), 1169 (m), 1148 (w), 1087 (m), 1072 (m), 1042 (m), 1017 (m), 956 (m), 864 (w), 828 (m), 792 (s), 744 (m), 727 (m), 688 (m), 643 (m), 628 (m), 606 (w), 589 (w), 556 (w), 493 (m).

*2.4.3.9 Synthesis of [(2-thio)⊂Zn(II)$_7$(OH)$_6$(L$_1$)$_6$](NO$_3$)$_2$ (**9**)*

To a 30 cm^3 methanolic solution of L_1H (0.139 g, 0.84 mmol) was added NaOH (0.034 g, 0.84 mmol) and $Zn(NO_3)_2 \cdot 6H_2O$ (0.250 g, 0.84 mmol). The resultant solution was allowed to stir for 1 hour before 2-thiophenecarboxaldehyde (0.79 cm^3, 8.4 mmol) was added and the solution stirred for a further 3 hours. The solution was then filtered and X-ray quality crystals of **9** were obtained in 14% yield after 2 weeks. Elemental analysis (%) calculated (found) for **9**.$2H_2O$ ($C_{59}H_{74}N_8O_{27}S_1Zn_7$): C 39.00 (38.82), H 4.11 (4.08), N 6.17 (5.61). FT-IR (cm^{-1}): 3432 (vb), 3084 (w), 2999 (w), 2964 (m), 2930 (m), 2825 (m), 2792 (w), 2698 (w), 2572 (w), 2416 (w), 2165 (w), 2046 (w), 1989 (w), 1933 (w), 1858 (w), 1787 (w), 1747 (w), 1653 (s), 1638 (s), 1602 (s), 1557 (m), 1474 (s), 1461 (s), 1437 (s), 1409 (s), 1353 (s/b), 1310 (s), 1240 (s), 1222 (s), 1172 (m), 1147 (m), 1093 (m), 1077 (m), 1032 (m), 1014 (m), 965 (m), 859 (m), 829 (w), 794 (m), 746 (s), 664 (m), 631 (m), 612 (m), 584 (w), 552 (w), 474 (m), 430 (w).

*2.4.3.10 Synthesis of [(2-thio)⊂Ni(II)$_7$(OH)$_6$(L$_1$)$_6$](NO$_3$)$_2$ (**10**)*

To a 30 cm^3 methanolic solution of L_1H (0.139 g, 0.86 mmol) was added NaOH (0.034 g, 0.86 mmol) and $Ni(NO_3)_2 \cdot 6H_2O$ (0.250 g, 0.86 mmol). The solution was allowed to stir for 1 hour before 2-thiophenecarboxaldehyde (0.80 cm^3, 8.6 mmol) was added and the reaction mixture stirred for a further 3 hours. The resultant solution was then filtered and X-ray quality crystals of **10** were obtained over a 3 week period (12% yield). Elemental analysis (%) calculated (found) for **10**.$4H_2O$ ($C_{59}H_{78}N_8O_{29}S_1Ni_7$): C 39.23 (38.85), H 4.35 (3.91), N 6.20 (5.65). FT-IR (cm^{-1}): 3568 (vb), 3084 (w), 3002 (w), 2932 (w), 2812 (w), 1656 (m), 1626 (s), 1603 (m), 1549 (w), 1520 (w), 1459 (s), 1437 (m), 1407 (m), 1335 (s), 1315 (s), 1239 (m), 1222 (s), 1209 (s), 1170 (m), 1148 (m), 1087 (m), 1072 (m), 1041 (m), 1017 (m), 956 (m), 863 (m), 828 (w), 792 (m), 743 (s), 727 (s), 665 (m), 641 (m), 627 (m), 605 (m), 589 (w), 555 (w), 492 (m).

*2.4.3.11 Synthesis of [(2-acetylfuran)⊂[Zn(II)$_7$(OH)$_6$(L$_1$)$_6$(NO$_3$)$_2$] (**11**)*

To a 30 cm^3 methanolic solution of L_1H (0.139 g, 0.84 mmol) was added NaOH, (0.034 g, 0.84 mmol) and $Zn(NO_3)_2.6H_2O$ (0.25 g, 0.84 mmol. The resultant solution was stirred for 1 hour before 2-acetylfuran (0.84 cm^3, 8.4 mmol) was added. The subsequent reaction mixture was stirred for a further 3 hours before being filtered. X-ray quality crystals of **11** were obtained (10%) over a three week period. Elemental analysis (%) calculated (found) for **11**.$3H_2O$ ($C_{61}H_{78}N_8O_{29}Zn_7$): C 39.71 (39.54), H 4.26 (4.62), N 6.07 (5.72). FT-IR (cm^{-1}): 3404 (vb), 2998 (w), 2930 (b), 2824 (m), 2041 (w), 1986 (w), 1963 (w), 1667 (w), 1636 (s), 1601 (m), 1560 (w), 1435 (s), 1408 (m), 1334 (s), 1308 (s), 1240 (s), 1229 (s), 1173 (w), 1147 (m), 1092 (w), 1076 (w), 1013 (w), 967 (w), 859 (w), 828 (w), 791 (w), 743 (s), 630 (m), 612 (m), 596 (w), 584 (m), 551 (w), 473 (m), 428 (w).

*2.4.3.12 Synthesis of [(2-acetylfuran) ⊂[Ni(II)$_7$(Ome)$_6$(L$_1$)$_6$](NO$_3$)$_2$·3H$_2$O (**12**)*

To a 30 cm^3 methanolic solution of L_1H (0.142 g, 0.86 mmol) was added NaOH, (0.034 g, 0.86 mmol) and $Ni(NO_3)_2.6H_2O$ (0.25 g, 0.86 g). The resultant solution stirred for 1 hour before 2-acetylfuran (0.86 cm^3, 8.6 mmol) was then added. The reaction mixture was stirred for a further 3 hours and allowed to settle for 30 minutes prior to being gravity filtered. X-ray quality crystals of **12** were obtained in 10% yield over a period of three weeks. Elemental analysis (%) calculated (found) for **12** ($C_{66}H_{90}N_8O_{29}Ni_7$): C 42.38 (42.42), H 4.85 (4.62), N 5.99 (6.36). FT-IR (cm^{-1}): 3528 (vb), 3001 (w), 2932 (b), 2813 (m/b), 1665 (w), 1626 (s), 1602 (m), 1560 (m), 1550 (w), 1460 (s), 1437 (w), 1407 (m), 1335 (s), 1315 (s), 1239 (s), 1222 (s), 1210 (w), 1170 (m), 1148 (m), 1087 (w), 1072 (m), 1042 (m), 1017 (m), 957 (m), 915 (m), 906 (m), 882 (m), 864 (w), 829 (w), 791 (m), 744 (s), 726 (m), 641 (w), 627 (w), 591 (w), 555 (w), 491 (m), 442 (w).

*2.4.3.13 Synthesis of [(2-acetylfuran)⊂Co(II)$_7$(Ome)$_6$(L$_1$)$_6$](NO$_3$)$_2$·7H$_2$O (**13**)*

To a 30 cm^3 methanolic solution of L$_1$H (0.142 g, 0.86 mmol) was added NaOH, (0.034 g, 0.86 mmol) and Co(NO$_3$)$_2$.6H$_2$O (0.25 g, 0.86 g). The resultant solution stirred for 1 hour before 2-acetylfuran (0.86 cm^3, 8.6 mmol), was then added. The reaction mixture was stirred for a further 3 hours and allowed to settle for 30 minutes prior to being gravity filtered. X-ray quality crystals of **13** were obtained in 20% yield over a period of three weeks. Elemental analysis (%) calculated (found) for **13**.3H$_2$O ($C_{66}H_{90}N_8O_{29}Co_7$): C 42.35 (42.10), H 4.85 (4.75), N 5.99 (5.62). FT-IR (cm^{-1}): 3546 (w), 3464 (w, b), 3003 (m), 2933 (w), 2822 (w), 2702 (w), 2655 (w), 2577 (w), 2377 (w), 2331 (w), 2044 (w), 1742 (vw), 1670 (m), 1627 (s), 1602 (m), 1563 (m), 1475 (sh), 1460 (s), 1433 (m), 1404 (s), 1343 (s), 1300 (s), 1230 (m), 1215 (s), 1168 (s), 1149 (m), 1090 (m), 1075 (s), 1030 (m), 1014 (m), 964 (m), 913 (w), 882 (m), 859 (m), 831 (s), 792 (m), 738 (s), 728 (sh), 631 (m), 619 (m), 553 (m), 477 (s).

*2.4.3.14 Synthesis of [(acetoph)⊂Zn(II)$_7$(OH)$_6$(L$_1$)$_6$](NO$_3$)$_2$ (**14**)*

To a 30 cm^3 methanolic solution of L$_1$H (0.139 g, 0.84 mmol) was added NaOH (0.034 g, 0.84 mmol) and Zn(NO$_3$)$_2$.6H$_2$O (0.25 g, 0.84 mmol). The solution was stirred for 1 hour before acetophenone (0.98 cm^3, 8.4 mmol), was introduced. The resultant solution was left to stir for a further 3 hours and allowed to settle for 30 minutes prior to being gravity filtered. X-ray quality crystals of **14** were obtained in 10% yield over a three week period. Elemental analysis (%) calculated (found) for **14** ($C_{62}H_{74}N_8O_{25}Zn_7$): C 41.62 (41.82), H 4.17 (4.58), N 6.26 (6.41). FT-IR (cm^{-1}): 3404 (vb), 2937 (b), 2820 (m), 1676 (m), 1637 (s), 1600 (m), 1561 (w), 1474 (s), 1458 (s), 1435 (s), 1408 (m), 1335 (s), 1308 (s), 1271 (m), 1240 (s), 1219 (s), 1194 (w), 11714 (w), 1093 (w), 1077 (w), 1029 (m), 1012 (m), 969 (m), 859 (w), 794 (w), 745 (s), 690 (m), 631 (m), 612 (m), 585 (m), 550 (w), 473 (m).

*2.4.3.15 Synthesis of [(acetoph)⊂[Ni(II)$_7$(Ome)$_6$(L$_1$)$_6$](NO$_3$)$_2$ (**15**)*

To a 30 cm^3 methanolic solution of L$_1$H (0.142 g, 0.86 mmol) was added NaOH (0.034 g, 0.86 mmol) and Ni(NO$_3$)$_2$.6H$_2$O (0.25 g, 0.86 mmol). The solution was stirred for 1 hour before acetophenone (1.00 cm^3, 8.6 mmol), was added. The resultant solution was stirred for a further 3 hours and allowed to settle for 30 minutes prior to being

gravity filtered. X-ray quality crystals of **15** were obtained in 18% yield over a three week period. Elemental analysis (%) calculated (found) for **15** ($C_{68}H_{86}N_8O_{25}Ni_7$): C 44.72 (44.65), H 4.75 (4.43), N 6.14 (6.11). FT-IR (cm^{-1}): 3435 (vb), 3001 (w), 2932 (b/m), 2814 (m), 1674 (m), 1627 (s), 1602 (m), 1560 (m), 1459 (s), 1436 (m), 1408 (m), 1334 (s), 1314 (s), 1271 (w), 1240 (s), 1221 (s), 1170 (m), 1147(m), 1080 (w), 1072 (m), 1041 (m), 1017 (m), 963 (m), 864 (m), 792 (m), 744 (s), 690 (m), 642 (w), 627 (w), 588 (w), 555 (w), 491 (m), 440 (w), 406 (w).

*2.4.3.16 Synthesis of [(acetoph)⊂[Co(II)$_7$(Ome)$_6$(L$_1$)$_6$](NO$_3$)$_2$·7H$_2$O (**16**)*

To a 30 cm^3 methanolic solution of L_1H (0.142 g, 0.86 mmol) was added NaOH (0.034 g, 0.86 mmol) and $Co(NO_3)_2.6H_2O$ (0.25 g, 0.86 mmol). The solution was stirred for 1 hour before acetophenone (1.00 cm^3, 8.6 mmol) was added. The resultant solution was stirred for a further 3 hours and allowed to settle for 30 minutes prior to being gravity filtered. X-ray quality crystals of **16** were obtained in 15% yield over a three week period. Elemental analysis (%) calculated (found) for **16** ($C_{68}H_{100}N_8O_{32}Co_7$): C 41.80 (42.03), H 5.16 (4.84), N 5.73 (5.92). FT-IR (cm^{-1}): 3455 (w, b), 3058 (w), 3005 (w), 2933 (m), 2816 (w), 2361 (w), 1676 (m), 1625 (s), 1600 (m), 1559 (m), 1474 (sh), 1458 (s), 1435 (m), 1407 (s), 1330 (s), 1304 (s), 1271 (m), 1240 (m), 1217 (s), 1170 (s), 1145 (m), 1088 (m), 1073 (s), 1009 (m), 964 (m), 857 (m), 828 (s), 791 (m), 742 (s,b), 728 (sh), 691 (m), 629 (m), 617 (m), 584 (m), 555 (m), 479 (s).

2.5 References

1. (a) X. Yang, J.-K. Sun, M. Kitta, H. Pang and Q. Xu. *Nature Catalysis,* 2018, **1**, 214-220. (b) C. Deraedt and D. Astruc. *Coord. Chem. Rev.,* 2016, **324**, 106-122. (c) D. M. Vriezema, M. C. Aragones, J. A. A. W. Elemans, J. L. M. Cornelissen, A. E. Rowan and R. J. M. Nolte. *Chem. Rev.,* 2005, **105(4)**, 1445-1490. (d) F. Hof, S. L. Craig, C. Nuckolls and J. Rebek Jr. *Angew. Chem. Int. Ed.,* 2002, **41**, 1488-1508.

2. (a) J. Zhou and B. Wang. *Chem. Soc. Rev.,* 2017, **46**, 6927-6945. (b) T. A. Makal, J.-R. Li, W. Wu and H.-C. Zhou. *Chem. Soc. Rev.,* 2012, **41**, 7761-7779**.** (c) P. Mal, B. Breiner, K. Rissanen and J. R. Nitschke. *Science,* 2009, **324**, 1697-1699. (d) D. Fielder, R. G. Bergman and K. N. Raymond. *Angew. Chem.,* 2006, **118**, 759-762.

3. (a) H. Li, L. Li, R.-B. Lin, W. Zhou, Z. Zhang, S. Xiang and B. Chen. *EnergyChem.,* 2019, **1**, 1000006. (b) L. Chen, P. S. Reiss, S. Y. Chong, D. Holden, K. E. Jelfs, T. Hasell, M. A. Little, A. Kewley, M. E. Briggs, A. Stephenson, K. M. Thomas, J. A. Armstrong, J. Bell, J. Busto, R. Noel, J. Liu, D. M. Strachan, P. K. Thallapally and A. I. Cooper. *Nat. Mater.,* 2014, **13**, 954-960. (c) Y. Peng, T. Gong, K. Zhang, X. Lin, Y. Liu, J. Jiang and Y. Cui. *Nat. Commun*., 2014, **5**, 4406.

4. (a) S. Pullen, J. Tessarolo and G. H. Clever. *Chem. Sci.,* 2021, **12**, 7269-7293. (b) T. Y. Kim, L. Digal, M. G. Gardiner, N. T. Lucas and J. D. Crowley. *Chem. Eur. J.,* 2017, **23**, 1-10. (c) M. Yoshizawa, J. K. Klosterman and M. Fujita. *Angew. Chem,. Int. Ed.* 2009, **48**, 3418-3438.

5. (a) T. Hasell and A. I. Cooper. *Nature Reviews Materials.* 2016, **1**, 1-14. (b) J. D. Evans, C. J. Sumby and C. J. Doonan. *Chem. Lett.,* 2015, **44(5)**, 582-588. (c) T. Towaza, J. T. A. Jones, S. I. Swamy, S. Jiang, D. J. Adams, S. Shakespeare, R. Cloers, D. Bradshaw, T. Hasell, S. Y. Chong, C. Tang, S. Thompson, J. Parker, A. Trewin, J. Bacsa, A. M. Z. Slawin, A. Steiner and A. I. Cooper. *Nature Materials.* 2009, **8**, 973-978.

6. (a) P. J. Waller, F. Gandara and O. M. Yaghi. *Acc. Chem. Res*., 2015, **48(12)**, 3053-3063. (b) X. Feng, X. Ding and D. Jiang. *Chem. Soc. Rev.,* 2012, **41**, 6010-6022. (c) A. Thomas*. Angew. Chem. Int. Ed.,* 2010, **49**, 8328-8344. (d) A. P. Cote, A. I. Benin, N. W. Ockwig, M. O'Keeffe, A. J. Matzger and O. M. Yaghi. *Science.,* 2005, **310**, 1166-1170.

7. (a) X. Zhang, Z. Chen, X. Liu, S. L. Hanna, X. Wang, R. Taheri-Ledari, A. Maleki, P. Li and O. K. Farha. *Chem. Soc. Rev*., 2020, **49**, 7406-7427. (b) Y. Cui, B. Li, H. He,

W. Zhou, B. Chen and G. Qian. *Acc. Chem. Res*., 2016, **49(3)**, 483-493. (c) H.-C. Zhou, J. R. Long and O. M. Yaghi. *Chem. Rev.,* 2012, **112(2)**, 673-674. (d) A. U. Czaja, N. Truckhan and U. Müller. *Chem. Soc. Rev.,* 2009, **38**, 1284-1293. (e) S. L. James. *Chem. Soc. Rev.,* 2003, **32**, 276-288.

8. S. T. Meally, C. McDonald, G. Karotsis, G. S. Papaefstathiou, E. K. Brechin, P. W. Dunne, P. McArdle, N. P. Power, L. F. Jones. *Dalton Trans.,* 2010, **39**, 4809 – 4816.

9. L. Clougherty, J. Sousa and G. Wyman. *J. Org. Chem.,* 1957, 22, **4**, 462-462.

10. B. Weckler and H. D. Ludz. *Spectrochim. Acta. A.* 1996, **52**, 1507-1513.

11. (a) S. T. Meally, C. McDonald, P. Kealy, S. M. Taylor, E. K. Brechin and L. F. Jones. *Dalton Trans.,* 2012, **41(18)**, 5610-5616. (b) S. T. Meally, G. Karotsis, E. K. Brechin, G. S. Papaefstathiou, P. W. Dunne, P. McArdle, L. F. Jones. *CrystEngComm.,* 2010, **12, 59-63.**

12. For other examples of complexes with body-centred hexagonal [M_7] (M = Co(II), Ni(II), Zn(II)) disc-like inorganic cores: (a) R. Gheorghe, Georgiana A. Ionita, C. Maxim, A. Caneschi, L. Sorace, M. Andruh. *Polyhedron* 2019, **171**, 269–278. (b) F. Kobayashi, R. Ohtani, S. Teraoka, W. Kosaka, H. Miyasaka, Y. Zhang, L. F. Lindoy, S. Hayami and M. Nakamura. *Dalton Trans*., 2017, **46**, 8555–8561. (c) S.-H. Zhang, R.-X. Zhao, G. Li, H.-Y. Zhang, C.-L. Zhang, G. Muller. *RSC Advances*. 2014, **4**, 54837-54846. (d) C. Ding, C. Gao, S. Ng, B. Wang and Y. Xie. *Chem. Eur. J*. 2013, **19**, 9961–9972. (e) L.-Q.Wei, K. Zhang, Y.-C. Feng, Y.-H. Wang, M.-H. Zeng and M. Kurmoo. *Inorg. Chem.* 2011, **50**, 7274–7283. (f) J. Zhang, P. Teo, R. Pattacini, A. Kermagoret, R. Welter, G. Rogez, T. S. A. Hor and P. Braunstein. *Angew. Chem. Int. Ed*. 2010, **49**, 4443–4446. (g) W. Leong and J. J. Vittal. *New J. Chem*., 2010, **34**, 2145–2152.

13. A. L. Spek, *Acta Crystallogr., Sect. C: Struct. Chem.,* 2015, **71**, 1–9.

14. C. F. Macrae, I. Sovago, S. J. Cottrell, P. T. A. Galek, P. McCabe, E. Pidcock, M. Platings, G. P Shields, J. S. Stevens, M. Towler and P. A. Wood. *J. Appl. Cryst.* 2020, **53**, 226-235.

15. Brown, I. D. & Altermatt, D. (1985). Acta Cryst. B41, 244-247.

16. O. V. Dolomanov, L. J. Bourhis, R. J. Gildea, J. A. K. Howard and H. Puschmann. *J. Appl. Cryst.* 2009, **42**, 339-341.

17. J. J. McKinnon, M. A. Spackman and A. S. Mitchell. *Acta Cryst. Sect. B.,* 2004, **B60**, 627-668.

18. N. R. Voss, M. Gerstein, *Nucleic Acids Res.* 2010, **38**, W555–W562.

19. S. Mecozzi and J. Rebek Jr. *Chem. Eur. J.* 1998, **4**, 1016-1022.

20. K. Rissansen, *Chem. Soc. Rev.,* 2017, **46**, 2638-2648.

21. Rigaku OD, CrysAlis PRO, Rigaku Oxford Diffraction Ltd, Yarnton, England, 2015.

22. G. M. Sheldrick, Acta Crystallogr., *Sect. C: Struct. Chem*., 2015, **71**, 3.

Chapter 3:

Crowding Out: Ligand modification and their structure directing effects on brucite-like $\{M_x(\mu_3\text{-}OH)_y\}$ (M = Co(II), Ni(II)) core growth within polymetallic cages

3.1 Introduction

Previous work in the Jones group has described the utilisation of the ligands 2-methoxy-6-[(methylimino)methyl]phenol (L_1H) and 2-methoxy-6-[(phenylimino)methyl]phenol (L_2H; Scheme 3.1), in the formation the pseudo metallocalix[6]arenes $[M_7(\mu_3\text{-}OH)_6(L_x)_6](NO_3)_y$ (M = Ni(II), x = 1, y = 2 and Co(II/III) x = 2, y = 3) (Figure 3.1).[1-3] Each of these complexes exhibit a double-bowl topology and in the solid state, form molecular cavities that are able to act as hosts for guests such as small organics and counter anions.[1-3] The heptanuclear inorganic cores in $[Ni(II)_7(\mu_3\text{-}OH)_6(L_1)_6](NO_3)_2$ and $[(NO_3)_2\subset Co(III)Co(II)_6(\mu_3\text{-}OH)_6(L_2)_6](NO_3)$ are best described as comprising six edge-sharing triangular $\{M_3(\mu_3\text{-}OH)\}$ (M = Ni(II) / Co(II/III)) units, resulting in their planar sheet-like body-centred hexagonal arrays (Figure 3.1), whereby each octahedral metal centre is connected by μ_3-bridging OH^- ions. Indeed, such sheet-like $\{M_x(\mu_3\text{-}OH)_y\}$ topologies are regularly observed in the literature for a variety of transition metal cages of numerous nuclearities such as $[M_4]$ (M = Mn,[4-7] Fe,[8-10] Co,[11] Ni[12-14] and Zn[15-19]), $[Ni_5]$,[20] $[Ni_6]$,[21] $[M_7]$ (M = Mn,[22,23,29] Fe,[24] Co,[3,25,26] Ni[1,2,27,28] and Zn[2,29]), $[Mn_{10}]$,[30] $[Co_{12}]$,[31] $[Fe_{17}]$,[32,33] $[Ni_{18}]$,[34] $[M_{19}]$ (M = Mn,[35] Fe[32,33]) and $[Co_{28}]$.[31]

Moreover, to observe such planar topologies is not surprising when we consider their similarities with respect to the sheet-like brucite topologies observed within minerals such as the α- and β- polymorphs of $Co(OH)_2$[36] and $Ni(OH)_2$[37] (as well as the familiar brucite structure of $Mg(OH)_2$). Interestingly, cobalt and nickel hydroxides hold significant interest in the field of water splitting catalysis. More specifically, in 2008 Nocera and co-workers devised an efficient $Co(OH)_2$ / phosphate catalyst produced through its electrode surface deposition and has been shown to exhibit topological similarities with the sheet-like structure in (for instance) β-$Co(OH)_2$ and many $M_x(\mu_3\text{-}OH)_y$ transition metal cages (*vida supra*).[38-42] It should also be noted here that $Ni(OH)_2$-borate thin film electrocatalysts have more recently been produced by the same research group.[43,44] Interestingly and to emphasise these similarities, the triflate analogues to our previously described homo- and heterovalent pseudo metallocalix[6]arenes $[Co(II)_7(\mu_3\text{-}OH)_6(L_1)_6](NO_3)_2$ and $[(NO_3)_2\subset Co(II)_6Co(III)(\mu_3\text{-}OH)_6(L_2)_6](NO_3)$, respectively, were employed by Nocera and co-workers as models

towards investigating the electron transfer kinetics of their cobalt-phosphate (Co-OEC) water splitting catalysts.[45]

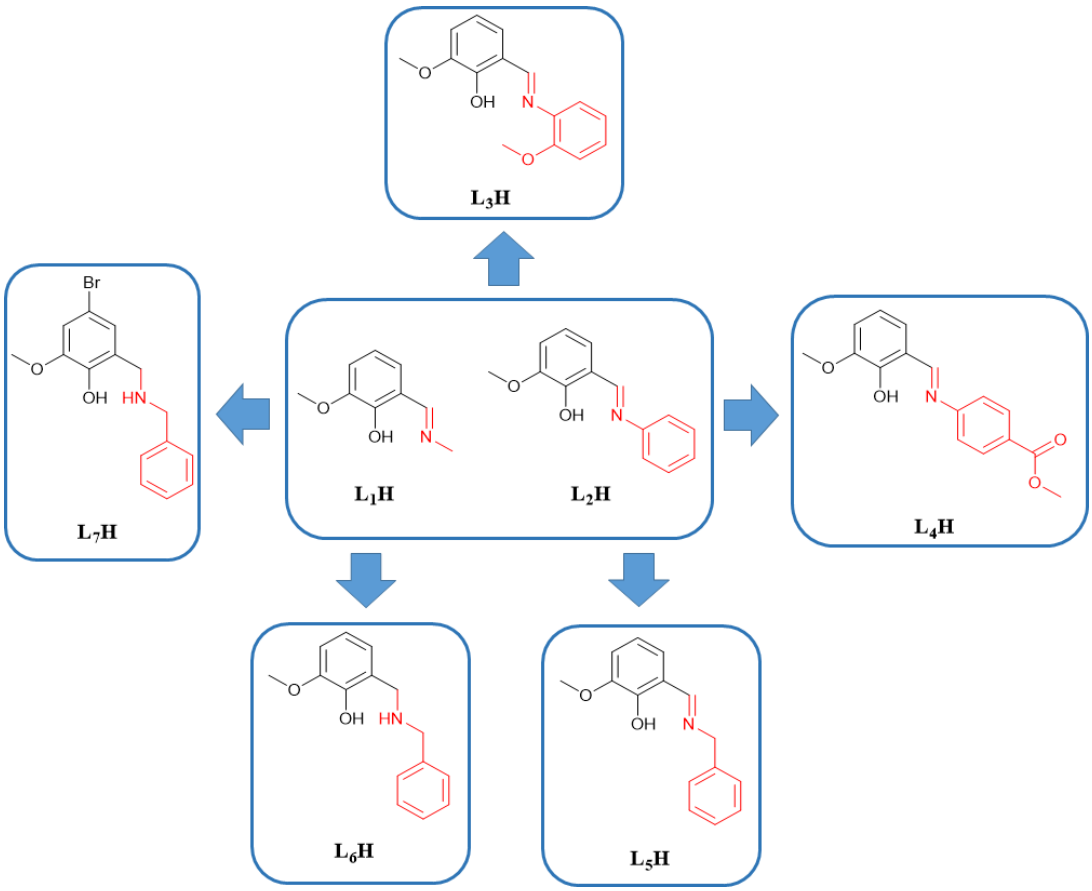

Scheme 3.1 ChemDraw representation of the ligands 2-methoxy-6-[(methylimino)methyl]phenol (L_1H) and 2-methoxy-6-[(phenylimino)methyl]phenol (L_2H), used previously in the formation of [M_7] (M = Co(II/III), Ni(II), Zn(II)) pseudo metallocalix[6]arenes (see main text for details). ChemDraw representations of the ligands 2-methoxy-6-{[(2-methoxybenzyl)imino]methyl}phenol (L_3H), methyl-(E)-4-((2-hydroxy-3-methoxybenzylidene)amino)benzoate (L_4H), 2-[(benzylimino)methyl]-6-methoxyphenol (L_5H), 2-[(benzylamino)methyl]-6-methoxyphenol (L_6H) and 2-[(benzylamino)methyl]-4-bromo-6-methoxyphenol (L_7H) employed in this chapter.

Our aim in this work was to strategically modify the shape and electronic nature of the [M_7] metallocalix[6]arene-directing ligands $L_{1\text{-}2}H$ (Scheme 3.1) and monitor any changes in resultant complex nuclearity and topology (e.g. $M_x(OH)_y$} sheet size) upon subsequent Co(II) and Ni(II) complexation. To this end, we report here the successfully synthesis of the novel ligands 2-methoxy-6-{[(2-methoxybenzyl)imino]methyl}phenol (L_3H), methyl (E)-4-((2-hydroxy-3-

methoxybenzylidene)amino)benzoate (L_4H) 2-[(benzylimino)methyl]-6-methoxyphenol (L_5H), 2-[(benzylamino)methyl]-6-methoxyphenol (L_6H) and 2-[(benzylamino)methyl]-4-bromo-6-methoxyphenol (L_7H) (Scheme 3.1). We also present the first examples of transition metal complexation of ligands $L_{3\text{-}7}H$ in the form of complexes: $[Ni(II)_2(L_3)_3(H_2O)](NO_3)\cdot 2H_2O\cdot 3MeOH$ (**17**), $[Na(I)Ni(II)_2(\mu\text{-}OH)(L_4H)(L_4)_3(H_2O)_2](NO_3)$ (**18**), $[Ni(II)(L_5)_2]$ (**19**), $[Co(III)(L_5)_3]\cdot H_2O\cdot MeOH$ (**20a**) and along with the tetranuclear siblings: $[(NO_3)\subset Co(II)_4(\mu_3\text{-}OH)_2(L_6)_4(H_2O)_2](NO_3)\cdot H_2O$ (**21**), $[(NO_3)\subset Ni(II)_4(\mu_3\text{-}OH)_2(L_6)_4(H_2O)_2](NO_3)\cdot H_2O$ (**22**) and $[Ni(II)_4(\mu_3\text{-}OH)_2(L_7)_4(NO_3)_2]\cdot MeCN$ (**23**). Complexes **17**-**23** represent the first examples of transition metal coordination of ligands $L_{3\text{-}7}H$.

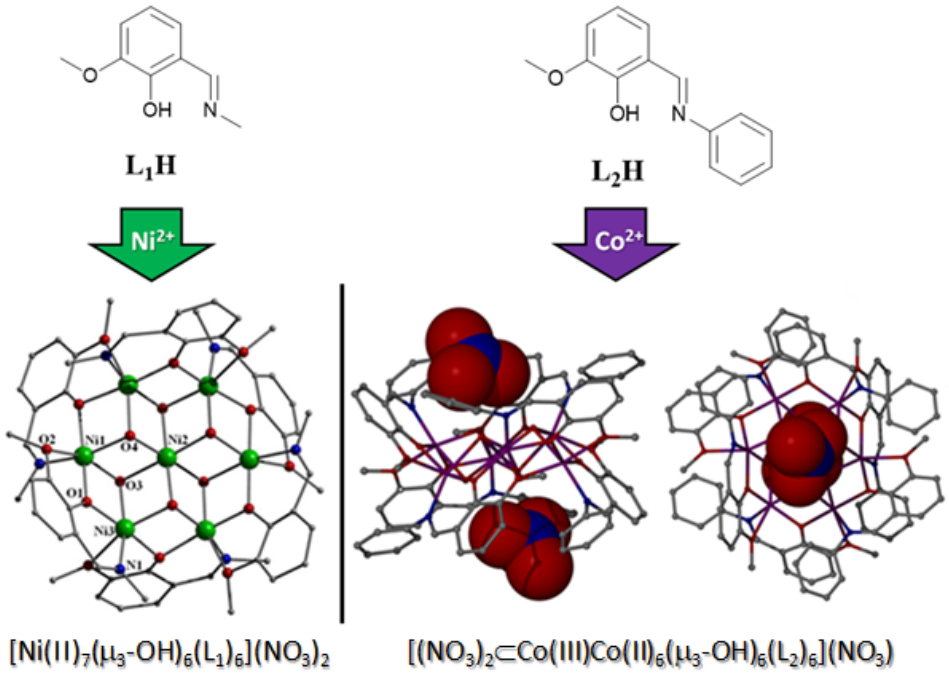

Figure 3.1 Schematic depicting the coordination chemistry of ligands L_1H and L_2H upon reactions with Ni(II) and Co(II/III) ions. Single crystal X-ray data was used to produce the $[Ni(II)_7]$ and $[Co(III)Co(II)_6]$ figures.[1-3] Colour code (used throughout this work): Green (Ni), Purple (Co), Red (O), Blue (N), Grey (C). Hydrogen atoms omitted for clarity and NO_3^- counter anions represented in space-fill mode.

3.2 Results and Discussion

We began our investigations by looking at the complexation of the ligand 2-methoxy-6-{[(2-methoxybenzyl)imino]methyl}phenol (L_3H) and Ni(II), which gives rise to the dimetallic complex $[Ni(II)_2(L_3)_3(H_2O)](NO_3)\cdot 2H_2O\cdot 3MeOH$ (**17**) and crystallises in the monoclinic $P2_1/n$ space group (Figure 3.2). The two Ni(II) ions (Ni1 and Ni2) are bridged by phenolic oxygens (O1 and O5) of two L_3^- ligands exhibiting $\eta^1{:}\eta^2{:}\eta^1{:}\eta^1$ μ- and $\eta^2{:}\eta^1$ μ-bridging motifs, to give the angles 101.77 º (Ni1-O1-Ni2) and 96.11 º (Ni1-O5-Ni2), respectively. The third L_3^- unit sits at approximately right angles to the $Ni1\text{-}O1_{phen}\text{-}Ni2$ plane and chelates (tridentate) at the Ni2 centre to complete its distorted octahedral geometry. The $\eta^2{:}\eta^1$: μ-bridging ligand in **17** has a much more contorted shape than the remaining two near planar L_3^- ligands, with its two aromatic rings twisted away from one another through rotation of the $N_{imine}\text{-}C_{arom}$ (N2-C22) single bond (Figure 3.2). Interestingly, this twisting is also observed in all six L_2^- ligands used in constructing the pseudo metallocalix[6]arene $[(NO_3)_2{\subset}Co(II)_6Co(III)(\mu_3\text{-}OH)_6(L_2)_6](NO_3)$ (Fig. 2.1). The introduction of the OMe group, along with the fact that the remaining two L_3^- ligands in **17** remain almost planar play a decisive role in the resultant dimeric topology. The final coordination site at Ni2 is taken by a single terminally bound H_2O ligand (Ni1-O10 = 2.08 Å). The NO_3^- counter anions (N4, O18-O20) in **17** act as molecular mortar in connecting the individual $\{Ni(II)_2\}$ units through extensive H-bonding with aromatic protons of nearby bridging L_3^- ligands (C40(H40)···O18 = 2.56 Å, C36(H36)···O19 = 2.52 Å and C34(H34)···O20 = 2.39 Å). These dimeric units in **17** arrange in the common brickwork motif along the *bc* plane of the unit cell, while these 2D sheets pack in superimposable rows along the *a* unit cell direction (Figure 3.3).

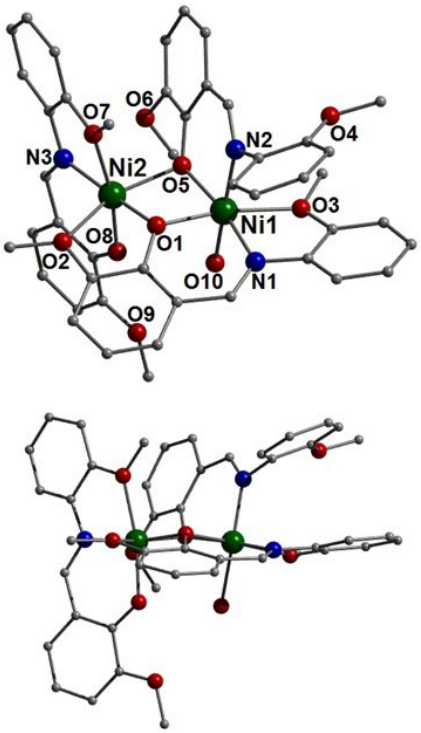

Figure 3.2 Crystal structure of $[Ni(II)_2(L_3)_3(H_2O)](NO_3)\cdot 2H_2O\cdot 3MeOH$ (**17**) as viewed off-set and parallel to the Ni-O(R)-Ni plane. Hydrogen atoms have been omitted for clarity.

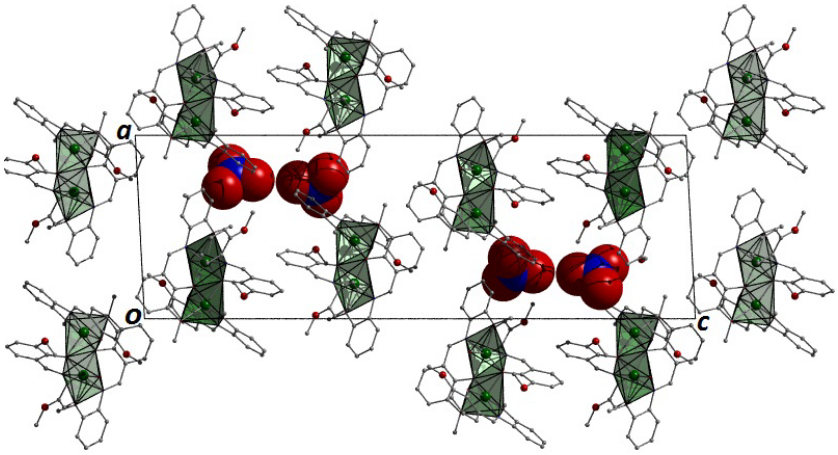

Figure 3.3 Polyhedral representation of the packing arrangement of $[Ni(II)_2(L_4)_3(H_2O)](NO_3)\cdot 2H_2O\cdot 3MeOH$ (**17**) as viewed along the *b* unit cell direction. All solvents of crystallisation have been omitted for clarity. The NO_3^- counter anions are space-fill represented. All hydrogen atoms have been omitted for clarity.

The complex $[Na(I)Ni(II)_2(\mu\text{-}OH)(L_4H)(L_4)_3(H_2O)_2](NO_3)$ (**18**) forms in methanol upon reaction with $Ni(NO_3)_2.6H_2O$ and L_4H in the presence of NaOH (base). Complex **18** crystallises in the Triclinic P-1 space group whose V-shaped trimeric Ni(II)···Ni(II)···Na(I) inorganic core is formed by a combination of three singly deprotonated L_4^- ligands and a single chelating L_4H moiety (Figure 3.4). More specifically, the two distorted octahedral Ni(II) ions (Ni1 and Ni2) are bridged by phenolic oxygens (O1 and O10) of two L_4^- ligands exhibiting $\eta^1{:}\eta^2{:}\eta^1$ μ -bridging motifs, to give the angles 104.28º (Ni1-O1-Ni2) and 93.76º (Ni1-O10-Ni2), respectively. The distorted octahedral Na(I) ion is also bound to the central Ni1 centre by two L_4^- units exhibiting $\eta^1{:}\eta^2{:}\eta^1$ μ- and $\eta^1{:}\eta^2{:}\eta^1$ μ_3- bonding motifs, respectively. A μ-bridging OH^- ion also bridges Ni1 to Na1, while two terminal H_2O ligands complete the coordination sphere at the Na(I) centre. The one chelating L_4H ligand is bound to Ni2 at distances of 2.07 Å (Ni2-N4) and 2.03 Å (Ni2-O14).

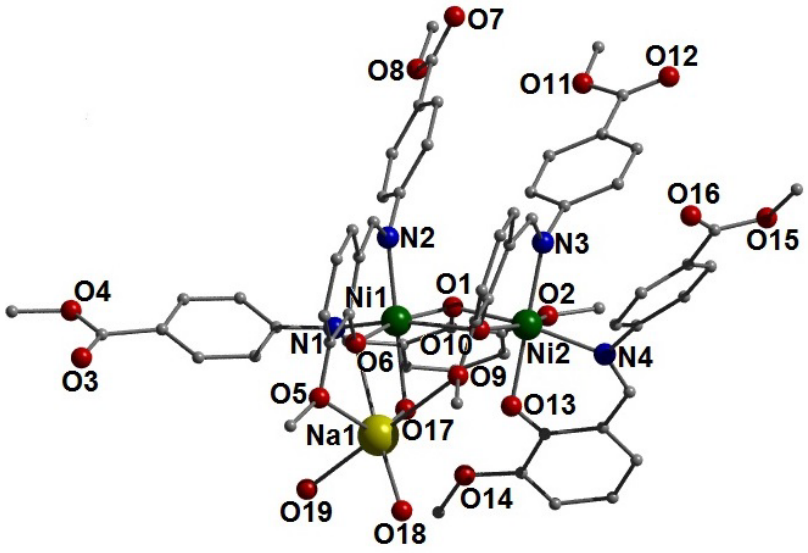

Figure 3.4 Crystal structure of $[NaNi(II)_2(\mu\text{-}OH)(L_4H)(L_4)_3(H_2O)_2](NO_3)$ (**18**) as viewed perpendicular (a – c). Colour code: Ni (green), O (red), N (blue), C (grey). Majority of hydrogen atoms have been omitted for clarity.

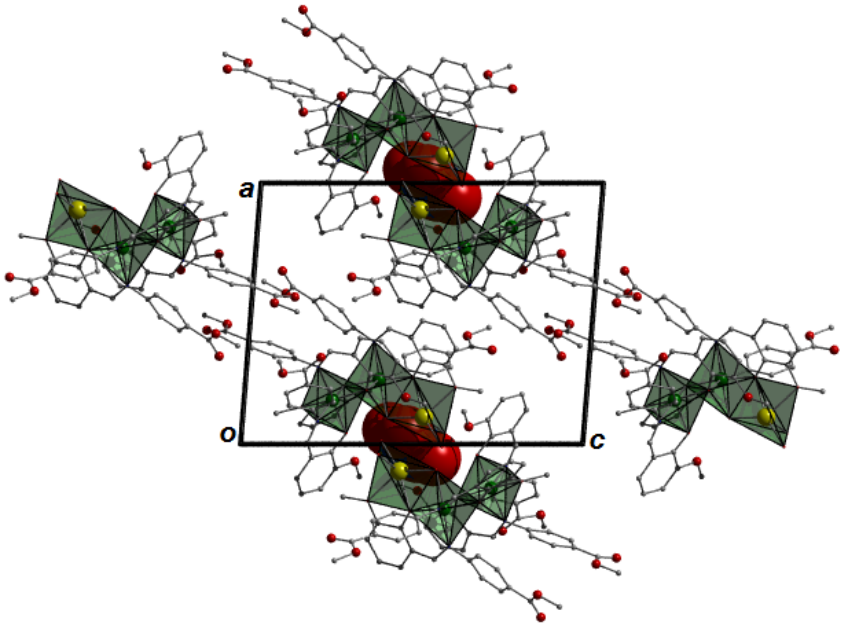

Figure 3.5 Packing in **18** as viewed down the *b* cell directions. Hydrogen atoms have been removed for clarity.

The monometallic complex [Ni(II)(L_5)$_2$] (**19**) crystallises from methanol in the triclinic space group (Z = 1) after reaction of Ni(NO_3)$_2$.6H_2O and L_5H in the presence of NaOH (base). The core in **19** comprises a single Ni(II) centre whose purely square planar geometry (N1-Ni1-N1 = 180°) is templated by two chelating L_5^- ligands through their O_{phen} (O1) and imine N atoms (N1) (Figure 3.6). This topology is vastly different to the heptanuclear cores in [Ni(II)$_7$(μ_3-OH)$_6$(L_1)$_6$](NO_3)$_2$ and [(NO_3)$_2$⊂Co(II)$_6$Co(III)(μ_3-OH)$_6$(L_2)$_6$](NO_3) (Figure 3.1 *cf.* Figure 3.6) and is attributed to the introduced –CH_2- bridge between the imine and lower rim phenyl group in L_5H. Upon chelation the OMe and benzyl imine groups in the symmetry related L_5^- moieties in **19** significantly deviate from the plane of their phenolic rings, resulting in a U-shaped topology and N1-C7-C6 and C13-O2-C15 angles of 111.11° and 112.45°, respectively (Figure 3.6). This is in stark contrast to the near planar topologies exhibited by the 2-methoxy-6-[(methylimino)methyl]phenol (L_1H) and 2-methoxy-6-[(phenylimino)methyl]phenol (L_2H) ligands in our previously reported family of [M_7] (M = Co(II/III) and Ni(II) pseudo metallocalix[6]arenes (Scheme 3.1 and Figure 3.1). Numerous intermolecular interactions stabilise and direct the topology in **19**. More specifically, the two symmetry equivalent L_4^- ligands partake in H-

bonding as shown as dashed lines in Figure 2.4 (O1···H7B′(C7′) = 2.19 Å, O2···H5′(C5′) = 2.34 Å and the long contact: C7(H7B)···O2′ = 2.91 Å. Intramolecular H-bonding interactions between O atoms (O2) of the unbound –OMe group on L_5^- and neighbouring aromatic protons (H5) effectively link the {Ni_1} units into superimposable H-bonded rows along the *c* direction of the unit cell in **19** (O2···(H4′)C4′ = 2.65 Å) (Figure 3.7). Powder XRD was carried out on the bulk to ensure the single crystals data obtained was consistent with the bulk of the product (Figure 3.8).

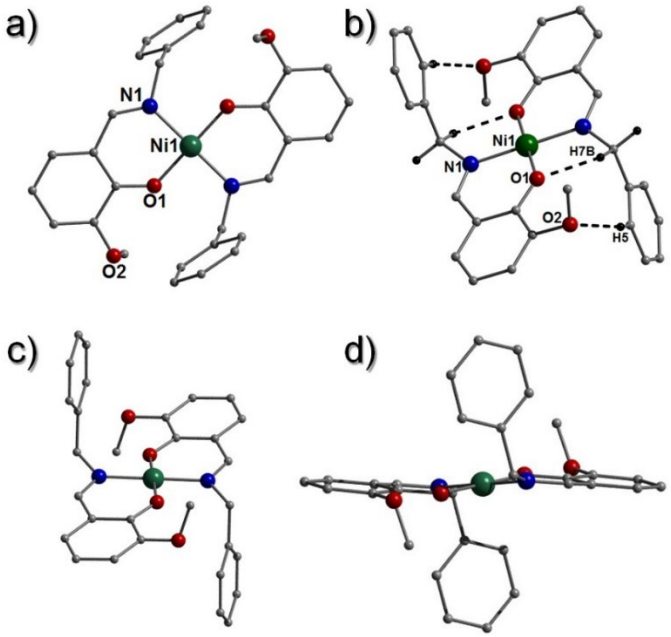

Figure 3.6 Crystal structure of [Ni(II)(L_5)$_2$] (**19**) as viewed perpendicular (a – c) and parallel (d) to the equatorial plane. Colour code: Ni (green), O (red), N (blue), C (grey). Majority of hydrogen atoms have been omitted for clarity. Dashed lines are H-bonds at distances: O1···H7B′(C7′) = 2.19 Å and O2···H5′(C5′) = 2.34 Å.

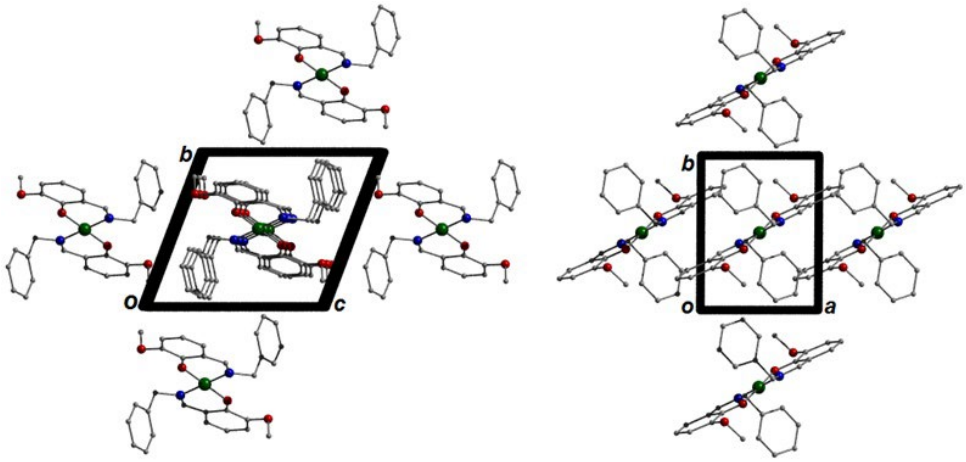

Figure 3.7 Packing in **19** as viewed down the *a* (left) and *c* (right) cell directions. Hydrogen atoms have been removed for clarity.

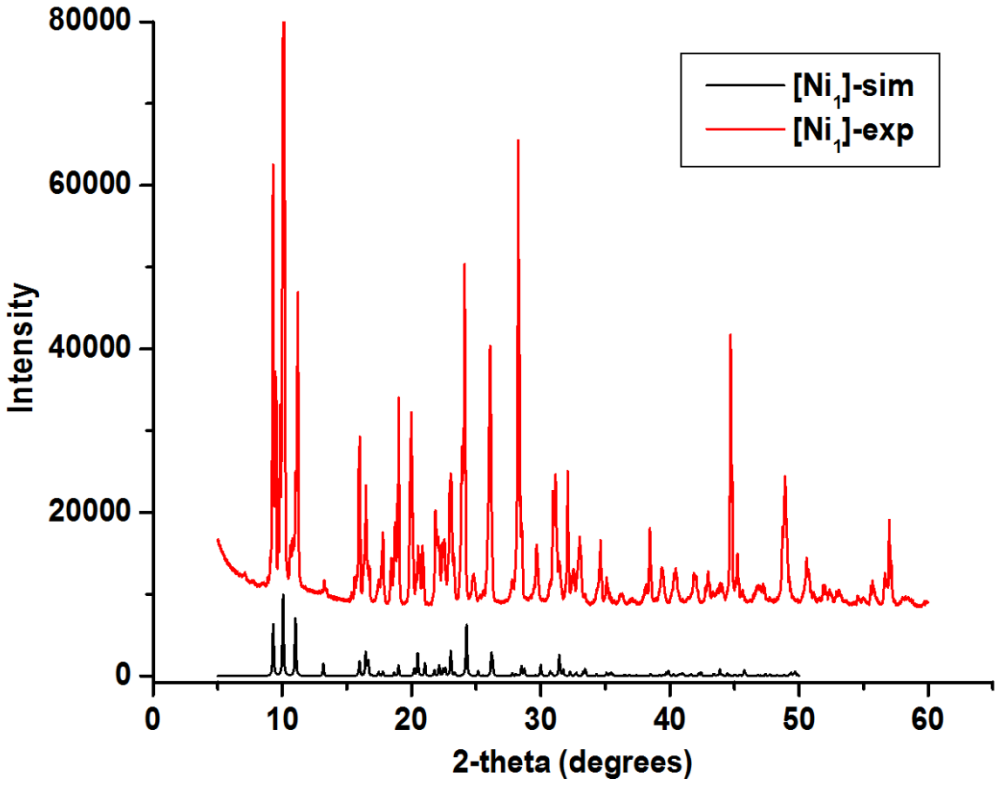

Figure 3.8 Experimental and simulated (from single crystal data) powder X-ray diffraction spectra obtained for [Ni(II)(L_5)$_2$] (**19**).

Building on our initial success, the reaction of L_5H with Co(II)(NO_3)$_2$.6H_2O gives rise to the co-crystallisation of the monometallic complex [Co(III)(L_5)$_3$]·H_2O·MeOH (**20a**; purple needle-like crystals and predominant product), along with a much smaller

quantity of red hexagonal crystals, which were found to be the complex $[Co(II)_7(OMe)_6(L_5)_6](NO_3)_2{\cdot}0.5H_2O{\cdot}4MeOH$ (**20b**); akin to the previously described $[M(II/(III)_7]$ (M = Co, Ni) pseudo metallocalix[6]arenes (*cf.* Figure 3.1 and Figure 3.11). Interestingly from a synthetic view point, the deliberate oxidation of Co(II) using hydrogen peroxide efficiently promotes the sole crystallisation of $[Co(III)(L_5)_3]{\cdot}H_2O{\cdot}MeOH$ (**20a**), over the formation of $[Co(II)_7(OMe)_6(L_5)_6](NO_3)_2{\cdot}0.5H_2O{\cdot}4MeOH$ (**20b**). Attempts were made to use various reducing agents to deliberately synthesise solely **20b** but were unsuccessful.

The single Co(III) centre in **20a** (BVS score = 3.22; Table 3.1) is enveloped by three singly deprotonated L_5^- ligands that chelate the metal centre through their N_{imine} and O_{phen} atoms (bond length range: 1.882(2) – 1.961(2) Å) (Fig. 3.9). A single water of crystallisation (O9) lies juxtaposed to the core in **20a** and sits in a pocket at H-bonding distance from three O atoms (O1-O3) located on two separate L_5^- ligands (O1···O9 = 2.99 Å, O2···O9 = 2.86 Å and O3···O9 = 2.79 Å). At a distance of ~2.75 Å from this water molecule lies a disordered (see crystallographic section for details) methanol solvent of crystallisation and is situated at H-bonding distances from protons (H8 and H11) belonging to nearby L_5^- units (O10A···H8(C8) = 2.312 Å and O10B···H11(C11) = 2.50 Å). Together these solvents of crystallisation provide the necessary connectivity between the individual $[Co(III)_1]$ units in **20a** (Figure 3.10).

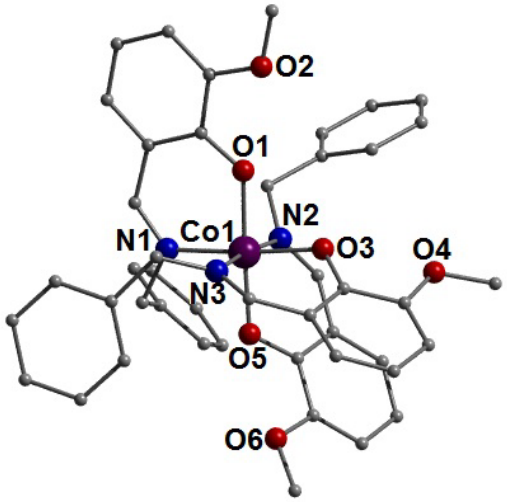

Figure 3.9 Crystal structure of $[Co(III)(L_5)_3]{\cdot}H_2O{\cdot}MeOH$ (**20a**). Hydrogen atoms have been omitted for clarity.

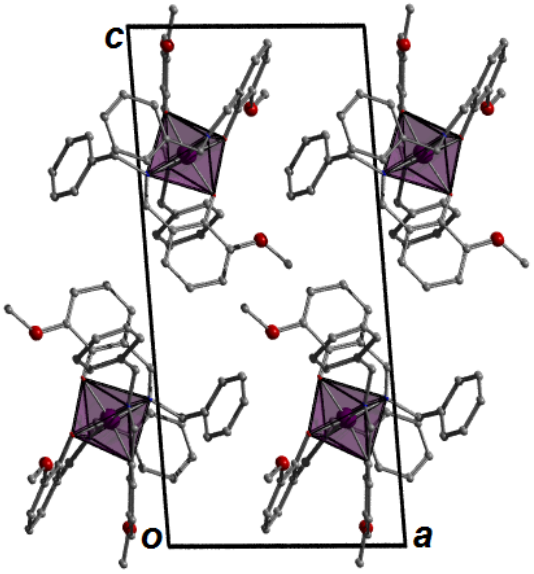

Figure 3.10 Packing arrangement of $[Co(III)(L_5)_3]\cdot H_2O\cdot MeOH$ (**20a**) as viewed along the *b* cell direction. Solvent molecules and hydrogen atoms have been omitted for clarity.

$[Co(II)_7(OMe)_6(L_5)_6](NO_3)_2\cdot 0.5H_2O\cdot 4MeOH$ (**20b**) crystallises in the monoclinic $P2_1/c$ space group and there are two 'half' $\{Co(II)_7\}$ units in the asymmetric unit (labelled Co1–Co4 and Co5–Co8, respectively; centres Co1 and Co5 lie on inversion centres). The inorganic core in **20b** exhibits a planar body centred hexagonal array of Co(II) ions linked together with a combination of μ_3-bridging −OMe and −OH ions (50 : 50 occupancy; see crystallography section for details). The Co(II) oxidation states were assigned using BVS and charge balancing considerations. The outer Co(II) ions (Co2–Co4 and Co6–Co8, respectively) are further connected through $\eta^1{:}\eta^2{:}\eta^1$ μ-bridging L_5^- ligands that lie alternately above and below the planar $\{Co(II)_7\}$ core in **20b**, thus forming the double-bowl pseudo metallocalix[6]arene as observed in our previous studies (Fig. 3.1 *cf.* Fig. 3.11). As with complexes **19** and **20a**, the phenyl ligand groups in **20b** twist away from their corresponding O_{phen} aromatic rings. Interestingly, the torsion angles produced in **20b** vary much more widely when compared with complexes **19** and **20a**, with values including 5.69° (C23–N2–C24–C25), 21.56° (C56–N4–C57–C58) and 89.19° (C86–N6–C87–C89). Thus the ligand conformational flexibility in L_5H, governed by free rotation along the N_{imine}–CH_2 bond, allows the feasible construction of both low (**19** and **20a**) and high nuclearity complexes (**20b**). The individual $[Co(II)_7]$ units arrange in superimposable rows along

the *a* unit cell direction and pack along the *bc* plane in the space-efficient brickwork motif (Fig. 3.12).

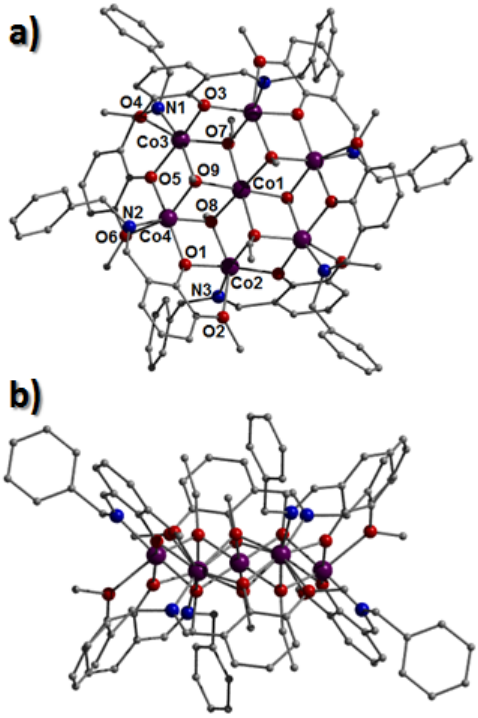

Figure 3.11 Crystal structure observed in $[Co(II)_7(OMe)_6(L_5)_6](NO_3)_2{\cdot}0.5H_2O{\cdot}3MeOH$ (**20b**) as viewed perpendicular (a) and parallel (b) to the $\{Co(II)_7\}$ plane. Hydrogen atoms have been omitted for clarity.

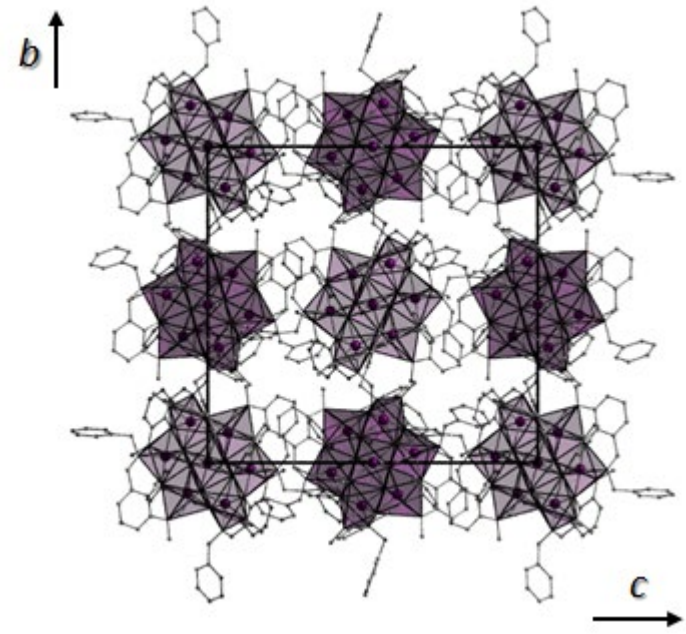

Figure 3.12 Packing arrangement of the [Co(II)$_7$] pseudo metallocalix[6]arenes in **20b** as viewed along the *a* direction of the unit cell. NO_3^- counter anions and H-atoms have been omitted for clarity.

It was decided that by reducing the imine (C=N) bond in L_5H (to give ligand L_6H) we could manipulate ligand shape and allow multiple metal centre coordination and growth of a more complex inorganic core. This proved to be the case when Co(II) / Ni(II) metalation of L_6H (and L_7H) gave rise to the tetranuclear complexes: $[(NO_3)\subset Co(II)_4(\mu_3\text{-}OH)_2(L_6)_4(H_2O)_2](NO_3)\cdot H_2O$ (**21**), $[(NO_3)\subset Ni(II)_4(\mu_3\text{-}OH)_2(L_6)_4(H_2O)_2](NO_3)\cdot H_2O$ (**22**) and $[Ni(II)_4(\mu_3\text{-}OH)_2(L_7)_4(NO_3)_2]\cdot MeCN$ (**23**).

The analogous complexes $[(NO_3)\subset Co(II)_4(\mu_3\text{-}OH)_2(L_6)_4(H_2O)_2](NO_3)\cdot H_2O$ (**21**) and $[(NO_3)\subset Ni(II)_4(\mu_3\text{-}OH)_2(L_6)_4(H_2O)_2](NO_3)\cdot H_2O$ (**22**) crystallise in the triclinic P-1 space group (Z = 1) and each exhibits a butterfly inorganic core whereby the body and wing-tip M(II) (M = Co, Ni) centres are connected by two μ_3-OH^- ions (O1(H1) and s.e.). The Co(II) oxidation states in **21** were confirmed using Bond Valence Sum calculations and charge balancing considerations (Table 3.1). In both **21** and **22**, two of the four singly deprotonated L_6^- ligands exhibit $\eta^1{:}\eta^2{:}\eta^1$ μ-bonding modes while the remaining two demonstrate $\eta^1{:}\eta^2$ μ-bridging arrays whereby their methoxy

functional groups forge long contacts with nearby Co(II) and Ni(II) centres (Co1···O3 = 2.58 Å and Ni1···O5 = 2.31 Å), respectively. The remaining metal centres are six coordinate distorted octahedral sites (Figure 3.13). Terminal water ligands complete the coordination sphere at Co1 at a distance of 2.03 Å (Co1-O6 and s.e) and Ni1 at a distance of 2.04 Å (Ni1-O6 and s.e.). The protons of these terminal waters also participate in H-bonding with a juxtaposed NO_3^- counter anion lying at the periphery of the structures in **21** and **22**. The second nitrate ion in both analogues are situated above the planar {M(II)$_4$} (M = Co, Ni) cores and are disordered over two sites (50:50 occupation and related by a centre of inversion).

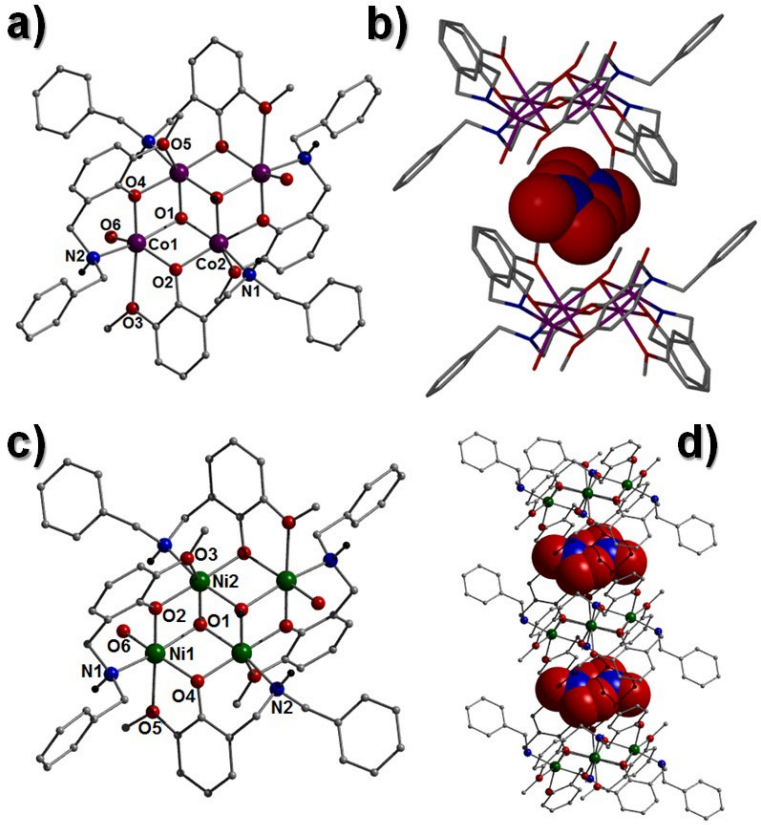

Figure 3.13 (Left) Crystal structures of [(NO$_3$)⊂Co(II)$_4$(μ$_3$-OH)$_2$(L$_6$)$_4$(H$_2$O)$_2$](NO$_3$)·H$_2$O (**21**; a) and [(NO$_3$)⊂Ni(II)$_4$(μ$_3$-OH)$_2$(L$_6$)$_4$(H$_2$O)$_2$](NO$_3$)·H$_2$O (**22**; c). (Right) Space-fill representations of the disordered NO_3^- guests within the molecular cavities formed by two {Co(II)$_4$} metallocalix[4]arene units in **21** (b) and three {Ni(II)$_4$} units in **22** (d). Hydrogen atoms have been omitted for clarity in all cases.

3.2.1 Bond valence model (BVS).

The bond valence model is a popular method in coordination chemistry for using bond lengths to estimate the oxidation state of atoms within a crystal structure.[46,47] In this work the BVS calculations assisted in determining the oxidation states of the cobalt atoms in **20a**, **20b** and **21** as can be seen in Table 3.1.

Table 3.1: BVS calculations on complexes **20a, 20b** and **21**.

Complex	Atom label	BVS result
20a	Co1	3.22
20b*	Co1 (central)	1.96
	Co2 (outer ring)	2.01
	Co3 (outer ring)	2.03
	Co4 (outer ring)	2.00
	Co5 (central)	1.96
	Co6 (outer ring)	2.05
	Co7 (outer ring)	1.99
	Co8 (outer ring)	2.06
21	Co1 (wing-tip)	1.94
	Co2 (body)	2.01

***** There are two independent $\{Co(II)_7\}$ units in the asymmetric unit.

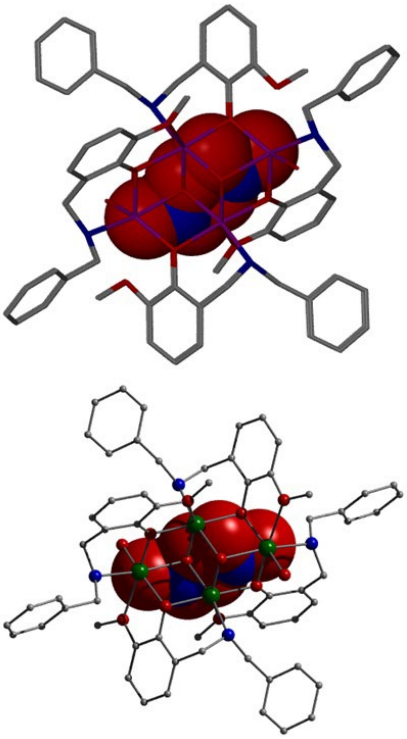

Figure 3.14 Crystal structures of **21** and **22** as viewed perpendicular to the {Co(II)$_4$} plane (top) and {Ni(II)$_4$} plane (bottom), respectively. Disordered NO_3^- counter anions are represented in space-fill mode. Hydrogen atoms have been omitted for clarity.

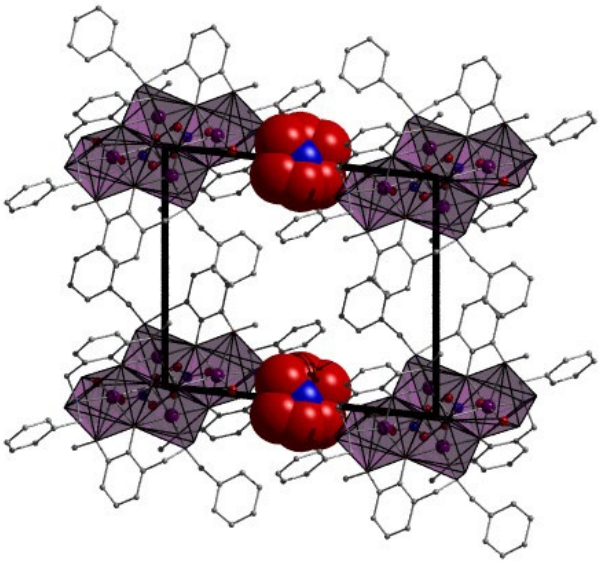

Figure 3.15 Polyhedral representation of the packing arrangement observed in **21** as viewed along the *a*- axis of the unit cell. Hydrogen atoms have been omitted for clarity and NO_3^- anions are space-fill represented.

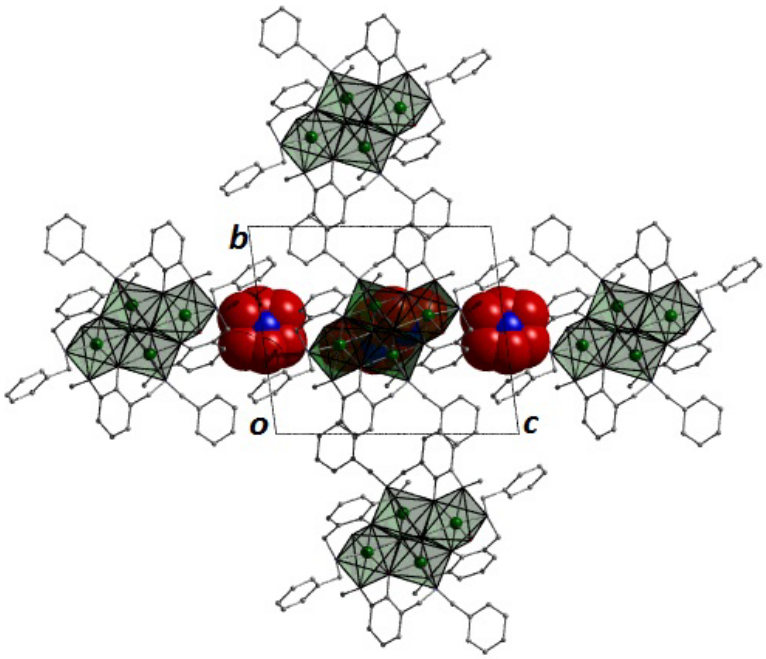

Figure 3.16 Polyhedral representation of the packing arrangement observed in **22** as viewed along the *a* axis of the unit cell. Hydrogen atoms have been omitted for clarity and NO_3^- anions are space-fill represented.

The topologies in **21** (and **22**) also share other structural similarities to that of the previously described heptanuclear metallocalix[6]arene $[(NO_3)_2{\subset}Co(III)Co(II)_6(\mu_3\text{-}OH)_6(L_2)_6](NO_3)$. More specifically and akin to the L_2^{-} ligands in $[(NO_3)_2{\subset}Co(III)Co(II)_6(\mu_3\text{-}OH)_6(L_2)_6](NO_3)$ (Scheme 3.1), the four singly deprotonated L_6^{-} ligands in **21** and **22** sit alternately above and below their planar $\{M(II)_4(\mu_3\text{-}OH)_2\}^{6+}$ (M = Co, Ni) cores. This gives rise to pseudo metallocalix[4]arene topologies in both analogues, where one of the two previously described NO_3^- counter anions occupies the molecular cavity formed by two superimposed $\{M(II)_4\}$ (M = Co, Ni) units as they stack along the *a* axis of the unit cells in both **21** and **22** (Figure 3.13b and Figure 3.13d). These nitrate anions (labelled N3 and O7-9 in both cases) are held in position through H-bonding interactions with protons of nearby μ_3- bridging OH^- ions (O1) and ligated waters (O6) at distances of O1(H1)···O9 = 1.83 Å and O7···O6 = 2.70 Å in **21** and O1(H1)···O9 = 1.82 Å and O7···O6 = 2.74 in **22**, respectively.

On closer inspection we notice that the planar inorganic cores in **21** and **22** may also be described as comprising half of a $\{M(II)_7(\mu_3\text{-}OH)_6\}^{8+}$ (M = Co, Ni) unit as exhibited in (for instance) $[(NO_3)_2{\subset}Co(III)Co(II)_6(\mu_3\text{-}OH)_6(L_2)_6](NO_3)$ and highlighted in Figure 3.13. Indeed, we can assume from these findings that the employment of ligand L_6H has sterically hindered core growth, leading to the formation of the tetrametallic cores in **21** and **22** as opposed to the larger heptametallic core previously observed when using the 2-methoxy-6-[(phenylimino)methyl]phenol ligand (L_2H in Scheme 3.1). This overcrowding and resultant nuclearity change is caused by the introduction of the trigonal pyramidal secondary amine group along with the additional aliphatic carbon atom. The result is a much more distorted ligand shape and although a planar $\{M_x(\mu_3\text{-}OH))_y\}$ (M = Co, Ni) core is achieved, its size has been limited accordingly.

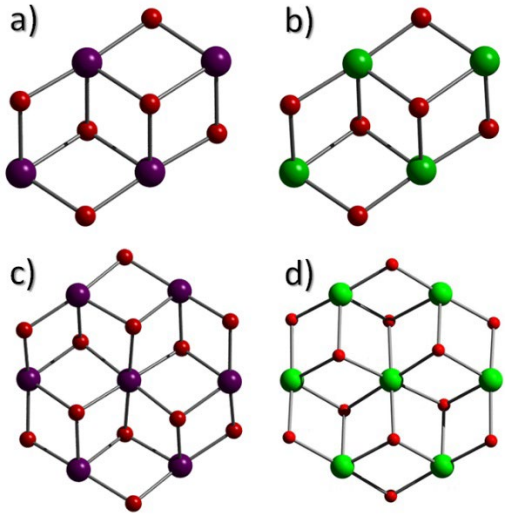

Figure 3.17 The "butterfly" inorganic $\{Co(II)_4(\mu_3\text{-}OH)_2\}^{6+}$ and $\{Ni(II)_4(\mu_3\text{-}OH)_2\}^{6+}$ cores in **21** (a), **22** and **23** (b). The heptanuclear $\{Co(III)Co(II)_6(\mu_3\text{-}OH)_6\}^{9+}$ and $\{Ni(II)_6(\mu_3\text{-}OH)_6\}^{8+}$ cores as observed in (c) the original pseudo metallocalix[6]arene complexes $[(NO_3){\subset}Co(III)Co(II)_6(\mu_3\text{-}OH)_6(L_2)_6](NO_3)_2$ (c) and $[Ni(II)_7(\mu_3\text{-}OH)_6(L_1)_6](NO_3)_2$ (d).[1-3] Hydrogen atoms have been omitted for clarity. Colour code: Co (purple), Ni (green), O (red).

The tetranuclear butterfly $\{Ni(II)_4\}$ core in **22** is once again observed upon the construction of the complex $[Ni(II)_4(\mu_3\text{-}OH)_2(L_7)_4(NO_3)_2]\cdot MeCN$ (**23**). Complex **23** was obtained from the reaction of $Ni(NO_3)_2.6H_2O$ and L_7H (Br analogue to L_6H) in the presence of a suitable base (NaOH) using either MeOH or MeCN as reaction media (see experimental section for details). Complex **23** crystallises in the Triclinic P-1 space group and comprises two complete $\{Ni(II)_4\}$ units in the asymmetric unit. Akin

to **21** and **22**, the butterfly cores in **23** are connected by two μ_3-bridging OH^- ions (O5 and s.e.) and a combination of $\eta^1{:}\eta^2{:}\eta^1$ μ- and $\eta^1{:}\eta^2$ μ-bridging L_7^- ligands (Figure 3.18). However, complex **23** does differ from **21** and **22** in that the NO_3^- counter anions do not sit within the molecular cavities in **23** and instead occupy the remaining ligation spots at the distorted octahedral metal centres (Ni1 and Ni3) through chelation. This significant difference expectedly gives rise to a different packing topology in **23** (*cf.* **21** and **22**). Here, the individual $\{Ni(II)_4\}$ units are connected to one another through H-bonding interactions between their μ_3-OH^- protons and Br- groups of neighbouring cages ((e.g. O5(H5)···Br4 = 2.54 Å and O105(H105)···Br2 = 2.62 Å; Fig. 3.19). Intramolecular H-bonds are observed between the tertiary amine protons and chelating NO_3^- counter anions (i.e. N2(H2)···O7 = 2.23 Å and N102(H102)···O107 = 2.17 Å) and oxygen atoms belonging to OMe groups on each L_7^- unit (N1(H1)···O3 = 2.19 Å and N101(H101)···O103 = 2.21 Å). Intermolecular interactions also arise between aromatic L_7^- protons (i.e. H3 and H127) and chelating NO_3^- anions (i.e. O8) at distances of (Å): 2.48 (C3(H3)···O8) and 2.60 (C127(H127)···O8). Weak intermolecular H-bonding also occurs between the protons of aromatic rings (i.e. H11) and OMe groups (H16A) of the L_7^- ligands with juxtaposed Br atoms also belonging to nearby ligand units (C16(H16A)···Br1 = 3.03 Å and C11(H11)···Br1 = 2.98 Å). The individual $\{Ni(II)_4\}$ units in **23** pack in a space efficient brickwork manner as shown in Figure 3.20.

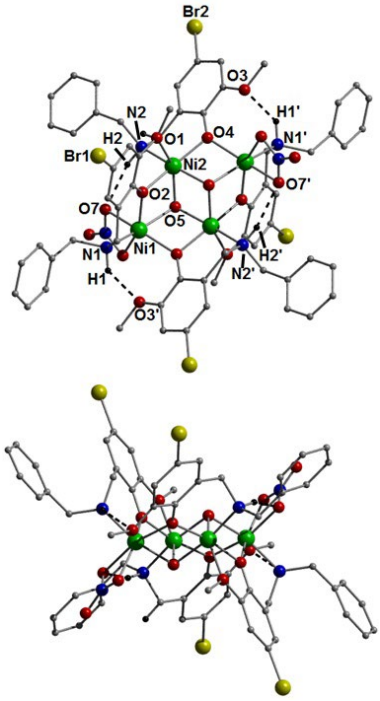

Figure 3.18 Crystal structure of one of the two $[Ni(II)_4(\mu_3\text{-}OH)_2(L_7)_4](NO_3)_2$ units observed in the a.s.u of **23** as viewed perpendicular (top) and parallel (bottom) to the $\{Ni(II)_4\}$ plane. Majority of H-bonds have been omitted for clarity. Dashed lines represent intramolecular H-bonds at distances (Å): N1(H1)···O3′ = 2.19 and N2(H2)···O7′ = 2.23.

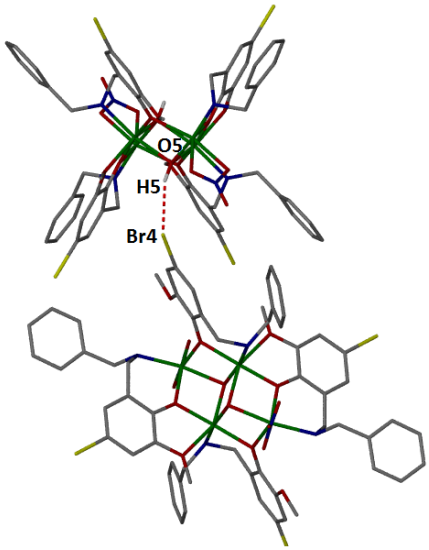

Figure 3.19 Intermolecular H-bonding interaction (red dashed line) between two $\{Ni(II)_4\}$ units in **23** (O5(H5)···Br4 = 2.54 Å). Hydrogen atoms omitted for clarity.

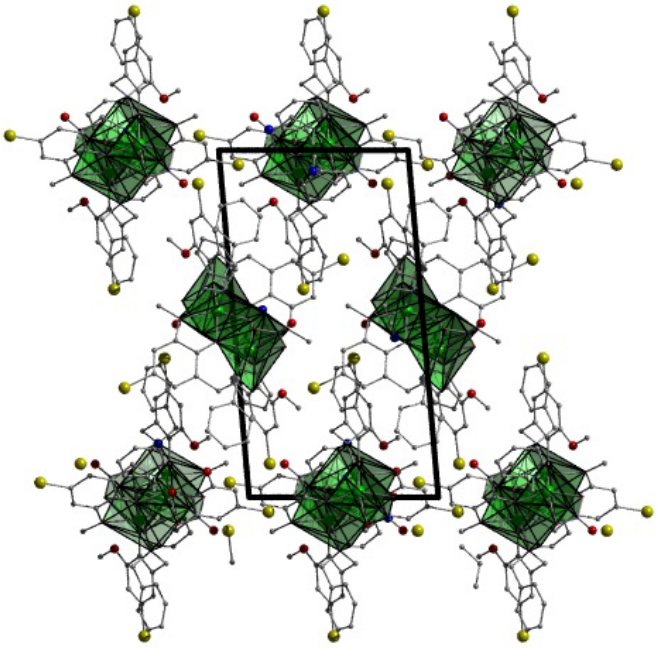

Figure 3.20 Polyhedral representation of the packing arrangement observed in **23** as viewed along the *b* axis of the unit cell. Hydrogen atoms and NO_3^- anions have been omitted for clarity.

3.3 Magnetic studies

The dc (direct current) molar magnetic susceptibility, χ_M, of polycrystalline samples of (**17**), (**21**) and (**23**) were measured in an applied magnetic field, B, of 0.1 T, in the T = 2-300 K temperature range. The experimental results are shown in Figure 3.21 in the form of the $\chi_M T$ products, where $\chi = M/B$, and M is the magnetisation of the sample. For **17**, the $\chi_M T$ product of 2.10 $cm^3\ mol^{-1}\ K$ at T = 280 K is close to that expected for two non-interacting Ni(II) ions (2.40 $cm^3\ mol^{-1}\ K$) assuming $g_{Ni} = 2.2$, where g_{Ni} is the g-factor of Ni(II). Upon cooling, the value of $\chi_M T$ increases reaching a maximum of 2.93 $cm^3\ mol^{-1}\ K$ at 13 K, before decreasing to 1.76 $cm^3\ mol^{-1}\ K$ at 2 K. This increase is indicative of weak intramolecular ferromagnetic exchange interactions between the phenoxo-bridged Ni(II) ions, with the sharp decrease in the value of $\chi_M T$ at low temperature attributed to antiferromagnetic intermolecular interactions between neighbouring dimers and/or zero-field splitting (zfs) effects. The susceptibility and magnetisation data were fitted simultaneously using the program PHI and a spin-Hamiltonian of the form.[48,49]

$$\hat{H} = -2\sum_{i,j>i}^{n} \hat{S}_i J_{ij} \hat{S}_j + \mu_B \sum_{i=1}^{n} \vec{B}\, g_i \hat{S}_i + \sum_{i=1}^{n} D\left[\hat{S}_{z,i}^2 - S_i(S_i+1)/3\right] \quad (1)$$

where $\hat{S}$ is a spin operator, J is the pairwise isotropic magnetic exchange interaction between constitutive N(II) centres, μ_B the Bohr magneton, $\vec{B}$ the external static magnetic field, g the isotropic g-factor of Ni(II) (fixed to g = 2.2; see EPR section below), the indices *i* and *j* refer to the two Ni ions, *D* is the second-order single-ion uniaxial anisotropy parameter of Ni(II) and $\hat{S}_{z,i}^2$ is the Cartesian component of spin operator $\hat{S}$ of the i^{th} Ni(II) centre along the z-direction of the local coordinate frame. The best-fit parameters obtained were $2J = 7.70$ cm^{-1} and $D_{Ni} = 7.42$ cm^{-1}. These values are close to that obtained from simulations of the EPR spectra (*vide infra*). The fit of the susceptibility data can be improved marginally through the addition of an intermolecular interaction, $zJ' = -0.09$ cm^{-1}. Examples of ferromagnetically coupled phenoxo-bridged Ni(II) dimers are rather rare,[50,51] with most being either heteroleptic,[52,53] or homoleptic and possessing Ni-O-Ni bridging angles less than 99 °.[54] Note that the asymmetric Ni-O-Ni bridging angles in (**17**) are of 96.11° and 101.77° (see Figure 3.22 for the Zeeman energy diagram for **17**).

The susceptibility data for (**21**) and (**23**) are also given in Figure 3.21. The $\chi_M T$ value of (**23**) at 300 K is 4.85 cm^3 mol^{-1} K which is in excellent agreement with the expected high temperature value for four $S = 1$ ions ($g_{Ni} = 2.2$, $\chi_M T = 4.84$ cm^3 mol^{-1} K). Upon cooling, the value of $\chi_M T$ remains essentially constant until approximately 60 K where it begins to decrease rapidly reaching a minimum of 0.150 cm^3 mol^{-1} K at 2 K. This behaviour is indicative of weak antiferromagnetic exchange between the metal ions, and/or zfs effects. The susceptibility and magnetisation data were fit simultaneously as described above using the exchange coupling scheme depicted in the inset of Figure 3.21 (bottom). The best-fit parameters obtained were $J_1 = -2.84$ cm^{-1}, $J_2 = 17.85$ cm^{-1} and $D_{Ni} = 12.43$ cm^{-1} (see Figure 3.23 for the corresponding Zeeman energy diagram for **23**).

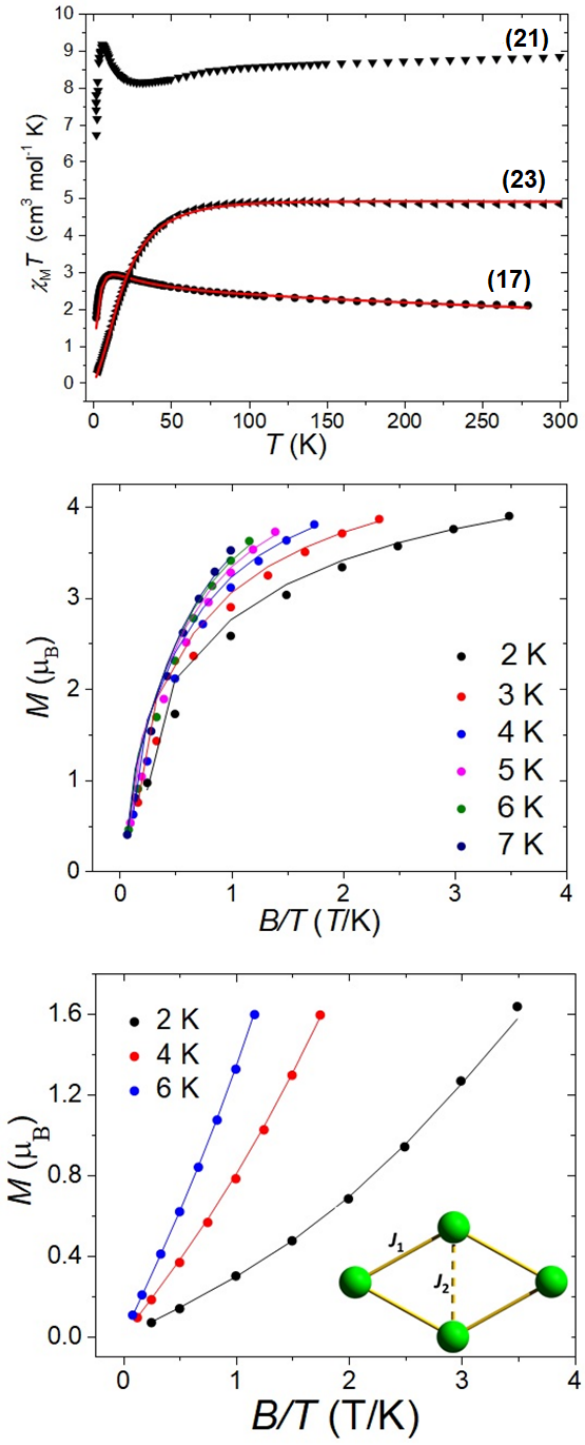

Figure 3.21 Top: Plot of $\chi_M T$ versus T for complexes (**17**), (**21**) and (**23**). Middle: Reduced magnetisation data for complex (**17**). Bottom: Reduced magnetisation data for complex (**23**). The inset shows the exchange coupling scheme used to fit the data; $\hat{H} = -2J_1(\hat{S}_1 \cdot \hat{S}_2 + \hat{S}_2 \cdot \hat{S}_3 - \hat{S}_3 \cdot \hat{S}_4 + \hat{S}_4 \cdot \hat{S}_1) - 2J_2(\hat{S}_2 \cdot \hat{S}_4)$. The solid lines represent a simultaneous best-fit of the experimental susceptibility and magnetisation data as described in the main text.

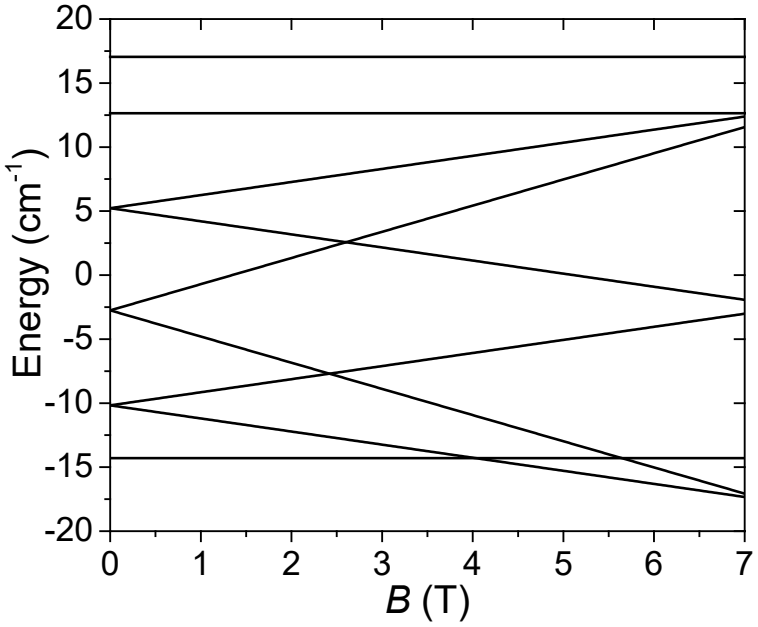

Figure 3.22 Zeeman diagram for complex (**17**) generated from the best fit parameters obtained from a simultaneous fit of the susceptibility and magnetization data.

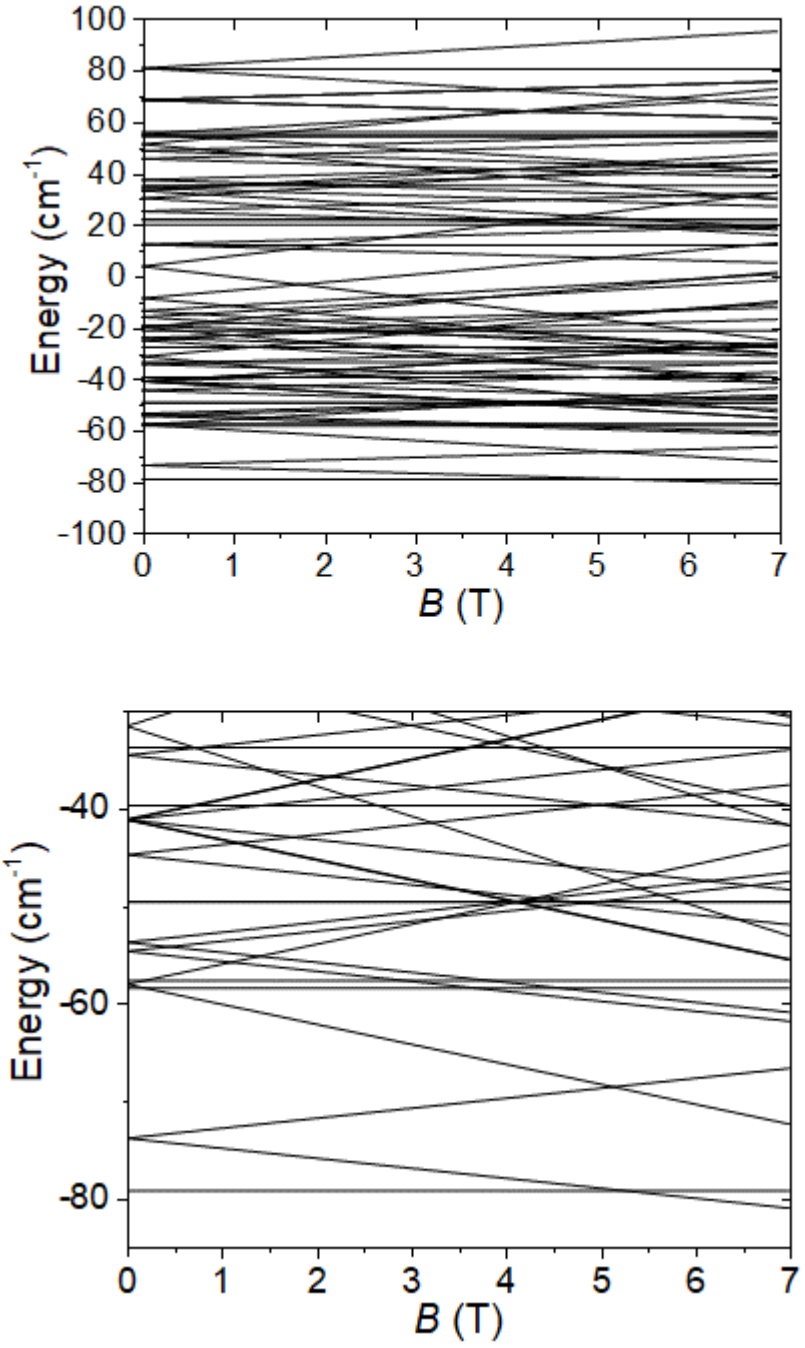

Figure 3.23 (top) Zeeman diagram for complex (**23**) generated from the best fit parameters obtained from a simultaneous fit of the susceptibility and magnetization data. See main text for details. (bottom) Zeeman diagram highlighting the lowest lying energy levels for complex (**23**) generated from the best fit parameters obtained from a simultaneous fit of the susceptibility and magnetization data. See main text for details.

The coupling constants obtained are in line with that derived for previously published, structurally analogous [Ni(II)$_4$] systems; the dominant structural parameter being the average Ni-O-Ni angle of the cubane faces.[54] Ferromagnetic exchange interactions would be expected for Ni-O-Ni angles < 99° (Ni2-O-Ni4, ~95°), with antiferromagnetic exchange interactions at Ni-O-Ni angles ≳ 99° (Ni1-O-Ni4 and Ni2-O-Ni3, ~99°; Ni1-O-Ni2 and Ni3-O-Ni4, ~98-105°).[55,56] The D_{Ni} value extracted from the fits is in the same range as that found in (**17**) and that previously reported for Ni(II) ions in a distorted octahedral environment with similar donor atoms.[57]

For (**21**) the value of $\chi_M T$ at 300 K is 8.84 cm^3 mol^{-1} K (Figure 3.21), a value close to that expected for four non-interacting Co(II) ions (S = 3/2, g_{Co} = 2.2, $\chi_M T$ = 9.07 cm^3 mol^{-1} K). Upon cooling the value of $\chi_M T$ decreases, reaching a minimum of 8.14 cm^3 mol^{-1} K at 28 K, before increasing to a maximum value of 9.18 cm^3 mol^{-1} K at 6 K, and then decreasing to 6.72 cm^3 mol^{-1} K at 2 K. This behaviour is commonly observed for complexes containing octahedral Co(II) ions: the initial decrease in $\chi_M T$ is due to the orbital contribution of the Co(II) ions, the increase to the maximum at T = 6 K due to the presence of some ferromagnetic interactions, with the decrease below this temperature attributed to antiferromagnetic exchange interactions and/or zfs effects.[57-60]

Magnetisation data is consistent with the presence of competing F/AF exchange and the presence of significant anisotropy (Figure 3.24). First order spin orbit coupling effects associated with the octahedral Co(II) ion preclude any simple quantitative analysis of the data. No out-of-phase ac signals were observed for **21**, even in the presence of an applied dc field.

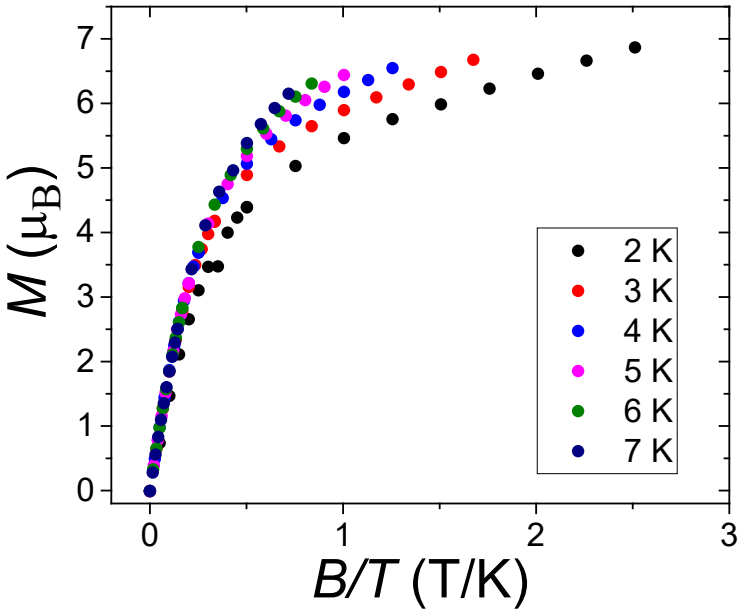

Figure 3.24 Reduced magnetisation (M/μ_B) vs. B/T (T/K) data obtained from a polycrystalline sample of **21** measured within the 2-7 K temperature range and 0-7 T magnetic field range.

3.3.1 MF / HF EPR spectroscopy

In order to refine the values obtained from the fitting of the magnetic measurements for complex **17**, multi-frequency/high-field EPR was employed on a powdered and pelletised sample. Spectra were recorded at several frequencies ranging from 95 to 662 GHz and in the temperature range 5-25 K (Figures 3.25 and 3.26 and 3.27).

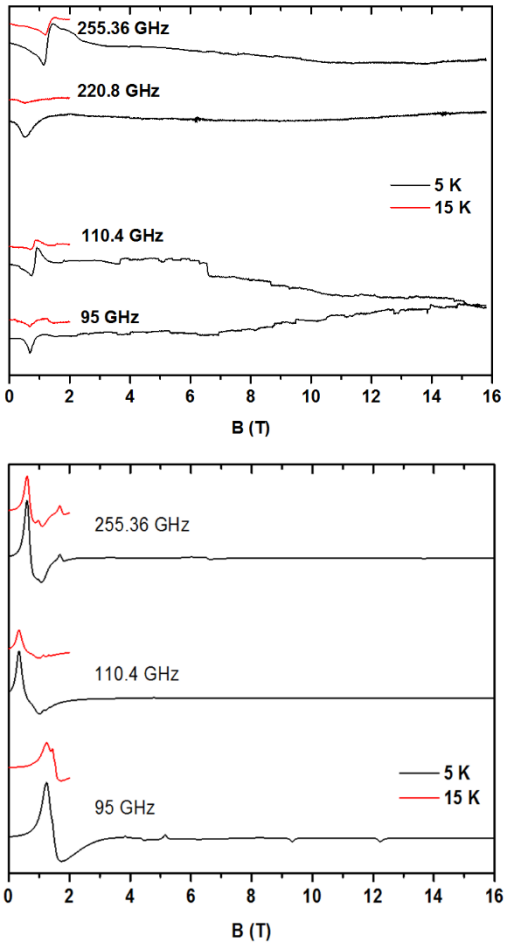

Figure 3.25 (top) Experimental MF/HF-EPR spectra obtained on a polycrystalline pelletised sample of **17** exhibiting a close to zero field transition. The intensity decrease with the increase of temperature indicates that these signals arise from the ground state spin level. Intensities have been rescaled from one frequency to the other. (Bottom) Simulated MF/HF-EPR spectra of **17** with the multispin model and the parameters described in the main text. Intensities have been rescaled from one frequency to the other.

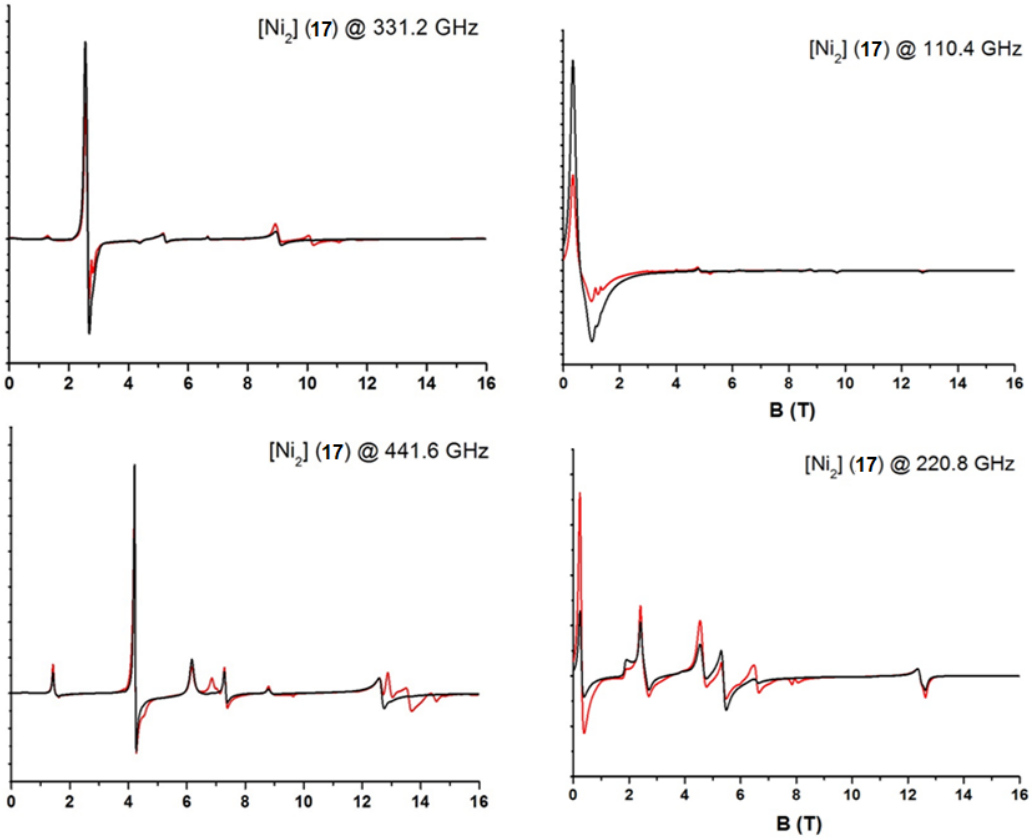

Figure 3.26 Simulated HF EPR spectra for [Ni(II)$_2$] (**17**) at frequencies 110.4 (top right) and 220.8 GHz (bottom right) at 15 K (red line) and 5 K (black line). Simulated HF EPR spectra for [Ni(II)$_2$] (**17**) at frequencies 331.2 (top left) and 441.6 GHz (bottom left) at 15 K (red line) and 5 K (black line).

For all frequencies, only a few signals were observed whose intensities change with temperature. At 331 and 442 GHz, besides the strong forbidden transition (at ~2.55 and ~3.88 T, respectively), small signals at higher fields (9 to 10 T at 331.2 GHz and 12 to 14 T at 442 GHz) were also recorded. These permitted signals are attributed to the accessing of successive energy levels from the lowest level group (which would belong to the $S = 2$ multiplet in the strong coupling limit) for the y orientation. At 110 GHz and for the frequency range 220-255 GHz, we observe close to zero signals and is indicative of the existence of gaps, in the spin energy diagram, of approximately 3.6 and 7.3 cm^{-1}, respectively. The structure of the spectra does not allow for a simple analysis, as expected from the results of the magnetic measurements, which suggest that $|D_1|$, $|D_2|$ and $|2J|$ are comparable. Simulations of the spectra were thus performed in the frame of the following Hamiltonian for a coupled Ni(II) dimer:

Eqn. 2: $H_{-}=\mu_B\, gB\cdot(S_1+S_2) - 2J\, S_1.S_2 + D_1\,(S_{1z}^2 - S(S+1)/3) + E_1\,(S_{1x}^2 - S_{1y}^2) + D_2\,(S_{2z}^2 - S(S+1)/3) + E_2\,(S_{2x}^2 - S_{2y}^2)$

where μ_B is the Bohr magneton, g is the single ion g-matrix, *J* is the magnetic exchange parameter, *S* is the spin quantum number, and *D* and *E* are the ZFS and rhombic parameters, respectively. In order to avoid over parameterization, the description of the system is simplified significantly, due to the reduced number of (independent) transitions detected in the experimental spectra. The assumption of the collinearity of both ZFS tensors is the most drastic. In addition, both g values were taken as identical and the anisotropy of the g factors neglected. These last approximations are expected to affect the calculated spectra much less, due to the masking effect of the ZFS terms over variations of the Zeeman effect. Simulations of the experimental spectra, for which the resonance positions are rather well reproduced (Figure 3.26), were obtained for the following set of parameters: D_1 = 10(1) cm^{-1}, E_1 = 2.5(6) cm^{-1}, D_2 = 9(1) cm^{-1}, E_2 = 2.25(65) cm^{-1}, $g_1 = g_2 = g$ = 2.2(2) and $2J$ = 7.5(1.5) cm^{-1}. The D_i (I = 1,2) and $2J$ values obtained compare well with those obtained from the magnetic studies. The E_i values reported have been chosen, among the possible sets of values, so that they lead to the same E_i / D_i ratio. Indeed, the three or four lowest energy levels of the system behave very similarly to changes on E_i if E_1+E_2 is constant. One may notice a discrepancy in the temperature behaviour of the signals associated to the *y* orientation at 331 and 442 GHz. This can be corrected through a change on E_i (i = 1, 2) values, at the expense of worsening the simulation of the low field signals (observed at 110 and 220-255 GHz frequencies). Despite our best efforts, it has not been possible to find parameters fully satisfying for all the identified signals, most probably as a result of the simplified model used. Finally, the spectra clearly shows that the magnetic anisotropy of **17** is rather rhombic (Ei/Di = 0.25) for both Ni(II) ions.

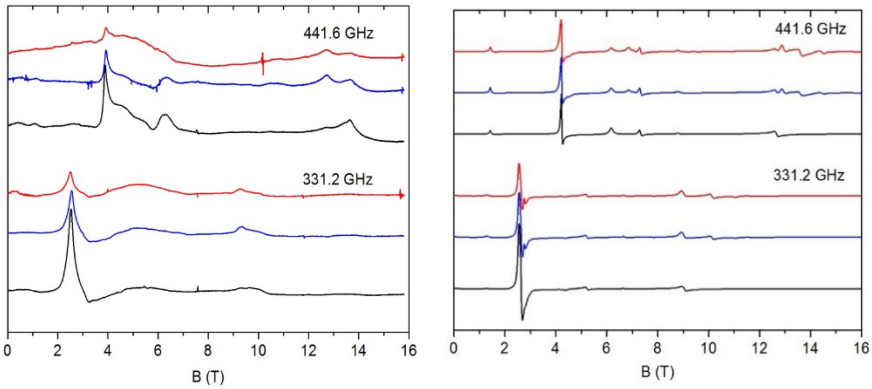

Figure 3.27 Experimental (top) and simulated (bottom) MF / HF-EPR spectra obtained on a polycrystalline pelletised sample of $[Ni(II)_2(L_3)_3(H_2O)](NO_3)\cdot 2H_2O\cdot 3MeOH$ (**17**) at frequencies of 331.2 and 441.6 GHz and temperatures of 25 K (red line), 15 K (blue line) and 5 K (black line).

Table 3.2 X-ray crystallographic data obtained from complexes **17**-**20a**.

	17.2H_2O.3MeOH	**18**.4MeOH.6H_2O	**19**	**20a**·H_2O·MeOH
Formula[a]	$C_{48}H_{60}N_4O_{18}Ni_2$	$C_{64}H_{58}N_5O_{21}Na_1Ni_2$	$C_{30}H_{28}N_2O_4Ni_1$	$C_{46}H_{48}N_3O_8Co_1$
M_W	1098.39	1373.56	539.25	829.82
Crystal System	Monoclinic	Triclinic	Triclinic	Triclinic
Space group	$P2_1/n$	P-1	P-1	P-1
a/Å	12.6966(4)	12.9739(4)	6.7178(3)	10.3690(2)
b/Å	10.1709(3)	14.7434(4)	9.3940(4)	10.7727(3)
c/Å	38.0873(11)	18.7650(6)	10.1699(4)	20.5457(7)
α/°	90	83.407(2)	69.232(4)	85.474(2)
β/°	92.904(3)	81.431(2)	87.650(4)	84.339(2)
γ/°	90	74.414(2)	89.471(4)	63.261(3)
V/Å^3	4912.1(3)	3408.22(18)	599.58(5)	2038.05(10)
Z	4	2	1	2
T/K	100(2)	100(2)	100(2)	100(2)
λ[b]/Å	0.71073	0.71073	0.71075	0.71073
D_c/g cm^{-3}	1.307	1.338	1.493	1.271
μ(Mo-Ka)/ mm^{-1}	0.829	0.634	0.851	0.472
Meas./indep.(R_{int}) refl.	50784 / 8992 (0.0628)	16889 / 12490 (0.0683)	6995 / 3018 (0.0221)	
Restraints, Parameters	7, 563	2, 831	0, 170	41114 / 7469 (0.0366)
wR2 (all data)	0.1965	0.1806	0.0889	0, 499
$R1$[d,e]	0.0683	0.0656	0.0293	0.0929
Goodness of fit on F^2	1.057	1.020	1.185	0.0469

[a] Includes guest molecules (Note: Solvents of crystallisation in **21** and **24b** are not counted in formula due to the employment of the SQUEEZE program). [b] Mo-Kα radiation, graphite monochromator. [c] $wR2 = [\Sigma w(|F_o^2| - |F_c^2|)^2 / \Sigma w|F_o^2|^2]^{1/2}$. [d]For observed data. [e] $R1 = \Sigma||F_o| - |F_c|| / \Sigma|F_o|$.

Table 3.3 X-ray crystallographic data obtained from complexes **20b-23**.

	20b.0.5H_2O.4MeOH	**21**·H_2O	**22**·H_2O	**23.**MeCN
Formula[a]	$C_{97}H_{110}N_8O_{28.5}Co_7$	$C_{60}H_{72}N_6O_{19}Co_4$	$C_{60}H_{72}N_6O_{19}Ni_4$	$C_{62}H_{65}Br_4N_7O_{16}Ni_4$
M_W	2256.48	1414.94	1416.07	1718.69
Crystal System	Monoclinic	Triclinic	Triclinic	Triclinic
Space group	$P2_1/c$	P-1	P-1	P-1
a/Å	19.8705(5)	9.0455(6)	9.0156(2)	11.1808(5)
b/Å	22.1327(4)	12.6133(9)	12.5137(2)	15.8405(5)
c/Å	23.1956(4)	14.4430(10)	14.5497(2)	20.5877(5)
α/°	90	92.607(6)	93.1290(10)	105.986(2)
β/°	94.902(2)	104.914(6)	105.662(2)	90.324(3)
γ/°	90	103.757(6)	105.280(2)	105.805(3)
V/Å^3	10163.8(4)	1536.64(18)	1510.62(5)	3359.9(2)
Z	4	1	1	2
T/K	100(2)	100(2)	100(2)	100(2)
λ[b]/Å	0.71073	0.71073	0.71073	0.71075
D_c/g cm^{-3}	1.309	1.529	1.557	1.699
μ(Mo-Ka)/ mm^{-1}	1.177	1.139	2.027	3.553
Meas./indep.(R_{int}) refl.	23280 / 19171 (0.0726)	19357 / 5605 (0.0592)	28299 / 5493 (0.0403)	35525 / 12305(0.0522)
Restraints, Parameters	6, 1133	8, 460	18, 459	36, 851
wR2 (all data)	0.3316	0.0968	0.1036	0.1597
$R1$[d,e]	0.1737	0.0454	0.0374	0.0580
Goodness of fit on F^2	1.335	1.048	1.029	1.044

[a] Includes guest molecules (Note: Solvents of crystallisation in **21** and **24b** are not counted in formula due to the employment of the SQUEEZE program). [b] Mo-Kα radiation, graphite monochromator. [c] $wR2 = [\Sigma w(|F_o^2| - |F_c^2|)^2 / \Sigma w|F_o^2|^2]^{1/2}$. [d]For observed data. [e] $R1 = \Sigma||F_o| - |F_c|| / \Sigma|F_o|$.

3.4 Concluding remarks.

We have described the synthesis and characterisation of a family ligands in the form of 2-methoxy-6-{[(2-methoxybenzyl)imino]methyl}phenol (L_3H), methyl (E)-4-((2-hydroxy-3-methoxybenzylidene)amino)benzoate (L_4H) 2-[(benzylimino)methyl]-6-methoxyphenol (L_5H), 2-[(benzylamino)methyl]-6-methoxyphenol (L_6H) and 2-[(benzylamino)methyl]-4-bromo-6-methoxyphenol (L_7H). Their subsequent complexation with Co(II) and Ni(II) ions gave rise to the dimetallic complex $[Ni(II)_2(L_3)_3(H_2O)](NO_3).2H_2O.3MeOH$ (**17**) and $[Na(I)Ni(II)_2(\mu\text{-}OH)(L_4H)(L_4)_3(H_2O)_2](NO_3)$ (**18**), the monometallic complexes $[Ni(II)(L_5)_2]$ (**19**) and $[Co(III)(L_5)_3]\cdot H_2O\cdot MeOH$ (**20a**) species (initially co-crystallised with $[Co(II)_7(OMe)_6(L_5)_6](NO_3)_2\cdot 0.5H_2O\cdot 3MeOH$ (**20b**) along with the tetranuclear siblings $[(NO_3)\subset Co(II)_4(\mu_3\text{-}OH)_2(L_6)_4(H_2O)_2](NO_3)\cdot H_2O$ (**21**), $[(NO_3)\subset Ni(II)_4(\mu_3\text{-}OH)_2(L_6)_4](NO_3)\cdot H_2O$ (**22**) and $[Ni(II)_4(\mu_3\text{-}OH)_2(L_7)_4(NO_3)_2]\cdot MeCN$ (**23**). Complexes **17**-**23** represent the first examples of transition metal coordination of ligands $L_{3\text{-}7}H$. The inorganic planar cores in **21**-**23** ($\{M(II)_4(\mu_3\text{-}OH)_2\}^{6+}$ (M = Co and Ni)) may be viewed as fragments of the $\{M(II)_7(\mu_3\text{-}OH)_6\}^{8+}$ (M = Co, Ni) and $\{Co(III)Co(II)_6(\mu_3\text{-}OH)_6\}^{9+}$ cores observed within our previously reported pseudo metallocalix[6]arenes,[1-3] which were constructed using similar Schiff base ligands (L_1H and L_2H in Scheme 3.1).

This work shows how even minor modifications to the ligand employed gives rise to dramatic changes with respect to the polymetallic cage topologies formed (i.e. (ranging from $[M_1]$ to $[M_7]$). SQUID measurements on $[Ni(II)_2(L_3)_3(H_2O)](NO_3)\cdot 2H_2O\cdot 3MeOH$ (**17**) reveal weak ferromagnetic exchange interactions between the two Ni(II) ions; a simultaneous fit of the susceptibility and magnetisation data affording $2J = 7.70$ cm^{-1} and $D_{Ni} = 7.42$ cm^{-1}, in agreement with simulations of the EPR data. Thus complex (**17**) is therefore a rather rare example of a ferromagnetically coupled diphenoxo-bridged $[Ni(II)_2]$ complex, especially given the unusual Ni-O-Ni bridging angles. Even if it has not been possible to obtain a fully reliable set of parameters from the MF/HF EPR spectra of **17**, the analysis of the spectra do confirm the ferromagnetic character of the coupling. Indeed, the forbidden transition evolves with a g_{eff} value close to 8 and more generally the spectra exhibit

similarities with the S = 2 spectra obtained for the strong coupling limit of the single ion parameters. This is because the signals observed come from the lowest energy levels, corresponding to the S = 2 levels in the strong coupling limit. However, changing the *J* value modifies the resonance positions. The best fit of the susceptibility and magnetisation data of $[Ni(II)_4(\mu_3\text{-}OH)_2(L_7)_4(NO_3)_2]\cdot MeCN$ (**23**), assuming a butterfly-like structure incorporating two different exchange interactions (wing-body and body-body) provided $2J_1$ = -5.68 cm^{-1}, $2J_2$ = 35.70 cm^{-1} and D_{Ni} = 12.43 cm^{-1}, values entirely consistent with previously published data on complexes with a similar diamond-like arrangement of the metal ions. The tetrameric $[(NO_3)\subset Co(II)_4(\mu_3\text{-}OH)_2(L_6)_4(H_2O)_2](NO_3)\cdot H_2O$ (**21**) cluster demonstrates competing anti- and ferromagnetic exchange along with significant anisotropy.

3.5 Experimental Section

3.5.1 General details

Infra-red spectra for all complexes were obtained from a newly acquired Bruker Alph*a* FT-IR *Platinum ATR* spectrometer (School of Chemistry, Bangor University). Elemental analysis was carried out at the OEA Laboratories Ltd (Kelly Bray, Cornwall, UK). MALDI TOF-MS measurements on complexes **21** and **23** were carried out at the EPSRC UK National Mass Spectrometry Facility at Swansea University. Powder XRD was carried out using a PANalytical Philips X`Pert 3040/60 diffractometer at 45 kV and 35 mA between 5 and 60° 2θ using Ni-Filtered Cu-$K_{\alpha 1}$ radiation (λ = 1.5405 Å) at the School of Chemistry, Bangor University.

3.5.2 Crystallographic details

All complexes were collected on an Rigaku AFC12 goniometer equipped with an enhanced sensitivity (HG) Saturn724+ detector mounted at the window of an FR-E+ Super Bright molybdenum rotating anode generator with HF Varimax optics (100m focus). The cell determination and data collection of all complexes were carried out using the CrystalClear-SM Expert package (Rigaku, 2012). Each data reduction, cell refinement and absorption correction were carried out using CrysAlisPro

software (Rigaku OD, 2015),[61] while all structures were initially solved and refined using SHELXT and SHELXL-2014[62] within OLEX-2.[63] All structures were refined and completed in-house by full matrix least squares using SHELXL-97[64] and refined with OSCAIL packages.[65]

3.5.3 Collection and refinement details

Due to modelling difficulties the residual electron densities representing solvent entities within the solvent accessible voids (total volume ~971 $Å^3$) in **17** were modelled using the SQUEEZE program.[66] The NO_3^- counter anion required the DFIX, DANG and FLAT restraints and remained isotropic. All protons in **17** were assigned to calculated positions.

The NO_3^- counter anion in $[Na(I)Ni(II)_2(\mu\text{-}OH)(L_4H)(L_4)_3(H_2O)_2](NO_3)$ (**18**) is modelled as disordered over two sites (50:50). All other non hydrogen atoms were modelled as anisotropic. All hydrogen atoms were assigned to calculated positions.

All non hydrogen atoms were modelled as anisotropic in **19**, while all hydrogen atoms were assigned to calculated positions. The SQUEEZE program was also employed in the treatment of **20a**, giving a total void volume of 551 $Å^3$ and resulting in the removal of 55 electrons from the structure. This electron density has been assigned as representing 1 x MeOH and 1 x H_2O solvent molecule per $[Co_1]$ molecule (Z = 2).

The μ_3-bridging $^-$OMe ions in **20b** were best modelled as sharing 50:50 occupancy with bridging $^-$OH moieties. At two of these positions, half occupancy waters of crystallisation (labelled O50 and s.e.) lie above these bridging $^-$OMe / $^-$OH ions and are presumed to partake in H-bonding with the $^-$OH moieties at distances of 2.84 Å (O18···O50). DFIX restraints were employed on the O-CH_3 distances of all bridging –OMe functional groups in **20b**. All non-hydrogen atoms in **20b** apart from the bridging $^-$OMe carbons (labelled C46-C48 and C94-96) were refined anisotropically and all protons were assigned to calculated positions. Due to modelling difficulties the residual electron densities representing NO_3^- counter anions and solvent entities within

the solvent accessible voids (total volume ~1911 Å^3; ~77 electrons per cage) in **20b** were modelled using the SQUEEZE program to give the final formula $[Co(II)_7(OMe)_6(L_4)_6](NO_3)_2{\cdot}0.5H_2O{\cdot}4MeOH$.[66]

All non-hydrogen atoms in complexes **21** and **22** were modelled as anisotropic. Both the NO_3^- counter anions in **21** were restrained using the DFIX command. The $^-$OH proton (H1) and the terminal water protons (H6A and H6B) in **21** were assigned to calculated positions, while the corresponding water protons in **22** (H6A and H6B) were located in the difference map. All other protons were assigned to calculated positions. In complexes **21** and **22**, both nitrates were found to be disordered over two sites (one of which lies at a special position while the other shares space with a water of crystallisation (labelled O7A in **21** and O13 in **22**). Both were modelled at half occupancy. The selected single crystal in **23** contains light green hexagonal plates. Most crystals within the sample looked twinned and gave multicomponent diffraction patterns. A small clean fragment was selected for collection (Fig. 3.30). Large residual electron density peaks observed were attributed to small twin domains within the crystal, which contributed to the observed diffraction pattern.

3.5.4 Synthesis of ligands $L_{3\text{-}8}H$.

3.5.4.1 Synthesis of 2-methoxy-6-(((2-methoxyphenyl)imino)methyl)phenol (L_3H)

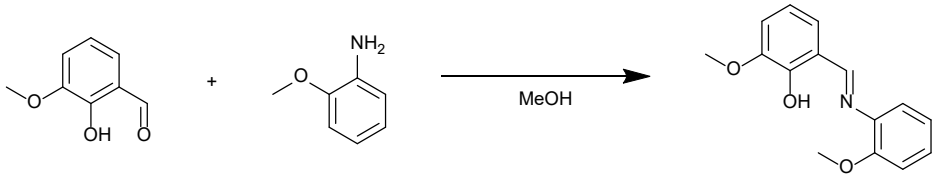

Scheme 3.2 Reaction scheme for the synthesis of 2-methoxy-6-{[(2-methoxybenzyl)imino]methyl}phenol (L_3H).

To a 50 cm^3 ethanolic solution was added o-vanillin (3.0 g, 19.72 mmol, 1 eq.) and o-anisidine (2.23 ml, 19.72 mmol). The resultant mixture was allowed to stir at room

temperature overnight. The mixture changed from a dark orange to a dark red colour during this time. A precipitate was produced and subsequently filtered off using suction filtration and washed with minimum amounts of solvent (ethanol). The solid was then dried under reduced pressure to give L_3H in 87% yield (4.41 g). ^{1}H NMR (400 MHz, $CDCl_3$) δ 8.71 (s, 1H), 7.26 – 7.22 (m, 2H), 6.99 (td, *J* = 9.2, 1.2 Hz, 4H), 6.85 (t, *J* = 7.9 Hz, 1H), 3.94 (s, 3H), 3.90 (s, 3H). ^{13}C NMR (100 MHz, $CDCl_3$) δ 161.48, 153.21, 152.81, 148.91, 136.47, 128.15, 123.62, 121.05, 119.29, 118.10, 114.47, 112.11, 56.26, 55.99. Elemental analysis (%) calculated (found) for L_3H ($C_{15}H_{15}N_1O_3$): C 70.02 (70.21), H 5.88 (6.02), N 5.44 (5.37). FT-IR (cm^{-1}): 2967 (w), 2836 (w), 1611 (s), 1585 (w), 1574 (w), 1495 (w), 1477 (w), 1455 (s), 1402 (w), 1361 (w), 1335 (w), 1301 (w), 1285 (w), 1273 (m), 1248 (s), 1194 (m), 1172 (m), 1162 (m), 1092 (w), 1078 (w), 1048 (w), 1021 (s), 970 (s), 937 (w), 888 (w), 854 (s), 835 (w), 780 (s), 761 (s), 737 (s), 636 (w), 587 (w), 521 (w), 480 (w). ESI-MS [M + H$^+$] (*m/z*): 257.14 (Calc. 257.29).

3.5.4.2 Synthesis of methyl (E)-4-((2-hydroxy-3-methoxybenzylidene)amino)benzoate (L_4H)

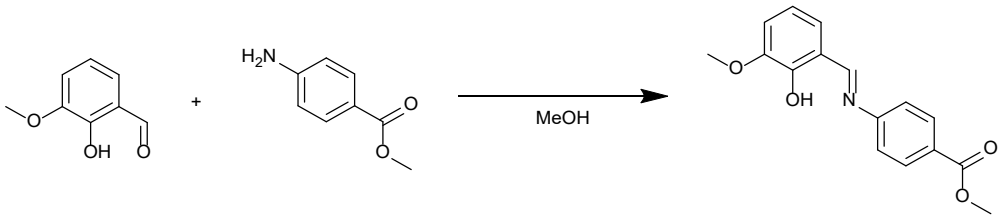

Scheme 3.3 Reaction scheme for the synthesis of methyl (E)-4-((2-hydroxy-3-methoxybenzylidene)amino)benzoate (L_4H).

To a 50 cm^3 methanolic solution of o-vanillin (2.50 g, 16.4 mmol) was added 2.48 g (16.4 mmol) of methyl 4-aminobenzoate. The resultant solution was stirred at room temperature for 2 hours and formed a bright orange ppt, this was filtered to give L_4H in yield 98%. ^{1}H NMR (400 MHz, $CDCl_3$) δ 8.65 (s, 1H), 8.11 (d, *J* = 8.4 Hz, 2H), 7.32 (d, *J* = 8.4 Hz, 2H), 7.04 (dd, *J* = 11.6, 7.9 Hz, 2H), 6.91 (t, *J* = 7.9 Hz, 1H), 3.94 (d, *J* = 4.0 Hz, 6H). ^{13}C NMR (100 MHz, $CDCl_3$) δ 166.56, 164.20, 152.25, 151.53, 148.54, 131.60, 131.08, 128.45, 124.55, 124.07, 121.18, 119.58, 118.84, 115.34,

56.24, 52.20. Elemental analysis (%) calculated (found) for L_4H ($C_{16}H_{15}NO_4$): C 67.36 (67.42), H 5.30 (5.30), N 4.91 (4.84). FT-IR (cm^{-1}): 2947 (w), 2837 (w), 1717 (s), 1617 (w), 1593 (m), 1571 (m), 1465 (s), 1431 (s), 1408 (m), 1360 (m), 1308 (w), 1271 (s), 1256 (s), 1189 (m), 1168 (s), 1097 (s), 1076 (m), 1010 (w), 963 (s), 855 (s), 836 (m), 781 (s), 769 (m), 732 (s), 693 (s), 669 (w), 634 (w), 582 (m), 570 (m), 552 (w), 505 (m), 465 (w).

3.5.4.3 Synthesis of (E)-2-[(benzylimino)methyl]-6-methoxyphenol (L_5H).

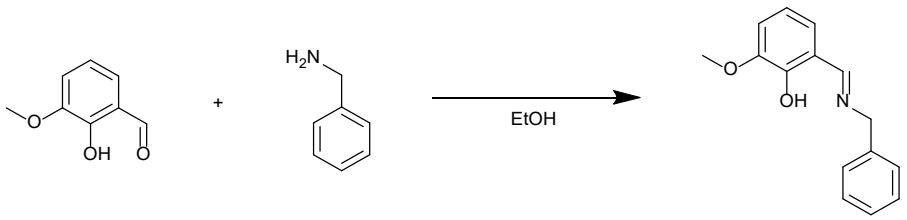

Scheme 3.4 Reaction scheme for the synthesis of 2-(benzylimino)methyl)-6-methoxyphenol (L_5H).

To a 100 cm^3 ethanolic solution of o-vanillin (4.00 g, 26.3 mmol) was added 2.85 cm^3 (26.3 mmol) of benzylamine. The solution was covered in parafilm and left to stir overnight. The resulting solution was concentrated under reduced pressure and then placed into an ice bucket to promote crystallisation. The resultant yellow polycrystalline powder was then dried on a Buchner funnel to afford 6.18 g (98%) of L_5H. ^1H NMR (400 MHz, $CDCl_3$) δ 13.90 (s, 1H), 8.43 (s, 1H), 7.37 – 7.27 (m, 5H), 6.92 (dd, J = 12.8, 7.3 Hz, 2H), 6.82 (t, J = 7.8 Hz, 1H), 4.83 (s, 2H), 3.90 (s, 3H). ^{13}C NMR (100 MHz, $CDCl_3$) δ 165.78, 151.94, 148.63, 138.17, 128.80, 127.76, 127.48, 123.14, 118.76, 118.11, 114.23, 62.84, 56.24. Elemental analysis (%) calculated (found) for L_5H ($C_{15}H_{17}N_1O_2$): C 74.05 (74.88), H 7.04 (6.41), N 5.76 (5.76). FT-IR (cm^{-1}): 3027 (w), 2997 (w), 2957 (w), 2938 (w), 2884 (w), 2834 (w), 2587 (w), 1630 (m), 1578 (w),1494 (w), 1459 (s), 1452 (s), 1435 (m), 1413 (m), 1379 (w), 1343 (w), 1332 (w), 1302 (w), 1249 (s), 1187 (w), 1169 (w), 1153 (m), 1081 (m), 1052 (m), 1029 (w), 992 (w), 973 (w), 949 (w), 880 (w), 835 (w), 778 (w), 749 (s), 734 (s), 697 (s), 635 (w), 573 (w), 562 (w), 538 (w), 471 (w), 447 (w). ESI-MS [M^+] (*m/z*): 241.06 (Calc. 243.30).

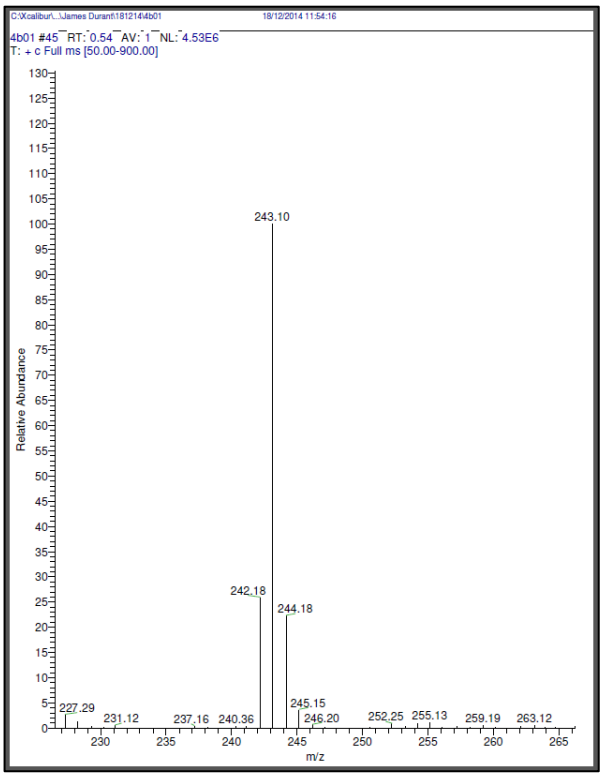

Figure 3.28 ESI+ Mass spectrum obtained from L_5H.

3.5.4.4 Synthesis of 2-[(benzylamino)methyl]-6-methoxyphenol (L_6H).

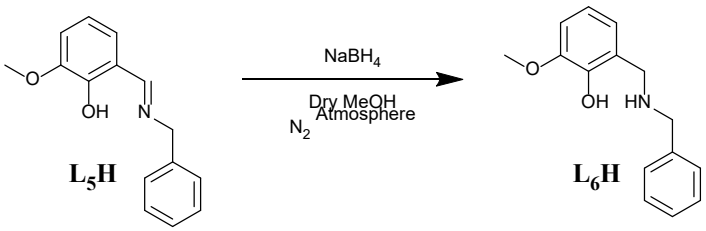

Scheme 3.5 Reaction scheme for the reduction of ligand L_5H to 2-[(benzylamino)methyl]-6-methoxyphenol (L_6H).

To a 50 cm^3 methanolic solution of L_5H (2.50 g, 10.4 mmol) was added 0.47 g (12.4 mmol) of $NaBH_4$. The resultant solution was stirred at room temperature for 18 hours and the solvent subsequently removed under reduced pressure. The clear, yellow tinted oily residue was added to 100 cm^3 of ethyl acetate and 30 cm^3 of saturated potassium carbonate. The aqueous phase was extracted with three 30 cm^3 portions of ethyl acetate

and the combined organic extracts were dried ($MgSO_4$) and concentrated under reduced pressure to afford 2.25 g (89%) of L_6H as a white / light cream solid (Fig. A3). ^{1}H NMR (400 MHz, $CDCl_3$) δ 7.33 (s, 5H), 6.83 (d, J = 8.1 Hz, 1H), 6.76 (t, J = 7.8 Hz, 1H), 6.65 (d, J = 7.5 Hz, 1H), 4.03 (s, 2H), 3.89 (s, 3H), 3.84 (s, 2H). ^{13}C NMR (100 MHz, $CDCl_3$) δ 148.22, 147.33, 138.09, 128.83, 128.64, 127.80, 122.46, 120.91, 118.99, 111.20, 56.07, 52.61, 51.35. Elemental analysis (%) calculated (found) for L_6H ($C_{15}H_{19}N_1O_2$): C 73.44 (73.28), H 7.81 (7.07), N 5.71 (5.64). FT-IR (cm^{-1}): 3304 (w), 2835 (w), 1584 (w), 1489 (m), 1474 (m), 1453 (m), 1407 (m), 1356 (w), 1262 (w), 1231 (s), 1186 (w), 1094 (w), 1084 (w), 1070 (s), 1055 (w), 1026 (w), 990 (m), 939 (m), 923 (w), 901 (w), 878 (w), 857 (w), 831 (m), 781 (w), 764 (m), 745 (s), 730 (s), 710 (m), 699 (s), 616 (w), 588 (w), 565 (w), 557 (w), 482 (w). ESI-MS [M^+] (*m/z*): 243.10 (Calc. 245.32).

3.5.4.5 Synthesis of (E)-2-((benzylimino)methyl)-4-bromo-6-methoxyphenol (PC1) and 2-[(benzylamino)methyl]-4-bromo-6-methoxyphenol (L_7H).

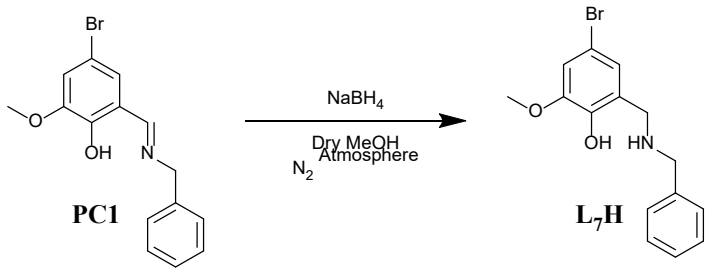

Scheme 3.6 Reaction scheme for the reduction of ligand PC1 to 2-[(benzylamino)methyl]-4-bromo-6-methoxyphenol (L_7H).

3.5.4.6 Synthesis of precursor 1: (E)-2-((benzylimino)methyl)-4-bromo-6-methoxyphenol (PC1).

To a 100 cm^3 ethanolic solution of bromo-vanillin (4.00 g, 17.3 mmol) was added 1.90 cm^3 (17.3 mmol) of benzylamine. The solution was covered in parafilm and left to stir overnight. The resulting solution was concentrated under reduced pressure and placed into an ice bucket to promote crystallisation. The resultant yellow polycrystalline solid

was then dried on a Buchner funnel to afford 5.38 g (97%) of PC1. ^{1}H NMR (400 MHz, $CDCl_3$) δ 8.26 (s, 1H), 7.35 – 7.28 (m, 2H), 7.23 (d, J = 11.8 Hz, 2H), 6.95 (dd, J = 12.9, 2.0 Hz, 2H), 4.78 (s, 2H), 3.84 (s, 3H).^{13}C NMR (100 MHz, CDCl3) δ 164.54, 151.77, 149.67, 137.57, 128.89, 127.84, 127.69, 125.01, 119.30, 117.14, 109.28, 62.52, 56.42. Elemental analysis (%) calculated (found) for $C_{15}H_{16}N_1O_2Br_1$: C 55.92 (56.10), H 5.01 (4.40), N 4.35 (4.21). FTIR (cm^{-1}): 3436 (vb), 3386 (w), 3014 (w), 2960 (w), 2925 (w), 2834 (w), 1627 (s), 1574 (w), 1489 (s), 1450 (m), 1441 (m), 1376 (m), 1346 (m), 1319 (w), 1256 (m), 1252 (s), 1536 (w), 1081 (w), 1052 (w), 1025 (w), 1001 (w), 981 (w), 843 (m), 820 (w), 757 (m), 734 (w), 710 (m), 702 (w), 660 (w), 607 (w), 574 (m), 492 (w), 453 (w), 416 (w). ESI-MS [M+] (m/z): 320.98 (Calc. 322.20).

3.5.4.7 Synthesis of 2-[(benzylamino)methyl]-4-bromo-6-methoxyphenol (L_7H).

To a methanolic solution (50 cm^3) of PC1 (2.86 g, 8.94 mmol) was added 0.405 g (10.7 mmol) of $NaBH_4$. The resultant solution was stirred at room temperature for 18 hours and the solvent was removed under reduced pressure. The clear, yellow tinted oily residue was added to 100 cm^3 of ethyl acetate and 30 cm^3 of saturated potassium carbonate. The aqueous phase was extracted with three 30 cm^3 portions of ethyl acetate and the combined organic extracts were dried ($MgSO_4$) and concentrated to afford 2.72 g (94%) of L_7H as a white solid. ^{1}H NMR (400 MHz, $CDCl_3$) δ 7.33 (dd, *J* = 16.3, 6.1 Hz, 5H), 6.93 (d, *J* = 2.0 Hz, 1H), 6.77 (d, *J* = 2.0 Hz, 1H), 3.97 (s, 2H), 3.87 (s, 3H), 3.81 (s, 2H). ^{13}C NMR (100 MHz, $CDCl_3$) δ 148.96, 146.74, 138.11, 128.81, 128.63, 128.47, 127.76, 127.15, 123.95, 123.14, 114.32, 110.37, 56.20, 52.65, 51.21. Elemental analysis (%) calculated (found) for $C_{15}H_{18}N_1O_2Br_1$: C 55.57 (55.86), H 5.60 (5.92), N 4.32 (4.15). FT-IR (cm^{-1}): 3454 (vb), 3306 (m), 3292 (m), 3030 (w), 2996 (w), 2933 (w), 2851 (w), 1575 (w), 1483 (s), 1442 (s), 1398 (s), 1358 (m), 1264 (m), 1232 (s), 1212 (m), 1186 (w), 1077 (m), 1025 (w), 991 (m), 951 (w), 911 (w), 858 (m), 829 (m), 752 (s). ESI-MS [M^+] (*m/z*): 322.41 (Calc. 324.21).

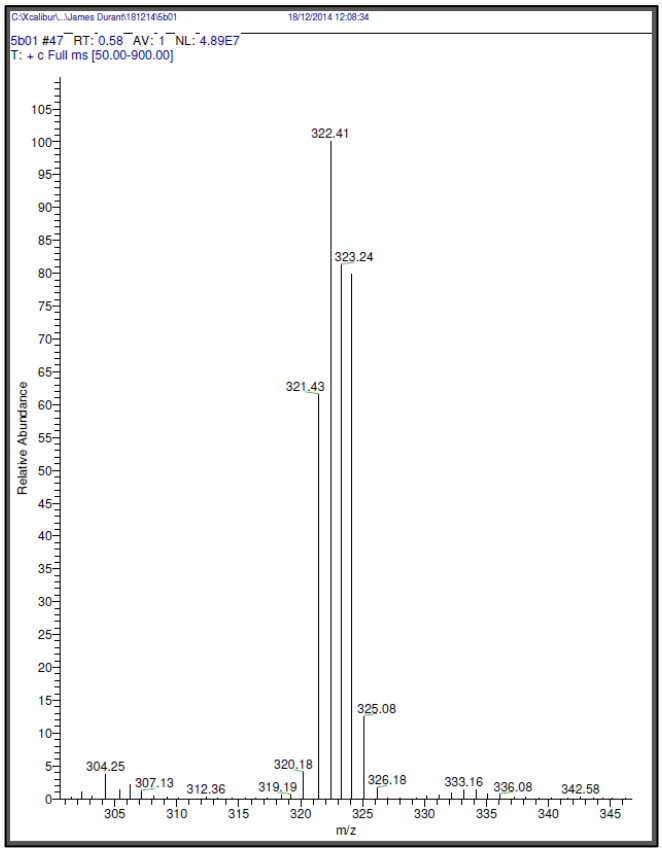

Figure 3.29 ESI+ Mass spectrum obtained from $\mathbf{L_7H}$.

3.5.5 Preparation of complexes

All reactions were performed under aerobic conditions and all reagents and solvents were used as purchased. *Caution*: Although no problems were encountered in this work, care should be taken when manipulating the potentially explosive nitrate salts.

3.5.5.1 Synthesis of $[Ni(II)_2(L_3)_3(H_2O)](NO_3)\cdot 2H_2O\cdot 3MeOH$ (17)

$Ni(NO_3)_2\cdot 6H_2O$ (0.25 g, 0.85 mmol), L_3H (0.22 g, 0.85 mmol) and NaOH (0.034 g, 0.85 mmol) were dissolved in methanol (30 cm^3) and stirred for 4 hours. The resultant lime green solution was filtered and X-ray quality crystals of **17** were obtained upon slow evaporation in 30% yield after 3 weeks. Elemental analysis (%) calculated (found) for **17** ($C_{48}H_{58}N_4O_{17}Ni_2$): C 53.36 (53.40), H 5.41 (4.81), N 5.19 (5.37). FT-IR (cm^{-1}): 3368 (vb), 3056 (w), 2942 (w), 2834 (w), 1611 (s), 1588 (s), 1541 (m), 1493 (s), 1467 (s), 1441 (s), 1384 (s), 1336 (s), 1297 (s), 1228 (s), 1192 (s), 1173 (s), 1118

(m), 1078 (m), 1046 (m), 1011 (m), 974 (m), 870 (w), 850 (w), 828 (w), 785 (m), 742 (s), 638 (m), 587 (m), 527 (m), 474 (w), 440 (w), 425 (w).

*3.5.5.2 Synthesis of [NaNi(II)$_2$(μ-OH)(L$_4$H)(L$_4$)$_3$(H$_2$O)$_2$](NO$_3$) (**18**)*

$Ni(NO_3)_2 \cdot 6H_2O$ (0.250 g, 0.86 mmol), L_4H (0.245 g, 0.86 mmol) and NaOH (0.034 g, 0.86 mmol) were dissolved in methanol (30 cm^3) and stirred for 4 hours. The resultant lime green solution was filtered and X-ray quality crystals of **18** were obtained upon slow evaporation in 30% yield after 3 weeks. Elemental analysis (%) calculated (found) for **18** ($C_{68}H_{90}N_5O_{32}Ni_2Na$): C 53.36 (52.99), H 5.41 (5.10), N 5.19 (5.32).

*3.5.5.3 Synthesis of [Ni(II)(L$_5$)$_2$] (**19**)*

$Ni(NO_3)_2 \cdot 6H_2O$ (0.25 g, 0.85 mmol), L_5H (0.20 g, 0.85 mmol) and NaOH (0.034 g, 0.85 mmol) were dissolved in methanol (30 cm^3) and stirred for 4 hours. The resultant lime green solution was filtered and X-ray quality crystals of **19** were obtained upon slow evaporation in 25% yield after 2 weeks. Elemental analysis (%) calculated (found) for **19** ($C_{30}H_{28}N_2O_4Ni_1$): C 66.82 (66.56), H 5.23 (4.98), N 5.20 (5.12). FT-IR (cm^{-1}): 3464 (b), 3055 (w), 3020 (w), 2928 (w), 2903 (w), 2852 (w), 2828 (w), 1836 (w), 1615 (s), 1551 (m), 1495 (m), 1471 (s), 1452 (s), 1434 (s), 1399 (m), 1332(m), 1319 (m), 1241 (s), 1164 (m), 1115 (w), 1094 (w), 1056 (m), 1031 (m), 984 (w), 957 (m), 914 (w), 874 (m), 858 (w), 791 (w), 762 (m), 737 (s), 699 (s), 656 (m), 602 (w), 524 (w), 490 (m), 447 (m), 417 (m).

*3.5.5.4 Synthesis of [Co(III)(L$_5$)$_3$]·H$_2$O·MeOH (**20a**) and [Co(II)$_7$(OMe)$_6$(L$_5$)$_6$](NO$_3$)$_2$·0.5H$_2$O·4MeOH (**20b**) co-crystals*

$Co(NO_3)_2 \cdot 6H_2O$ (0.25 g, 0.85 mmol), L_5H (0.20 g, 0.85mmol) and NaOH (0.034 g, 0.85 mmol) were dissolved in methanol (30 cm^3) and stirred for 4 hours. The resultant purple solution was filtered and X-ray quality crystals of **20a** (purple) and **20b** (red) were obtained upon slow evaporation of the mother liquor after 3 weeks. FT-IR (cm^{-1}): 3501 (vb), 3053 (w), 3024 (w), 2985 (w), 2910 (m), 2853 (w), 2824 (w), 1623 (s), 1548 (w), 1472 (s), 1450 (s), 1384 (s), 1322 (s), 1244 (s), 1221 (s), 1167 (m), 1109

(w), 1077 (m), 1036 (m), 1012 (m), 859 (m), 759 (m), 732 (s), 703 (m), 628 (w), 601 (w), 477 (w), 451 (w), 432 (w).

*3.5.5.5 Sole synthesis of [Co(III)(L_5)$_3$]·H_2O·MeOH (**20a**)*

$Co(NO_3)_2 \cdot 6H_2O$ (0.25 g, 0.86 mmol) was dissolved in methanol (30 cm^3) along with one equivalent of hydrogen peroxide (1 cm^3, 0.86 mmol). The resultant purple solution was then introduced to L_5H (0.20 g, 0.85 mmol) and NaOH (0.034 g, 0.85 mmol). X-ray quality crystal of **20a** were obtained upon slow evaporation in 25% yield after 2 weeks. Elemental analysis (%) calculated (found) for **20a**·H_2O ($C_{46}H_{48}N_3O_8Co_1$): C 65.17 (65.15), H 5.94 (5.58), N 4.96 (5.00). FT-IR (cm^{-1}): 3650 (w), 3503 (w), 3325 (w), 2986 (m), 2910 (m), 2821 (w), 2361 (w), 2344 (w), 2028 (w), 1869 (w), 1845 (w), 1802 (w), 1624 (s), 1609 (s), 1595 (s), 1559 (m), 1544 (m), 1508 (s), 1492 (s), 1470 (s), 1437 (m), 1412 (m), 1394 (m), 1342 (s), 1316 (s), 1242 (s), 1221 (s), 1193 (m), 1167 (m), 1109 (m), 1075 (m), 1049 (m), 1035 (m), 1026 (m), 966 (m), 953 (m), 904 (m), 858 (m), 767 (s), 756 (m), 730 (m), 694(m), 638 (m), 624 (m), 600 (m), 575 (m), 541 (m), 497 (w), 483 (w), 450 (w), 434 (w), 424 (w).

*3.5.5.6 Synthesis of [(NO_3)⊂Co(II)$_4$(μ_3-OH)$_2$(L_6)$_4$(H_2O)$_2$](NO_3)·H_2O (**21**)*

$Co(NO_3)_2 \cdot 6H_2O$ (0.25 g, 0.86 mmol), L_6H (0.21 g, 0.86 mmol) and NaOH (0.034 g, 0.86 mmol) were dissolved in MeCN and the solution stirred at room temperature for 4 hours. X-ray quality crystals of **21** were obtained in 20% yield upon filtration and subsequent slow evaporation of the mother liquor. Elemental analysis (%) calculated (found) for **21**·$2H_2O$ ($C_{60}H_{76}N_6O_{22}Co_4$): C 49.60 (48.95), H 5.27 (4.97), N 5.78 (6.28). FT-IR (cm^{-1}): 3577 (m), 3502 (m), 3274 (m), 3208 (vb), 3022 (m), 2926 (m), 2855 (m), 1639 (w), 1602 (m), 1579 (m), 1481 (s), 1389 (s), 1359 (s), 1330 (s), 1296 (m), 1255 (m), 1234 (m), 1207 (m), 1087 (m), 1066 (m), 1040 (m), 1028 (m), 1003 (m), 922 (s), 854 (s), 740 (s), 699 (s), 633 (m), 610 (m), 560 (w), 515 (w), 458 (w), 432 (w). MALDI-TOF MS (in DBTC-MeCN matrix) (%, m/z): 301 (5, $[Co(II)(L_6)]^+$), 364 (81, $[\{Co(II)(L_6)](NO_3) + H^+\}]$, 637 (12, $[Co(II)_4(\mu_3\text{-}OH)_2(L_6)_4(H_2O)_2]^{2+}$), 664 (100, $[Co(II)_4(\mu_3\text{-}OH)_2(L_6)_4(H_2O)_5]^{2+}$), 755 (42, $[Co(II)_4(\mu_3\text{-}OH)_2(L_6)_4(H_2O)_6(MeCN)_4]^{2+}$), 966 (22, $\{[Co(II)_4(\mu_3\text{-}OH)_4(L_6{*})_4(H_2O)_2] + H^+\}$), 1027 (6, {[Co(II)$_4$($\mu_3$-

$OH)_2(L_6*)_4(H_2O)_2](NO_3)\}^+$), 1055 (25, $\{[Co(II)_4(\mu_3\text{-}OH)_2(L_6*)_4](NO_3)_2 + H^+\}$). *Note*: L_6* = L_6^- - C_6H_5 (loss of pendant Ph group).

*3.5.5.7 Synthesis of $[(NO_3)\subset Ni(II)_4(\mu_3\text{-}OH)_2(L_6)_4(H_2O)_2](NO_3)\cdot H_2O$ (**22**)*

$Ni(NO_3)_2\cdot 6H_2O$ (0.25 g, 0.86 mmol), L_6H (0.21 g, 0.86 mmol) and NaOH (0.034 g, 0.86 mmol) were dissolved in MeCN and the solution stirred at room temperature for 4 hours. X-ray quality crystals of **22** were obtained in 20% yield upon filtration and subsequent slow evaporation of the mother liquor after 2 weeks. Elemental analysis (%) calculated (found) for **22**$\cdot H_2O$ ($C_{60}H_{74}N_6O_{20}Ni_4$): C 50.25 (50.65), H 5.20 (5.15), N 5.86 (6.19). FT-IR (cm^{-1}): 3576 (w), 3537 (w), 3478 (w), 3268 (w), 3187 (w/vb), 3019 (w), 2841 (w), 1599 (w), 1577 (w), 1478 (s), 1442 (m), 1384 (m), 1360 (m), 1322 (m), 1298 (s), 1256 (m), 1229 (s), 1210 (m), 1168 (w), 1112 (w), 1085 (m), 1072 (w), 1042 (w), 1024 (w), 1001 (m), 921 (w), 880 (m), 851 (w), 817 (w), 778 (w), 768 (w), 739 (s), 697 (s), 643 (w), 633 (w), 614 (m), 555 (w), 540 (w), 519 (w), 493 (w), 460 (w), 433 (w), 416 (w).

*3.5.5.8 Synthesis of $[Ni(II)_4(\mu_3\text{-}OH)_2(L_7)_4(NO_3)_2]\cdot MeCN$ (**23**)*

Method A: $Ni(NO_3)_2\cdot 6H_2O$ (0.25 g, 0.86 mmol), L_7H (0.28 g, 0.86 mmol) and NaOH (0.0344 g, 0.86 mmol) were dissolved in MeCN and the solution stirred at room temperature for 4 hours. X-ray quality crystals of **23** were obtained in 15% yield upon filtration and subsequent slow evaporation of the mother liquor after 3 weeks. *Method B:* $Ni(NO_3)_2\cdot 6H_2O$ (0.25 g, 0.86 mmol), **L_7H** (0.28 g, 0.86 mmol) and NaOH (0.0344 g, 0.86 mmol) were dissolved in MeOH and the solution stirred at room temperature for 4 hours. The precipitous solution was then evaporated to dryness and re-dissolved in MeCN. X-ray quality crystals of **23** were obtained in 20% yield upon filtration and subsequent slow evaporation of the mother liquor. Elemental analysis (%) calculated (found) for **23** ($C_{60}H_{62}N_6O_{16}Br_4Ni_4$): C 42.96 (43.06), H 3.73 (3.76), N 5.01 (4.95). FT-IR (cm^{-1}): 3616 (s), 3268 (s), 3085 (w), 3062 (w), 3028 (w), 3004 (w), 2959 (w), 2937 (w), 2861 (w), 1567 (m), 1484 (s), 1442 (sh), 1358 (m), 1331 (m), 1300 (m), 1247 (m), 1233 (s), 1207 (m), 1095 (m), 1052 (m), 1035 (m), 1019 (m), 1009 (m), 929 (m), 883 (m), 864 (m), 809 (w), 779 (s), 746 (s), 700 (s), 659 (w), 620 (m), 570 (w), 553 (w), 504 (w), 479 (w), 422 (w). MALDI-TOF MS (in DBTC-MeCN matrix) (%,

m/z): 795 (100, $[Ni(II)_4(\mu_3\text{-}OH)_2(L_7)_4(H_2O)_2]^{2+}$), 820 (12, $[Ni(II)_4(\mu_3\text{-}OH)_2(L_7)_4(MeCN)_2]^{2+}$), 1632 (30, $\{[Ni(II)_4(\mu_3\text{-}OH)_2(L_7)_4(H_2O)] + (NO_3)\}^{+}$).

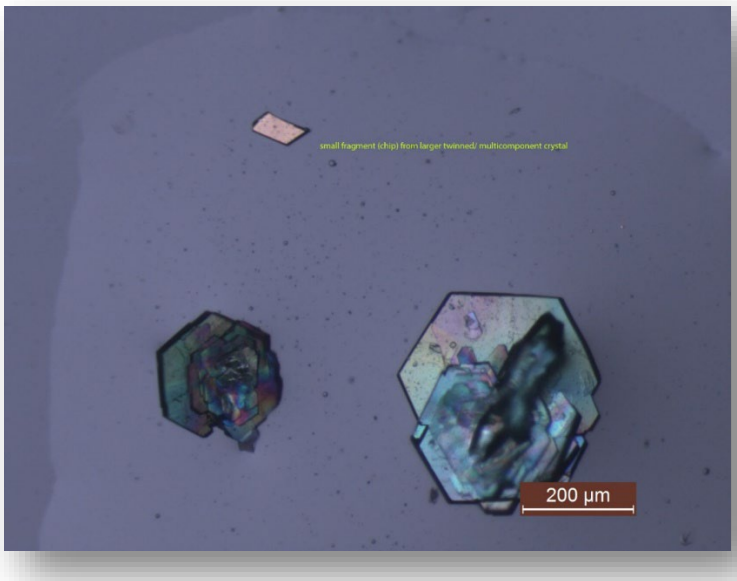

Figure 3.30 The crystal morphology in **23** showing the small fragment of crystal collected (top middle) after being chipped from a larger twinned multicomponent crystal.

3.6 References

1. S. T. Meally, G. Karotsis, E. K. Brechin, G. S. Papaefstathiou, P. W. Dunne, P. McArdle and L. F. Jones. *CrystEngComm.,* 2010, **12, 59.**

2. S. T. Meally, C. McDonald, G. Karotsis, G. S. Papaefstathiou, E. K. Brechin, P. W. Dunne, P. McArdle, N. P. Power and L. F. Jones. *Dalton Trans.,* 2010, **39**, 4809.

3. S. T. Meally, C. McDonald, P. Kealy, S. M. Taylor, E. K. Brechin and L. F. Jones. *Dalton Trans.,* 2012, **41(18)**, 5610.

4. M. Coletta, R. McLellan, P. Murphy, B. T. Leube, S. Sanz, R. Clowes, K. J. Gagnon, S. J. Teat, A. I. Cooper, M. J. Paterson, E. K. Brechin and S. J. Dalgarno. *Chem. Eur. J*. 2016, **22**, 8791-8795.

5. T. C. Stamatatos, R. Adam, C. P. Raptopoulou, V. Psycharis, R. Ballesteros, B. Aberca, S. P. Perlepes and A. K. Boudalis. *Inorg. Chem. Commun*., 2012, **15**, 73-77.

6. S. M. Taylor, G. Karotsis, R. D. McIntosh, S. Kennedy, S. J. Teat, C. M. Beavers, W. Wernsdorfer, S. Piligkos, S. J. Dalgarno and E. K. Brechin. *Chem. Eur. J.,* 2011, **17**, 7521-7530.

7. Y. Sunatsuki, H. Shimada, T. Matsuo, M. Nakamura, F. Kai, N, Marsumoto and N. Re. *Inorg. Chem.,* 1998, **37**, 5566-5574.

8. A.-A. H. Abu-Nawwas, C. A. Muryn and M. A. Malik. *Inorg. Chem. Commun*., 2009, **12**, 125-127.

9. I.-P. Lorenz, W. Pohl and H. Nöth. *Angew. Chem. Int. Ed.,* 1997, **36**, 54-56.

10. K.-H. Lii and Y.-F. Huang. *Chem. Commun.,* 1997, 839-840.

11. P. King, R. Clérac, W. Wernsdorfer, C. E. Anson and A. K. Powell. *Dalton Trans.,* 2004, 2670-2676.

12. B.-C. Tsai, Y.-H. Liu, S.-M. Peng and S.-T. Liu. *Eur. J. Inorg. Chem*., 2016, 2783-2790.

13. S.-H. Zhang, N. Li, C.-M. Ge, C. Feng and L.-F. Na. *Dalton Trans.,* 2011, **40**, 3000-3007.

14. G. Chaboussant, R. Basler, H.-U. Güdel, S. Oschenbein, A. Parkin, S. Parsons, G. Rajaraman, A. Sieber, A. A. Smith, G. A. Timco and R. E. Winpenny. *Dalton Trans*., 2004, 2758-2766.

15. K. F. Konidaris, V. Bekiari, E. Katsoulakou, C. P. Raptapoulou, V. Psycharis, E. Manessi-Zoupa, G. E. Kostakis and S. P. Perlepes. *Dalton Trans*., 2012, **41**, 3797-3806.

16. J. Martinez, I. Aiello, A. Bellusci, A. Crispini and M. Ghedini. *Inorg. Chim. Acta.,* 2008, **361**, 2677-2682.

17. Zoupa, S. P. Perlepes and D. P. Kessissoglou. Eur. J. *Inorg. Chem.,* 2005, 1964-1978.

18. J. Hermann and A. Erxleben, *Inorg. Chim. Acta.,* 2000, **304**, 125-129.

19. A. J. Stemmler, J. F. Kampf and V. L. Pecoraro. *Inorg. Chem.,* 1995, **34**, 2271-2272.

20. P. S. Perlepe, L. Cunha-Silva, V. Bekiari, K. J. Gagnon, S. KJ. Teat, A. Escuer and T. C. Stamatatos. *Dalton Trans*., 2016, **45**, 10256-10270.

21. M. Mikuriya, K. Tanaka, N. Inoue, D. Yoshioka and J.-W. Lim. *Chem. Lett.,* 2003, **32**, 126-127.

22. N. C. Harden, M. A. Bolcar, W. Wernsdorfer, K. A. Abboud, W. E. Streib and G. Christou, *Inorg. Chem.,* 2003, **42**, 7067.

23. M. A. Bolcar, S. M. J. Aubin, K. Folting, D. N Hendrickson and G. Christou, *Chem. Commun*., 1997, 1485.

24. M. Menelaou, E. Vournari, V. Psycharis, C. P. Raptopoulou, A. Terzis, V. Tangoulis, Y. Sanakis, C. Mateescu and A. Salifoglou. *Inorg. Chem.,* 2013, **52**, 13849-13860.

25. E.-C. Yang, Z.-Y. Liu, L. Zhang, N. Yang and X.-J. Zhao. *Dalton Trans*., 2016, **45**, 8134.

26. D.-M. Chen, X.-Z. Ma, X.-J. Zhang, N. Xu and P. Cheng, *Inorg. Chem*., 2015, **54**, 2976-2982.

27. W. L. Leong and J. J. Vittal. *New J. Chem.,* 2010, **34**, 2145-2152.

28. K. Mitsumoto, M. Nihei, T.Shiga, and H. Oshio. *Chem. Lett.,* 2008, **37**, 966-967.

29. S.-H. Zhang and C. Feng. *J. Mol. Struct.* 2010, **977**, 62-66.

30. M. Manoli, A. Collins, S. Parsons, A. Candini, M. Evengelisti and E. K. Brechin. *J. Am. Chem. Soc*., 2008, **130**, 11129-11139.

31. T. D. Keene, M. E. Light, M. B. Hursthouse and D. J. Price. *Dalton Trans*., 2011, **40**, 2983.

32. J. C. Goodwin, R. Sessoli, D. Gatteschi, W. Wernsdorfer, A. K. Powell and S. L. Heath. *Dalton Trans.,* 2000, 1835-1840.

33. S. L. Heath and A. K. Powell. *Angew. Chem. Int. Ed*., 1992, **31**, 191-193.

34. A. V. Pestov, P. A. Slepukhin and Y. G. Yatluk. *Russ. J. Coord. Chem*., 2011, **37(8)**, 619-624.

35. Y.-K. Deng, H.-F. Su, J.-H. Xu, W.-G. Wang, M. Kurmoo, S.-C. Lin, Y.-Z. Tan, J. Jia, D. Sun and L.-S. Zheng. *J. Am. Chem. Soc.,* 2016, **138**, 1328-1334.

36. For the structure of α-$Co(OH)_2$ see: M. Rajamathi, P. Vishnu Kamath and R. Seshadri. *M. Res. Bull.,* 2000, **35**, 271-278. For the structure of β-$Co(OH)_2$ see: Ch. Mockenhaupt, Th. Zeiske and H. D. Lutz. *J. Mol. Struct.* 1998, **443**, 191-196.

37. D. S. Hall, D. J. Lockwood, C. Bock and B. R. MacDougall. *Proc. R. Soc. A*., 2014, **471**, 20140792.

38. M. W. Kanan and D. G. Nocera. *Science*. 2008, **321**, 1072.

39. M. W. Kanan, Y. Surendranath and D. G. Nocera. *Chem. Soc. Rev.,* 2009, **38**, 109-114.

40. Y. Surendranath, D. A. Lutterman, Y. Li and D. G. Nocera. *J. Am. Chem. Soc.,* 2012, **134**, 6326-6336.

41. C. L. Farrow, D. K. Bediako, Y. Surendranath, D. G. Nocera and S. J. L. Billinge. *J. Am. Chem. Soc.,* 2013, 6403-6406.

42. M. W. Kanan, J. Yano, Y. Surendranath, M. Dincã, V. K. Yachandra and D. G. Nocera. *J. Am. Chem. Soc.,* 2010, **132**, 13692-13701.

43. D. K. Bediako, Y. Surendranath and D. G. Nocera, *J. Am. Chem. Soc*. 2013, **135**, 3362-3674.

44. D. K. Bediako, B. Lasalle-Kaiser, Y. Surendranath, J. Yano, V. K. Yachandra and D. G. Nocera. *J. Am. Chem. Soc*., 2012, **134**, 6801.

45. A. M. Ullman and D. G. Nocera. *J. Am. Chem. Soc*., 2013, **135**, 15053.

46. D. Altermatt and I. D. Brown. *Acta Cryst. 1985.* **B41**,240-244

47. I. D. Brown. *Chem. Rev.* 2009, **109**, 6858–6919

48. N. F. Chilton, R. P. Anderson, L. D. Turner, A. Soncini and K. S. Murray*, J. Comput. Chem.,* 2013, **34**, 1164–1175.

49. O. Khan, Molecular Magnetism, VCH, New York, 1993.

50. R. J. Butcher, C. J. O'Connor and E. Sinn, *Inorg. Chem.,* 1981, **20**, 3486– 3493.

51. E. Loukopoulos, B. Berkoff, K. Griffiths, V. Keeble, V. N. Dokorou, A. C. Tsipis, A. Escuer and G. E. Kostakis, *CrystEngComm*, 2015, **17**, 6753–6764.

52. S. Banerjee, M. G. B. Drew, C.-Z. Lu, J. Tercero, C. Diaz and A. Ghosh, *Eur. J. Inorg. Chem*., 2005, 2376–2383.

53. L. Rodríguez, E. Labisbal, A. Sousa-Pedrares, J. A. García-Vázquez, J. Romero, M. L. Durán, J. A. Real and A. Sousa, *Inorg. Chem.,* 2006, **45**, 79037914.

54. P. S. Perlepe, A. A. Athanasopoulou, K. I. Alexopoulou, C. P. Raptopoulou, V. Psycharis, A. Escuer, S. P. Perlepes and T. C. Stamatatos, *Dalton Trans.,* 2014, **43**, 16605–16609.

55. A. Das, F. J. Klinke, S. Demeshko, S. Meyer, S. Dechert and F. Meyer. *Inorg. Chem.,* 2012, **51**, 8141–8149.

56. M. A. Halcrow, J.-S. Sun, J. C. Huffman and G. Christou, *Inorg. Chem.,* 1995, **34**, 4167–4177.

57. R. Boča, *Coord. Chem. Rev.,* 2004, **248**, 757–815.

58. R.-X. Yao, X.-H. Qiao, X. Cui, X.-X. Jia and X.-M. Zhang, *Inorg. Chem. Front.,* 2016, **3**, 78–85.

59. X. M. Zhang, J. Q. Li, S. J. Liu, M. B. Luo, W. Y. Xu and F. Luo, *CrystEngComm,* 2014, **16**, 2570-2573.

60. H.-H. Chen, J. Yang, Y.-Y. Liu and J.-F. Ma, *CrystEngComm,* 2013, **15**, 5168-5178.

61. P. Khakhlary, C. E. Anson, A. Mondal, A. K. Powell and J. B. Baruah, *Dalton Trans.,* 2015, **44**, 2964–2969.

62. Rigaku OD (2015). *CrysAlis PRO*. Rigaku Oxford Diffraction Ltd, Yarnton, England.

63. G. M. Sheldrick. *Acta Crystallogr. Sect. C Struct. Chem.* 2015, **71**, 3.

64. O. V. Dolomanov, L. J. Bourhis, R. J. Gildea, J. A. K. Howard and H. J. Puschmann. *Appl. Crystallogr.* 2009, **42**, 339.

65. G. M. Sheldrick, *Acta. Crystallogr., Sect. A: Found. Crystallogr.,* 1990, **A46**, 467.

66. A. L. Spek. *Acta Cryst. C: Structural Chem.,* 2015, **71**, 9-18.

Chapter 4

Upper and Lower Rim modifications of *pseudo* metallocalix[6]arene directing ligands towards molecular cavity wall extensions and other topology changes

4.1 Introduction

The pursuit of new discrete and extended molecular structures equipped with premeditated application driven properties has never been more intense. Once discovered and fully characterised, such materials often require varying levels of structural and / or electronic modification in order to optimise their operational potential. To this end, synthetic tools at our disposal include post-synthetic ligand modification, a technique often employed to fine tune structural properties while maintaining the integrity of the core molecule. Indeed, such endeavours lend themselves to the structural adjustment of both discrete molecules (e.g. the linking of magnetic complexes using Cu-ACC click chemistry)[1] and extended architectures such as Metal-Organic Frameworks (MOFs),[2] and Covalent Organic Frameworks (COFs).[3] An alternative route towards targeted structural fine-tuning would be to use de novo synthetic techniques, where the ligand used in the construction of the prototype material is replaced with a modified / functionalised version that imparts the required topology and / or functionality onto the novel material.[4] For instance, replacing monotopic ligands with di- / multitopic analogues has been shown to be an effective way to template / organise discrete molecules into extended network assemblies. One example is the facile substitution of benzoate ($^{-}O_2CPh$) ligands within the Single-Molecule Magnet $[Mn(III)_6(\mu_3\text{-}O)_2(Et\text{-}sao)_6(O_2CPh)_2]$ ($Et\text{-}saoH_2$ = 2-hydroxypropiophenone oxime) with succinate (or isophthalate) directs 1-D chain formation.[5] Another benefit to this methodology is that the synthetic chemist is often able to control / modify the second coordination sphere associated with their prototype materials. Indeed, there are numerous examples where careful ligand selection has allowed the assembly of (for instance) molecular cavities that are able to entice guest ingression within their host architectures / containers.[6]

To date, the Jones group have successfully encapsulated a variety of guest organic moieties within the molecular cavities of our *pseudo* $[M(II)_7(OH)_6(L_{1\text{-}2})_6](NO_3)_2$ metallocalix[6]arene hosts and include solvent molecules of crystallisation (MeOH, $MeNO_2$, MeCN)[7] and as described in Chapter 2, a number of small organics of similar shape and functionality (2- and 3-furaldehyde (2-, 3-fur), benzaldehyde (bzal), 2-thiophenecarboxaldehyde (2-thio), 2-acetylfuran (2-acetylfuran) and acetophenone (acetoph). Moreover, through ligand modification the encapsulation of counter NO_3^- anions was achieved in the heptanuclear *pseudo* metallocalix[6]arene

$[(NO_3)_2 \subset Co(III)Co(II)_6(OH)_6(L)_6](NO_3)\cdot 3MeCN$ (where LH = 2-iminophenyl-6-methoxyphenol).[8]

4.2 Results and Discussion

Given our enduring desire to encapsulate more diverse and interesting guests within our [M(II/III)$_7$] (M = Co, Ni, Zn) host units, it was postulated that by further functionalising L_1H at the 4-position of the phenol ring (i.e. the upper rim of the *pseudo* metallocalix[6]arene; Figure 4.1), we were effectively carrying out a molecular cavity wall extension upon *pseudo* metallocalix[6]arene formation. It was proposed that this ligand adaptation would provide adequate space and π-character for the attraction and therefore accommodation of larger and more elaborate guest species. In pursuit of this goal the ligand 4-phenyl-2-iminomethyl-6-methoxyphenol (L_3H) was synthesised via a Suzuki coupling reaction followed by Schiff base coupling (see experimental section for details). L_3H possesses a phenyl group at the 4-position of the phenolic ring and therefore we believed that potential guests possessing a high degree of aromatic (π) character would be readily encapsulated, through edge-to-face π···π stacking and C-H···π interactions within the host framework.

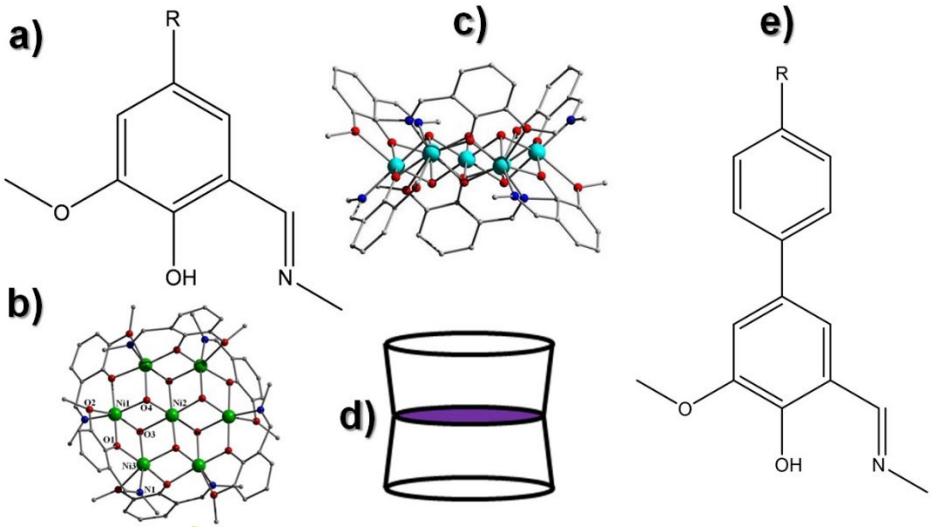

Figure 4.1 (a) The ligand 2-methoxy-6-((R-imino)methyl)phenol (R = H (L_1H) or Br (L_2H)) used in the construction of our heptanuclear double bowl *pseudo* metallocalix[6]arenes. Perpendicular (b) and side-on (c) views of a [Ni$_7$] and [Zn$_7$] metallocalix[6]arene, respectively. Colour code: Light blue (Zn), Green (Ni), Grey (C), Dark blue (N), Red (O) as used throughout this chapter. Hydrogen and NO_3^- counter anions have been omitted for clarity. (d) Schematic highlighting the double bowl topology. (e) The new ligands 2-Methoxy-4-phenyl-6-[(E)-

(methylimino)methyl]phenol (R = H, L_8H) and 2-Methoxy-4-tolyl-6-[(E)-(methylimino)methyl]phenol (R = CH_3, L_9H) used in this work to form larger molecular cavities upon metallocalix[6]arene assembly.

4.2.1 Upper rim ligand modification leads to molecular cavity wall extensions

To this end the heptanuclear complex $[Co(II)_7(OMe)_6(L_8)_6](NO_3)_2{\cdot}H_2O{\cdot}3MeOH$ (**24**) was isolated via the reaction of $Co(NO_3)_2.6H_2O$ with L_8H and NaOH in methanol (first synthesised by the previous Jones group member Sean T. Meally at NUI Galway).[9] Complex **24** crystallises as purple-brown plates in the monoclinic C2/c space group and complete X-ray structural details are given in Table 4.4. Indeed, all crystallographic details emerging from this Chapter can be found in Tables 4.4 and 4.5. Akin to previously described $[M(II)_7]$ (M = Co, Ni and Zn) systems,[7-8] the asymmetric unit of **24** comprises four crystallographically unique Co(II) ions (Co1-Co4), whose oxidation states were confirmed via BVS (Table 4.6), bond length and charge-balancing analyses. The seven Co(II) ions in **24** are held in a planar body centred hexagonal array by a combination of μ_3-bridging $^-$OMe and $^-$OH ions (50:50 occupancy; see crystallography section for details). The six outer cobalt ions (Co2-Co4 and s.e.) are linked by six $\eta^1{:}\eta^2{:}\eta^1$-μ bridging L_8^- ligands sitting above and below the planar heptanuclear core in **24** in an alternating fashion. The result is a double-bowl pseudo metallocalix[6]arene structure in **24**. The construction of **24** using our pre-designed L_8H ligands dictates double bowl topology formation with dimensions exceeding those of its previously reported siblings (e.g. $[Co(II)_7(OH)_6(L_1)_6](NO_3)_2$ in Fig. 4.2a, where L_1H = 2-methoxy-6-((methylimino)methyl)phenol: base × depth × rim diameter (Å) = 6.25 × 4.83 × 13.24 *cf.* 6.24 × 7.84 × 19.12 (**24**); Fig. 4.2a vs. b). This feature highlights the influence that ligand modification has on the topology of our $[M(II)_7]$ framework. Two charge balancing NO_3^- counter anions lie at the periphery of the structure in **24**. Upon further scrutiny of the bridging L_8^- ligands within the crystal structure of **24**, we observed considerable out-of-plane twisting of the phenyl groups with respect to their counterpart phenolic rings. These structural distortions can be quantified by measuring the torsion angles generated between the upper rim phenyl groups and their associated phenolic rings of each L_8^- ligand, which in complex **24** range from 24.32 to 42.91°.

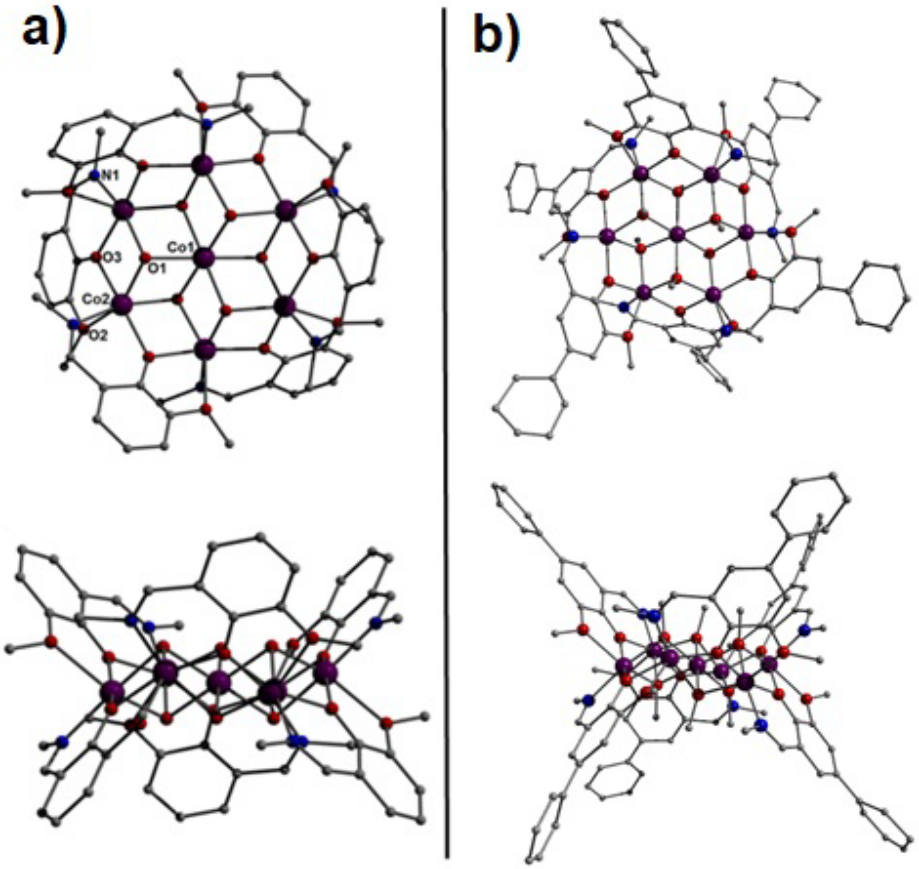

Figure 4.2 Crystal structure of the siblings (a) $[(MeOH)_2 \subset Co(II)_7(OH)_6(L_1)_6](NO_3)_2$ (L_1H = 2-Methoxy-6-[(E)-(methylimino)methyl]phenol**)** (MeOH guests have been omitted for clarity) and (b) $[Co(II)_7(OMe)_6(L_8)_6](NO_3)_2 \cdot H_2O \cdot 3MeOH$ (**24**) (L_8H = 2-Methoxy-6-{(E)-[(2-methoxyphenyl)imino]methyl}phenol) as synthesised by Seán Meally et al.[9] Both analogues are viewed perpendicular (bottom) and parallel (top) to their planar $[Co(II)_7]$ cores. Colour code: Purple (Co), Red (O), Blue (N), Grey (C) (used throughout this work). Hydrogen atoms and NO_3^- counter anions have been omitted for clarity.

The crystal packing arrangement observed in **24** is different to those of our previously reported $[M(II)_7]$ (M = Co, Ni, Zn) siblings in that the individual $[Co(II)_7]$ units in **24** do not arrange into superimposable 1D columns and therefore no appreciable molecular cavities are observed. Instead, the packing in **24** is much more space efficient and is facilitated by interdigitation of the $[Co(II)_7]$ units, with ligand moieties from two independent heptanuclear units penetrating into a third $[Co(II)_7]$ assembly via edge-to-face (T-shaped) C-H$\cdots\pi$ stacking between individual L_8^- upper rim phenyl groups in each pair (i.e. $[C17\text{-}C28]_{centroid}\cdots(H38')C38'$ = 2.74 Å and $[C32\text{-}C43]_{centroid}\cdots H8'(C8')$ = 2.69 Å) (Figure 4.3). The interdigitating ligand phenyl groups

also partake in C-H···π interactions with the bridging methoxide ions of the interpenetrated [Co(II)$_7$] unit (e.g. C47′(H47A′)···[C5-C10]$_{centroid}$ = 3.75 Å). As a result of these interactions, the individual [Co(II)$_7$] units in **24** arrange themselves into the space efficient brickwork patterns along the *ab* plane of the unit cell and these planes pack as superimposable sheets along the *c* unit cell direction (Fig. 4.3-right).

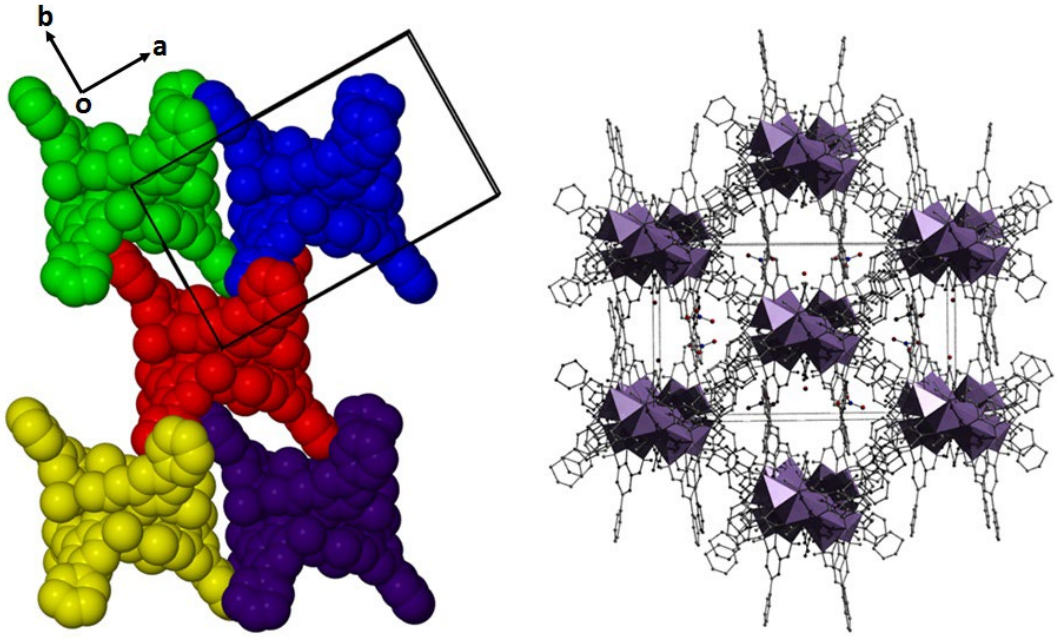

Figure 4.3 (left) Interdigitation of the individual colour coded [Co(II)$_7$] units in **24** (i.e. red unit) facilitated via T-shaped C-H···π stacking interactions between ligand moieties on pairs of [Co(II)$_7$] complexes (i.e. yellow + purple and green + blue units). (Right) Polyhedral representation of the packing in **24** as viewed along the *c*-axis of the unit cell. Hydrogen atoms and NO_3^- counter anions have been omitted for clarity.

Analogues to complex [Co(II)$_7$(OMe)$_6$(L$_8$)$_6$](NO$_3$)$_2$·3MeOH·H$_2$O (**24**) have also been obtained in the form of [Ni(II)$_7$(OMe)$_6$(L$_8$)$_6$](NO$_3$)$_2$·2H$_2$O (**25**) and [Zn(II)$_7$(OH)$_2$(OMe)$_4$(L$_8$)$_6$](NO$_3$)$_2$·4MeOH·10H$_2$O (**26**). Complexes **25** and **26** are isolated via a similar synthetic route to that of **24** (see experimental section for details) and crystallise in the monoclinic P2$_1$/n and C2/c space groups as green and pale-yellow blocks, respectively. Both **25** and **26** comprise body centred hexagonal cores connected through μ$_3$-OR$^-$ (R = H, Me) bridging ions (R = Me in **25** and a combination of both in **26**) along with six L$_8^-$ ligand units (Fig. 4.4a/b and 4.5a). As observed in **24**, complexes **25** and **26** do not show guest encapsulation and instead the individual

[Ni(II)$_7$] and [Zn(II)$_7$] units pack efficiently through interdigitation via their peripheral ligand phenyl groups, interacting through C-H$\cdots\pi$ interactions with one another (e.g. C25(H25)$\cdots$[C39B-C44B]$_{centroid}$ = 3.460 Å in **25** and C14(H14)$\cdots$[C40B-C45B]$_{centroid}$ = 3.756 Å in **26**) and with nearby bridging μ_3-OMe$^-$ units (e.g. C48(H48B)$\cdots$[C24-C29]$_{centroid}$ = 3.87 Å in **25** and C46(H46C)$\cdots$[C10-C15]$_{centroid}$ = 3.763 Å in **26**) (Fig. 4.4c/d and 4.5b).

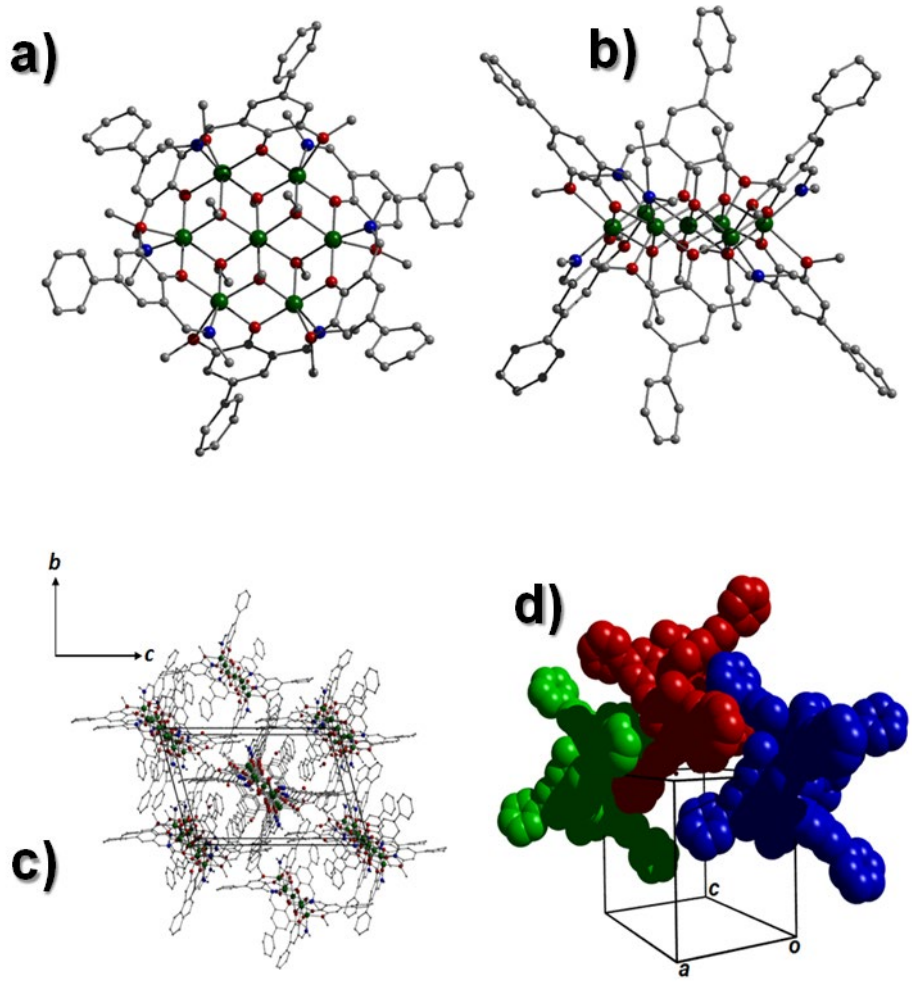

Figure 4.4 Crystal structure of **25** as viewed perpendicular (a) and parallel (b) to the planar [Ni(II)$_7$] core. Hydrogen atoms and NO_3^- counter anions have been omitted for clarity. **(c)** Packing arrangement in **25** as viewed along the *a* unit cell direction. (d) Space-fill and colour coded representation of the interdigitation observed between the individual [Ni$_7$] units in **25**. All solvent molecules of crystallisation have been omitted for clarity.

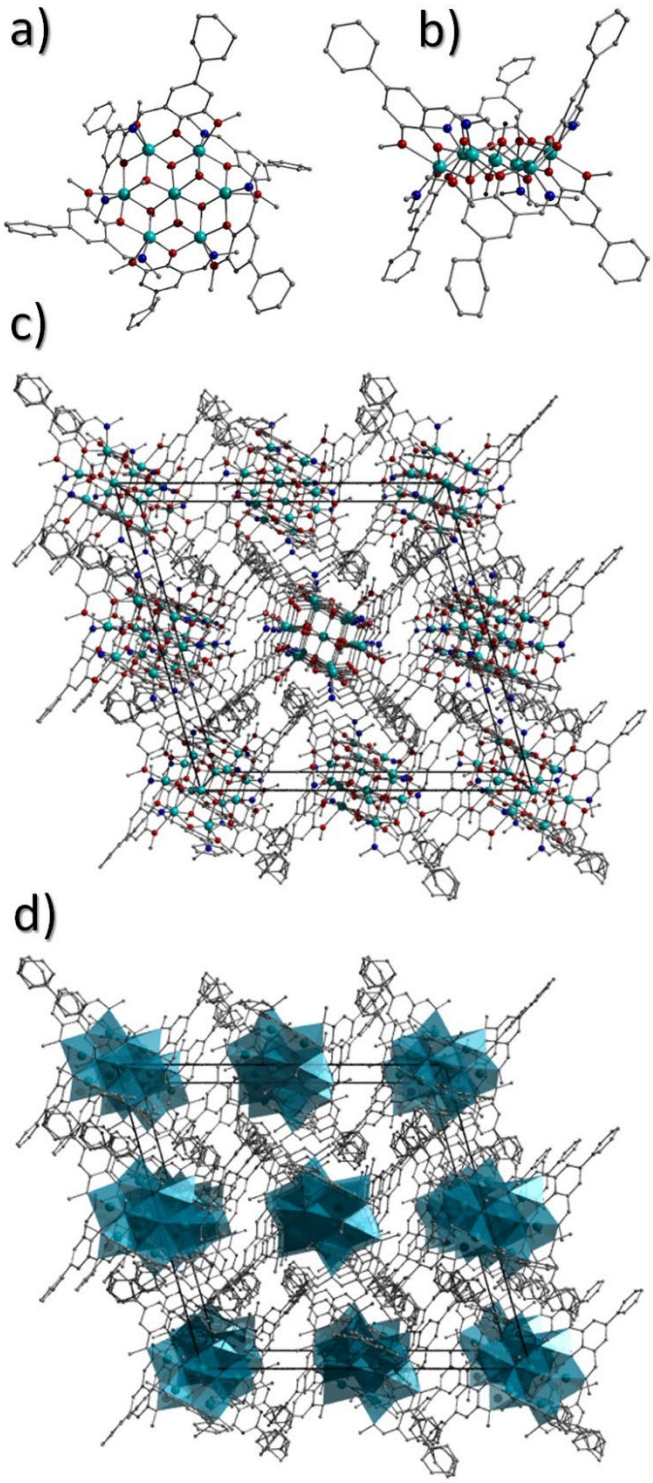

Figure 4.5 Crystal structure of $[Zn(II)_7(OH)_2(OMe)_4(L_8)_6](NO_3)_2{\cdot}4MeOH{\cdot}10H_2O$ (**26**) as viewed perpendicular (a) and parallel to its body centred heptanuclear $[Zn(II)_7]$ core. (c) Packing arrangement observed in **26** along with its polyhedral representation (d).

Using Suzuki coupling as described in Section 4.4.2, we decided to introduce a tolyl group at the upper rim position of our metallocalix[6]arene directing ligand to produce the novel ligand 2-Methoxy-4-tolyl-6-[(E)-(methylimino)methyl]phenol (L_9H). Its subsequent reaction with $Zn(II)(NO_3)_2.6H_2O$ gave rise to the heptanuclear complex $[Zn(II)_7(OMe)_6(L_9)_6](NO_3)_2$ (**27**): a direct analogue to complexes **24**-**26** and highlights functional group tolerance of this ever-growing family of pseudo $[M(II)_7]$ metallocalix[6]arenes. The resultant double-bowl topology in **27** provides the dimensions (Å): 6.22 (base) × 8.54 (depth) × 19.35 (rim) as given in Table 4.1, while an out-of-plane dihedral angle of 40.09° is generated within the six-symmetry equivalent L_9^- units in **27** (Fig. 4.6). Complex **27** differs to its analogues by way of its crystallisation in the trigonal R-3 space group (monoclinic C2/c in **24** and $P2_1/_n$ in 25 and **26**). Akin to **24**-**26**, no enclosed / confined molecular cavities are formed by the packing arrangement in **27** although an extremely large void space of **~** 4467 $Å^3$ is observed. As a result, the diffuse solvent required modelling using the SQUEEZE program (see crystallography section for details). Although the efficient packing arrangements in **24**-**27** thwart the targeted formation of larger / extended molecular cavities, the introduction of the extended ligands 2-Methoxy-4-phenyl-6-[(E)-(methylimino)methyl]phenol (L_8H) and 2-Methoxy-4-tolyl-6-[(E)-(methylimino)methyl]phenol (L_9H) have successfully extended both the depth and rim cavity dimensions within these complexes with ranges of 61 (in **25**) to 77% (in **27**) and 38 (in **26**) to 45% (in **27**), respectively (Table 4.1).

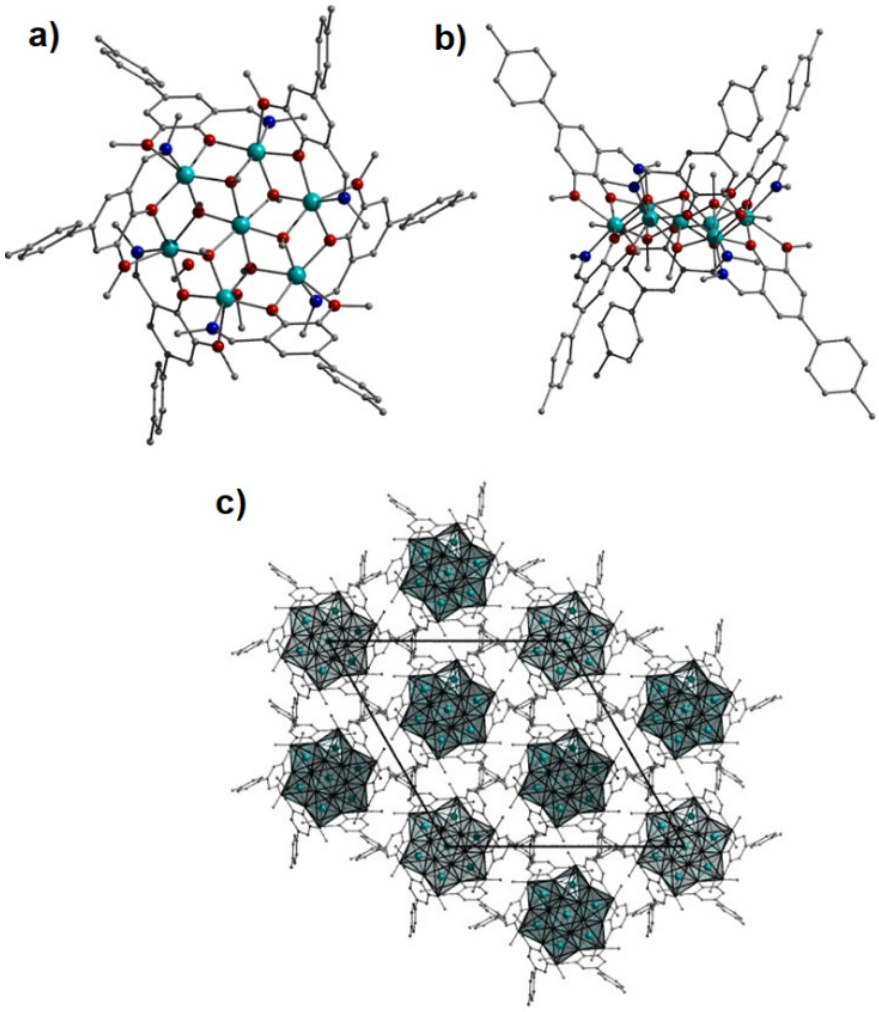

Figure 4.6 Crystal structure of **27** as viewed (perpendicular (a) and parallel (b) to the $\{Zn(II)_7\}$ plane. (c) Polyhedral representation of the packing arrangement in **27** as viewed along the *c* direction of the unit cell.

Table 4.1 Cavity dimensions observed in the crystals of **24-27** and a comparison with one of the original *pseudo* [M_7] (M = Co(II), Ni(II), Zn(II)) metallocalix[6]arenes.

Pseudo **metallocalix[6]arene**	**Cavity dimensions (Å)** **(base × depth × rim)**	**% increase in cavity depth** **(*cf.* corresponding [M_7]**	**% increase in cavity rim** **(*cf.* corresponding [M_7])**
[Co_7] (reference 8)	6.25 × 4.83 × 13.24	-	-
[Ni_7] (reference 7a)	6.20 × 4.99 × 12.76	-	-
[Zn_7] (reference 7b)	6.26 × 4.82 × 13.38	-	-
[Co_7] **(24)**	6.24 × 7.84 × 19.12	62	44
[Ni_7] **(25)**	6.19 × 8.04 × 18.00	61	41
[Zn_7] **(26)**	6.23 × 7.85 × 18.46	63	38
[Zn_7] (**27**)	6.22 × 8.54 × 19.35	77	45

4.2.2 Lower rim ligand modification and their metal coordination

It was decided that it would be interesting to introduce *lower rim* functionality to ligand L_8H in the form of the ligands 2-Methoxy-4-phenyl-6-{(E)-[(2-methoxyphenyl)imino]methyl}phenol ($L_{10}H$) and 2-[(E)-(Benzylimino)methyl]-4-phenyl-6-methoxyphenol ($L_{11}H$) as shown below (Scheme 4.1). We began with the reaction of $Ni(NO_3)_2.6H_2O$, $L_{10}H$ (deprotonated with NaOH) in acetonitrile, which led to the formation of the dimeric complex $[Ni(II)_2(L_{10})_2(H_2O)(NO_3)_2].2MeCN$ (**28**) (Fig. 4.7). The two distorted octahedral Ni(II) centres in **28** are connected by one L_{10}^- ligand (η^1:η^2:η^1:η^1 μ-bridging motif) and a bridging NO_3^- anion. The remaining L_{10}^- moiety chelates at the meridian coordination positions at Ni1 (via O6, N2 and O5) and as a result these two ligands lie at approximate right angles to one another (Figure 4.8). A ligated water and the second charge balancing NO_3^- anion complete the coordination sphere at the Ni2 centre by occupying the axial positions. The H_2O ligand is held in position by partaking in two intra-molecular H-bonding interactions with O_{phen} (O5) and OMe (O4) oxygen donor atoms belonging to a neighbouring L_{10}^- ligand (O7(H7A)···O5 = 2.027 Å and O7(H7A)···O4 = 2.336 Å). Likewise, the terminally

bound nitrate (via O9) interacts with a nearby ligand OMe proton (H42C) at a distance of 2.454 Å (C42(H42C)···O9), while the bridging NO_3^- also hydrogen bonds to a different juxtaposed OMe proton (H21B) belonging to the second ligand unit (C21(H21B)···O12 = 2.423 Å).

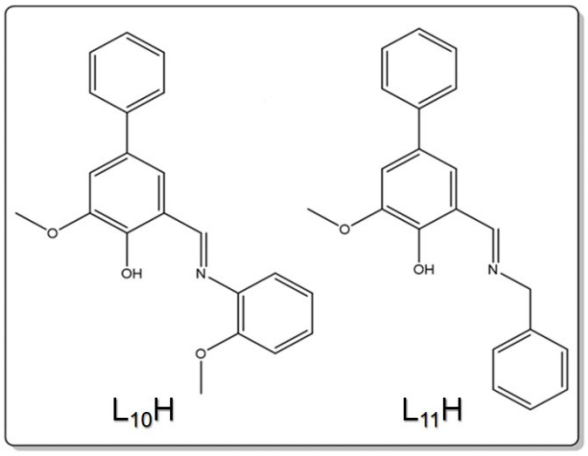

Scheme 4.1 The ligands 2-Methoxy-4-phenyl-6-{(E)-[(2-methoxyphenyl)imino]methyl}phenol ($L_{10}H$) and 2-[(E)-(Benzylimino)methyl]-4-phenyl-6-methoxyphenol ($L_{11}H$) used in this Chapter.

Intermolecular interactions are also commonplace within the structure of **28**. Once again, both the NO_3^- counter anions hydrogen bond to nearby ligand protons of neighbouring $\{Ni_2\}$ units (e.g. C12′(H12′)···O9 = 2.366 Å, C3′(H3B′)···O10 = 2.600 Å, C3′(H3C′)···O11 = 2.380 Å and C24′(H24A′)···O13 = 2.556 Å). Two crystallographically unique acetonitrile molecules of crystallisation lie near the $\{Ni(II)_2\}$ units in **28** and are locked in position through H-bonding interactions with ligated water protons (H7B) and nitrate O donor atoms (O13) at distances of 2.088 (O7(H7B)···N5) and 2.679 Å (O13···H46A(C46)), respectively. These MeCN molecules also act as molecular mortar by connecting the individual $\{Ni_2\}$ units in **28** through H-bonding interactions with neighbouring ligand protons (i.e. N6···H42A(C42) = 2.745 Å). Likwise, $\pi_{centroid}$-$\pi_{centroid}$ off-set parallel stacking interactions also aid the association of the dimeric moieties in **28** (e.g. $[C27\text{-}C32]_{centroid}$···$[C15'\text{-}C20']_{centroid}$ = 3.85 Å and $[C6\text{-}C11]_{centroid}$···$[C15'\text{-}C20']_{centroid}$ = 4.29 Å). Such extensive intermolecular interactions allow the individual units in **28** to arrange themselves into H-bonded 2D-sheets along the *ab* plane of the unit cell and these are connected along the *c*-direction via spacer MeCN solvents of crystallisation

(Fig. 4.9). Interestingly, the structure in **28** is akin to our complex $[Ni(II)_2(L_3)_3(H_2O)](NO_3)\cdot 2H_2O\cdot 3MeOH$ (**17**) previously discussed in Chapter 3, which was constructed with the similar ligand 2-methoxy-6-{[(2-methoxyphenyl)imino]methyl}phenol. For a full structural and magnetic discussion on this complex see reference 10. On the face of it, it is perhaps not surprising that these structurally similar ligands 2-Methoxy-6-{(E)-[(2-methoxyphenyl)imino]methyl}phenol (L_3H) and 2-Methoxy-4-phenyl-6-{(E)-[(2-methoxyphenyl)imino]methyl}phenol ($L_{10}H$) forge dimeric complexes in the form of $[Ni(II)_2(L_3)_3(H_2O)](NO_3)\cdot 2H_2O\cdot 3MeOH$ (**17**) and $[Ni(II)_2(L_{10})_2(H_2O)(NO_3)_2]\cdot 2MeCN$ (**28**), respectively (Fig. 4.7). However, upon closer inspection they do exhibit more subtle differences in terms of the number of ligands incorporated (2 vs. 3) and the location / binding of the nitrate counter anions (metal bound vs. unbound).

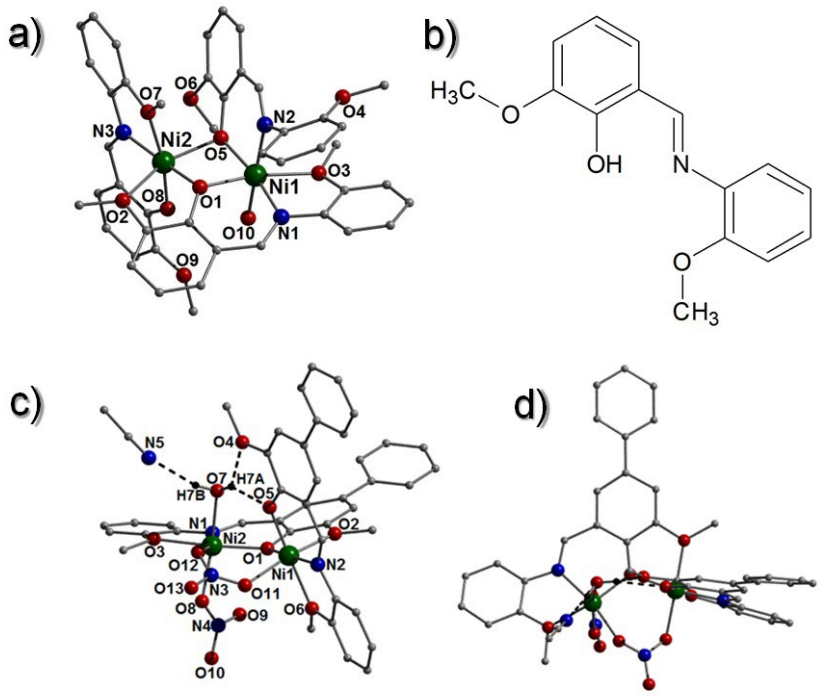

Figure 4.7 (a) Crystal structure of the dimeric complex $[Ni(II)_2(L_3)_3(H_2O)](NO_3)\cdot 2H_2O\cdot 3MeOH$ (**17**) previously discussed in Chapter 3, constructed with the ligand 2-Methoxy-6-{(E)-[(2-methoxyphenyl)imino]methyl}phenol; L_3H) (b). The structure of $[Ni(II)_2(L_{10})_2(H_2O)(NO_3)_2]\cdot 2MeCN$ (**28**) as viewed off-set (c) and perpendicular (d) to the Ni-O1-Ni plane. The dashed lines represent a selection of the intra- and intermolecular hydrogen bonding interactions observed in **28** (see main text for distances).

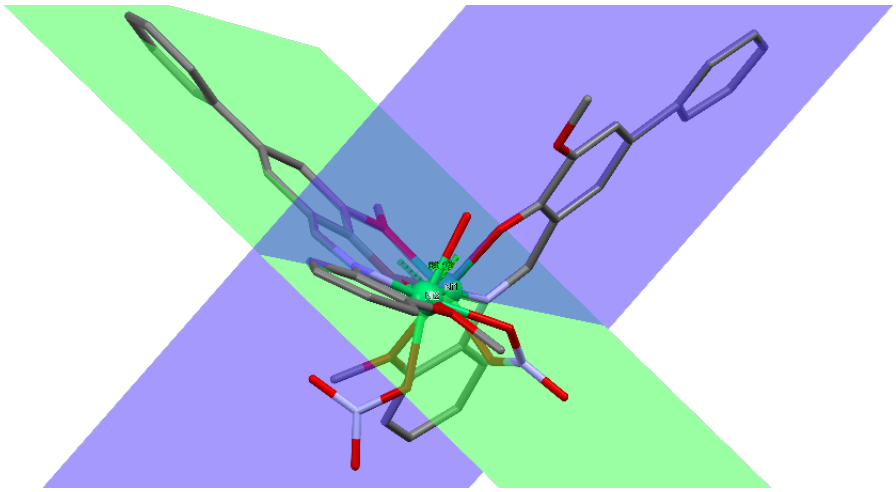

Figure 4.8 Two colour coded planes highlighting the 89.2° angle generated by the two L_{10}^{-} ligands units in $[Ni(II)_2(L_{10})_2(H_2O)(NO_3)_2]\cdot 2MeCN$ **28**. Intramolecular hydrogen bonds present in the complex marked by green dashed lines (right). Hydrogens have been omitted for clarity.

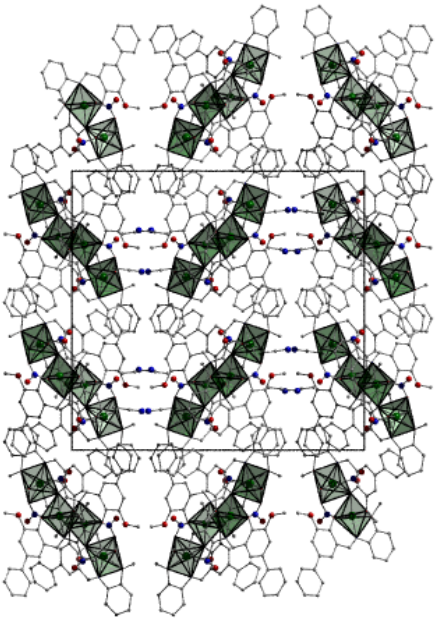

Figure 4.9 Polyhedral representation of the crystal packing arrangement in $[Ni(II)_2(L_{10})_2(H_2O)(NO_3)_2]\cdot 2MeCN$ (**28**) as viewed along the *a* unit cell direction.

The next iteration in ligand design gave rise to 2-[(E)-(Benzylimino)methyl]-4-phenyl-6-methoxyphenol (**$L_{11}H$**) and its methanolic reaction with $Zn(II)(NO_3)_2\cdot 6H_2O$ and NaOH (1:1:1) produced the monometallic H-bonded chain structure $[Zn(L_{11})_2]_n$ (**29**) (Fig. 4.10). The monomeric $[Zn(L_{11})_2]$ units in **29** comprises a distorted tetrahedral

Zn(II) centre ($\tau = 0.11$) bound to two singly deprotonated chelating L_{11}^- ligands (Zn1-O1 = 1.943 Å, Zn1-O3 = 1.930 Å, Zn1-N1 = 2.001 Å and Zn1-N2 = 1.999 Å). The structure in **29** shares similarities to the monomeric complexes $[Co(III)(L_5)_3]\cdot H_2O\cdot MeOH$ (**20a**) (b) and $[Ni(II)(L_5)_2]$ (**19**) previously discussed in Chapter 3 (Fig. 4.13). This is perhaps not surprising as $L_{11}H$ shares many similarities to the structure in 2-[(benzylimino)methyl]-6-methoxyphenol and differs only in its presence of a phenyl group at the 4-position of the phenolic backbone (out-of-plane dihedral angles of 31.16° and 31.42°). However, the introduction of this phenyl group has had a nuanced influence on the second coordination sphere in **29**. More specifically, the individual $\{Zn(L_{11})_2\}$ units arrange in the solid state as superimposable H-bonded chains propagating along the *b* unit cell direction (Fig. 4.11). The two ligands O_{phen} donor atoms (O1 and O3), along with the methoxy proton O2, partake in hydrogen bonding with the methylene bridge protons (H15B and H36B) belonging to neighbouring L_{11}^- ligands at distances of (Å): 2.440 ((O1···(H15B´)C15´), 2.339 ((O2···(H15B´)C15´) and 2.376 ((O3···(H36B´)C36´). The H-bonded chains in **29** pack in the space efficient brickwork motif along the *ac* plane of the unit cell (Fig. 4.12).

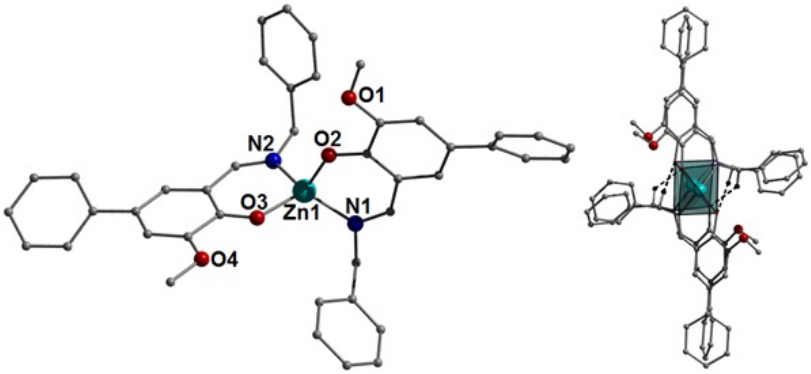

Figure 4.10 (a) The crystal structure of $[Zn(L_{11})_2]_n$ (**29**). (b) Polyhedral representation of one H-bonded chain propagating along the *b* unit cell direction in **29**.

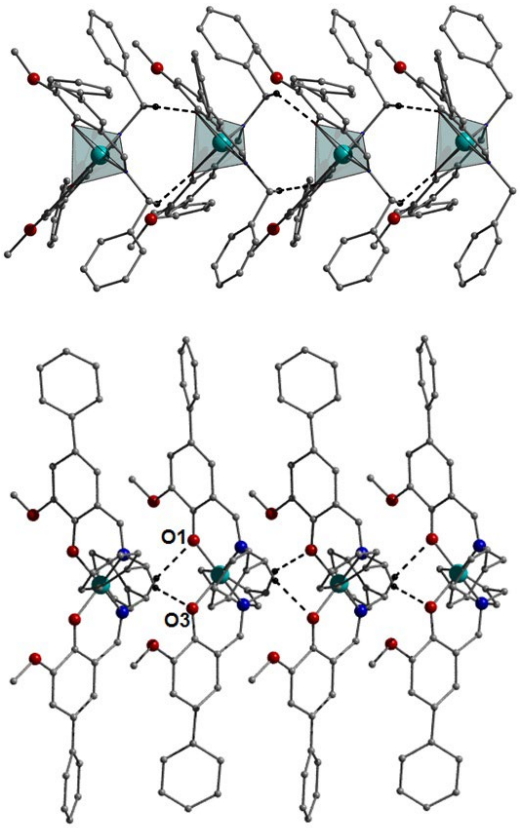

Figure 4.11 Crystal structure representations of the H-bonded chains in **29**. The dashed lines represent intermolecular H-bonding between the $\{Zn(L_{11})_2\}$ monomer units.

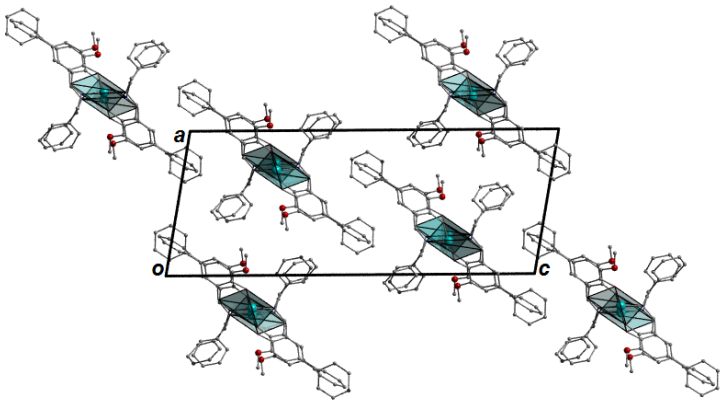

Figure 4.12 Polyhedral representation of the crystal packing arrangement in $[Zn(II)(L_{11})_2]n$ (**29**) showing the H-bonded chains propagating along the *b* direction of the unit cell.

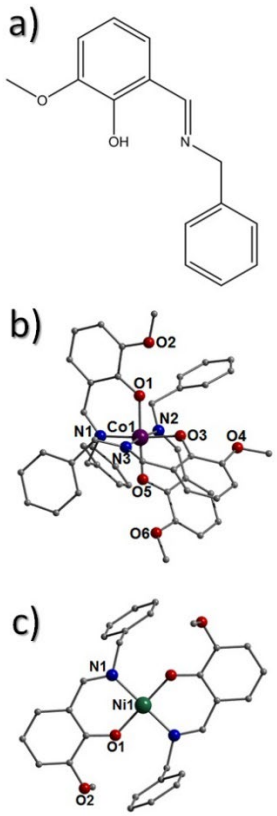

Figure 4.13 ChemDraw representation of the ligand 2-[(E)-(Benzylimino)methyl]-6-methoxyphenol (L_5H) used in the production of the complexes $[Co(III)(L_5)_3]\cdot H_2O\cdot MeOH$ (**20a**) (b) and $[Ni(II)(L_5)_2]$ (**19**) (c) as discussed in chapter 3.[10]

4.3 Concluding Remarks

The introduction of various functional groups at the upper rim (4-position) of the *pseudo* metallocalix[6]arene directing ligand 2-Methoxy-6-[(E)-(methylimino)methyl]phenol (L_1H) allows the deliberate introduction of molecular cavity wall extensions exampled by the heptanuclear complexes **24**-**27**. Although these complexes do indeed exhibit bowl dimensions which exceeded those of their previously reported siblings ($[M(II)_7(OH)_6(L_1)_6](NO_3)_2$; M = Co, Ni, Zn) they do not replicate their molecular cavities upon crystallisation. Instead, the individual $\{M(II)_7\}$ (M = Co, Ni, Zn) units in **24-27** pack through multiple interdigitated C-H$\cdots\pi$ intermolecular interactions between their aromatic ring L_x^- (x = 3, 4) units located at the upper rim of their metallocalix[6]arene structures. The result is a more space efficient packing arrangement at the expense of molecular cavity formation or guest

encapsulation. Work continues within the Jones group on the covalent connecting these individual {M(II)$_7$} units towards the deliberate design of organic cage-like permanent cavities comprising inorganic metallocalix[6]arene backbones.

We also presented in this work the synthesis of the novel ligands 2-Methoxy-4-phenyl-6-{(E)-[(2-methoxyphenyl)imino]methyl}phenol ($L_{10}H$) and 2-[(E)-(Benzylimino)methyl]-4-phenyl-6-methoxyphenol ($L_{11}H$) forged via the upper *and* lower rim functionalisation of the original *pseudo* metallocalix[6]arene producing ligand 2-methoxy-6-((methylimino)methyl)phenol. Investigations into their resultant metal ligation gave rise to the dimeric complex **[**$Ni(II)_2(L_{10})_2(H_2O)(NO_3)_2]\cdot 2MeCN$ (**28**) and the H-bonded 1-D chains in $[Zn(L_{11})_2]$ (**29**). We are awaiting magnetic susceptibility data on complexes $[Co(II)_7(OMe)_6(L_8)_6](NO_3)_2\cdot 3MeOH\cdot H_2O$ (**24**) and $[Ni(II)_7(OMe)_6(L_8)_6](NO_3)_2\cdot 2H_2O$ (**25**) and $[Ni(II)_2(L_{10})_2(H_2O)(NO_3)_2].2MeCN$ (**28**), in conjunction with the Brechin group at the University of Edinburgh. We expect similar magnetic behaviour to the previously reported complexes $[Co(II)_7(\mu_3\text{-}OH)_6(L_1)_6](NO_3)_2$ and $[Ni(II)_7(\mu_3\text{-}OH)_6(L_1)_6](NO_3)_2$.[7-8] Likewise, we expect complex 28 to show similar magnetic traits to the previously publishes complex $[Ni(II)_2(L_3)_3(H_2O)](NO_3)\cdot 2H_2O\cdot 3MeOH$ (**17**) (as described in Chapter 3).[10] Solid state photoluminescence studies on the H-bonded chain complex $[Zn(L_{11})_2]_n$ (**29**) are currently underway in collaboration with Igor Perepichka.

4.4 Experimental Section

Unless otherwise stated all materials (solvents and reagents) were purchased commercially and used as supplied without further purification. ***Caution:*** Although no difficulties were encountered in this work, great care must be taken when working with the potentially explosive nitrate salts. The infra-red spectra of **24** and **25** were recorded on a Perkin Elmer FT-IR *Spectrum One* spectrometer equipped with a Universal ATR Sampling accessory (NUI Galway). All other complexes in this work were measured at Bangor University on a Bruker Alpha FT-IR Platinum ATR. Elemental analysis on complexes **24** and **25** were carried using the School of Chemistry microanalysis service at NUI Galway. The elemental compositions of **26**-**29** were analysed at OEA Laboratories Ltd (Kelly Bray, Cornwall).

4.4.1 X-ray crystallography

The X-ray data for crystal structures of **24** and **25** were collected on an Xcalibur S single crystal diffractometer (Oxford Diffraction) using an enhanced Mo source, located at the School of Chemistry, NUI Galway. Each data reduction was carried out on the CrysAlisPro software package. The crystal structures were solved by direct methods (SHELXS-97) and refined by full matrix least squares using SHELXL-97.[11] SHELX operations were automated using the OSCAIL software package.[12] Complexes **26-29** were collected on an Rigaku AFC12 goniometer equipped with an enhanced sensitivity (HG) Saturn724+ detector mounted at the window of an FR-E+ Super Bright molybdenum rotating anode generator with HF Varimax optics (100m focus) (National Crystallography Service, School of Chemistry, University of Southampton). The cell determination and data collection of all complexes were carried out using the CrystalClear-SM Expert package (Rigaku, 2012). Each data reduction, cell refinement and absorption correction were carried out using CrysAlisPro software (Rigaku OD, 2015),[13] while all structures were initially solved and refined using SHELXT and SHELXL-2014[14] within OLEX-2.[15]

4.4.1.1 Collection and refinement details

With cell volumes of over approximately 10,000 $Å^3$, when analysing the data from complexes $[Co(II)_7(OMe)_6(L_8)_6](NO_3)_2 \cdot 3MeOH \cdot H_2O$ (**24**), $[Zn(II)_7(OH)_2(OMe)_4(L_8)_6](NO_3)_2 \cdot 4MeOH \cdot 10H_2O$ (**26**) and $[Zn(II)_7(OMe)_6(L_9)_6](NO_3)_2 \cdot 10MeOH \cdot 13H_2O$ (**27**) we were unable to successfully model the NO_3^- counter anions nor the diffuse solvent (MeOH and H_2O) in either data set and so we implemented the SQUEEZE program. From this we discovered that the two solvent accessible voids in **26** occupied a void volume of 1606 $Å^3$ each and contained approximately 465 electrons per void (2 voids located) and therefore 232.5 electrons per $[Zn_7]$ unit (Z = 4). From this, the formula in **26** was produced. Similarly, the large single solvent accessible void in **27** (void volume = 4467 $Å^3$) equates to 381 electrons per $[Zn_7]$ unit (Z = 3) and from this we determined the given formula. The disordered phenyl groups at the periphery of the structure in **26** was modelled over two sites (50:50 occupancy). The DFIX and FLAT restraints were subsequently required. All other non-hydrogen atoms in **26** were modelled as anisotropic. All hydrogen atoms

were placed in calculated positions. Likewise, all non-hydrogen atoms in **27** were given as anisotropic and all protons were placed in calculated positions.

All non-hydrogen atoms in $[Ni(II)_2(L_{10})_2(H_2O)(NO_3)_2].2MeCN$ (**28**) were given as anisotropic (including the acetonitrile molecules of crystallisation), while all H-atoms remained isotropic and placed in calculated positions. All non-hydrogen atoms in **28** were modelled as anisotropic. The ligated water protons (H7A and H7B) were found in the difference map and restrained using the DFIX tool. All other protons were modelled in calculated positions. All non-hydrogen atoms in **29** were modelled as anisotropic while the hydrogen atoms were placed in calculated positions. The aromatic carbon atoms C13 and C37 (on separate L_{11}^- moieties) required the ISOR restraint.

4.4.2 Ligand preparation (L_8H-$L_{11}H$)

All ligands employed in this work ($L_{8\text{-}11}H$) were synthesised in a two-stage process: *1)* Suzuki coupling of an arylboronic acid and 5-Bromo-3-methoxysalicylaldehyde to give the corresponding aldehyde precursor and *2)* Schiff base condensation of aldehyde with the required amine. Unless otherwise stated all materials (solvents and reagents) were purchased commercially and used as supplied without further purification.

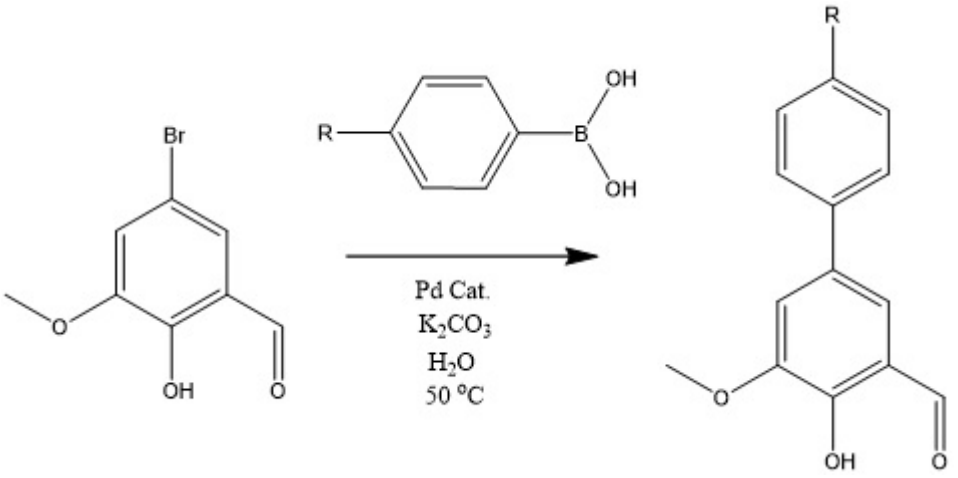

Scheme 4.2 General scheme of Suzuki coupling employed in the synthesis of 5-(4-R-phenyl)-3-methoxysalicyaldehyde (R = H (**PC1**); CH_3 (**PC2**).

4.4.2.1 Synthesis of 4-hydroxy-5-methoxy-3-biphenylcarbaldehyde ***(PC1**: precursor to L_8H)*

The first step in the synthesis of the Schiff base ligand 2-Methoxy-4-phenyl-6-[(E)-(methylimino)methyl]phenol (L_8H) involves the synthesis of 4-hydroxy-5-methoxy-3-biphenylcarbaldehyde (Precursor 1 (**PC1**) in Scheme 4.2) from its bromo precursor (5-Bromo-3-methoxysalicylaldehyde) via a Suzuki coupling reaction. The reaction was performed under a N_2 atmosphere and the reaction solvent (Millipore H_2O) was degassed via the freeze-pump-thaw technique.

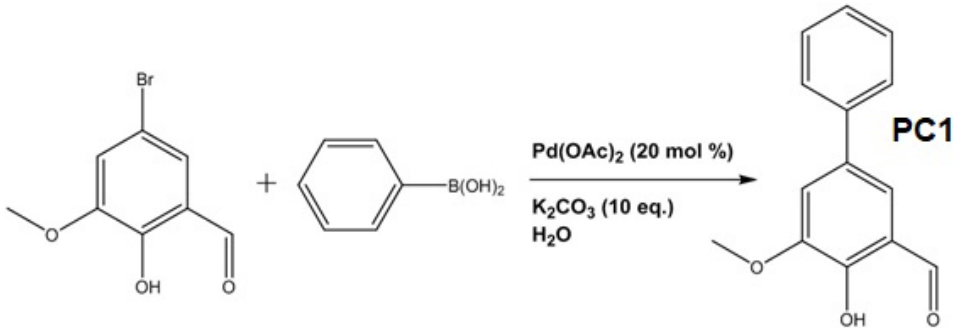

Scheme 4.3 Reaction scheme for the synthesis of 4-hydroxy-5-methoxy-3-biphenylcarbaldehyde (**PC1**)

To a solid mixture of 5-Bromo-3-methoxysalicylaldehyde (2.30 g, 9.95 mmol, 1.0 eq.), phenylboronic acid (1.58 g, 12.92 mmol, 1.30 eq.) and finely ground potassium carbonate (K_2CO_3) (13.75 g, 99.5 mmol, 10 eq.) in a 3-neck round-bottomed flask (250 cm^3), was added palladium acetate (0.50 g, 2.23 mmol, ~20 mol%) via a solid-addition 'fish-hook' adapter. Degassed millipore H_2O (~150 cm^3) was then added via cannula to the now evacuated reaction vessel (Scheme 3.1). The resultant dirty yellow suspension was stirred under high agitation to afford maximum dissolution of the solid reactants. After 4 hours stirring the suspension had adopted a brown appearance and was stirred for a further 2 days under N_2. The pH of the mixture was subsequently adjusted (pH = 7 using 6M HCl). Dichloromethane (CH_2Cl_2) (50 cm^3) was added and the mixture stirred for ~5 minutes. Two distinct phases were observed with the organic phase exhibiting a very dark red-brown appearance. The mixture was filtered over Celite to remove the palladium catalyst and the mother liquor transferred to a 500 cm^3 separation funnel. The organic layer was extracted with CH_2Cl_2 (3 x 50 cm^3) as an opaque red-orange solution. The aqueous layer was separated off as a sludge-like residue. The organic phase was further filtered over celite to yield a transparent red

mother liquor which was evaporated *in vacuo*. Dichloromethane (~50 cm^3) was then added to the resultant oil and the solution pre-adsorbed onto a small quantity of silica gel. The product was purified via Dry-Column-Vacuum-Chromatography using an 80:20 CH_2Cl_2: Petroleum Ether solvent system, while the separation itself was monitored via TLC. The resultant bright yellow transparent solution was evaporated *in vacuo* to yield a bright yellow solid (5-phenyl-2-hydroxy-3-methoxybenzaldehyde; **PC1**) in 74% yield (1.68 g). ^1H NMR (500 MHz, $CDCl_3$): δ 11.09 (s, 1H, CHO), 9.99 (s, 1H OH), 7.34-7.55 (m, Ar-H), 4.00 (s, 3H, O-CH_3). Elemental analysis (%) calculated (found) for $C_{14}H_{12}O_3$: C 73.67 (73.73), H 5.30 (5.17). FT-IR (cm^{-1}): 3062 (w), 2999 (w), 2967 (w), 2848 (w), 1644 (s), 1591 (m), 1471 (m), 1456 (w), 1443 (s), 1390 (m), 1355 (w), 1323 (m), 1297 (m), 1273 (s), 1231 (m), 1202 (s), 1184 (m), 1103 (m), 1069 (m), 1031 (w), 963 (s), 887 (m), 870 (m), 842 (w), 800 (w), 775 (w), 765 (s), 746 (m), 722 (s), 696 (s).

4.4.2.2 Synthesis of 2-Methoxy-4-phenyl-6-[(E)-(methylimino)methyl]phenol (L_8H*)*

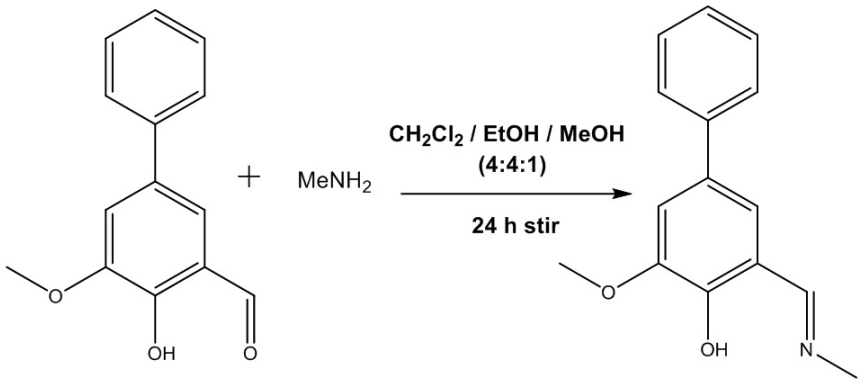

Scheme 4.4 Reaction scheme for the synthesis of 2-Methoxy-4-phenyl-6-[(E)-(methylimino)methyl]phenol (L_8H).

PC1 (1.68 g, 7.37 mmol, 1.0 eq.) was dissolved in CH_2Cl_2 (40 cm^3). $MeNH_2$ (0.229g, 7.37 mmol, 1.0 eq.) was then added resulting in the precipitation of a yellow solid. EtOH (40 cm^3) and MeOH (10 cm^3) were added to the mixture resulting in dissolution of the solid material and formation of a bright yellow-orange solution. This solution was subsequently stirred for a further 24 hours under ambient conditions after which time the solvent was evaporated *in vacuo* to yield a dark red-orange, viscous oil. This oil was dissolved in Et_2O (40 cm^3) to yield a bright orange solution. This was then placed in the fridge at ~4°C for 48 hrs after which time L_3H recrystallised as bright yellow needles in 80% yield (1.42 g). Elemental analysis (%) calculated (found) for

$C_{15}H_{15}N_1O_2$: C 74.67 (74.34), H 6.27 (6.47), N 5.81 (5.43). FT-IR (cm^{-1}): 1630 (m), 1596 (w), 1463 (m), 1441 (m), 1397 (m), 1271 (m), 1229 (w), 1208 (s), 1190 (m), 1104 (m), 1070 (m), 1005 (w), 969 (m), 888 (w), 874 (w), 853 (m), 779 (m), 758 (s), 716 (m), 696 (s). ^{1}H NMR (500 MHz, $CDCl_3$): δ 8.36 (s, 1H, N=CH).7.07-7.55 (m, Ar-H), 3.97 (s, 3H, O-CH_3), 3.51 (s, 3H, N-CH_3).MeOH: λ_{max} [nm] (ε_{max} 10^3 dm^3 mol^{-1} cm^{-1}): 224 (6980), 273 (13113), 434 (1346) MeCN: λ_{max} [nm] (ε_{max} 10^3 dm^3 mol^{-1} cm^{-1}): 208 (6828), 256 (12203), 339 (1128).

*4.4.2.3 Synthesis of 4-hydroxy-5-methoxy-4'-methyl-3-biphenylcarbaldehyde (**PC2**, precursor to L_9H)*

A suspension of 5-Bromo-3-methoxysalicylaldehyde (0.50 g, 2.16 mmol), 4-methylphenyl-boronic acid (0.40 g, 2.94 mmol), 20 mol% palladium acetate and potassium carbonate (3.32 g, 24.02 mmol) was stirred in 50 cm^3 deionised water for 2 days at 50 °C under a N_2 atmosphere. The deionised water was degassed with N_2 bubbling before being added to the reaction vessel containing the solid reagents. The reaction mixture was stirred and further N_2 bubbling took place for 30 mins before the mixture was heated to 50°C. During the course of the reaction the reaction mixture turned from a yellow to brown colour. The mixture was then adjusted to pH 7 using HCl (37%) and the product extracted with dichloromethane (3 × 50 cm^3). The crude product was pre-absorbed onto silica and purified via column chromatography using silica and an 80:20 dichloromethane: petroleum ether solvent system. The process was monitored by TLC and the resulting liquid was evaporated under vacuum to yield a yellow solid (yield = 48%). ^{1}H NMR ($CDCl_3$): δ (ppm) = 11.06 (s, 1H, OH), 9.98 (s, 1H, CHO), 7.45 (d, J = 7.18 Hz, 2H, CH), 7.37 (d, J = 2.01 Hz, 1H, CH), 7.32 (d, J = 1.82 Hz, 1H, CH), 7.27 (d, J = 6.80 Hz, 2H, CH), 3.99 (s, 3H, OCH_3), 2.41 (s, 3H, p-$C_6H_4CH_3$). ^{13}C NMR ($CDCl_3$): δ (ppm) = 196.89, 150.98, 148.69, 137.52, 137.02, 133.44, 129.83, 126.72, 122.63, 120.93, 117.08, 56.58, 21.24. ESI MS: m/z (% Rel. Ab.); 242.06 (100%, PC2), 243.01 (23%, PC4 + H^+), 196.20 (14%, PC4 -OH, -CHO). FT-IR (KBr): υ (cm^{-1}) = 3459.8 (b), 3083.5 - 2859.9 (w), 1658.7 (vs), 1475.9 (s), 1392.4 (s), 1333.2 (m), 1266.3 (vs), 1220.9 (s), 1204.3 (s), 962.1 (s), 815.6 (s), 761.9 (s), 733.3 (s), 501.9 (m).

4.4.2.4 Synthesis of 2-Methoxy-4-tolyl-6-[(E)-(methylimino)methyl]phenol (L_9H).

To a suspension 4-hydroxy-5-methoxy-4'-methyl-3-biphenylcarbaldehyde (PC2, 0.20 g, 0.83 mmol) in 30 mL methanol, 40% aqueous methylamine solution (2 mL, 45 mmol) was added and the solution stirred at ambient temperature for 4 hours. 50 cm^3 saturated brine water was then added and the organic layer extracted with chloroform (3 × 30 cm^3). The resulting organic mixture was dried with $MgSO_4$ and gravity filtrated and evaporated under vacuum, yielding a red / orange solid (yield 85%). ^{1}H NMR ($CDCl_3$): δ (ppm): 8.40 (s, 1H, C*H*N), 7.45 (d, J = 8.01 Hz, 2H, C*H*), 7.24 (d, J = 7.95 Hz, 2H, C*H*), 7.16 (s, 1H, C*H*), 7.14 (s, 1H, C*H*), 3.96 (s, 3H, OCH_3), 3.52 (s, 3H, NCH_3), 2.39 (s, 3H, p-$C_6H_4CH_3$). ^{13}C NMR ($CDCl_3$): δ (ppm) = 166.33, 151.80, 148.82, 137.90, 136.57, 131.08, 129.51, 126.49, 120.88, 118.49, 112.84, 56.21, 45.53, 21.06. ESI MS: m/z (% Rel. Ab.); 255.07 (100%, L_4H), 240.09 (89%, L_4H–CH_3), 255.99 (19%, L_4H^+), 238.16 (16%, L_4H –OH). FT-IR (KBr): υ (cm^{-1}) = 3472.1 (b), 3024.2 – 2855.8 (w), 1634.9 (vs), 1478.5 (s), 1396.8 (m), 1270 (s), 1218.4 (s), 1203.4 (s), 1104.9 (s), 969.7 (m), 891.2 (m), 822 (s), 811.8 (s), 764.7 (m), 505.5 (m).

4.4.2.5 General synthesis of ligands $L_{10}H$ and $L_{11}H$

4-hydroxy-5-methoxy-3-biphenylcarbaldehyde (**PC1**) was placed in a 250 cm^3 round-bottomed flask and dissolved in 100 cm^3 of methanol. The primary amine is added (1.05 eq) with vigorous stirring and the solution the reaction allowed to proceed under a N_2 atmosphere for 4 h. The resultant target ligands were obtained after solvent removal under reduced pressure. The specific amounts and resultant yields are given in the Table below:

Table 4.2 Data for 2-Methoxy-4-phenyl-6-{(E)-[(2-methoxyphenyl)imino]methyl}phenol ($L_{10}H$).

	PC1	**o-anisidine**	**$L_{10}H$**
Mass	1.08 g	612 mg	1.46 g
Yield		-	93%

^{1}H NMR (400 MHz, $CDCl_3$) δ 8.78 (s, 1H), 7.58 (dd, J = 12.3, 5.0 Hz, 3H), 7.44 (t, J = 7.6 Hz, 3H), 7.34 (dd, J = 4.8, 2.5 Hz, 1H), 7.21 (dd, J = 12.3, 1.9 Hz, 2H), 7.05 – 6.97 (m, 2H), 4.01 (s, 3H), 3.91 (s, 3H). Elemental analysis (%) calculated (found) for **$L_{10}H$**·0.5H_2O ($C_{21}H_{20}N_1O_{3.5}$): C 73.66 (73.97), H 5.89 (5.44), N 4.09 (4.39). FTIR (cm^{-1}): 3362 (w,b), 3000 (w), 2935 (w), 2834 (w), 1614 (s), 1493 (s), 1460 (s), 1397 (m), 1370 (m), 1342 (m), 1269 (s), 1249 (s), 1220 (s), 1192 (s), 1174 (s), 1117 (s), 1025 (s), 972 (s), 930 (w), 889 (w), 860 (s), 787 (m), 739 (s), 695 (s), 627 (m), 579 (m), 525 (m), 470 (m). ESI-MS (m/z): 333.13 ($L_{10}H + H^+$).

Table 4.3 Data for 2-[(E)-(Benzylimino)methyl]-4-phenyl-6-methoxyphenol **(**$L_{11}H$).

	PC1	**Benzylamine**	**$L_{11}H$**
Mass	954.80 mg	470.67 mg	1.21 g
Yield			91%

^{1}H NMR (400 MHz, $CDCl_3$) δ 8.49 (s, 1H), 7.55 (d, J = 7.2 Hz, 2H), 7.43 (t, J = 7.4 Hz, 3H), 7.37 – 7.31 (m, 3H), 7.14 (dd, J = 19.0, 1.9 Hz, 2H), 4.85 (d, J = 10.9 Hz, 2H), 3.97 (s, 3H). FTIR (cm^{-1}): 3290 (m), 3054 – 2946 (w,b), 1627 (m), 1560 (m), 1449 (s), 1382 (s), 1328 (s), 1298 (s), 1269 (s), 1037 (m), 812 (m), 735 (s), 694 (s), 627 (s), 575 (s), 474 (m). ESI-MS (m/z): 317.11 ($L_{11}H + H^+$).

4.4.3 Preparation of complexes 25-29

*4.4.3.1 Synthesis of [Ni(II)$_7$(OMe)$_6$(L_8)$_6$](NO_3)$_2$·2H_2O (**25**)*

To a solution of $Ni(NO_3)_2.6H_2O$ (0.10 g, 0.34 mmol) in MeOH (20 cm^3) were added L_8H (0.083 g, 0.34 mmol) and solid NaOH (0.014 g, 0.34 mmol) and the mixture stirred to afford an opaque bright green solution. The solution was stirred for a further 3 hours, following which it was filtered to afford a bright green mother liquor. The mother liquor was diffused with Et_2O, which afforded green needles of **25** in 15% yield. Elemental analysis (%) calculated (found) for **25** ($C_{96}H_{106}N_8O_{26}Ni_7$): C 52.44 (52.20), H 4.86 (4.38), N 5.10 (5.49). FT-IR (cm^{-1}): 3395 (b), 1639 (s), 1548 (w), 1472 (s), 1393 (s), 1312 (s), 1258 (s), 1207 (s), 1095 (s), 848 (m), 837 (w), 825 (w), 760 (s), 720 (s).

*4.4.3.2 Synthesis of $[Zn(II)_7(OH)_2(OMe)_4(L_8)_6](NO_3)_2 \cdot 4MeOH \cdot 10H_2O$ (**26**)*

A solution of $Zn(NO_3)_2.6H_2O$ (0.10 g, 0.33 mmol) in MeOH (20 cm^3) was mixed with L_8H (0.081 g, 0.33 mmol) and solid NaOH (0.013 g, 0.33 mmol) and the mixture stirred to afford complete dissolution of the solids. The resultant yellow solution was stirred for a further 3 hours, after which time it was filtered to afford a bright yellow mother liquor. The mother liquor was allowed to slowly concentrate via slow evaporation of the solvent to yield **26** as pale yellow blocks in 15% yield. Elemental analysis (%) calculated (found) for **26**$\cdot 3H_2O$ ($C_{100}H_{116}N_8O_{27}Zn_7$): C 51.78 (51.90), H 5.04 (4.72), N 4.83 (4.55). FT-IR (cm^{-1}): 3390 (b), 2932 (b), 1631 (s), 1599 (m), 1558 (w), 1476 (s), 1458 (s), 1398 (m), 1313 (s), 1268 (s), 1203 (s), 1100 (m), 1073 (w), 1038 (w), 1015 (w), 970 (m), 862 (m), 803 (m), 759 (s), 724 (m), 697 (m).

*4.4.3.3 Synthesis of $[Zn(II)_7(OMe)_6(L_9)_6](NO_3)_2 \cdot 10MeOH \cdot 13H_2O$ (**27**)*

To a methanolic (30 cm^3) solution $Zn(NO_3)_2.6H_2O$ (0.25 g. 0.84 mmol), L_9H (0.215 g, 0.84 mmol) and NaOH (0.034 g, 0.84 mmol) were added. The resultant pale yellow solution was stirred for 4 h and allowed to settle for 30 minutes before being gravity filtered. X-ray quality crystals of **27** were obtained in 20% yield upon slow evaporation of the mother liquor over a period of 2-3 weeks. Elemental analysis (%) calculated (found) for **27**$\cdot 4MeOH \cdot 5H_2O$ ($C_{106}H_{114}N_8O_{33}Zn_7$): C 51.22 (51.60), H 4.62 (4.52), N 4.51 (4.35). FT-IR (cm^{-1}): 3429 (b), 2932 (b), 2831 (b), 1635 (s), 1577 (w), 1558 (w), 1517 (m), 1479 (s), 1460 (s), 1398 (m), 1384 (m), 1352 (w), 1313 (m), 1269 (s), 1245 (s), 1203 (s), 1179 (m), 1097 (s), 1074 (m), 1030 (s), 969 (s), 893 (w), 870 (w), 829 (s), 811 (s), 778 (w), 759 (w), 710 (w), 636 (w), 579 (w), 564 (w).

*4.4.3.4 Synthesis of $[Ni(II)_2(L_{10})_2(H_2O)(NO_3)_2].2MeCN$ (**28**)*

To a methanolic solution (35 cm^3) of $Ni(NO_3)_2.6H_2O$ (0.25 g, 0.85 mmol) was added $L_{10}H$ (0.28 g, 0.85 mmol) and NaOH (0.034 g, 0.85 mmol). The resultant green solution was stirred for 4 hours before being filtered and reduced to dryness under reduced pressure. The resultant solid was re-dissolved in acetonitrile to give X-ray quality crystals of **28** upon slow Et_2O diffusion after four days in 20% yield. Elemental

analysis (%) calculated (found) for **28** ($C_{46}H_{44}N_6O_{13}Ni_2$): C 54.91 (54.72), H 4.41 (4.47), N 8.35 (8.03).

*4.4.3.5 Synthesis of [Zn(II)(L_{10})$_2$] (**29**)*

To a methanolic solution (30 cm^3) of $Zn(NO_3)_2.6H_2O$ (0.25 g, 0.85 mmol) was added $L_{11}H$ (0.26 g, 0.85 mmol) and NaOH (0.034 g, 0.85 mmol). The resultant mixture was stirred for 4 hours and was subsequently gravity filtered. X-ray quality crystals of **29** were subsequently obtained upon slow evaporation of the mother liquor over a period of one week. Elemental analysis (%) calculated (found) for **29** ($C_{42}H_{36}N_2O_4Zn_1$): C 72.26 (72.20), H 5.20 (5.11), N 4.01 (4.42). FT-IR (cm^{-1}): 1616 (s), 1598 (s), 1543 (m), 1518 (m), 1498 (m), 1457 (m), 1333 (m), 1305 (m), 1272 (s), 1206 (s), 1139 (w), 1113 (w), 1074 (w), 1020 (w), 973 (w), 959 (w), 914 (w), 895 (w), 861 (w), 835 (w), 824 (w), 802 (w), 754 (s), 719 (w), 697 (s), 641 (w), 628 (w), 598 (w), 577 (w), 564 (w), 542 (w), 494 (w), 484 (w).

Table 4.4 Crystallographic data obtained from complexes **24**-**26**.

	24·2H$_2$O·3MeOH	**25**·2H$_2$O	**26**·2H$_2$O
Formula[a]	$C_{96}H_{114}N_8O_{27}Co_7$	$C_{93}H_{97}N_8O_{26}Ni_7$	$C_{104}H_{146}N_8O_{38}Zn_7$
M_W	2165.33	2015.62	2573.95
Crystal System	Monoclinic	Monoclinic	Monoclinic
Space group	C2/c	P2$_1$/n	C2/c
a/Å	26.7878(12)	14.6830(7)	26.9617(12)
b/Å	15.1243(7)	14.3260(5)	15.1167(7)
c/Å	28.0186(10)	24.1964(11)	28.0457(10)
α/°	90	90	90
β/°	105.301(4)	106.598(5)	105.778(4)
γ/°	90	90	90
V/Å^3	10949.3(8)	4877.6(4)	11000.0(8)
Z	4	2	4
T/K	150(2)	100(2)	150(2)
λ[b]/Å	0.71073	0.71073	0.71073
D_c/g cm^{-3}	1.314	1.372	1.225
μ(Mo-Ka)/ mm^{-1}	1.103	1.389	1.558
Meas./indep.(R_{int}) refl.	10025 / 6252 (0.0535)	8924 / 5819 (0.0532)	25142 / 12696 (0.0737)
Restraints, parameters	10, 568	15, 562	20, 562
wR2 (all data)[c]	0.2267	0.2435	0.2082
$R1$[d,e]	0.0710	0.0756	0.1729
Goodness of fit on F^2	1.039	1.097	0.992

[a] Includes guest molecules.[b] Mo-Kα radiation, graphite monochromator. [c] $wR2 = [\Sigma w(|F_o^2| - |F_c^2|)^2 / \Sigma w|F_o^2|^2]^{1/2}$. [d]For observed data. [e] $R1 = \Sigma||F_o| - |F_c|| / \Sigma|F_o|$.

Table 4.5 Crystallographic data obtained from complexes **27-29**.

	27·13H_2O·10MeOH	**28**·2MeCN	**29**
Formula[a]	$C_{102}H_{114}N_8O_{24}Zn_7$	$C_{46}H_{44}N_6O_{13}Ni_2$	$C_{42}H_{36}N_2O_4Zn_1$
M_W	2822.10	1006.29	698.10
Crystal System	Trigonal	Orthorhombic	Monoclinic
Space group	R-3	Pbca	$P2_1/n$
a/Å	23.6952(4)	14.06900(10)	11.6792(6)
b/Å	23.6952(4)	24.61980(10)	9.8090(5)
c/Å	21.8157(3)	25.76250(10)	29.3921(15)
α/°	90	90	90
β/°	90	90	99.865(4)
γ/°	120	90	90
V/Å^3	10607.7(3)	8923.51(8)	3317.4(3)
Z	3	8	4
T/K	100(2)	100(2)	100(2)
λ[b]/Å	0.71073	1.54184	0.71073
D_c/g cm^{-3}	1.019	1.498	1.398
μ(Mo-Ka)/ mm^{-1}	1.215	0.918	0.788
Meas./indep.(R_{int}) refl.	13254 / 4319 (0.0167)	79050 / 8150 (0.0355)	23290 / 5180 (0.2194)
Restraints, parameters	0, 205	2, 618	0, 434
wR2 (all data)[c]	0.1690	0.1827	0.4179
$R1$[d,e]	0.0442	0.0561	0.1500
Goodness of fit on F^2	1.171	1.062	1.107

[a] Includes guest molecules. [b] Mo-Kα radiation, graphite monochromator. [c] $wR2 = [\Sigma w(|F_o^2| - |F_c^2|)^2 / \Sigma w|F_o^2|^2]^{1/2}$. [d] For observed data. [e] $R1 = \Sigma||F_o| - |F_c|| / \Sigma|F_o|$.

Table 4.6 Bond Valence Sum calculations on $[Co(II)_7(OMe)_6(L_3)_6](NO_3)_2 \cdot H_2O \cdot 3MeOH$ (**24**).

Metal ion	BVS score
Co1	1.95
Co2	2.01
Co3	2.00
Co4	2.06

4.5 References

1. C. Plenk, J. Krause, M. Beck and E. Rentschler. *Chem. Commun.,* 2015, **51**, 6524-6527.

2. A. D. Burrows, C. G. Frost, M. F. Mahon and C. Richardson. *Angew. Chem., Int. Ed.,* 2008, **47(44)**, 8482-8486.

3. J. L. Segura, S. Royuela and M. Mar Ramos. *Chem. Soc. Rev.,* 2019, **48**, 3903-3945.

4. For examples of Single-Molecule Magnet templation / fine-tuning using careful ligand selection:
(a) A. Fetoh, G. Cosquer, M. Morimoto, M. Irie, O. El-Gammal, G. Abu El-Reash, B. K. Breedlove and M. Yamashita. *Sci. Reports.,* 2016, **6**, 23785. (b) K. S. Pedersen, J. Bendix and R. Clérac. *Chem. Commun*., 2014, **50**, 4396-4415. (c) L. M. C. Beltram and J. R. Long. *Acc. Chem. Res.,* 2005, **4**, 325-334. For other (non SMM) examples see: (a) Y.-L. Lu, W.-L. Lan, W. Shi, Q.-H. Jin and Peng Cheng. *Dalton Trans.,* 2021, **50**, 13124-13137. (b) Y. Gao, M. Aerts, C. S. Suchand Sandeep, E. Talgorn, T. J. Savenije, S. Kinge, L. D. A. Siebbeles and A. J. Houtepen. *ACS Nano,* 2012, **6(11)**, 9606-9614.

5. L. F. Jones, A. Prescimone, M. Evangelisti and E. K. Brechin. *Chem. Commun.,* 2009, 2023-2025.

6. (a) F.-R. Dai, Y. Qiao and Z. Wang. *Inorg. Chem. Front.,* 2016, **3**, 243-249. For reviews on molecular containers see: (b) M. Yoshizawa, J. K. Klosterman, M. Fujita. *Angew. Chem. Int. Ed.,* 2009, **48**, 3418-3438. (c) P. Ballester, M. Fujita, J. Rebek Jr. *Chem. Soc. Rev.,* 2015, **44**, 392-393.

7. (a) S. T. Meally, G. Karotsis, E. K. Brechin, G. S. Papaefstathiou, P. W. Dunne, P. McArdle and L. F. Jones. *CrystEngComm.,* 2010, **12, 59. (b)** S. T. Meally, C. McDonald, G. Karotsis, G. S. Papaefstathiou, E. K. Brechin, P. W. Dunne, P. McArdle, N. P. Power and L. F. Jones. *Dalton Trans.,* 2010, **39**, 4809.

8. S. T. Meally, C. McDonald, P. Kealy, S. M. Taylor, E. K. Brechin and L. F. Jones. *Dalton Trans.,* 2012, **41(18)**, 5610.

9 S.T. Meally, Investigating the structural and magnetic characteristics of polynuclear complexes including the solid-state hosting abilities of [M_7] (M = Ni(II), Zn(II)M Co(II/III) metallocalix[6]arene discs. PhD thesis, NUI Galway, Ireland. 2012.

10. M. E. Slater-Parry, J. P. Durrant, J. M. Howells, M. B. Pitak, P. N. Horton, W. T. Klooster, S. J. Coles, H. M. O`Connor, E. K. Brechin, A.-L. Barra and L. F. Jones. *Dalton Trans*., 2019, **48**, 1477-1488.

11. G. M. Sheldrick, *Acta. Crystallogr., Sect. A: Found. Crystallogr.,* 1990, **A46**, 467.

12. P. McArdle, P. Daly and D. Cunningham, *J. Appl. Crystallogr*., 2002, **35**, 378.

13. Rigaku OD (2015). *CrysAlis PRO*. Rigaku Oxford Diffraction Ltd, Yarnton, England.

14. G. M. Sheldrick. *Acta Crystallogr. Sect. C Struct. Chem.* 2015, **71**, 3.

15. O. V. Dolomanov, L. J. Bourhis, R. J. Gildea, J. A. K. Howard and H. J. Puschmann. *Appl. Crystallogr.* 2009, *42*, 339.

Chapter 5

Concluding Remarks and Future Work

5.1 Concluding Remarks

Previous work from the Jones group showed how a family of *pseudo* [M_7] (M = Co(II), Ni(II) and Zn(II)) metallocalix[6]arenes of general formulae [$M(II)_7(\mu_3\text{-}OH)_6(L_1)_6](NO_3)_2$ (where L_1H = 2-Methoxy-6-[(E)-(methylimino)methyl]phenol; Fig. 5.1a-b) were able to accommodate various solvent guest molecules (MeCN, $MeNO_2$, MeOH) within the molecular cavities formed in the solid state upon their crystallisation (see Figure 5.1c-inset).[1] Part of this PhD study set out to further investigate the guest accommodating power of this family of complexes. To this end and as described in Chapter 2, a total of six new guest molecules (see Fig. 5.1c) were successfully encapsulated within these *pseudo* metallocalix[6]arene complexes. Examples include [(2-fur)⊂$Zn(II)_7(OMe)_6(L_1)_6](NO_3)_2{\cdot}3H_2O$ (**1**), [(benz)⊂$Ni(II)_7(OH)_6(L_1)_6](NO_3)_2$ (**8**) and [(acetoph)⊂[$Co(II)_7(OMe)_6(L_1)_6](NO_3)_2{\cdot}7H_2O$ (**16**) (where 2-fur = 2-furaldehyde; benz = benzophenone and acetoph = acetophenone).

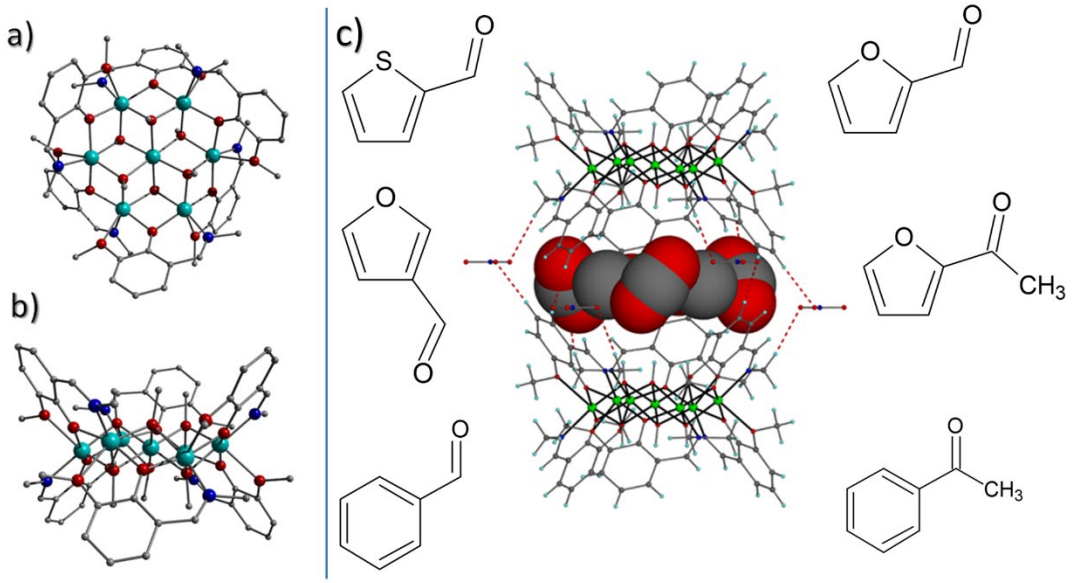

Figure 5.1 Crystal structure of the complex [(2-fur)⊂$Zn(II)_7(OMe)_6(L_1)_6](NO_3)_2{\cdot}3H_2O$ (**1**) (where L_1H = 2-Methoxy-6-[(E)-(methylimino)methyl]phenol) as viewed perpendicular (a) and parallel (b) to the planar body centred hexagonal core (guest 2-furaldehyde has been omitted). The NO_3^- counter anions and the majority of H atoms have been omitted for clarity. Colour code: Light blue (Zn), Red (O), Blue (N), Grey (C). (c) The eight guest organic molecules used in this work and described in detail in Chapter 2: (2- and 3-furaldehyde (2-, 3-

Fur), benzaldehyde (bzal), 2-thiophenecarboxaldehyde (2-thio), 2-acetylfuran (2-acetylfuran) and acetophenone (acetoph). Inset: A typical host *pseudo* metallocalix[6]arene in the form of the complex $[(MeOH)_2 \subset Ni(II)_7(OH)_6(L_1)_6](NO_3)_2$ exhibiting a molecular cavity that accommodates (in this instance) MeOH guest moieties (space-fill represented).[1] Colour code: Green (Ni), Red (O), Blue (N), Grey (C), Light blue (H). Dashed lines represent H-bonding interactions.

The work described in Chapters 3 and 4 describe the design and synthesis of nine (9) new ligands (L_3H-$L_{11}H$; see Figures 5.2 and 5.3) whose structures are best described as modifications upon the original *pseudo* metallocalix[6]arene ligand 2-Methoxy-6-[(E)-(methylimino)methyl]phenol (L_1H). More specifically, ligands L_3H-L_7H are each modified at the *lower rim* positions as shown in the inset of Figure 5.2. Metal complexation of these ligands have produced a number of new complexes ranging in topologies of one (e.g. $[Ni(II)(L_5)_2]$ (**19**) and $[Co(III)(L_5)_3]\cdot H_2O\cdot MeOH$ (**20a**)) to seven ($[Co(II)_7(OMe)_6(L_5)_6](NO_3)_2\cdot 0.5H_2O\cdot 3MeOH$ (**20b**)). From these findings it becomes clear that introducing such bulky functional groups near the binding site ligand positions often hinders polymetallic complexation and favours lower nuclearity topology formation. Indeed, this is also the case when the upper and lower rim modified ligands 2-Methoxy-4-phenyl-6-{(E)-[(2-methoxyphenyl)imino]methyl}phenol ($L_{10}H$) and 2-[(E)-(Benzylimino)methyl]-4-phenyl-6-methoxyphenol ($L_{11}H$) form the di- and monometallic complexes $[Ni(II)_2(L_{10})_2(H_2O)(NO_3)_2]$.2MeCN (**28**) and $[Zn(II)(L_{11})_2]_n$ (**29**), respectively (Fig. 5.3). As (perhaps) expected, when only the upper rim ligand position is functionalised (e.g. in the form of the ligands 2-Methoxy-4-phenyl-6-[(E)-(methylimino)methyl]phenol (**(**L_8H) and 2-Methoxy-4-tolyl-6-[(E)-(methylimino)methyl]phenol (L_9H)), *pseudo* metallocalix[6]arene formation is maintained as exampled in the complexes $[Ni(II)_7(OMe)_6(L_8)_6](NO_3)_2\cdot 2H_2O$ (**25),** $[Zn(II)_7(OH)_2(OMe)_4(L_8)_6](NO_3)_2\cdot 4MeOH\cdot 10H_2O$ (**26**) and $[Zn(II)_7(OMe)_6(L_9)_6](NO_3)_2\cdot 10MeOH\cdot 13H_2O$ (**27**) (Fig. 5.3).

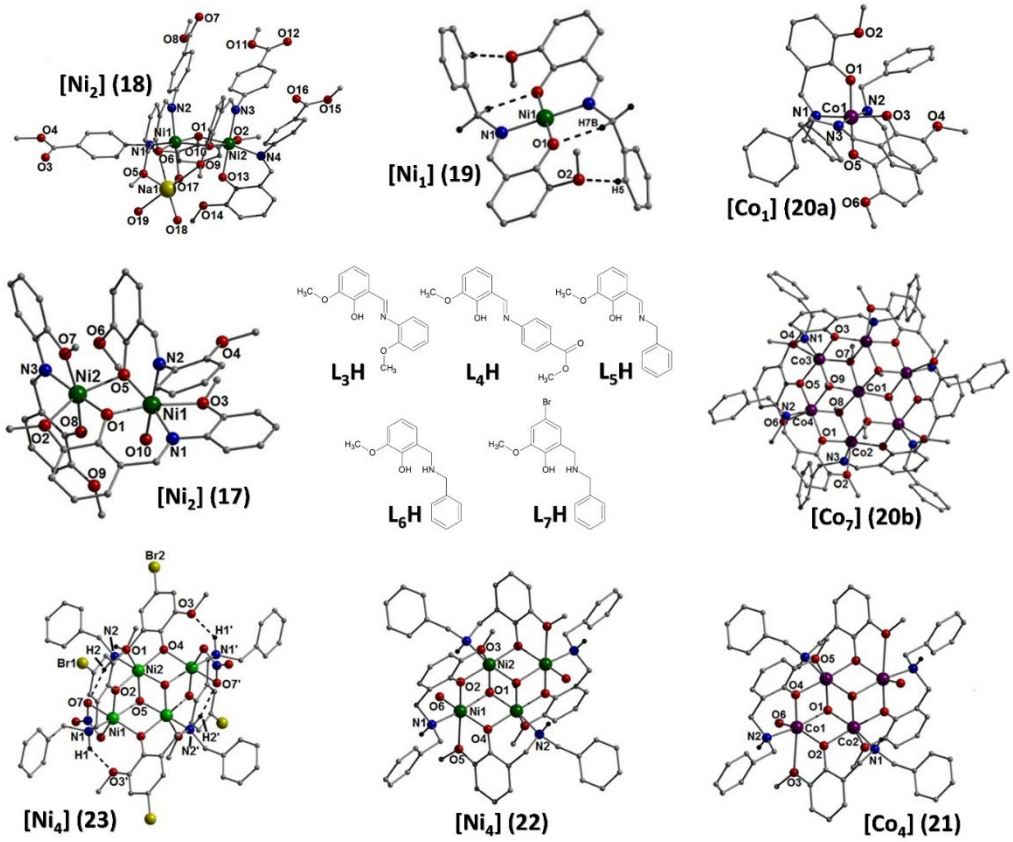

Figure 5.2 Schematic highlighting the *lower rim* modified ligands 2-Methoxy-6-{(E)-[(2-methoxyphenyl)imino]methyl}phenol (L_3H), methyl 4-[(E)-(2-hydroxy-3-methoxybenzylidene)amino]benzoate (L_4H), 2-[(E)-(Benzylimino)methyl]-6-methoxyphenol (L_5H), 2-[(Benzylamino)methyl]-6-methoxyphenol (L_6H) and 2-[(benzylamino)methyl]-4-bromo-6-methoxyphenol (L_7H) along with examples of Ni(II) and Co(II) complexes constructed with these ligands as described in Chapter 3. The majority of H atoms have been omitted for clarity. Dashed lines represent intramolecular H-bonding interactions. Colour code: Green (Ni), Purple (Co), Red (O), Blue (N), Grey (C), Black (H) and Yellow (Br).

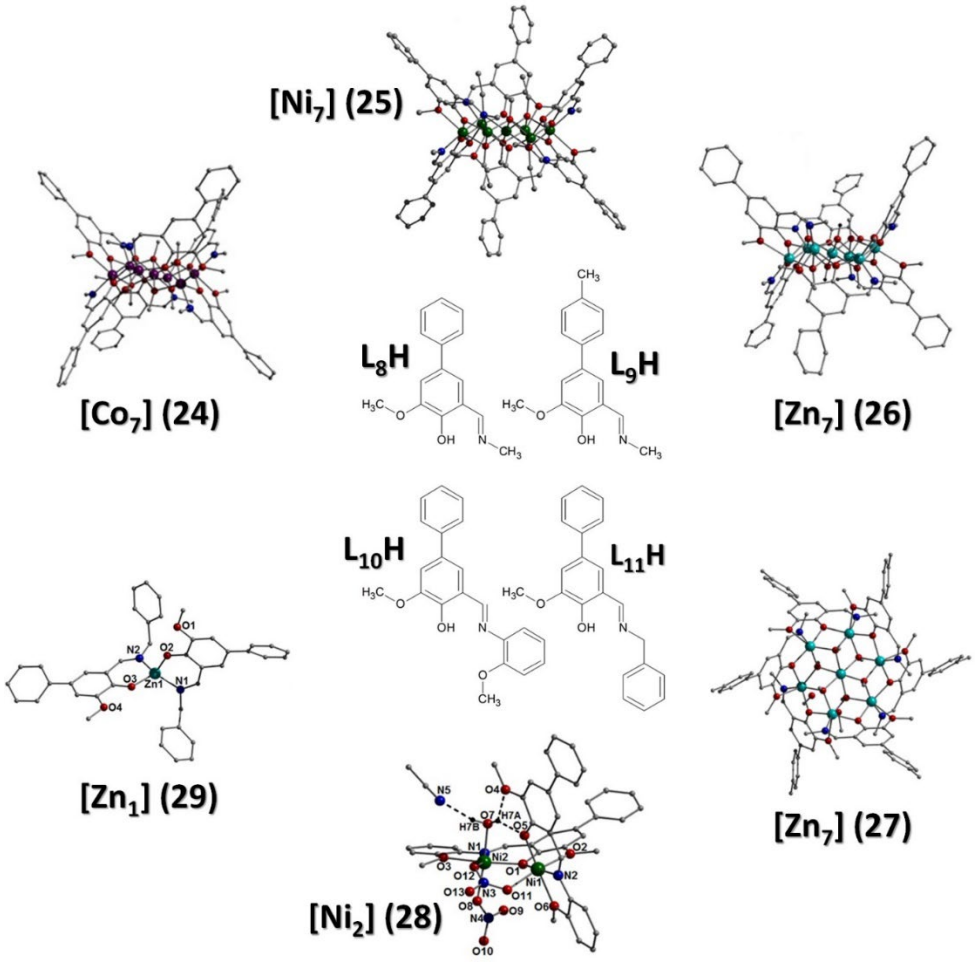

Figure 5.3 Schematic highlighting the *upper* **and** *lower rim* modified ligands 2-Methoxy-4-phenyl-6-[(E)-(methylimino)methyl]phenol (L_8H), 2-Methoxy-4-tolyl-6-[(E)-(methylimino)methyl]phenol (L_9H), 2-Methoxy-4-phenyl-6-{(E)-[(2-methoxyphenyl)imino]methyl}phenol ($L_{10}H$) and 2-[(E)-(Benzylimino)methyl]-4-phenyl-6-methoxyphenol ($L_{11}H$), surrounded by examples of Ni(II) and Co(II) and Zn(II) complexes (**24**-**29**) constructed with these ligands as described in Chapter 4. The majority of H atoms have been omitted for clarity. Colour code: Green (Ni), Purple (Co), Red (O), Blue (N), Grey (C) and Black (H).

5.2 Future work

Work within the Jones group has already shifted towards the strategic design and formation of permanent molecular cavities within the family of *pseudo* metallocalix[n]arenes (previously discussed in Chapter 2). It is envisaged this will be achieved by building upon the work described in both chapters 3 and 4 of this work;

where the metallocalix[6]arene forming ligands have been structurally modified towards altered cavity formation. As highlighted in these chapters, such modifications often led to either poor cavity formation (more efficient packing in the solid state) or an entirely new metal topology (moving away from the $[M_7]$ and $[M_4]$ motifs towards lower nuclearity complexes. With these thoughts in mind, work will focus on the covalent dimerization of these ligands in the hope that a permanent molecular cavity may be achieved upon metal complexation. By doing this we may form permanently porous extended materials capable of hosting guest molecules towards catalytic and / or storage properties. Other future work emanating from this thesis are given below.

5.2.1 Future magnetic susceptibility studies

Although not the focus of the work, the Jones group will pursue magnetic susceptibility studies on a selection of the paramagnetic host-guest complexes of general formula $[(guest)\subset M(II)_7(OMe)_6(L)_6](NO_3)$ (M = Co(II); Ni(II)), as discussed in Chapter 2. We envisage that their properties will mirror the previously published analogues $[Ni(II)_7(\mu_3\text{-}OH)_6(L_1)_6](NO_3)_2$,[1] $[Co(II)_7(\mu_3\text{-}OH)_6(L_1)_6](NO_3)_2$ and $[(NO_3)\subset Co(III)Co(II)_6(\mu_3\text{-}OH)_6(L_2)_6](NO_3)_2$ (where L_1H = 2-methoxy-6-[(methylimino)methyl]phenol and L_2H = 2-methoxy-6-[(phenylimino)methyl]phenol).[2]

5.2.2 Investigations into a new branch of the ligand family

More recent work by the Jones group has focused on investigating the coordination chemistry of the analogous ligands 5-phenyl-2-hydroxy-3-methoxybenzaldehyde (Figure 5.4) and 5-(4-chlorophenyl)-2-hydroxy-3-methoxybenzaldehyde (Fig. 5.6). Close inspection of these ligands shows that they are in fact precursors to the ligands 5-(4-R-phenyl)-3-methoxysalicyaldehyde (R = H (L_8H) and CH_3 (L_9H)) employed in Chapter 4 of this work (where the synthesis has been halted prior to the Schiff base condensation step). Initial Cu(II) coordination studies have produced the 1-D chain $[Cu(II)Na(I)(L)_2(MeOH)(NO_3)]_n$ (where LH = 5-phenyl-2-hydroxy-3-methoxybenzaldehyde; Figure 5.4) along with the intermolecular H-bonded dimeric complex $[Cu(II)(L)_2(H_2O)]$ (where LH = 5-chlorophenyl-2-hydroxy-3-methoxybenzaldehyde; Fig. 5.6). The Jones group will continue investigating the

coordinating power of these ligands with a range of paramagnetic 3d (eg. Fe(II/III), Mn(II/III/IV), Cu(II) and Ni(II)) and 4f (e.g. Gd(III) and Dy(III)) metal ions. Gadolinium would have an isotropic effect while dysprosium would have an anisotropic effect which could produce a SMM. All new complexes will be studied using a number of techniques (e.g. XRD, UV-vis, FT-IR and SQUID magnetometry).

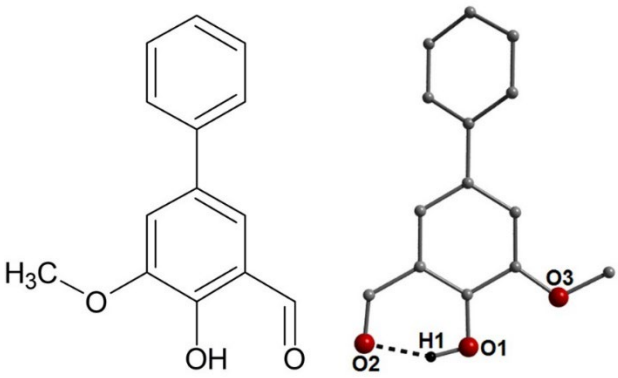

Figure 5.4 ChemSketch and crystal structure of the ligand 5-phenyl-2-hydroxy-3-methoxybenzaldehyde (LH). The dashed line represents an intramolecular H-bond at a distance of (O1(H1)···O2 = 1.72 Å. Colour code: Red (O), Blue (N), Grey (C).

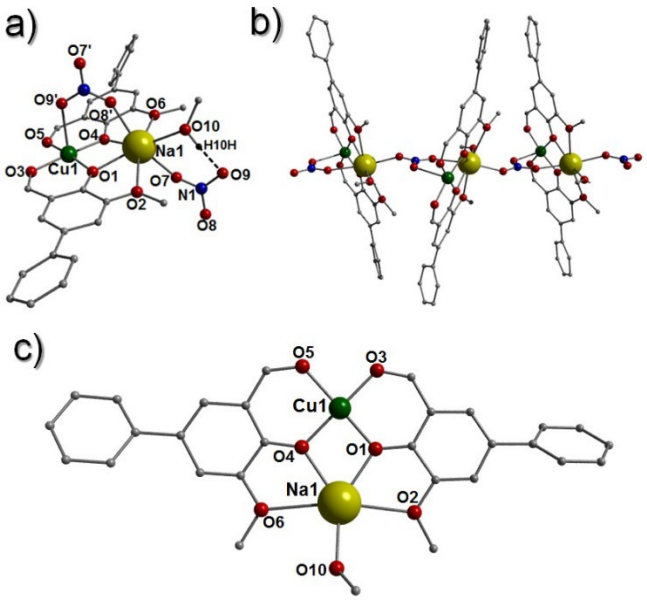

Figure 5.5 Crystal structure of 1-D chain complex $[Cu(II)Na(I)(L)_2(MeOH)(NO_3)]_n$ (where LH = 5-phenyl-2-hydroxy-3-methoxybenzaldehyde). The dashed line represents an intramolecular H-bond at a distance of (O1(H10H)···O9 = 2.30 Å. Colour code: Green (Cu), Yellow (Na), Red (O), Blue (N), Grey (C) and Black (H). The bound NO_3^- anion and terminal

MeOH ligand has been omitted in figure c for clarity. The majority of hydrogen atoms have been omitted for clarity.

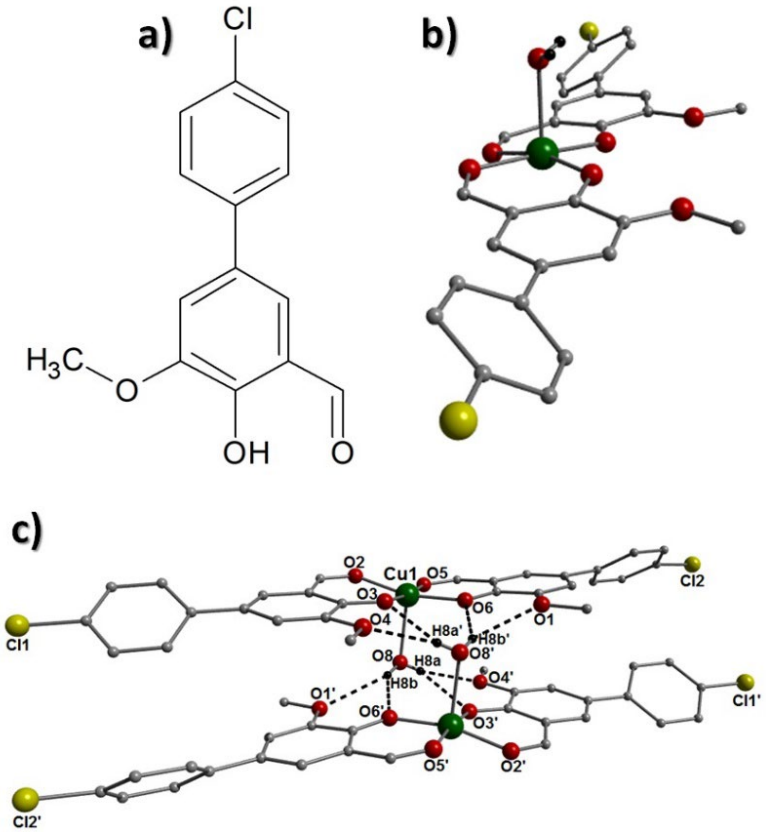

Figure 5.6 (a) Chemsketch representation of the ligand 5-(4-chlorophenyl)-2-hydroxy-3-methoxybenzaldehyde (LH). (b) Crystal structure of the monometallic complex $[Cu(II)(L)_2(H_2O)]$ whose extensive intermolecular interactions (dashed lines) allow the formation of the dimeric topology shown in (c). Intramolecular distances: O8(H8a)···O3′ = 2.304 Å, O8(H8a)···O4′ = 2.451 Å, O8(H8b)···O1′ = 2.429 Å and O8(H8b)···O6′ = 2.183 Å. The majority of hydrogen atoms have been omitted for clarity. Colour code: Green (Cu), Red (O), Blue (N), Grey (C), Black (H) and Yellow (Cl).

5.3 References

1. (a) S. T. Meally, C. McDonald, G. Karotsis, G. S. Papaefstathiou, E. K. Brechin, P. W. Dunne, P. McArdle, N. P. Power, L. F. Jones. *Dalton Trans.,* 2010, **39**, 4809 – 4816. (b) S. T. Meally, G. Karotsis, E. K. Brechin, G. S. Papaefstathiou, P. W. Dunne, P. McArdle, L. F. Jones. *CrystEngComm.,* 2010, **12, 59-63.** For other examples of complexes with body-centred hexagonal [M_7] (M = Co(II), Ni(II), Zn(II)) disc-like inorganic cores: (c) R. Gheorghe, Georgiana A. Ionita, C. Maxim, A. Caneschi, L. Sorace, M. Andruh. *Polyhedron* 2019, **171**, 269–278. (d) F. Kobayashi, R. Ohtani, S. Teraoka, W. Kosaka, H. Miyasaka, Y. Zhang, L. F. Lindoy, S. Hayami and M. Nakamura. *Dalton Trans*., 2017, **46**, 8555–8561. (e) S.-H. Zhang, R.-X. Zhao, G. Li, H.-Y. Zhang, C.-L. Zhang, G. Muller. *RSC Advances*. 2014, **4**, 54837-54846. (f) C. Ding, C. Gao, S. Ng, B. Wang and Y. Xie. *Chem. Eur. J*. 2013, **19**, 9961–9972. (g) L.-Q.Wei, K. Zhang, Y.-C. Feng, Y.-H. Wang, M.-H. Zeng and M. Kurmoo. *Inorg. Chem.* 2011, **50**, 7274–7283. (h) J. Zhang, P. Teo, R. Pattacini, A. Kermagoret, R. Welter, G. Rogez, T. S. A. Hor and P. Braunstein. *Angew. Chem. Int. Ed*. 2010, **49**, 4443–4446. (h) W. Leong and J. J. Vittal. *New J. Chem*., 2010, **34**, 2145–2152.

2. S. T. Meally, C. McDonald, P. Kealy, S. M. Taylor, E. K. Brechin and L. F. Jones. *Dalton Trans.,* 2012, **41(18)**, 5610-5616.